

DTIC FILE COPY

AGARD-AG-301 VOL. I

①

AGARD-AG-301 VOL. I

# AGARD

ADVISORY GROUP FOR AEROSPACE RESEARCH & DEVELOPMENT

7 RUE ANTOINE LÉON, 92000 NEUILLY SUR SEINE, FRANCE

AD-A223 563

AGARDograph No.301

## Aircraft Trajectories Computation—Prediction—Control

(La Trajectoire de l'Avion  
Calcul—Prédiction—Contrôle)

Volume 1

DISTRIBUTION STATEMENT A

Approved for public release;  
Distribution Unlimited.

DTIC  
ELECTE  
JUL 02 1990  
S B D

NORTH ATLANTIC TREATY ORGANIZATION



is AGARD:

DISTRIBUTION AND AVAILABILITY  
ON BACK COVER

90 06 29 058

AGARD-AG-301  
Volume 1

NORTH ATLANTIC TREATY ORGANIZATION  
ADVISORY GROUP FOR AEROSPACE RESEARCH AND DEVELOPMENT  
(ORGANISATION DU TRAITE DE L'ATLANTIQUE NORD)

AGARDograph No.301

# **Aircraft Trajectories Computation—Prediction—Control**

(La Trajectoire de l'Avion  
Calcul—Prédiction—Contrôle)

## VOLUME 1

**Part I** Fundamentals  
**Part II** Flight in Critical Atmospheric Conditions  
**Part III** Impact of New On-Board Technologies on Aircraft Operation

Edited by

André Benoit  
Programme Director

**DISTRIBUTION STATEMENT A**  
Approved for public release;  
Distribution Unlimited

This AGARDograph has been sponsored by the Guidance and Control Panel of AGARD.

# The Mission of AGARD

According to its Charter, the mission of AGARD is to bring together the leading personalities of the NATO nations in the fields of science and technology relating to aerospace for the following purposes:

- Recommending effective ways for the member nations to use their research and development capabilities for the common benefit of the NATO community;
- Providing scientific and technical advice and assistance to the Military Committee in the field of aerospace research and development (with particular regard to its military application);
- Continuously stimulating advances in the aerospace sciences relevant to strengthening the common defence posture;
- Improving the co-operation among member nations in aerospace research and development;
- Exchange of scientific and technical information;
- Providing assistance to member nations for the purpose of increasing their scientific and technical potential;
- Rendering scientific and technical assistance, as requested, to other NATO bodies and to member nations in connection with research and development problems in the aerospace field.

The highest authority within AGARD is the National Delegates Board consisting of officially appointed senior representatives from each member nation. The mission of AGARD is carried out through the Panels which are composed of experts appointed by the National Delegates, the Consultant and Exchange Programme and the Aerospace Applications Studies Programme. The results of AGARD work are reported to the member nations and the NATO Authorities through the AGARD series of publications of which this is one.

Participation in AGARD activities is by invitation only and is normally limited to citizens of the NATO nations.

The content of this publication has been reproduced directly from material supplied by AGARD or the authors.

Published March 1990  
Copyright © AGARD 1990  
All Rights Reserved  
ISBN 92-835-0547-6



Printed by Specialised Printing Services Limited  
40 Chigwell Lane, Loughton, Essex IG10 3TZ

# Préface

Nécessaire pour les besoins d'un large éventail d'applications, la détermination de la trajectoire d'un aéronef fait intervenir une multitude d'éléments. Dans ce manuel, nous limitons notre propos à des aspects précis du calcul, de la prévision et du contrôle des trajectoires, et du guidage des vols.

L'ouvrage s'articule autour de deux grands thèmes: d'une part, les éléments fondamentaux qui interviennent dans la détermination des trajectoires compte tenu des connaissances et des technologies actuelles, de l'autre, la gestion et le contrôle de la circulation aérienne, ce qui suppose l'existence de méthodes et de techniques permettant de calculer en temps réel le cheminement d'un grand nombre d'aéronefs, ainsi que la possibilité de les guider dans les meilleures conditions de sécurité et d'efficacité dans les régions fortement encombrées.

Ces deux thèmes sont développés respectivement dans les volumes 1 et 2. Un troisième volume contient les résumés des contributions, une importante bibliographie, ainsi que la liste des auteurs des différentes contributions, avec l'indication du nom et de l'adresse de leur entreprise ou de leur organisation (un index complète chacune de ces deux dernières parties).

Ce premier volume se compose de trois parties:

- Part I:** Aspects Fondamentaux
- Part II:** Navigation Aérienne dans des Conditions Atmosphériques Difficiles
- Part III:** Incidence des Technologies Nouvelles sur les Pilotage des Aéronefs

En fait, les première et deuxième parties forment un tout: le lecteur constatera en effet que la structure des contributions reflète les liens étroits qui existent entre les sujets traités, à savoir les trajectoires optimales, les modèles non linéaires et les vols par vents non uniformes. Cela tient à la nature même du présent ouvrage: la contribution de chacun tend à privilégier un point particulier et revêt souvent un caractère autonome.

Après une introduction illustrant les relations entre les divers éléments influant sur le mouvement d'un aéronef, les auteurs traitent ensuite de la détermination des trajectoires optimales et du vol en présence de vents variables. Plusieurs applications sont envisagées: recherche de la trajectoire optimale pour la phase de décollage, définition de lois de pilotage — optimales et non optimales — pour la conduite d'aéronefs par vent cisailant et établissement de directives concernant les interceptions militaires. Les auteurs présentent en outre plusieurs modèles prenant en compte de façon réaliste le facteur vent et ses variations temporelles et spatiales dans les simulateurs de vol.

La troisième partie traite de l'incidence de la nouvelle conception technologique des équipements de bord sur la conduite des aéronefs. Elle comprend deux contributions. La première est consacrée à l'utilisation d'ordinateurs de bord en vue d'améliorer l'efficacité du transport aérien, la seconde aborde, sujet difficile s'il en est, le rôle de l'homme devant l'automatisation croissante du poste de pilotage, et l'incidence de ce phénomène sur l'exécution du vol.

André Benoît  
Directeur du programme  
Membre de la Commission Guidage et Pilotage



Accession For	
NTIS GRA&I	<input checked="" type="checkbox"/>
DTIC TAB	<input type="checkbox"/>
Unannounced	<input type="checkbox"/>
Justification	
By	
Distribution/	
Availability Codes	
Dist	Avail and/or Special
A-1	

## Preface

The determination of the motion of aircraft exhibits a very great number of facets and this is required in a wide range of applications. It is accordingly our intention to limit the scope of this manual to specific aspects related to the computation, prediction and control of trajectories, and guidance of flights.

Within this framework, the work will be structured around two main themes: on the one hand the fundamentals of the computation of a trajectory in terms of present knowledge and technologies and, on the other, the handling of air traffic, implying the availability of methods and techniques to compute on-line the future paths of a large number of aircraft and the possibility of guiding their flights safely and efficiently in dense traffic, and even, in congested areas.

These two themes are developed in two separate volumes, numbered 1 and 2 respectively. A third volume will include the book of abstracts, an extensive bibliography and the list of contributors, including affiliations and professional addresses; these last two parts being complemented by adequate indexes.

This first volume has been divided into three parts, namely:

- Part I** Fundamentals
- Part II** Flight in Critical Atmospheric Conditions
- Part III** Impact of New On-Board Technologies on Aircraft Operation

Parts I and II actually constitute a single entity: the reader will note that the structure of the contributions presented reflects the tight coupling between the subjects covered, mainly optimum trajectories/non-linear models/flight in non-uniform wind. This results from the inherent nature of this work; each individual contribution tending to be autonomous, although placing the emphasis on a particular topic.

After an introduction illustrating relationships between the elements affecting the motion of an aircraft, the emphasis is placed on determination of optimal trajectories and the computation of flight paths in the presence of wind variations. Several applications are treated, including the derivation of optimal trajectories for the take-off phase, the determination of control laws — optimal and non-optimal — to fly aircraft in the presence of windshear and the generation of directives relating to military interceptions. Further, models are proposed to account realistically for wind and wind variations in flight simulations.

Part III affords a picture of the impact of new on-board technologies on aircraft operation. It is made up of two contributions. The first one presents the use of on-board computers to improve efficiency in air transport, while the second treats the difficult subject of the role of man in the face of increasing automation in the cockpit, and the resulting effect on the conduct of the flight.

Dr André Benoit  
Programme Director and Editor  
Guidance and Control Panel

# Guidance and Control Panel Officers

**Chairman:** Ir P.Ph. van den Broek  
Department of Aerospace Engineering  
Delft University of Technology  
Kluyverweg, 1  
2629 HS Delft  
Netherlands

**Deputy Chairman:** Prof. E.B.Stear  
Executive Director  
Washington Technology Center  
University of Washington  
376 Loew Hall — FH-10  
1013 NE 40th Street  
Seattle, WA 98195  
United States

## TECHNICAL PROGRAMME

Programme Director and Editor: Dr André Benoit  
Faculté des Sciences Appliquées  
Université Catholique de Louvain  
B-1348 Louvain-la-Neuve  
Belgium

European Organisation for the Safety of Air Navigation  
EUROCONTROL  
Engineering Directorate  
72, rue de la Loi  
B-1040 Bruxelles  
Belgium

## PANEL EXECUTIVE

**From Europe**  
CDT Moustafa Mouhamad (FAF)  
Executive, GCP  
AGARD-NATO  
92200 Neuilly-sur-Seine  
France  
Telephone: 33(1)4738 5780 — Telex: 610 176F

**From USA and Canada**  
Executive, GCP  
AGARD-NATO  
APO New York 09777

## ACKNOWLEDGEMENT/REMERCIEMENTS

The Guidance and Control Panel wishes to express its appreciation to all authors and co-ordinators who contributed to this AGARDograph, and made its publication possible.

La Commission Guidage et Pilotage tient à remercier tous les auteurs et coordonnateurs qui contribuèrent à la réalisation et la publication de cette AGARDographie.

# Activities in Air Traffic Handling

Over the past 20 years, the Guidance and Control Panel of the Advisory Group for Aerospace Research and Development to the North Atlantic Treaty Organization has devoted part of its activities to the fascinating field known historically as Air Traffic Control.

The Panel's contributions listed below cover in particular, the air and ground components considered as parts of a single system, the methods, techniques and technologies applicable to or usable for the management of the flows of aircraft and the control of individual flights, the integration of control phases over extended areas such as in the *Zone of Convergence* type concepts, the 4-D guidance of aircraft in critical conditions, the ever-increasing level of automation and its impact on the essential role of the human acting on-line in the control loop.

## **AIR TRAFFIC CONTROL SYSTEMS**

Guidance and Control Symposium, Edinburgh, Scotland,  
26-29 June 1972.  
AGARD-CP-105, April 1973.

## **A SURVEY OF MODERN AIR TRAFFIC CONTROL**

AGARDograph AG-209, Vols. I and II  
July 1975.

## **PLANS AND DEVELOPMENTS FOR AIR TRAFFIC SYSTEMS**

Guidance and Control Panel Symposium, Cambridge, Mass., United States  
20-23 May 1975.  
AGARD-CP-188, February 1976.

## **AIR TRAFFIC MANAGEMENT: Civil/Military Systems and Technologies**

Guidance and Control Symposium, Copenhagen, Denmark,  
9-12 October 1979.  
AGARD-CP-273, February 1980.

## **AIR TRAFFIC CONTROL IN FACE OF USERS' DEMAND AND ECONOMY CONSTRAINTS**

Guidance and Control Symposium, Lisbon, Portugal,  
15 October 1982.  
AGARD-CP-340, February 1983.

## **EFFICIENT CONDUCT OF INDIVIDUAL FLIGHTS AND AIR TRAFFIC**

or Optimum Utilisation of Modern Technology  
(Guidance, control, navigation, surveillance and processing facilities)  
for the Overall Benefit of Civil and Military Airspace Users  
Guidance and Control Symposium, Brussels, Belgium,  
10-13 June 1986.  
AGARD-CP-410, December 1986.

## **AIRCRAFT TRAJECTORIES: Computation - Prediction - Control**

AGARDograph AG-301, Vols. 1, 2 and 3:

### **Volume 1 FUNDAMENTALS**

**FLIGHT IN CRITICAL ATMOSPHERIC CONDITIONS  
IMPACT OF NEW ON-BOARD TECHNOLOGIES ON AIRCRAFT OPERATION**

### **Volume 2 AIR TRAFFIC HANDLING AND GROUND-BASED GUIDANCE OF AIRCRAFT**

### **Volume 3 ABSTRACTS - BIBLIOGRAPHY - CONTRIBUTORS**

## **ON-LINE HANDLING OF AIR TRAFFIC**

**Guidance & Control Aspects**  
AGARDograph AG-321, in preparation

# Condensed Contents

Detailed Contents of all three volumes follow

## VOLUME 1

**PREFACE**

**PART I FUNDAMENTALS**

**PART II FLIGHT IN CRITICAL ATMOSPHERIC CONDITIONS**

**PART III IMPACT OF NEW ON-BOARD TECHNOLOGIES ON AIRCRAFT OPERATION**

## VOLUME 2

**PART IV AIR TRAFFIC HANDLING**

**PART V GUIDANCE OF AIRCRAFT IN A TIME-BASED CONSTRAINED ENVIRONMENT**

**PART VI SURVEILLANCE**

**PART VII METEOROLOGICAL FORECASTS**

**PART VIII AIRCRAFT OPERATION IN AIR TRAFFIC HANDLING SIMULATION**

## VOLUME 3

**PART IX BOOK OF ABSTRACTS**

**PART X BIBLIOGRAPHY (with Index)**

**PART XI LIST OF CONTRIBUTORS (with Index)**

# Contents

## VOLUME 1

	Page
PREFACE (F)	iii
PREFACE (E)	iv
GUIDANCE AND CONTROL PANEL OFFICERS AND PROGRAMME DIRECTOR	v
GCP ACTIVITIES IN AIR TRAFFIC HANDLING	vi
CONDENSED CONTENTS	vii
	Reference
<b>PART I – FUNDAMENTALS</b>	
<i>A – GENERAL OUTLINE OF THE PROBLEM</i>	
INTRODUCTION A L'ETUDE DES TRAJECTORIES D'AVION: Schéma Général des Problèmes Posés par Frédéric Haus	1F
INTRODUCTION TO THE STUDY OF AIRCRAFT TRAJECTORIES: General Outline of the Problem by Frédéric Haus	1E
<i>B – COMPUTATION OF OPTIMAL TRAJECTORIES</i>	
OPTIMAL TRAJECTORIES OF AIRCRAFT AND SPACECRAFT by Antonio Miele	2
<i>C – NON-LINEAR MODELS OF AIRCRAFT</i>	
COMPARISON OF A MATHEMATICAL ONE-POINT MODEL AND A MULTI-POINT MODEL OF AIRCRAFT MOTION IN MOVING AIR by R.Brockhaus	3
DETERMINATION DES LOIS DE GUIDAGE QUASI-OPTIMALES EN TEMPS REEL POUR DES TRAJECTOIRES D'AVIONS DE COMBAT (Computation of Sub-Optimal Real-Time Guidance Laws for Combat Aircraft Trajectories) par H.T.Huynh	4
<b>PART II – FLIGHT IN CRITICAL ATMOSPHERIC CONDITIONS</b>	
<i>A – GENESIS OF WIND AND INFLUENCE ON AIRPLANE TRAJECTORIES</i>	
CRITICAL ASPECTS OF TRAJECTORY PREDICTION: Flight in Non-Uniform Wind by Bernard Etkin and David Alexandre Etkin	5
EFFECT OF WIND AND WIND VARIATION ON AIRCRAFT FLIGHT – PATHS K.U.Hahn, T.Heintsch, B.Kaufmann, G.Schänzer and M.Swolinsky	6
<i>B – FLIGHT CONTROL IN WINDSHEAR</i>	
AIRCRAFT FLIGHT IN WINDSHEAR by D.McLean	7
HOW TO FLY WINDSHEAR by Paul Camus	8

**C – FLIGHT SIMULATION**

- WIND MODELS FOR FLIGHT SIMULATION** 9  
by K.U.Hahn, T.Heintsch, B.Kaufmann, G.Schänzer and M.Swolinsky

**PART III – IMPACT OF NEW ON-BOARD TECHNOLOGIES ON AIRCRAFT OPERATION****A – FLIGHT MANAGEMENT IN AIR TRANSPORT**

- AIRCRAFT TRAJECTORY – PREDICTION AND CONTROL IN THE AIR TRANSPORT** 10  
**FLIGHT MANAGEMENT COMPUTER SYSTEM**  
by Peter J.Howells

**B – CREW/AUTOMATION INTERFACE**

- IMPACT OF NEW TECHNOLOGY ON OPERATIONAL INTERFACE: From Design Aims** 11  
**to Flight Evaluation and Measurement**  
by J.J.Speyer, C.Monteil, R.D.Blomberg and J.P.Fouillot

**VOLUME 2****PART IV – AIR TRAFFIC HANDLING****A – REQUIREMENT: INTEGRATION OF CONTROL PHASES**

- OPTIMUM ON-LINE HANDLING OF AIR TRAFFIC OVER WESTERN EUROPE** 12E  
by André Benoit and Sip Swierstra

- REGULATION TEMPS REEL OPTIMALE DU TRAFIC AERIEN EN EUROPE OCCIDENTALE** 12F  
par André Benoit et Sip Swierstra

**B – PROSPECT: A FUTURE EUROPEAN AIR TRAFFIC SYSTEM CONCEPT**

- THE EUROCONTROL FUTURE ATS SYSTEM CONCEPT AND THE PROGRAMME OF** 13E  
**STUDIES, TESTS AND TRIALS**  
by V.Vachiéry

- LE CONCEPT DU FUTUR SYSTEME ATS EUROCONTROL ET LE PROGRAMME** 13F  
**D'ETUDES, ESSAIS ET EXPERIMENTATIONS**  
par V.Vachiéry

**C – ON-LINE PREDICTION OF AIRCRAFT TRAJECTORIES****(i) General Discussion**

- PREDICTION OF AIRCRAFT TRAJECTORIES** 14  
by Stanley Ratcliffe

**(ii) Fundamentals**

- AIRCRAFT DYNAMICS FOR AIR TRAFFIC CONTROL** 15  
by P.Y.Willems

**(iii) Applications**

- THE APPLICATION OF TRAJECTORY PREDICTION ALGORITHMS FOR PLANNING** 16  
**PURPOSES IN THE NETHERLANDS ATC-SYSTEM**  
by J.N.P.Beers, T.B.Dalm, J.M. ten Have and H.Vischer

- GENERATION OF AIRCRAFT TRAJECTORIES FOR ON-LINE OPERATION** 17  
by André Benoit and Sip Swierstra

**D – AIR TRAFFIC MANAGEMENT***(i) Optimisation: Models and Techniques*

**OPTIMIZATION MODELS AND TECHNIQUES TO IMPROVE AIR TRAFFIC MANAGEMENT** 18  
by Lucio Bianco

*(ii) Man/Computer Interface*

**THE HIGH-RESOLUTION GRAPHIC DISPLAY** 19  
A possible man/machine interface for a computer assisted ATC management system  
by Carlos García Avello

**PART V – GUIDANCE OF AIRCRAFT IN A TIME-BASED  
CONSTRAINED ENVIRONMENT**

**A – CONTEXT – OBJECTIVES – PLANS**

**4-D CONTROL OF CURRENT AIR-CARRIERS IN THE PRESENT ENVIRONMENT:** 20E  
Objectives – Status – Plans  
by André Benoit

**REGULATION 4-D DANS L'INFRASTRUCTURE ACTUELLE: Point de la Situation  
et Objectifs à Atteindre** 20F  
par André Benoit

**NAVIGATION 4-D EN CIRCULATION AERIENNE** 21  
par Nicole Imbert et Marc Pèlerin

**B – GENERAL DISCUSSION**

**ON THE AUTOMATION OF FUTURE ATC CENTRES IN THE LIGHT OF THE  
CONCEPT OF THE "ZONE OF CONVERGENCE"** 22  
by Victor Attwooll

**C – GUIDANCE AND CONTROL: PRINCIPLES AND CONCEPTS**

**THE CONTROL OF INBOUND FLIGHTS: Basic Principles** 23E  
by André Benoit and Sip Swierstra

**LE GUIDAGE DES VOLS JUSQU'AU SEUIL DE PISTE: Principes Généraux** 23F  
par André Benoit et Sip Swierstra

**GUIDANCE CONCEPTS FOR TIME-BASED FLIGHT OPERATIONS** 24  
by Dan D. Vicroy

**4-D DESCENT TRAJECTORY GENERATION TECHNIQUES UNDER REALISTIC  
OPERATING CONDITIONS** 25  
by David H. Williams and Charles E. Knox

**D – CONDUCT OF AIR TRAFFIC CONTROL IN A ZONE OF CONVERGENCE**

**EXPERT SYSTEMS FOR THE GENERATION OF TERMINAL AREA ARRIVAL PATHS  
FOR CIVIL TRANSPORT** 26  
by Robert W. Simpson

**A DESCRIPTION AND EVALUATION OF "TIMER": A Time-Based Terminal Flow-Control  
Concept** 27  
by Léonard Credeur and William R. Capron

**USE OF 4D RNAV IN TIME-BASED EN ROUTE ARRIVAL METERING** 28  
by R.L. Erwin and K.H. Izumi

**AIR TRAFFIC MANAGEMENT AND AIRCRAFT GUIDANCE IN A ZONE OF  
CONVERGENCE** 29  
by André Benoit and Sip Swierstra

	Reference
<b>E -- GROUND-BASED 4-D GUIDANCE OF AIRCRAFT IN MOVING ATMOSPHERE</b>	
GROUND-BASED 4-D GUIDANCE OF FLIGHTS IN STRONG WIND by André Benoit and Sip Swierstra	30E
GUIDAGE QUADRIDIMENSIONNEL A PARTIR DU SOL DE VOLS OPERANT PAR VENT FORT par André Benoit et Sip Swierstra	30F
A PILOTED SIMULATOR EVALUATION OF GROUND-BASED 4D DESCENT ADVISOR ALGORITHM by Thomas J.Davis, Steven M.Green and Heinz Erzberger	31
<b>F -- THE COMPUTER/CONTROLLER/PILOT DIALOGS</b>	
THE AIR TRAFFIC CONTROLLER FACING AUTOMATION: Conflict or Co-Operation by André Benoit, Sip Swierstra and René de Wispelaere	32E
LE CONTROLEUR DE LA CIRCULATION AERIENNE ET L'AUTOMATISATION: Conflit d'Intérêts ou Convergence? par André Benoit, Sip Swierstra et René de Wispelaere	32F
<b>PART VI -- SURVEILLANCE</b>	
<b>A -- RADAR TRACKING</b>	
AIRCRAFT TRAJECTORY RECONSTITUTION ON THE BASIS OF MULTI-RADAR PLOT INFORMATION by Pieter van der Kraan	33
BAYESIAN MULTI-SENSOR TRACKING FOR ADVANCED AIR TRAFFIC CONTROL SYSTEMS by H.A.P.Blom, R.A.Hogendoorn and F.J. van Schaik	34
THE USE OF DOWNLINKED MEASUREMENTS TO TRACK CIVIL AIRCRAFT by Chris C.Lefas	35
<b>B -- SATELLITE TECHNIQUES</b>	
L'APPORT DES TECHNIQUES SATELLITAIRES A LA SURVEILLANCE DE LA NAVIGATION AERIENNE (Contribution of the Satellite Techniques to the Surveillance of Air Traffic) par Olivier Carel	36
<b>PART VII -- METEOROLOGICAL FORECASTS</b>	
<b>A -- IMPACT OF FORECASTS QUALITY ON TRAJECTORY PREDICTION</b>	
DEVELOPMENTS TO ENHANCE METEOROLOGICAL FORECASTING FOR AIR TRAFFIC SERVICES by M.E.Cox and D.A.Forrester	37
<b>PART VIII -- AIRCRAFT OPERATION IN AIR TRAFFIC HANDLING SIMULATION</b>	
<b>A -- REALISTIC OPERATION AND MOTION OF AIRCRAFT</b>	
INTEGRATION OF AIRCRAFT CAPABILITY IN AIR TRAFFIC HANDLING SIMULATIONS by André Benoit, S.Swierstra and Yves Delnatte	38
<b>B -- FLIGHT OPERATIONS WITHIN A TERMINAL AREA</b>	
SIMULATION OF AUTOMATED APPROACH PROCEDURES CONSIDERING DYNAMIC FLIGHT OPERATIONS by Manfred Ficke and Adreas Hörmann	39

**Reference**

**VOLUME 3**

**PART IX – BOOK OF ABSTRACTS**

**A**

**PART X – BIBLIOGRAPHY**

**B**

**A – GLOSSARY**

**B – REFERENCES**

**C – INDEX**

**PART XI – LIST OF CONTRIBUTORS**

**C**

**A – CONTRIBUTORS AND AFFILIATIONS**

**B – INDEX**

**PART I**

**Fundamentals**

## INTRODUCTION A L'ETUDE DES TRAJECTOIRES D'AVION

par

Frédéric Haus  
 Professeur Emérite aux Universités de Gand et Liège  
 99 rue Colonel Chaltin  
 B-1180 Bruxelles  
 Belgium

\* \* \*

## Schéma général des problèmes posés

Le transport aérien résulte du bon fonctionnement d'un système formé par :

- l'avion
- l'atmosphère
- le pilote
- les aides terrestres à la navigation.

Dans ce qui suit, le terme avion désigne l'ensemble constitué par la structure de l'avion, l'organe de propulsion et tous les systèmes mécaniques existant à bord.

Le terme atmosphère désigne l'ensemble de tous les éléments variables définissant le milieu dans lequel se déplace l'avion.

Le terme pilote désigne l'ensemble de l'équipage intervenant dans la conduite de l'avion.

Le terme aide terrestre désigne toute information transmise à partir du sol et, éventuellement, toute action exercée au sol.

Le programme "Calcul des trajectoires" nécessite l'établissement de relations numériques entre des variables de nature très différente. Il s'étend à la recherche de la manière dont le pilote doit gérer le vol en vue d'optimiser l'une ou l'autre des variables du système, telles la durée du vol reliant le point de départ au point d'arrivée, la consommation totale de combustible, etc.

Un organigramme décrivant les relations entre les différentes parties du système ainsi défini, est présenté ci-après. Il répartit en douze groupes les problèmes soulevés par le vol d'un avion. Cet organigramme présente ces groupes sous forme de blocs et indique les relations les plus importantes qui les unissent.

Le premier bloc comprend la définition de la mission envisagée, l'évaluation de la quantité de combustible à prendre à bord, la vérification par le pilote du bon fonctionnement des systèmes les plus importants. Le résultat de l'activité représentée par ce bloc est l'établissement d'un plan de vol, tenant compte des caractéristiques mécaniques de l'avion et des informations issues des blocs 2 et 3.

Le bloc 2 définit l'état de l'atmosphère au moment du départ et prévoit, dans la mesure du possible, les modifications qui pourraient survenir pendant le vol.

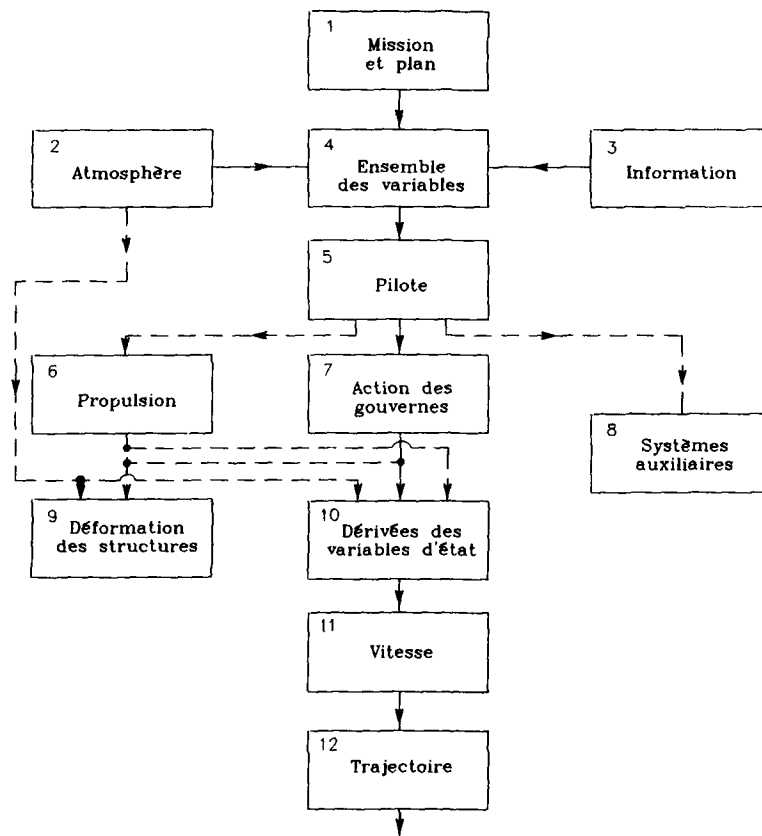
Le bloc 3 englobe toutes les informations que les services de contrôle de la circulation aérienne peuvent rassembler sur l'état d'occupation de l'atmosphère par d'autres avions, tant au moment du départ que pendant toute la durée du vol. Ces informations conduisent toujours à restreindre le choix que le pilote peut exercer en matière de trajectoire.

Le bloc 4 schématise l'ensemble des variables définissant, à chaque instant l'état dans lequel se trouve l'avion, sa position et son mouvement. Les moyens d'information dont dispose le pilote constituent le support matériel de ce bloc.

Le bloc 5 schématise l'action du pilote qui s'étend :

- a. au traitement de l'information et à la vérification de la conformité du vol réel (bloc 4) avec le plan de vol (bloc 1) ;
- b. à la prise des décisions nécessaires à la poursuite du vol dans les meilleures conditions ;
- c. à l'exécution des actions nécessaires à cette fin.

Des instruments de calcul et, dans certains cas, des appareils automatiques peuvent aider le pilote dans ce travail.



CALCUL DES TRAJECTOIRES  
Organigramme

Le bloc 6 représente le système de propulsion. Le fonctionnement de ce dernier est commandé par le pilote et produit :

- a. une poussée ;
- b. la diminution continue de la masse de l'avion, par suite de la consommation de combustible ;
- c. l'émission d'un bruit correspondant à un nombre élevé de décibels ;
- d. des vibrations.

Le bloc 7 définit l'action des commandes et des gouvernes. Il est indispensable de rappeler la définition que l'ISO donne de ces termes.

Les gouvernes sont des organes destinés à altérer l'écoulement de l'air autour de l'avion, et à modifier ainsi les forces extérieures agissant sur celui-ci. Ces organes sont en fait des parties de la structure susceptibles de subir de faibles déplacements commandés par le pilote. On doit remarquer que des jets d'air modulables et dirigés de l'intérieur de l'avion vers l'extérieur, constitueraient aussi des gouvernes si on les utilisait.

Le terme commande désigne l'organe sur lequel le pilote agit pour mettre la gouverne en action.

Il existe nécessairement tout un mécanisme entre la commande et la gouverne. Ce mécanisme peut, dans certains cas, être actionné par des signaux indiquant un écart entre la grandeur souhaitée des variables d'état et leur grandeur réelle.

Ce mécanisme constitue la partie matérielle du groupe 7. La connaissance de son action est essentielle dans l'étude de la mécanique de l'avion.

Le bloc 8 représente (pour mémoire) les systèmes auxiliaires qui peuvent être mis en service par le pilote.

Les blocs 9 et 10 déterminent l'action d'entrées consistant en :

- perturbations atmosphériques
- variations de poussée
- déplacements de gouvernes.

Ces entrées peuvent produire des déformations de structure de l'avion, prévues par le bloc 9. Elles exercent un effet direct sur le mouvement de l'avion défini par le bloc 10.

Dans les deux cas, ces entrées exercent des forces et des moments dépendant des caractéristiques aérodynamiques de l'avion. Ces caractéristiques sont définies par ce qu'on peut appeler le modèle aérodynamique de l'avion. Une bonne connaissance de celui-ci est indispensable si on veut, à l'aide des équations de la mécanique, prévoir l'effet des blocs 9 et 10.

Cette situation serait sans conséquences graves si les déformations de la structure de l'avion ne constituaient pas une entrée supplémentaire au bloc 10, ce qui conduit à la possibilité de couplages entre les déformations de structure et les mouvements de l'avion, devant lesquels le pilote se trouverait désarmé.

C'est au moment de la conception de l'avion que les techniciens doivent veiller à ce que de tels couplages ne puissent atteindre une grandeur dangereuse dans les limites d'utilisation des avions.

L'organigramme est tracé dans l'hypothèse où, ni les sorties du bloc 9, ni celles du bloc 8 n'exercent d'effet sur le bloc 10. Ceci exclut l'examen du système "manoeuvre du train d'atterrissage" ainsi que tout problème de flutter.

Les sorties du bloc 10 sont les dérivés des variables d'état par rapport au temps.

Le bloc 11 schématise l'intégration de ces dérivés. Il décrit par conséquent l'évolution des variables d'état par rapport au temps.

Le bloc 12 schématise l'intégration des vitesses et définit la trajectoire parcourue.

## INTRODUCTION TO THE STUDY OF AIRCRAFT TRAJECTORIES

by

Frédéric Haus  
Emritus Professor, Universities of Gand and Liège  
99 rue Colonel Chaltin  
B-1180 Bruxelles  
Belgium

\*

\* \*

### General outline of the Problem

Air transport depends on the smooth operation of a system made up of the following elements:

- the aircraft
- the atmosphere
- the pilot
- the ground-based navigation aids.

For the purposes of this paper, the term "aircraft" is taken to mean the whole made up of the structure of the aircraft, its propulsion system and all the mechanical systems on board.

The term "atmosphere" covers all the variables defining the space in which the aircraft travels.

The term "pilot" refers to all the crew involved in flying the aircraft.

The term "ground-based aids" means all information transmitted from the ground, together, potentially, with all actions originating on the ground.

The "computation of trajectory" program requires the establishment of numerical relations between variables of very different kinds. It covers research into how the pilot should manage the flight so as to optimise one or other of the variables in the system (e.g. flight time between the point of departure and the point of arrival, total fuel consumption, etc.).

A flow chart illustrating the relation between the various parts of the system thus defined is given below. It divides the problems raised by the flight of an aircraft into twelve groups; these are shown as blocks and the major links between them indicated.

The first block embraces the definition of the intended flight, the evaluation of the amount of fuel to be taken on, and the pilot checks of the main systems. All this results in the establishment of a flight plan taking into account the mechanical features of the aircraft and the information in Blocks 2 and 3.

Block 2 defines the state of the atmosphere at the time of departure and gives, as far as possible, the charges which might occur during the flight.

Block 3 covers all the information the ATC services have been able to assemble regarding occupancy by other aircraft at the time of departure and during the entire flight. These factors always restrict the pilots' choice of trajectory.

Block 4 shows all the variables defining at any given moment the state of the aircraft, its position and its progress. The basis for this block is formed by the information resources at the pilots' disposal.

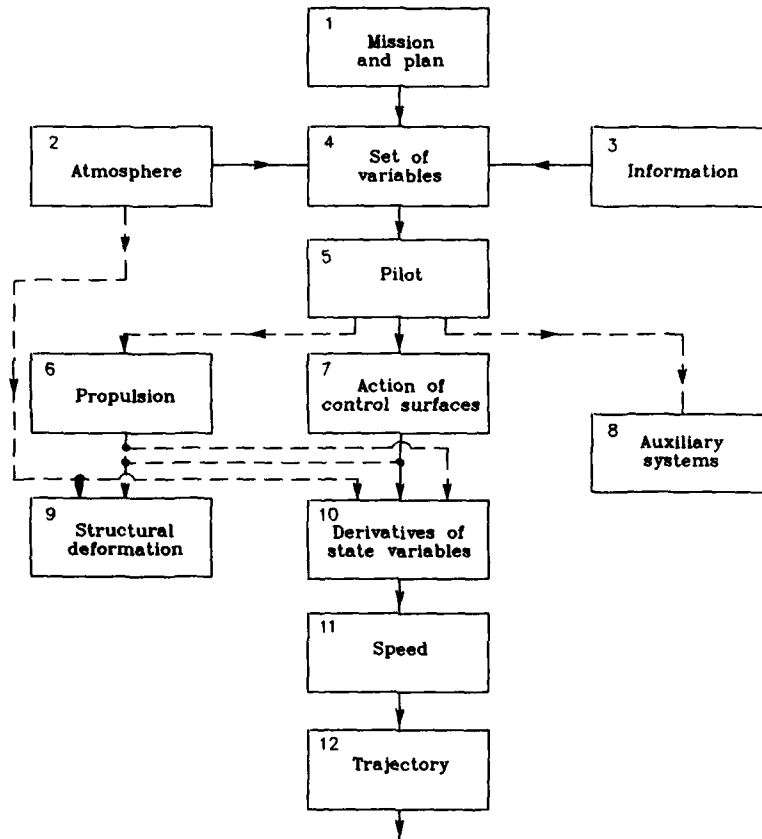
Block 5 is a representation of the pilots' action, covering:

- a. processing the information and checking the actual flight (Block 4) against the flight plan (Block 1)
- b. taking the decisions necessary to enable the flight to proceed under optimal conditions;

Computers, and in some cases automatic devices, may be used to assist the pilot in this.

Block 6 represents the propulsion-system. This is controlled by the pilot and produces :

- a. a thrust;
- b. a constant reduction in the mass of the aircraft as the weight of fuel is reduced;
- c. noise equivalent to a high level of decibels;
- d. vibration.



COMPUTATION OF TRAJECTORY  
Flow chart

Block 7 defines the action of the control (or actuators) and control surfaces. The definition attached to these terms by the ISO must be borne in mind.

It is this mechanism which makes up the material part of Block 7. An understanding of its action is essential in the study of the mechanics of the aircraft.

Block 8 shows, for the record, the auxiliary systems which may be used by the pilot.

Blocks 9 and 10 determine the effect of inputs such as:

- atmospheric disturbances
- variations in thrust
- displacements of control surfaces.

These may cause structural changes to the aircraft, as provide in Block 9. They have a direct effect on the movement of the aircraft as defined by Block 10.

In both cases, these inputs exert force and momentum depending on the aerodynamic features of the aircraft. These in turn are defined by what might be termed the aerodynamic model of the aircraft. This must be fully understood if the mechanical equations are to be used to predict the effect of Blocks 9 and 10.

This state of affairs would not matter very much if changes to the aircraft structure did not constitute an additional input in Block 10, opening the way for possible links between structural changes and aircraft movements, which would leave the pilot unprepared.

At the design stage the engineers should strive to ensure that such links never reach a dangerous level when the aircraft is used within the design limitations.

The flow chart is based on the assumption that neither Block 8 nor Block 9 will have any bearing on Block 10. Accordingly no account is taken of the "landing path manoeuvre" system or any flutter problem.

Block 10 outputs are derived from variations of state over time.

Block 11 shows the integration of these derivatives. It thus gives the trend in the variations of state over time.

Block 12 illustrates the integration of speeds and defines the trajectory followed.

OPTIMAL TRAJECTORIES OF AIRCRAFT AND SPACECRAFT<sup>1,2</sup>

by

A. Miele<sup>3</sup>  
Aero-Astronautics Group  
Rice University  
230 Ryon Building  
Houston, Texas 77251-1892  
United States

## SUMMARY

This paper summarizes some of the work done by the Aero-Astronautics Group of Rice University on algorithms for the numerical solutions of optimal control problems and their application to the computation of optimal flight trajectories of aircraft and spacecraft.

Part 1 deals with general considerations on calculus of variations, optimal control, numerical algorithms, and applications of these algorithms to real-world problems.

Part 2 deals with the sequential gradient-restoration algorithm (SGRA) for the numerical solution of optimal control problems of the Bolza type. Both the primal formulation and the dual formulation are discussed.

Part 3 deals with aircraft trajectories, in particular, the application of the dual sequential gradient-restoration algorithm (DSGRA) to the determination of optimal flight trajectories in the presence of windshear. Both take-off trajectories and abort landing trajectories are discussed. Take-off trajectories are optimized by minimizing the peak deviation of the absolute path inclination from a reference value. Abort landing trajectories are optimized by minimizing the peak drop of altitude from a reference value. The survival capability of an aircraft in a severe windshear is discussed, and the optimal trajectories are found to be superior to both constant pitch trajectories and maximum angle of attack trajectories.

Parts 4 and 5 deal with spacecraft trajectories, in particular, the application of the primal sequential gradient-restoration algorithm (PSGRA) to the determination of optimal flight trajectories for aeroassisted orbital transfer. Both the coplanar case (problem without plane change, Part 4) and the noncoplanar case (problem with plane change, Part 5) are discussed within the frame of three problems: minimization of the total characteristic velocity; minimization of the time integral of the square of the path inclination; and minimization of the peak heating rate. The solution of the second problem is called nearly-grazing solution, and its merits are pointed out as a useful engineering compromise between energy requirements and aerodynamics heating requirements.

Part 6 presents the conclusions. The references are given in Part 7.

<sup>1</sup>This research was supported by NASA Langley Research Center (Grant No. NAG-1-516), by Boeing Commercial Airplane Company, by Air Line Pilots Association, by United States Aviation Underwriters, by Jet Propulsion Laboratory (Contract No. 956415), and by Boeing Military Airplane Company.

<sup>2</sup>Discussions with Dr. T. Wang (Rice University), Mr. W. Y. Lee (Rice University), Captain W. W. Melvin (ALPA), and Dr. K. D. Mease (JPL) are acknowledged. Discussions with Dr. R. L. Bowles (NASA-LRC), Mr. C. R. Higgins (BCAC), and Dr. G. R. Hennig (BCAC) are also acknowledged.

<sup>3</sup>Professor of Aerospace Sciences and Mathematical Sciences, Aero-Astronautics Group, Rice University, Houston, Texas.

## PART 1. GENERAL CONSIDERATIONS

## 1.1. INTRODUCTION

In every branch of science, engineering, and economics, there exist systems which are controllable, that is, they can be made to behave in different ways depending on the will of the operator. Every time the operator of a system exerts an option, a choice in the distribution of the controls governing the system, he produces a change in the distribution of the states occupied by the system and, hence, a change in the final state. Therefore, it is natural to pose the following question: Among all the admissible options, what is the particular option which renders the system optimum? As an example, what is the option which minimizes the difference between the final value and the initial value of an arbitrarily specified function of the state of the system? The body of knowledge covering problems of this type is called calculus of variations or optimal control theory (Refs. 1-8). As stated before, applications occur in every field of science, engineering, and economics.

It must be noted that only a minority of current problems can be solved by purely analytical methods. Hence, it is important to develop numerical techniques enabling one to solve optimal control problems on a digital computer. These numerical techniques can be classified into two groups: first-order methods and second-order methods. First-order methods (or gradient methods) are those techniques which employ at most the first derivatives of the functions under consideration. Second-order methods (or quasilinearization methods) are those techniques which employ at most the second derivatives of the functions under consideration.

Both gradient methods and quasilinearization methods require the solution of a linear, two-point or multi-point boundary-value problem at every iteration. This being the case, progress in the area of numerical methods for differential equations is essential to the efficient solution of optimal control problems on a digital computer.

## 1.2. GRADIENT METHODS

In Part 2 of this paper, we review recent advances in the area of gradient methods for optimal control problems (Refs. 9-28). Because of space limitations, we make no attempt to cover every possible technique and every possible approach, a material impossibility in view of the large number of publications available. Thus, except for noting the early work performed by Kelley (Refs. 9-10) and Bryson (Refs. 11-14), we devote Part 2 of the paper to a review of the work performed in recent years by the Aero-Astronautics Group of Rice University (Refs. 15-28).

Also because of space limitations, we treat only single-subarc problems. More specifically, we consider the following Bolza problem of optimal control, called Problem (P) for easy identification.

Problem (P) consists of minimizing a functional  $I$  which depends on the state vector  $x(t)$ , the control vector  $u(t)$ , and the parameter vector  $\pi$ . At the initial point, the state and the parameter are required to satisfy a vector relation. At the final point, the state and the parameter are required to satisfy another vector relation. Along the interval of integration, the state, the control, and the parameter are required to satisfy a vector differential equation.

Problem (P) can be further complicated via the addition of a vector nondifferential equation to be satisfied everywhere along the interval of integration. The resulting generalized Bolza problem is called Problem (S); see, for example, Ref. 17.

In technical applications, there exist problems of optimal control whose format is different from, but is reducible to, the format of Problem (P) or that of Problem (S). In particular, this is the case with the Chebyshev problem or minimax problem [Problem (Q)]. For a particular transformation technique converting the Chebyshev problem into the Bolza problem, see Ref. 29.

### 1.3. SEQUENTIAL GRADIENT-RESTORATION ALGORITHM

One of the most effective first-order algorithms for solving trajectory optimization problems is the sequential gradient-restoration algorithm (SGRA, Refs. 15-24). Originally developed in the primal formulation (PSGRA, Refs. 15-21), this algorithm has been extended to incorporate a dual formulation (DSGRA, Refs. 22-24).

Both the primal formulation and the dual formulation involve a sequence of two-phase cycles, each cycle including a gradient phase and a restoration phase. The gradient phase involves one iteration and is designed to decrease the value of the functional, while the constraints are satisfied to first order. The restoration phase involves one or more iterations and is designed to force constraint satisfaction to a predetermined accuracy, while the norm squared of the variations of the control, the parameter, and the initial state is minimized. In turn, each iteration of the gradient phase and the restoration phase requires the solution of an auxiliary minimization problem (AMP).

In the primal formulation, the AMP is solved with respect to the variations of the state, the control, and the parameter. This leads to a linear, two-point boundary-value problem, which can be solved with the method of particular solutions (Refs. 25-28) or the method of complementary functions, employed in conjunction with some available integration scheme, for instance, Hamming's modified predictor-corrector method (Ref. 30).

In the dual formulation, the AMP is solved with respect to the Lagrange multipliers. Once more, advantageous use can be made of the method of particular solutions or the method of complementary functions.

A characteristic of the dual formulation is that the AMP's associated with the gradient phase and the restoration phase of SGRA can be reduced to mathematical programming problems involving a finite number of parameters as unknowns. This leads to particularly efficient versions of the sequential gradient-restoration algorithm (Refs. 22-24).

The principal property of the algorithms presented here is that a sequence of feasible suboptimal solutions is produced. In other words, at the end of each gradient-restoration cycle, the constraints are satisfied to a predetermined accuracy. Therefore, the values of the functional  $I$  corresponding to any two elements of the sequence are comparable.

### 1.4. AEROSPACE APPLICATIONS

Applications of the sequential gradient-restoration algorithm occur in various branches of science, engineering, and economics. With particular regard to aerospace engineering, various problems of atmospheric flight mechanics and suborbital flight mechanics can be solved by means of PSGRA and DSGRA. Generally speaking, PSGRA has proven to be more efficient in problems of suborbital flight mechanics, while DSGRA has proven to be more efficient in problems of atmospheric flight mechanics (Ref. 24).

Part 3 of this paper deals with aircraft trajectories: the application of the dual sequential gradient-restoration algorithm (DSGRA) to the determination of optimal flight trajectories in the presence

of windshear is shown (Refs. 31-60). Both take-off trajectories and abort landing trajectories are discussed. Take-off trajectories are optimized by minimizing the peak deviation of the absolute path inclination from a reference value. Abort landing trajectories are optimized by minimizing the peak drop of altitude from a reference value. The survival capability of an aircraft in a severe windshear is discussed, and the optimal trajectories are found to be superior to both constant pitch trajectories and maximum angle of attack trajectories.

Parts 4 and 5 deal with spacecraft trajectories: the application of the primal sequential gradient-restoration algorithm (PSGRA) to the determination of optimal trajectories for hypervelocity flight is shown (Refs. 61-95). Both coplanar aeroassisted orbital transfer (problem without plane change, Part 4) and noncoplanar aeroassisted orbital transfer (problem with plane change, Part 5) from high Earth orbit (HEO) to low Earth orbit (LEO) are discussed within the frame of three problems: minimization of the total characteristic velocity; minimization of the time integral of the square of the path inclination; and minimization of the peak heating rate. The solution of the second problem is called nearly-grazing solution, and its merits are pointed out as a useful engineering compromise between energy requirements and aerodynamic heating requirements (Refs. 83 and 92).

1.5. REMARK

For spacecraft trajectories, the procedure employed to optimize HEO-to-LEO transfers can be extended to include GEO-to-LEO transfers and LEO-to-LEO transfers (Ref. 92). Here, GEO denotes geosynchronous Earth orbit and LEO denotes low Earth orbit. Note that LEO-to-LEO transfers are of interest for the National Aero-Space Plane (NASP).

To sum up, the sequential gradient-restoration algorithm is a powerful and versatile algorithm for solving optimal trajectory problems of atmospheric flight mechanics, suborbital flight mechanics, and orbital flight mechanics. While the examples provided belong to the extreme regions of the velocity spectrum (low subsonic flight and hypervelocity flight), the sequential gradient-restoration algorithm can handle equally well optimal trajectory problems of supersonic and hypersonic aircraft as well as optimal trajectory problems for vehicles of the space shuttle type and the Hermes type.

## PART 2. SEQUENTIAL GRADIENT-RESTORATION ALGORITHM

### 2.1. OUTLINE

In Part 2, we present the algorithms useful for solving Bolza problems on a digital computer, specifically, sequential gradient-restoration algorithms. Both the primal formulation and the dual formulation are discussed.

Section 2.2 contains the notations, and Section 2.3 presents the Bolza problem of optimal control [Problem (P)]. The sequential gradient-restoration algorithm (SGRA) is introduced in Section 2.4 and is discussed in Section 2.5 (primal formulation, PSGRA) and Section 2.6 (dual formulation, DSGRA). The solution of the linear, two-point boundary-value problem is discussed in Section 2.7 (primal formulation, PSGRA) and Section 2.8 (dual formulation, DSGRA). The determination of the stepsize is discussed in Section 2.9, and a summary of the sequential gradient-restoration algorithm is given in Section 2.10. Primal-dual properties are presented in Section 2.11. Finally, the order of magnitude of the variations produced by SGRA is discussed in Section 2.12.

### 2.2. NOTATIONS

Throughout Part 2, vector-matrix notation is used for conciseness. All vectors are column vectors.

Let  $t$  denote the independent variable, and let  $x(t)$ ,  $u(t)$ ,  $\pi$  denote the dependent variables. The time  $t$  is a scalar; the state  $x(t)$  is an  $n$ -vector; the control  $u(t)$  is an  $m$ -vector; and the parameter  $\pi$  is a  $p$ -vector.

Let  $f(x, u, \pi, t)$  denote a scalar function of the arguments  $x, u, \pi, t$ . The symbol  $f_u$  denotes the  $m$ -vector function whose components are the partial derivatives of the scalar function  $f$  with respect to the components of the vector  $u$ . Analogous definitions hold for the symbols  $f_x$ ,  $f_\pi$ .

Similar definitions are employed for the partial derivatives  $h_x$ ,  $h_\pi$  of the scalar function  $h(x, \pi)$  and the partial derivatives  $g_x$ ,  $g_\pi$  of the scalar function  $g(x, \pi)$ .

Let  $\phi(x, u, \pi, t)$  denote an  $n$ -vector function of the arguments  $x, u, \pi, t$ . The symbol  $\phi_u$  denotes the  $m \times n$  matrix function whose elements are the partial derivatives of the components of the vector function  $\phi$  with respect to the components of the vector  $u$ . Analogous definitions hold for the symbols  $\phi_x$ ,  $\phi_\pi$ .

Similar definitions are employed for the partial derivatives  $\omega_x$ ,  $\omega_\pi$  of the vector function  $\omega(x, \pi)$  and the partial derivatives  $\psi_x$ ,  $\psi_\pi$  of the vector function  $\psi(x, \pi)$ .

The dot sign denotes derivative with respect to the time, that is,  $\dot{x} = dx/dt$ . The symbol  $T$  denotes transposition of vector or matrix. The subscript 0 denotes the initial point, and the subscript 1 denotes the final point.

The symbol  $N(y) = y^T y$  denotes the quadratic norm of a vector  $y$ .

Throughout Part 2, it is assumed that the interval of integration has been normalized to unity, using a suitable transformation. The actual final time  $\tau$ , if it is free, becomes a component of the vector parameter  $\pi$  being optimized.

### 2.3. OPTIMAL CONTROL PROBLEM

Problem (P). We consider the problem of minimizing the functional

$$I = \int_0^1 f(x, u, \pi, t) dt + [h(x, \pi)]_0 + [g(x, \pi)]_1, \quad (1)$$

with respect to the n-vector state  $x(t)$ , the m-vector control  $u(t)$ , and the p-vector parameter  $\pi$  which satisfy the constraints

$$\dot{x} + \phi(x, u, \pi, t) = 0, \quad 0 \leq t \leq 1, \quad (2a)$$

$$[\omega(x, \pi)]_0 = 0, \quad (2b)$$

$$[\psi(x, \pi)]_1 = 0. \quad (2c)$$

In the above equations,  $f$  is a scalar;  $h$  is a scalar;  $g$  is a scalar;  $\phi$  is a n-vector;  $\omega$  is an a-vector,  $a \leq n$ ; and  $\psi$  is a b-vector,  $b \leq n$ . We assume that the first and second derivatives of the functions  $f$ ,  $h$ ,  $g$ ,  $\phi$ ,  $\omega$ ,  $\psi$  with respect to the vectors  $x$ ,  $u$ ,  $\pi$  exist and are continuous. We also assume that the  $n \times a$  matrix  $\omega_x$  has rank  $a$  at initial point, that the  $n \times b$  matrix  $\psi_x$  has rank  $b$  at final point, and that the constrained minimum exists.

From calculus of variations, it is known that Problem (P) is of the Bolza type. It can be recast as that of minimizing the augmented functional

$$J = I + L, \quad (3)$$

subject to (2), where  $L$  denotes the Lagrangian functional

$$L = \int_0^1 \lambda^T (\dot{x} + \phi) dt + (\sigma^T \omega)_0 + (\mu^T \psi)_1. \quad (4)$$

In Eq. (4),  $\lambda(t)$  denotes an n-vector Lagrange multiplier,  $\sigma$  denotes an a-vector Lagrange multiplier, and  $\mu$  denotes a b-vector Lagrange multiplier.

Optimality Conditions. The first-order optimality conditions for Problem (P) take the form

$$\dot{\lambda} - f_x - \phi_x \lambda = 0, \quad 0 \leq t \leq 1, \quad (5a)$$

$$f_u + \phi_u \lambda = 0, \quad 0 \leq t \leq 1, \quad (5b)$$

$$\int_0^1 (f_\pi + \phi_\pi \lambda) dt + (h_\pi + \omega_\pi \sigma)_0 + (g_\pi + \psi_\pi \mu)_1 = 0, \quad (5c)$$

$$(-\lambda + h_x + \omega_x \sigma)_0 = 0, \quad (5d)$$

$$(\lambda + g_x + \psi_x \mu)_1 = 0. \quad (5e)$$

Summarizing, we seek the functions  $x(t)$ ,  $u(t)$ ,  $\pi$  and the multipliers  $\lambda(t)$ ,  $\sigma$ ,  $\mu$  such that the feasibility equations (2) and the optimality conditions (5) are satisfied.

Performance Indexes. The form of Eqs. (2) and (5) suggests that the following scalar performance indexes are useful in computational work:

$$P = \int_0^1 N(\dot{x} + \phi) dt + N(\omega)_0 + N(\psi)_1, \quad (6a)$$

$$\begin{aligned} Q = & \int_0^1 N(\dot{\lambda} - f_x - \phi_x \lambda) dt + \int_0^1 N(f_u + \phi_u \lambda) dt \\ & + N \int_0^1 (f_\pi + \phi_\pi \lambda) dt + (h_\pi + \omega_\pi \sigma)_0 + (g_\pi + \psi_\pi \mu)_1 \\ & + N(-\lambda + h_x + \omega_x \sigma)_0 + N(\lambda + g_x + \psi_x \mu)_1. \end{aligned} \quad (6b)$$

Here,  $P$  denotes the error in the constraints and  $Q$  denotes the error in the optimality conditions.

Convergence Conditions. Numerical convergence can be characterized by the relations

$$P \leq \epsilon_1, \quad (7a)$$

$$Q \leq \epsilon_2, \quad (7b)$$

where  $\epsilon_1, \epsilon_2$  are preselected, small positive numbers.

#### 2.4. SEQUENTIAL GRADIENT-RESTORATION ALGORITHM

The sequential gradient-restoration algorithm (SGRA) is an iterative technique which includes a sequence of two-phase cycles, each cycle including a gradient phase and a restoration phase. This technique is designed to achieve the decrease in the functional  $I$  between the endpoints of each cycle, while the constraints are satisfied to a predetermined accuracy. The two phases of a cycle are called the gradient phase and the restoration phase.

The gradient phase is started only when Ineq. (7a) is satisfied; it involves one iteration and is designed to decrease the value of the augmented functional  $J$ , while the constraints are satisfied to first order.

The restoration phase is started only when Ineq. (7a) is violated; it involves one or more iterations, each designed to decrease the constraint error  $P$ , while the constraints are satisfied to first order and the norm squared of the variations of the control vector, the parameter vector, and the initial state vector is minimized. The restoration phase is terminated whenever Ineq. (7a) is satisfied.

The algorithm as a whole is terminated whenever Ineqs. (7) are both satisfied.

Let  $x(t), u(t), \pi$  denote the nominal functions; let  $\bar{x}(t), \bar{u}(t), \bar{\pi}$  denote the varied functions; and let  $\Delta x(t), \Delta u(t), \Delta \pi$  denote the perturbations of  $x(t), u(t), \pi$  about the nominal values. Assume that the perturbations  $\Delta x(t), \Delta u(t), \Delta \pi$  are linear in the stepsize  $\alpha$ , where  $\alpha > 0$ ; and let  $A(t), B(t), C$  denote the perturbations per unit stepsize. Then, the following relations hold:

$$\bar{x}(t) = x(t) + \Delta x(t) = x(t) + \alpha A(t), \quad (8a)$$

$$\bar{u}(t) = u(t) + \Delta u(t) = u(t) + \alpha B(t), \quad (8b)$$

$$\bar{\pi} = \pi + \Delta \pi = \pi + \alpha C. \quad (8c)$$

Therefore, each iteration of the gradient phase and the restoration phase includes two distinct operations: (i) the determination of the basic functions  $A(t), B(t), C$ ; and (ii) the determination of the stepsize  $\alpha$ .

In the following sections, we describe the gradient phase and the restoration phase of the sequential gradient-restoration algorithm in both the primal formulation and the dual formulation.

#### 2.5. PRIMAL FORMULATION

In the primal formulation, the basic functions  $A(t), B(t), C$  are determined through the formulation of two auxiliary minimization problems, one for the gradient phase and one for the restoration phase.

Gradient Phase: Problem (GP). Minimize the quadratic functional

$$I_{GP} = \int_0^1 (f_x^T A + f_u^T B + f_\pi^T C) dt + (h_x^T A + h_\pi^T C)_0 + (g_x^T A + g_\pi^T C)_1 \\ + (1/2) \left[ \int_0^1 B^T B dt + C^T C + (A^T A)_0 \right], \quad (9)$$

with respect to the vectors  $A(t)$ ,  $B(t)$ ,  $C$  which satisfy the linearized constraints

$$\dot{A} + \phi_X^T A + \phi_U^T B + \phi_\pi^T C = 0, \quad 0 \leq t \leq 1, \quad (10a)$$

$$(\omega_X^T A + \omega_\pi^T C)_0 = 0, \quad (10b)$$

$$(\psi_X^T A + \psi_\pi^T C)_1 = 0. \quad (10c)$$

From calculus of variations, it is known that Problem (GP) is of the Bolza type. It can be recast as that of minimizing the augmented functional

$$J_{GP} = I_{GP} + L_{GP}, \quad (11)$$

subject to (10), where  $L_{GP}$  denotes the Lagrangian functional

$$L_{GP} = \int_0^1 \lambda^T (\dot{A} + \phi_X^T A + \phi_U^T B + \phi_\pi^T C) dt + \sigma^T (\omega_X^T A + \omega_\pi^T C)_0 + \mu^T (\psi_X^T A + \psi_\pi^T C)_1. \quad (12)$$

In Eq. (12),  $\lambda(t)$  denotes an  $n$ -vector Lagrange multiplier,  $\sigma$  an  $a$ -vector Lagrange multiplier, and  $\mu$  a  $b$ -vector Lagrange multiplier.

The first-order optimality conditions for Problem (GP) take the form

$$\dot{\lambda} - f_X - \phi_X \lambda = 0, \quad 0 \leq t \leq 1, \quad (13a)$$

$$f_U + \phi_U \lambda + B = 0, \quad 0 \leq t \leq 1, \quad (13b)$$

$$\int_0^1 (f_\pi + \phi_\pi \lambda) dt + (h_\pi + \omega_\pi \sigma)_0 + (g_\pi + \psi_\pi \mu)_1 + C = 0, \quad (13c)$$

$$(-\lambda + h_X + \omega_X \sigma + A)_0 = 0, \quad (13d)$$

$$(\lambda + g_X + \psi_X \mu)_1 = 0. \quad (13e)$$

Summarizing, we seek the functions  $A(t)$ ,  $B(t)$ ,  $C$  and the multipliers  $\lambda(t)$ ,  $\sigma$ ,  $\mu$  such that the feasibility equations (10) and the optimality conditions (13) are satisfied.

Restoration Phase: Problem (RP). Minimize the quadratic functional

$$I_{RP} = (1/2) \left[ \int_0^1 B^T B dt + C^T C + (A^T A)_0 \right], \quad (14)$$

with respect to the vectors  $A(t)$ ,  $B(t)$ ,  $C$  which satisfy the linearized constraints

$$\dot{A} + \phi_X^T A + \phi_U^T B + \phi_\pi^T C + (\dot{x} + \phi) = 0, \quad 0 \leq t \leq 1, \quad (15a)$$

$$(\omega_X^T A + \omega_\pi^T C + \omega)_0 = 0, \quad (15b)$$

$$(\psi_X^T A + \psi_\pi^T C + \psi)_1 = 0. \quad (15c)$$

From calculus of variations, it is known that Problem (RP) is of the Bolza type. It can be recast as that of minimizing the augmented functional

$$J_{RP} = I_{RP} + L_{RP}, \quad (16)$$

subject to (15), where  $L_{RP}$  denotes the Lagrangian functional

$$L_{RP} = \int_0^1 \lambda^T [\dot{A} + \phi_x^T A + \phi_u^T B + \phi_\pi^T C + (\dot{x} + \phi)] dt + \sigma^T (\omega_x^T A + \omega_\pi^T C + \omega)_0 + \mu^T (\psi_x^T A + \psi_\pi^T C + \psi)_1. \quad (17)$$

In Eq. (17),  $\lambda(t)$  denotes an  $n$ -vector Lagrange multiplier,  $\sigma$  an  $a$ -vector Lagrange multiplier, and  $\mu$  a  $b$ -vector Lagrange multiplier.

The first-order optimality conditions for Problem (RP) take the form

$$\dot{\lambda} - \phi_x \lambda = 0, \quad 0 \leq t \leq 1, \quad (18a)$$

$$\phi_u \lambda + B = 0, \quad 0 \leq t \leq 1, \quad (18b)$$

$$\int_0^1 \phi_\pi \lambda dt + (\omega_\pi \sigma)_0 + (\psi_\pi \mu)_1 + C = 0, \quad (18c)$$

$$(-\lambda + \omega_x \sigma + A)_0 = 0, \quad (18d)$$

$$(\lambda + \psi_x \mu)_1 = 0. \quad (18e)$$

Summarizing, we seek the functions  $A(t)$ ,  $B(t)$ ,  $C$  and the multipliers  $\lambda(t)$ ,  $\sigma$ ,  $\mu$  such that the feasibility equations (15) and the optimality conditions (18) are satisfied.

First Variation Properties. The basic functions  $A(t)$ ,  $B(t)$ ,  $C$  solving Problems (GP) and (RP) are endowed with some first variation properties, shown here without proof. These properties are important, because they dictate the choice of the functions to be considered in the determination of the stepsize.

For the gradient phase, it can be shown that

$$\delta I = \delta J = -\alpha Q, \quad (19a)$$

$$\delta P = 0, \quad (19b)$$

where  $I$  is the functional (1),  $J$  is the augmented functional (3),  $P$  is the constraint error (6a), and  $Q$  is the error in the optimality conditions (6b). Clearly, the decrease of the functionals  $I$  and  $J$  is guaranteed for a gradient stepsize  $\alpha$  sufficiently small.

For the restoration phase, it can be shown that

$$\delta P = -2\alpha P, \quad (20)$$

where  $P$  is the constraint error (6a). Clearly, the decrease of the constraint error  $P$  is guaranteed for a restoration stepsize  $\alpha$  sufficiently small.

## 2.6. DUAL FORMULATION

In the dual formulation, the multipliers  $\lambda(t)$ ,  $\sigma$ ,  $\mu$  are determined through the formulation of two auxiliary minimization problems, one for the gradient phase and one for the restoration phase.

Gradient Phase: Problem (GD). Minimize the quadratic functional

$$I_{GD} = (1/2) \left[ \int_0^1 B^T B dt + C^T C + E^T E \right], \quad (21)$$

with respect to the vectors  $\lambda(t)$ ,  $\sigma$ ,  $\mu$  and  $B(t)$ ,  $C$ ,  $E$  which satisfy the linear constraints

$$\dot{\lambda} - f_x - \phi_x \lambda = 0, \quad 0 \leq t \leq 1, \quad (22a)$$

$$f_u + \phi_u \lambda + B = 0, \quad 0 \leq t \leq 1, \quad (22b)$$

$$\int_0^1 (f_\pi + \phi_\pi \lambda) dt + (h_\pi + \omega_\pi \sigma)_0 + (g_\pi + \psi_\pi \mu)_1 + C = 0, \quad (22c)$$

$$(-\lambda + h_x + \omega_x \sigma)_0 + E = 0, \quad (22d)$$

$$(\lambda + g_x + \psi_x \mu)_1 = 0. \quad (22e)$$

From calculus of variations, it is known that Problem (GD) is of the Bolza type. It can be recast as that of minimizing the augmented functional

$$J_{GD} = I_{GD} + L_{GD}, \quad (23)$$

subject to (22), where  $L_{GD}$  denotes the Lagrangian functional

$$\begin{aligned} L_{GD} = & \int_0^1 A_*^T (\dot{\lambda} - f_x - \phi_x \lambda) dt - \int_0^1 B_*^T (f_u + \phi_u \lambda + B) dt \\ & - C_*^T \left[ \int_0^1 (f_\pi + \phi_\pi \lambda) dt + (h_\pi + \omega_\pi \sigma)_0 + (g_\pi + \psi_\pi \mu)_1 + C \right] \\ & - E_*^T (-\lambda + h_x + \omega_x \sigma)_0 + E] - F_*^T (\lambda + g_x + \psi_x \mu)_1. \end{aligned} \quad (24)$$

In Eq. (24),  $A_*(t)$  denotes an  $n$ -vector Lagrange multiplier,  $B_*(t)$  an  $m$ -vector Lagrange multiplier,  $C_*$  a  $p$ -vector Lagrange multiplier,  $E_*$  an  $n$ -vector Lagrange multiplier, and  $F_*$  an  $n$ -vector Lagrange multiplier.

The first-order optimality conditions for Problem (GD) take the form

$$\dot{A}_* + \phi_x^T A_* + \phi_u^T B_* + \phi_\pi^T C_* = 0, \quad 0 \leq t \leq 1, \quad (25a)$$

$$B - B_* = 0, \quad 0 \leq t \leq 1, \quad (25b)$$

$$(\omega_x^T E_* + \omega_\pi^T C_*)_0 = 0, \quad (25c)$$

$$(\psi_x^T F_* + \psi_\pi^T C_*)_1 = 0, \quad (25d)$$

$$C - C_* = 0, \quad (25e)$$

$$E - E_* = 0, \quad (25f)$$

$$(A_* - E_*)_0 = 0, \quad (25g)$$

$$(A_* - F_*)_1 = 0. \quad (25h)$$

Let the following substitutions be employed:

$$A_*(t) = A(t), \quad 0 \leq t \leq 1, \quad (26a)$$

$$B_*(t) = B(t), \quad 0 \leq t \leq 1, \quad (26b)$$

$$C_* = C, \quad (26c)$$

$$E_* = A(0), \quad (26d)$$

$$F_* = A(1). \quad (26e)$$

Then, one can readily verify that the feasibility equations and the optimality conditions of Problem (GD) reduce to the optimality conditions and the feasibility equations of Problem (GP), respectively. Clearly, after the transformation (26) is applied, the solution of Problem (GD) yields the solution of Problem (GP) and viceversa. This means that the multipliers  $\lambda(t)$ ,  $\sigma$ ,  $\mu$  associated with the gradient phase of SGRA are endowed with a duality property: They also minimize the quadratic functional (21), subject to (22), for given state, control, and parameter.

Restoration Phase: Problem (RD). Minimize the quadratic functional

$$I_{RD} = (1/2) \left[ \int_0^1 B^T B dt + C^T C + E^T E \right] - \left[ \int_0^1 \lambda^T (\dot{x} + \phi) dt + (\sigma^T \omega)_0 + (\mu^T \psi)_1 \right], \quad (27)$$

with respect to the vectors  $\lambda(t)$ ,  $\sigma$ ,  $\mu$  and  $B(t)$ ,  $C$ ,  $E$  which satisfy the linear constraints

$$\dot{\lambda} - \phi_x \lambda = 0, \quad 0 \leq t \leq 1, \quad (28a)$$

$$\phi_u \lambda + B = 0, \quad 0 \leq t \leq 1, \quad (28b)$$

$$\int_0^1 \phi_\pi \lambda dt + (\omega_\pi \sigma)_0 + (\psi_\pi \mu)_1 + C = 0, \quad (28c)$$

$$(-\lambda + \omega_x \sigma)_0 + E = 0, \quad (28d)$$

$$(\lambda + \psi_x \mu)_1 = 0. \quad (28e)$$

From calculus of variations, it is known that Problem (RD) is of the Bolza type. It can be recast as that of minimizing the augmented functional

$$J_{RD} = I_{RD} + L_{RD}, \quad (29)$$

subject to (28), where  $L_{RD}$  denotes the Lagrangian functional

$$\begin{aligned} L_{RD} = & \int_0^1 A_*^T (\dot{\lambda} - \phi_x \lambda) dt - \int_0^1 B_*^T (\phi_u \lambda + B) dt \\ & - C_*^T \left[ \int_0^1 \phi_\pi \lambda dt + (\omega_\pi \sigma)_0 + (\psi_\pi \mu)_1 + C \right] \\ & - E_*^T [(-\lambda + \omega_x \sigma)_0 + E] - F_*^T (\lambda + \psi_x \mu)_1. \end{aligned} \quad (30)$$

In Eq. (30),  $A_*(t)$  denotes an  $n$ -vector Lagrange multiplier,  $B_*(t)$  an  $m$ -vector Lagrange multiplier,  $C_*$  a  $p$ -vector Lagrange multiplier,  $E_*$  an  $n$ -vector Lagrange multiplier, and  $F_*$  an  $n$ -vector Lagrange multiplier.

The first-order optimality conditions for Problem (RD) take the form

$$\dot{A}_* + \phi_x^T A_* + \phi_u^T B_* + \phi_\pi^T C_* + (\dot{\lambda} + \phi) = 0, \quad 0 \leq t \leq 1, \quad (31a)$$

$$B - B_* = 0, \quad 0 \leq t \leq 1, \quad (31b)$$

$$(\omega_x^T E_* + \omega_\pi^T C_* + \omega)_0 = 0, \quad (31c)$$

$$(\psi_x^T F_* + \psi_\pi^T C_* + \psi)_1 = 0, \quad (31d)$$

$$C - C_* = 0, \quad (31e)$$

$$E - E_* = 0, \quad (31f)$$

$$(A_* - E_*)_0 = 0, \quad (31g)$$

$$(A_* - F_*)_1 = 0. \quad (31h)$$

Let the following substitutions be employed:

$$A_*(t) = A(t), \quad 0 \leq t \leq 1, \quad (32a)$$

$$B_*(t) = B(t), \quad 0 \leq t \leq 1, \quad (32b)$$

$$C_* = C, \quad (32c)$$

$$E_* = A(0), \quad (32d)$$

$$F_* = A(1). \quad (32e)$$

Then, one can readily verify that the feasibility equations and the optimality conditions of Problem (RD) reduce to the optimality conditions and the feasibility equations of Problem (RP), respectively. Clearly, after the transformation (32) is applied, the solution of Problem (RD) yields the solution of Problem (RP) and viceversa. This means that the multipliers  $\lambda(t)$ ,  $\sigma$ ,  $\mu$  associated with the restoration phase of SGRA are endowed with a duality property: They also minimize the quadratic functional (27), subject to (28), for given state, control, and parameter.

#### 2.7. LTP-BVP FOR THE PRIMAL FORMULATION

We return to the primal formulation and present a procedure for solving the linear, two-point boundary-value problems (LTP-BVP) associated with both the gradient phase [Eqs. (10) and (13)] and the restoration phase [Eqs. (15) and (18)].

Gradient Phase. We employ a backward-forward integration technique in combination with the method of particular solutions (Refs. 25-28). The technique requires the execution of  $b+1$  independent sweeps of the differential system (10) and (13), each characterized by a different value of the multiplier  $\mu$ . Here,  $b$  denotes the number of final conditions.

The generic sweep is started by assigning particular values to the components of the multiplier  $\mu$ . Then, the multiplier  $\lambda(1)$  is obtained from Eq. (13e). Next, Eq. (13a) is integrated backward to obtain the function  $\lambda(t)$ . With  $\lambda(t)$  known, Eq. (13b) is employed to obtain the function  $B(t)$ . The multiplier  $\sigma$  is obtained from the relation

$$(\omega_x^T \omega_x + \omega_\pi^T \omega_\pi)_0 \sigma + (\omega_\pi^T)_0 \int_0^1 (f_\pi + \phi_\pi \lambda) dt + (h_\pi)_0 + (g_\pi + \psi_\pi \mu)_1 + [\omega_x^T (-\lambda + h_x)]_0 = 0, \quad (33)$$

which arises by combining (10b), (13c), (13d). With  $\sigma$  known, Eq. (13c) is employed to compute  $C$  and Eq. (13d) is employed to compute  $A(0)$ . Then, the function  $A(t)$  is obtained by forward integration of Eq. (10a), subject to the computed values for  $C$  and  $A(0)$ . In this way, the sweep is completed. It leads to satisfaction of all the equations of the system (10) and (13), except Eq. (10c). This is because the values assigned to the components of the multiplier  $\mu$  are arbitrary.

In order to satisfy Eq. (10c), and because the system (10) and (13) is nonhomogeneous,  $b+1$  independent sweeps must be executed employing  $b+1$  different multiplier vectors  $\mu_i$ ,  $i = 1, 2, \dots, b, b+1$ . The first  $b$  sweeps are executed by choosing the vectors  $\mu_1, \mu_2, \dots, \mu_b$  to be the columns of the identity matrix of order  $b$ . The last sweep is executed by choosing  $\mu_{b+1}$  to be the null vector. As a result, one generates the functions and multipliers

$$A_i(t), B_i(t), C_i, \lambda_i(t), \sigma_i, \mu_i, \quad i = 1, 2, \dots, b, b+1. \quad (34)$$

Next, we form the following matrices, each having  $b+1$  columns:

$$\bar{A}(t) = [A_1(t), A_2(t), \dots, A_b(t), A_{b+1}(t)], \quad (35a)$$

$$\bar{B}(t) = [B_1(t), B_2(t), \dots, B_b(t), B_{b+1}(t)], \quad (35b)$$

$$\bar{C} = [C_1, C_2, \dots, C_b, C_{b+1}], \quad (35c)$$

$$\bar{\lambda}(t) = [\lambda_1(t), \lambda_2(t), \dots, \lambda_b(t), \lambda_{b+1}(t)], \quad (35d)$$

$$\bar{\sigma} = [\sigma_1, \sigma_2, \dots, \sigma_b, \sigma_{b+1}], \quad (35e)$$

$$\bar{\mu} = [\mu_1, \mu_2, \dots, \mu_b, \mu_{b+1}]. \quad (35f)$$

Note that  $\bar{\mu} = [I, 0]$ , where  $I$  is the identity matrix of order  $b$  and  $0$  is the null vector of dimension  $b$ . Also, we introduce the vectors

$$k = [k_1, k_2, \dots, k_b, k_{b+1}]^T, \quad (36a)$$

$$u = [1, 1, \dots, 1, 1]^T, \quad (36b)$$

each having  $b+1$  elements.

If the method of particular solutions is employed (Refs. 25-28), the general solution of the system (10) and (13) can be written in the form

$$A(t) = \bar{A}(t)k, \quad B(t) = \bar{B}(t)k, \quad C = \bar{C}k, \quad (37a)$$

$$\lambda(t) = \bar{\lambda}(t)k, \quad \sigma = \bar{\sigma}k, \quad \mu = \bar{\mu}k, \quad (37b)$$

with the following understanding: the components of the vector  $k$  must satisfy the scalar normalization condition

$$u^T k = 1, \quad (38a)$$

as well as the vector relation

$$(\psi_x^T \bar{A} + \psi_n^T \bar{C})_1 k = 0, \quad (38b)$$

which forces the satisfaction of Eq. (10c). Since the system (38) has dimension  $b+1$ , the components of the vector  $k$  can be computed. With  $k$  known, Eqs. (37) yield the solution of the LTP-BVP (10) and (13).

**Restoration Phase.** We employ a backward-forward integration technique in combination with the method of particular solutions (Refs. 25-28). The technique requires the execution of  $b+1$  independent sweeps of the differential system (15) and (18), each characterized by a different value of the

multiplier  $\mu$ . Here,  $b$  denotes the number of final conditions.

The generic sweep is started by assigning particular values to the components of the multiplier  $\mu$ . Then, the multiplier  $\lambda(1)$  is obtained from Eq. (18e). Next, Eq. (18a) is integrated backward to obtain the function  $\lambda(t)$ . With  $\lambda(t)$  known, Eq. (18b) is employed to obtain the function  $B(t)$ . The multiplier  $\sigma$  is obtained from the relation

$$(\omega_x^T \omega_x + \omega_n^T \omega_n) \sigma + (\omega_n^T)_0 \int_0^1 \phi_n \lambda dt + (\psi_n \mu)_1 - (\omega_x^T \lambda + \omega)_0 = 0, \quad (39)$$

which arises by combining (15b), (18c), (18d). With  $\sigma$  known, Eq. (18c) is employed to compute  $C$  and Eq. (18d) is employed to compute  $A(0)$ . Then, the function  $A(t)$  is obtained by forward integration of Eq. (15a), subject to the computed values for  $C$  and  $A(0)$ . In this way, the sweep is completed. It leads to satisfaction of all the equations of the system (15) and (18), except Eq. (15c). This is because the values assigned to the components of the multiplier  $\mu$  are arbitrary.

In order to satisfy Eq. (15c), and because the system (15) and (18) is nonhomogeneous,  $b+1$  independent sweeps must be executed employing  $b+1$  different multiplier vectors  $\mu_i$ ,  $i = 1, 2, \dots, b, b+1$ . The first  $b$  sweeps are executed by choosing the vectors  $\mu_1, \mu_2, \dots, \mu_b$  to be the columns of the identity matrix of order  $b$ . The last sweep is executed by choosing  $\mu_{b+1}$  to be the null vector. As a result, one generates the functions and multipliers

$$A_i(t), B_i(t), C_i, \lambda_i(t), \sigma_i, \mu_i, \quad i = 1, 2, \dots, b, b+1. \quad (40)$$

Next, we form the following matrices, each having  $b+1$  columns:

$$\bar{A}(t) = [A_1(t), A_2(t), \dots, A_b(t), A_{b+1}(t)], \quad (41a)$$

$$\bar{B}(t) = [B_1(t), B_2(t), \dots, B_b(t), B_{b+1}(t)], \quad (41b)$$

$$\bar{C} = [C_1, C_2, \dots, C_b, C_{b+1}], \quad (41c)$$

$$\bar{\lambda}(t) = [\lambda_1(t), \lambda_2(t), \dots, \lambda_b(t), \lambda_{b+1}(t)], \quad (41d)$$

$$\bar{\sigma} = [\sigma_1, \sigma_2, \dots, \sigma_b, \sigma_{b+1}], \quad (41e)$$

$$\bar{\mu} = [\mu_1, \mu_2, \dots, \mu_b, \mu_{b+1}]. \quad (41f)$$

Also, we introduce the vectors

$$k = [k_1, k_2, \dots, k_b, k_{b+1}]^T, \quad (42a)$$

$$u = [1, 1, \dots, 1, 1]^T, \quad (42b)$$

each having  $b+1$  elements.

If the method of particular solutions is employed (Refs. 25-28), the general solution of the system (15) and (18) can be written in the form

$$A(t) = \bar{A}(t)k, \quad B(t) = \bar{B}(t)k, \quad C = \bar{C}k, \quad (43a)$$

$$\lambda(t) = \bar{\lambda}(t)k, \quad \sigma = \bar{\sigma}k, \quad \mu = \bar{\mu}k, \quad (43b)$$

with the following understanding: the components of the vector  $k$  must satisfy the scalar normalization

condition

$$U^T k = 1, \quad (44a)$$

as well as the vector relation

$$(\psi_x^T \tilde{A} + \psi_n^T \tilde{C})_1 k + \psi_1 = 0, \quad (44b)$$

which forces the satisfaction of Eq. (15c). Since the system (44) has dimension  $b+1$ , the components of the vector  $k$  can be computed. With  $k$  known, Eqs. (43) yield the solution of the LTP-BVP (15) and (18).

## 2.8. LTP-BVP FOR THE DUAL FORMULATION

We return to the dual formulation and present a procedure for solving the linear, two-point boundary-value problems (LTP-BVP) associated with both the gradient phase [Eqs. (10) and (22)] and the restoration phase [Eqs. (15) and (28)]. In Section 2.7, these equations were solved directly. Here, these equations are solved indirectly by exploiting the duality properties established in Section 2.6. Indeed, it can be shown that the execution of an iteration of SGRA can be reduced to solving a mathematical programming problem involving a finite number of parameters as unknowns. Hence, the algorithmic efficiency of both the gradient phase and the restoration phase of SGRA can be enhanced.

Gradient Phase. First, we consider Eqs. (22a) and (22e). We observe that, if  $\mu$  is assigned,  $\lambda(1)$  can be computed with (22e) and  $\lambda(t)$  can be computed by backward integration of (22a). Next, we execute  $b+1$  backward integrations, using Eqs. (22a) and (22e) in combination with  $b+1$  different multiplier vectors  $\mu_i$ ,  $i = 1, 2, \dots, b, b+1$ . The first  $b$  integrations are executed by choosing the vectors  $\mu_1, \mu_2, \dots, \mu_b$  to be the columns of the identity matrix of order  $b$ . The last integration is executed by choosing  $\mu_{b+1}$  to be the null vector. As a result, one generates the multipliers

$$\lambda_i(t), \mu_i, \quad i = 1, 2, \dots, b, b+1. \quad (45)$$

Next, we form the following matrices, each having  $b+1$  columns:

$$\tilde{\lambda}(t) = [\lambda_1(t), \lambda_2(t), \dots, \lambda_b(t), \lambda_{b+1}(t)], \quad (46a)$$

$$\tilde{\mu} = [\mu_1, \mu_2, \dots, \mu_b, \mu_{b+1}]. \quad (46b)$$

Once more, we note that  $\tilde{\mu} = [I, 0]$ , where  $I$  is the identity matrix of order  $b$  and  $0$  is the null vector of dimension  $b$ . Also, we introduce the vectors

$$k = [k_1, k_2, \dots, k_b, k_{b+1}]^T, \quad (47a)$$

$$U = [1, 1, \dots, 1, 1]^T, \quad (47b)$$

each having  $b+1$  elements.

If the method of particular solutions is employed (Refs. 25-28), the general solution of Eqs. (22a) and (22e) can be written in the form

$$\lambda(t) = \tilde{\lambda}(t)k, \quad \mu = \tilde{\mu}k, \quad (48)$$

with the following understanding: the components of the vector  $k$  must satisfy the scalar normalization condition

$$U^T k = 1. \quad (49)$$

Next, we combine Eqs. (22b), (22c), (22d) with Eqs. (48) and obtain the relations

$$B = -f_u - \phi_u \tilde{\lambda} k, \quad 0 \leq t \leq 1, \quad (50a)$$

$$C = -\int_0^1 f_{\pi} dt + (h_{\pi})_0 + (g_{\pi})_1 - \int_0^1 \phi_{\pi} \tilde{\lambda} dt + (\psi_{\pi})_1 \tilde{\mu} k - (\omega_{\pi})_0 \sigma, \quad (50b)$$

$$E = -(h_x)_0 + (\tilde{\lambda})_0 k - (\omega_x)_0 \sigma. \quad (50c)$$

These relations show that B(t), C, E depend only on the parameters k,  $\sigma$ .

Finally, upon combining (21) and (50), we obtain the following quadratic function of k,  $\sigma$ :

$$I_{GD} = (1/2)k^T M_1 k + (1/2)\sigma^T M_2 \sigma + k^T M_3 \sigma + N_1^T k + N_2^T \sigma + (1/2)L. \quad (51)$$

Here, the matrices  $M_1$ ,  $M_2$ ,  $M_3$ , the vectors  $N_1$ ,  $N_2$ , and the scalar L are known. They are defined by

$$M_1 = \int_0^1 (\phi_u \tilde{\lambda})^T (\phi_u \tilde{\lambda}) dt + (\tilde{\lambda}^T \tilde{\lambda})_0 + \int_0^1 \phi_{\pi} \tilde{\lambda} dt + (\psi_{\pi})_1 \tilde{\mu} \int_0^1 \phi_{\pi} \tilde{\lambda} dt + (\psi_{\pi})_1 \tilde{\mu}, \quad (52a)$$

$$M_2 = (\omega_x^T \omega_x + \omega_{\pi}^T \omega_{\pi})_0, \quad (52b)$$

$$M_3 = \left[ \int_0^1 \phi_{\pi} \tilde{\lambda} dt + (\psi_{\pi})_1 \tilde{\mu} \right]^T (\omega_{\pi})_0 - (\tilde{\lambda}^T \omega_x)_0, \quad (52c)$$

$$N_1 = \left[ \int_0^1 \phi_{\pi} \tilde{\lambda} dt + (\psi_{\pi})_1 \tilde{\mu} \right]^T \left[ \int_0^1 f_{\pi} dt + (h_{\pi})_0 + (g_{\pi})_1 \right] + \int_0^1 (\phi_u \tilde{\lambda})^T f_u dt - (\tilde{\lambda}^T h_x)_0, \quad (52d)$$

$$N_2 = (\omega_{\pi})_0^T \left[ \int_0^1 f_{\pi} dt + (h_{\pi})_0 + (g_{\pi})_1 \right] + (\omega_x^T h_x)_0, \quad (52e)$$

$$L = \int_0^1 f_{\pi} dt + (h_{\pi})_0 + (g_{\pi})_1 \int_0^1 f_{\pi} dt + (h_{\pi})_0 + (g_{\pi})_1 + \int_0^1 f_u^T f_u dt + (h_x^T h_x)_0. \quad (52f)$$

Because of the duality property, the parameters k,  $\sigma$  can be obtained by minimizing (51), subject to (49). Clearly, this auxiliary minimization problem is a mathematical programming problem.

Let  $\beta$  denote a scalar Lagrange multiplier associated with the constraint (49). Let  $F_{GD}$  denote the augmented function

$$F_{GD} = (1/2)k^T M_1 k + (1/2)\sigma^T M_2 \sigma + k^T M_3 \sigma + N_1^T k + N_2^T \sigma + (1/2)L + \beta(U^T k - 1). \quad (53)$$

With this understanding, the first-order optimality conditions of the auxiliary minimization problem take the form

$$(F_{GD})_k = 0, \quad (F_{GD})_{\sigma} = 0. \quad (54)$$

Hence, the values of k,  $\sigma$ ,  $\beta$  are determined by solving the following linear algebraic system:

$$M_1 k + M_3 \sigma + U \beta + N_1 = 0, \quad (55a)$$

$$M_3^T k + M_2 \sigma + N_2 = 0, \quad (55b)$$

$$U^T k - 1 = 0, \quad (55c)$$

whose dimension is  $a+b+2$ . Once k,  $\sigma$ ,  $\beta$  are known, the multipliers  $\lambda(t)$  and  $\mu$  are determined with Eqs. (48). Then, B(t), C, E are obtained with Eqs. (22b), (22c), (22d). Finally, A(t) is determined by

forward integration of (10a) subject to  $A(0) = E$  and the computed value for  $C$ .

Restoration Phase. First, we consider Eqs. (28a) and (28e). We observe that, if  $\mu$  is assigned,  $\lambda(1)$  can be computed with (28e) and  $\lambda(t)$  can be computed by backward integration of (28a). Next, we execute  $b$  backward integrations, using Eqs. (28a) and (28e) in combination with  $b$  different multiplier vectors  $\mu_i$ ,  $i = 1, 2, \dots, b$ . Specifically, the vectors  $\mu_1, \mu_2, \dots, \mu_b$  are chosen to be the columns of the identity matrix of order  $b$ . As a result, one generates the multipliers

$$\lambda_i(t), \mu_i, \quad i = 1, 2, \dots, b. \quad (56)$$

Next, we form the following matrices, each having  $b$  columns:

$$\tilde{\lambda}(t) = [\lambda_1(t), \lambda_2(t), \dots, \lambda_b(t)], \quad (57a)$$

$$\tilde{\mu} = [\mu_1, \mu_2, \dots, \mu_b]. \quad (57b)$$

We note that  $\tilde{\mu} = I$ , where  $I$  is the identity matrix of order  $b$ . Also, we introduce the vectors

$$k = [k_1, k_2, \dots, k_b]^T, \quad (58a)$$

$$U = [1, 1, \dots, 1], \quad (58b)$$

each having  $b$  elements.

If the method of complementary functions is employed, the general solution of Eqs. (28a) and (28e) can be written in the form

$$\lambda(t) = \tilde{\lambda}(t)k, \quad \mu = \tilde{\mu}k. \quad (59)$$

Next, we combine Eqs. (28b), (28c), (28d) with Eqs. (59) and obtain the relations

$$B = -\phi_U \tilde{\lambda}k, \quad 0 \leq t \leq 1, \quad (60a)$$

$$C = -\left[ \int_0^1 \phi_\pi \tilde{\lambda} dt + (\psi_\pi)_1 \tilde{\mu} \right] k - (\omega_\pi)_0 \sigma, \quad (60b)$$

$$E = (\tilde{\lambda})_0 k - (\omega_x)_0 \sigma. \quad (60c)$$

These relations show that  $B(t)$ ,  $C$ ,  $E$  depend only on the parameters  $k, \sigma$ .

Finally, upon combining (27) and (60), we obtain the following quadratic function of  $k, \sigma$ :

$$I_{RD} = (1/2)k^T M_1 k + (1/2)\sigma^T M_2 \sigma + k^T M_3 \sigma + N_1^T k + N_2^T \sigma. \quad (61)$$

Here, the matrices  $M_1, M_2, M_3$  and the vectors  $N_1, N_2$  are known. They are defined by

$$M_1 = \int_0^1 (\phi_U \tilde{\lambda})^T (\phi_U \tilde{\lambda}) dt + (\tilde{\lambda}^T \tilde{\lambda})_0 + \left[ \int_0^1 \phi_\pi \tilde{\lambda} dt + (\psi_\pi)_1 \tilde{\mu} \right]^T \left[ \int_0^1 \phi_\pi \tilde{\lambda} dt + (\psi_\pi)_1 \tilde{\mu} \right], \quad (62a)$$

$$M_2 = (\omega_x^T \omega_x + \omega_\pi^T \omega_\pi)_0, \quad (62b)$$

$$M_3 = \left[ \int_0^1 \phi_\pi \tilde{\lambda} dt + (\psi_\pi)_1 \tilde{\mu} \right]^T (\omega_\pi)_0 - (\tilde{\lambda}^T \omega_x)_0, \quad (62c)$$

$$N_1 = -\int_0^1 \tilde{\lambda}^T (\tilde{\lambda} + \phi) dt - (\tilde{\mu}^T \psi)_1, \quad (62d)$$

$$N_2 = -(\omega)_0. \quad (62e)$$

Because of the duality property, the parameters  $k$ ,  $\sigma$  can be obtained by minimizing (61). Clearly, this auxiliary minimization problem is a mathematical programming problem, whose first-order optimality conditions take the form

$$(I_{RD})_k = 0, \quad (I_{RD})_\sigma = 0. \quad (63)$$

Hence, the values of  $k$ ,  $\sigma$  are determined by solving the following linear algebraic system:

$$M_1 k + M_3 \sigma + N_1 = 0, \quad (64a)$$

$$M_3 k + M_2 \sigma + N_2 = 0, \quad (64b)$$

whose dimension is  $a+b$ . Once  $k$ ,  $\sigma$  are known, the multipliers  $\lambda(t)$  and  $\mu$  are determined with Eqs. (59). Then,  $B(t)$ ,  $C$ ,  $E$  are obtained with Eqs. (28b), (28c), (28d). Finally,  $A(t)$  is determined by forward integration of (15a), subject to  $A(0) = E$  and the computed value for  $C$ .

#### 2.9. STEPSIZE DETERMINATION

The procedure for determining the basic functions  $A(t)$ ,  $B(t)$ ,  $C$  is different, depending on whether the primal formulation or the dual formulation is employed. However, the basic functions  $A(t)$ ,  $B(t)$ ,  $C$  are the same, regardless of whether the primal formulation or the dual formulation is used. Hence, the rules for the determination of the stepsize are common to both the primal formulation and the dual formulation.

Gradient Stepsize. With the functions  $A(t)$ ,  $B(t)$ ,  $C$  known, the one-parameter family of varied functions (8) can be formed. For this family, the functionals  $I$ ,  $J$ ,  $P$  take the following form:

$$\tilde{I} = \tilde{I}(\alpha), \quad \tilde{J} = \tilde{J}(\alpha), \quad \tilde{P} = \tilde{P}(\alpha). \quad (65)$$

Then, the gradient stepsize  $\alpha$  is computed by a one-dimensional search on the function  $\tilde{J}(\alpha)$  until the following relations are satisfied:

$$\tilde{J}(\alpha) < \tilde{J}(0), \quad (66a)$$

$$\tilde{P}(\alpha) \leq P_*, \quad (66b)$$

where  $P_*$  is a preselected number, not necessarily small.

The simplest way of ensuring satisfaction of (66) is to employ a bisection process, starting from the reference stepsize  $\alpha = \alpha_0$ . In turn, the reference stepsize  $\alpha_0$  can be obtained by the combination of a scanning process and a cubic interpolation process. With the scanning process, one brackets the minimum point of the function  $\tilde{J}(\alpha)$ . With the cubic interpolation process, either single-step or multi-step, one obtains an approximation to the reference stepsize  $\alpha_0$ . This is the stepsize which yields the minimum of the cubic approximation to  $\tilde{J}(\alpha)$ .

The details of the one-dimensional search can be found in Refs. 15-24 and related publications. They are omitted here, for the sake of brevity.

Restoration Stepsize. With the functions  $A(t)$ ,  $B(t)$ ,  $C$  known, the one-parameter family of varied functions (8) can be formed. For this family, the functional  $P$  takes the following form:

$$\tilde{P} = \tilde{P}(\alpha). \quad (67)$$

Then, the restoration stepsize  $\alpha$  is computed by a one-dimensional search on the function (67) until the following relation is satisfied:

$$\tilde{P}(\alpha) < \tilde{P}(0). \quad (68)$$

The simplest way of ensuring satisfaction of (68) is to employ a bisection process, starting from the reference stepsize  $\alpha = \alpha_0$ . Here, the correct reference stepsize is  $\alpha_0 = 1$ , in that it yields one-step restoration if the constraints (2) are linear.

#### 2.10. SUMMARY OF THE SEQUENTIAL GRADIENT-RESTORATION ALGORITHM

The sequential-gradient restoration algorithm involves a sequence of two-phase cycles, each cycle including a gradient phase and a restoration phase. In a complete gradient-restoration cycle, the value of the functional is decreased, while the constraints are satisfied to a predetermined accuracy; in the gradient phase, the value of the augmented functional is decreased, while avoiding excessive constraint violation; in the restoration phase, the constraint error is decreased, while avoiding excessive change in the value of the functional.

It must be noted that, while the gradient phase involves a single iteration, the restoration phase might involve several iterations. The decision of whether to execute a gradient iteration or a restorative iteration is based on the measurement of a single scalar quantity, the constraint error  $P$ , given by Eq. (6a). If the constraint error satisfies Ineq. (7a), a gradient iteration is executed; if the constraint error violates Ineq. (7a), a restorative iteration is executed.

For both gradient iterations and restorative iterations, the following terminology is employed:  $x(t)$ ,  $u(t)$ ,  $\pi$  denote the nominal functions;  $\bar{x}(t)$ ,  $\bar{u}(t)$ ,  $\bar{\pi}$  denote the varied functions;  $\Delta x(t)$ ,  $\Delta u(t)$ ,  $\Delta \pi$  denote the perturbations leading from the nominal functions to the varied functions; and  $A(t)$ ,  $B(t)$ ,  $C$  denote the perturbations per unit stepsize  $\alpha$ . Then, the following relations hold:

$$\bar{x}(t) = x(t) + \Delta x(t) = x(t) + \alpha A(t), \quad (69a)$$

$$\bar{u}(t) = u(t) + \Delta u(t) = u(t) + \alpha B(t), \quad (69b)$$

$$\bar{\pi} = \pi + \Delta \pi = \pi + \alpha C. \quad (69c)$$

Thus, each iteration involves two distinct operations: (i) the determination of the basic functions  $A(t)$ ,  $B(t)$ ,  $C$ ; and (ii) the determination of the stepsize  $\alpha$ .

Depending on whether the primal formulation is used or the dual formulation is used, one obtains a primal sequential gradient-restoration algorithm (PSGRA) or a dual sequential gradient-restoration algorithm (DSGRA).

**Gradient Iteration.** Its objective is to reduce the augmented functional  $J$ , while the constraints are satisfied to first order.

**Step 1.** Assume nominal functions  $x(t)$ ,  $u(t)$ ,  $\pi$  which satisfy the constraints (2) within the predetermined accuracy (7a).

**Step 2.** For the nominal functions, compute the basic functions  $A(t)$ ,  $B(t)$ ,  $C$  using either the procedure of Sections 2.5 and 2.7 (primal formulation) or the procedure of Sections 2.6 and 2.8 (dual formulation).

Step 3. With the functions  $A(t)$ ,  $B(t)$ ,  $C$  known, determine the gradient stepsize  $\alpha$  with the procedure of Section 2.9.

Step 4. Once the gradient stepsize  $\alpha$  is known, compute the varied functions  $\bar{x}(t)$ ,  $\bar{u}(t)$ ,  $\bar{\pi}$  with Eqs. (69). In this way, the gradient iteration is completed.

Restorative Iteration. Its objective is to reduce the constraint error  $P$ , while the constraints are satisfied to first order and the norm squared of the variations of the control vector, the parameter vector, and the initial state vector is minimized.

Step 1. Assume nominal functions  $x(t)$ ,  $u(t)$ ,  $\pi$  which violate at least one of the constraints (2).

Step 2. For the nominal functions, compute the basic functions  $A(t)$ ,  $B(t)$ ,  $C$  using either the procedure of Sections 2.5 and 2.7 (primal formulation) or the procedure of Sections 2.6 and 2.8 (dual formulation).

Step 3. With the functions  $A(t)$ ,  $B(t)$ ,  $C$  known, determine the restoration stepsize  $\alpha$  with the procedure of Section 2.9.

Step 4. Once the restoration stepsize  $\alpha$  is known, compute the varied functions  $\bar{x}(t)$ ,  $\bar{u}(t)$ ,  $\bar{\pi}$  with Eqs. (69). In this way, the restorative iteration is completed.

Gradient Phase. The gradient phase includes a single gradient iteration. Hence, the gradient phase is the same as the gradient iteration discussed previously.

Restoration Phase. The restoration phase might include several restorative iterations. In each restorative iteration, the constraint error is reduced in accordance with Ineq. (68). The restoration phase is terminated whenever the constraint error reaches a level compatible with Ineq. (7a).

Gradient-Restoration Cycle. As stated before, a complete gradient-restoration cycle includes a gradient phase and a restoration phase. After a restoration phase is completed, one must verify whether the following inequality is satisfied:

$$I < \hat{I}; \quad (70)$$

here,  $I$  denotes the value of the functional (1) at the end of the present restoration phase and  $\hat{I}$  denotes the value of the functional (1) at the end of the previous restoration phase. If Ineq. (70) is satisfied, one starts the next cycle of the sequential gradient-restoration algorithm. If Ineq. (70) is violated, one returns to the previous gradient phase and reduces the gradient stepsize (using a bisection process) until, after restoration, the functional  $I$  finally decreases.

Starting Condition. The present algorithm can be started with nominal functions  $x(t)$ ,  $u(t)$ ,  $\pi$  which either violate the constraints (2) or satisfy the constraints (2). If the nominal functions violate Ineq. (7a), the algorithm starts with a restoration phase; hence, the first cycle is a half cycle involving only a restoration phase. If the nominal functions satisfy Ineq. (7a), the algorithm starts with a gradient phase; hence, the first cycle is a complete cycle, involving both a gradient phase and a restoration phase.

Stopping Conditions. The present algorithm is terminated whenever Ineqs. (7a) and (7b) are satisfied simultaneously. Note that Ineq. (7a) is verified at the end of a restoration phase/beginning of a gradient phase. On the other hand, Ineq. (7b) must be verified at the beginning of a gradient phase, after the multipliers  $\lambda(t)$ ,  $\sigma$ ,  $\mu$  are computed and before the search for the gradient stepsize is executed.

## 2.11. PRIMAL-DUAL PROPERTIES

Some simple relations hold between the values of the functionals associated with the primal formulation and the values of the functionals associated with the dual formulation. These relations are stated below without proof.

For the gradient phase, the functionals  $I_{GP}$  and  $I_{GD}$ , associated with Problems (GP) and (GD), satisfy the relation

$$I_{GP} + I_{GD} = 0. \quad (71)$$

For the restoration phase, the functionals  $I_{RP}$  and  $I_{RD}$ , associated with Problems (RP) and (RD), satisfy the relation

$$I_{RP} + I_{RD} = 0. \quad (72)$$

## 2.12. REMARK

For a complete gradient-restoration cycle, the satisfaction of Ineq. (70) is guaranteed by the different order of magnitude of the variations of the gradient phase and those of the restoration phase. If  $\alpha_G$  is the gradient stepsize and  $\alpha_R$  is the restoration stepsize, it can be shown that the variations of the gradient phase are of  $O(\alpha_G)$ , while those of the restoration phase are of  $O(\alpha_R \alpha_G^2)$ . Hence, if the gradient stepsize  $\alpha_G$  is sufficiently small, the restorative corrections are negligible by comparison with the gradient corrections. This means that the descent property for the gradient phase implies a descent property for a complete gradient-restoration cycle.

## PART 3. OPTIMAL AIRCRAFT TRAJECTORIES FOR WINDSHEAR FLIGHT

## 3.1. OUTLINE

In Part 3, we present the application of the dual sequential gradient-restoration algorithm (DSGRA) to the determination of optimal flight trajectories in the presence of windshear. Both take-off trajectories and abort landing trajectories are discussed.

Section 3.2 contains the notations, and Section 3.3 contains some general considerations relative to flight in a windshear. The equations of motion are given in Section 3.4, and the system description is given in Section 3.5.

Optimal trajectories are discussed in Section 3.6 for the take-off problem and in Section 3.7 for the abort landing problem. A comparison between the optimal trajectories, the constant pitch trajectories, and the maximum angle of attack trajectories is presented in Section 3.8. Finally, the survival capability of an aircraft in a severe windshear is discussed in Section 3.9.

## 3.2. NOTATIONS

Throughout Part 3, the British engineering system is employed [the basic units are the foot, the pound (weight), and the second]. The following scalar notations are employed:

$C_D$ = drag coefficient;	$\alpha$ = relative angle of attack (wing), rad;
$C_L$ = lift coefficient;	$\alpha_e$ = absolute angle of attack (wing), rad;
$D$ = drag force, lb;	$\beta$ = engine power setting;
$g$ = acceleration of gravity, $\text{ft sec}^{-2}$ ;	$\gamma$ = relative path inclination, rad;
$h$ = altitude, ft;	$\gamma_e$ = absolute path inclination, rad;
$L$ = lift force, lb;	$\delta$ = thrust inclination, rad;
$m$ = mass, $\text{lb ft}^{-1} \text{sec}^2$ ;	$\theta$ = pitch attitude angle (wing), rad;
$S$ = reference surface, $\text{ft}^2$ ;	$\lambda$ = wind intensity parameter;
$t$ = time, sec;	$\rho$ = air density, $\text{lb ft}^{-4} \text{sec}^2$ ;
$T$ = thrust force, lb;	$\tau$ = final time, sec;
$V$ = relative velocity, $\text{ft sec}^{-1}$ ;	ARL = aircraft reference line;
$V_e$ = absolute velocity, $\text{ft sec}^{-1}$ ;	CPT = constant pitch trajectory;
$W$ = $mg$ = weight, lb;	LAC = landing configuration;
$W_h$ = h-component of wind velocity, $\text{ft sec}^{-1}$ ;	MAAT = maximum angle of attack trajectory;
$W_x$ = x-component of wind velocity, $\text{ft sec}^{-1}$ ;	OT = optimal trajectory;
$x$ = horizontal distance, ft;	TOC = take-off configuration.

## 3.3. FLIGHT IN A WINDSHEAR

Low-altitude windshear is a threat to the safety of aircraft in take-off or landing (Refs. 31-60). Over the past 20 years, some 30 aircraft accidents have been attributed to windshear. The most notorious ones are the crash of PANAM Flight 759 on July 9, 1982 at New Orleans International Airport (Boeing B-727 in take-off, Ref. 33) and the crash of Delta Airlines Flight 191 on August 2, 1985 at Dallas-Fort Worth International Airport (Lockheed L-1011 in landing, Refs. 39-40).

Low-altitude windshear is usually associated with a severe meteorological phenomenon, called the downburst (Fig. 1). In turn, a downburst involves a descending column of air, which then spreads horizontally in the neighborhood of the ground. This condition is hazardous, because an aircraft in take-off or landing might encounter a headwind coupled with a downdraft, followed by a tailwind coupled

with a downdraft. The transition from headwind to tailwind engenders a transport acceleration, and hence a windshear inertia force (the product of the transport acceleration and the mass of the aircraft). In turn, the windshear inertia force can be as large as the drag of the aircraft, and in some cases as large as the thrust of engines. Hence, an inadvertent encounter with a low-altitude windshear can be a serious problem for even a skilled pilot.

If the windshear can be predicted, the best way to deal with the problem is avoidance. Both the take-off and the landing should be delayed until the weather conditions improve. However, because windshear exists only for a short time and it happens locally and randomly, sometimes avoidance is not possible and an inadvertent encounter takes place.

Research on optimal trajectories is important for developing guidance schemes and piloting strategies for flight in a windshear. However, optimal trajectories are difficult to implement, for the following reasons: (i) for the computation of optimal trajectories, global information on the wind field is required, while global measurements are not available in today's technique; (ii) the rapid computation of optimal trajectories is beyond present onboard computer capability. Although the optimal trajectories are not implementable, they provide criteria for developing guidance trajectories which approximate the optimal trajectories. Thus, the windshear performance of an optimal trajectory sets up a benchmark; with this benchmark, the relative merits of different guidance schemes and piloting strategies can be evaluated.

#### 3.4. EQUATIONS OF MOTION

We make use of the relative wind-axes system (Fig. 2) in connection with the following assumptions: (a) the aircraft is a particle of constant mass; (b) flight takes place in a vertical plane; (c) Newton's law is valid in an Earth-fixed system; and (d) the wind flow field is steady.

With above premises, the equations of motion include the kinematical equations

$$\dot{x} = V \cos \gamma + W_x, \quad (73a)$$

$$\dot{h} = V \sin \gamma + W_h, \quad (73b)$$

and the dynamical equations

$$\dot{V} = (T/m) \cos(\alpha + \delta) - D/m - g \sin \gamma - (\dot{W}_x \cos \gamma + \dot{W}_h \sin \gamma), \quad (74a)$$

$$\dot{\gamma} = (T/mV) \sin(\alpha + \delta) + L/mV - (g/V) \cos \gamma + (1/V)(\dot{W}_x \sin \gamma - \dot{W}_h \cos \gamma). \quad (74b)$$

Because of assumption (d), the total derivatives of the wind velocity components and the corresponding partial derivatives satisfy the relations

$$\dot{W}_x = (\partial W_x / \partial x)(V \cos \gamma + W_x) + (\partial W_x / \partial h)(V \sin \gamma + W_h), \quad (75a)$$

$$\dot{W}_h = (\partial W_h / \partial x)(V \cos \gamma + W_x) + (\partial W_h / \partial h)(V \sin \gamma + W_h). \quad (75b)$$

These relations must be supplemented by the functional relations

$$T = T(h, V, \beta), \quad (76a)$$

$$D = D(h, V, \alpha), \quad (76b)$$

$$L = L(h, V, \alpha), \quad (76c)$$

$$W_x = W_x(x, h), \quad (76d)$$

$$W_h = W_h(x, h), \quad (76e)$$

and by the analytical relations

$$\gamma_e = \arctan[(V \sin \gamma + W_h)/(V \cos \gamma + W_x)], \quad (77a)$$

$$\theta = \alpha + \gamma. \quad (77b)$$

For a given value of the thrust inclination  $\delta$ , the differential system (73)-(76) involves four state variables [the horizontal distance  $x(t)$ , the altitude  $h(t)$ , the velocity  $V(t)$ , and the relative path inclination  $\gamma(t)$ ] and two control variables [the angle of attack  $\alpha(t)$  and the power setting  $\beta(t)$ ]. However, the number of control variables reduces to one (the angle of attack), if the power setting is specified in advance. The quantities defined by the analytical relations (77) can be computed a posteriori, once the values of the state and the control are known.

Angle of Attack Bounds. The angle of attack  $\alpha$  and its time derivative  $\dot{\alpha}$  are subject to the inequalities

$$\alpha \leq \alpha_*, \quad (78a)$$

$$-\dot{\alpha}_* \leq \dot{\alpha} \leq \dot{\alpha}_*, \quad (78b)$$

where  $\alpha_*$  is a prescribed upper bound and  $\dot{\alpha}_*$  is a prescribed, positive constant.

Ineqs. (78) are enforced indirectly via the following transformation technique:

$$\alpha = \alpha_* - u^2, \quad (79a)$$

$$\dot{u} = -(\dot{\alpha}_*/2u) \sin w, \quad |u| \geq \epsilon, \quad (79b)$$

$$\dot{u} = -(\dot{\alpha}_*/2u) \sin^2(\pi u/2\epsilon) \sin w, \quad |u| \leq \epsilon. \quad (79c)$$

Here,  $u(t)$ ,  $w(t)$  are auxiliary variables and  $\epsilon$  is a small, positive constant, which is introduced to prevent the occurrence of boundary singularities. Note that the right-hand sides of Eqs. (79b)-(79c) are continuous and have continuous first derivatives at  $|u| = \epsilon$ . Clearly, when using Eqs. (79) in conjunction with Eqs. (73)-(76), one must regard  $\alpha(t)$ ,  $u(t)$  as state variables and  $w(t)$  as control variable.

### 3.5. SYSTEM DESCRIPTION

In this section, we supply an analytical specification of the system functions (76).

Thrust. The thrust  $T$  is written in the form

$$T = \beta T_*, \quad (80a)$$

$$T_* = A_0 + A_1 V + A_2 V^2, \quad (80b)$$

where  $\beta$  is the power setting and  $T_*$  is a reference thrust, specifically, the thrust corresponding to the power setting  $\beta = 1$ .

In the take-off problem (Section 3.6), it is assumed that maximum power setting is employed, that is,

$$\beta = 1. \quad (81)$$

In the abort landing problem (Section 3.7), it is assumed that the power setting is increased at a constant time rate until maximum power setting is reached; afterward, the power setting is held constant. This yields the relations

$$\beta = \beta_0 + \dot{\beta}_0 t, \quad 0 \leq t \leq \sigma, \quad (82a)$$

$$\beta = 1, \quad \sigma \leq t \leq \tau. \quad (82b)$$

Here,  $\beta_0$  is the initial power setting,  $\dot{\beta}_0$  is the constant rate of increase of the power setting,  $\sigma = (1 - \beta_0)/\dot{\beta}_0$  is the time at which maximum power setting is reached, and  $\tau$  is the final time.

Drag. The drag  $D$  is written in the form

$$D = (1/2)C_D \rho S V^2, \quad (83a)$$

$$C_D = B_0 + B_1 \alpha + B_2 \alpha^2, \quad \alpha \leq \alpha_*, \quad (83b)$$

where  $\rho$  is the air density (assumed constant),  $S$  is a reference surface,  $V$  is the relative velocity, and  $C_D$  is the drag coefficient.

Lift. The lift  $L$  is written in the form

$$L = (1/2)C_L \rho S V^2, \quad (84a)$$

$$C_L = C_0 + C_1 \alpha, \quad \alpha \leq \alpha_{**}, \quad (84b)$$

$$C_L = C_0 + C_1 \alpha + C_2 (\alpha - \alpha_{**})^2, \quad \alpha_{**} \leq \alpha \leq \alpha_*, \quad (84c)$$

where  $\rho$  is the air density (assumed constant),  $S$  is a reference surface,  $V$  is the relative velocity, and  $C_L$  is the lift coefficient.

Weight. The mass  $m$  of the aircraft is regarded to be constant. Hence, the weight

$$W = mg \quad (85)$$

is regarded to be constant.

Aircraft Data. The numerical examples of the subsequent sections refer to a Boeing B-727 aircraft powered by three JT8D-17 turbofan engines. It is assumed that the runway is located at sea-level altitude and that the ambient temperature is 100 deg F.

Two different configurations are considered, a take-off configuration (TOC) and a landing configuration (LAC). For the TOC, it is assumed that the gear is up, the flap setting is  $\delta_F = 15$  deg, and the weight is  $W = 180,000$  lb. For the LAC, it is assumed that the gear is down, the flap setting is  $\delta_F = 30$  deg, and the weight is  $W = 150,000$  lb.

Figure 3 shows the thrust function  $T_*(V)$ ; Fig. 4 shows the drag coefficient function  $C_D(\alpha)$  for both the take-off configuration and the landing configuration; and Fig. 5 shows the lift coefficient function  $C_L(\alpha)$  for both the take-off configuration and the landing configuration.

Wind Model. In this paper, the following particular wind model is assumed:

$$W_x = \lambda A(x), \quad (86a)$$

$$W_h = \lambda(h/h_*)B(x), \quad (86b)$$

with

$$\lambda = \Delta W_x / \Delta W_{x*}, \quad (86c)$$

The function  $A(x)$  represents the distribution of the horizontal wind versus the horizontal distance (Fig. 6); the function  $B(x)$  represents the distribution of the vertical wind versus the horizontal distance (Fig. 6); the parameter  $\lambda$  characterizes the intensity of the shear/downdraft combination;  $\Delta W_x$  is the horizontal wind velocity difference (maximum tailwind minus maximum headwind);  $\Delta W_{x*} = 100 \text{ ft sec}^{-1}$  is a reference value for the horizontal wind velocity difference; and  $h_* = 1000 \text{ ft}$  is a reference value for the altitude.

The one-parameter family of wind models (86) has the following properties: (a) it represents the transition from a uniform headwind to a uniform tailwind, with nearly constant shear in the core of the downburst; (b) the downdraft achieves maximum negative value at the center of the downburst; (c) the downdraft vanishes at  $h = 0$ ; and (d) the functions  $W_x$ ,  $W_h$  nearly satisfy the continuity equation and the irrotationality condition in the core of the downburst.

Decreasing values of  $\lambda$  (hence, decreasing values of  $\Delta W_x$ ) correspond to milder windshears; conversely, increasing values of  $\lambda$  (hence, increasing values of  $\Delta W_x$ ) correspond to more severe windshears. If one excludes the 1983 windshear episode at Andrews AFB, the highest value of  $\lambda$  ever recorded is  $\lambda = 1.40$ , corresponding to  $\Delta W_x = 140 \text{ ft sec}^{-1}$ . Hence, values of  $\lambda$  in the following range are considered:

$$0.8 \leq \lambda \leq 1.4, \quad (87a)$$

corresponding to values of  $\Delta W_x$  in the following range:

$$80 \leq \Delta W_x \leq 140 \text{ ft sec}^{-1}. \quad (87b)$$

### 3.6. TAKE-OFF PROBLEM

For the take-off problem, we assume that: (i) maximum power setting is employed; hence, the only control is the angle of attack; (ii) the constraints (73)-(79) must be satisfied; (iii) the initial conditions are given; and (iv) at the final point, gamma recovery is required, that is,

$$\gamma_\tau = \gamma_0 = \gamma_{*}, \quad (88)$$

where  $\gamma_*$  is the path inclination for quasi-steady steepest climb (TOC).

The performance index being minimized is the peak value of the modulus of the difference between the absolute path inclination and a reference value,

$$I = \max_t |\gamma_e - \gamma_{eR}|, \quad 0 \leq t \leq \tau; \quad (89)$$

here,  $\gamma_e$  is given by Eq. (77a) and  $\gamma_{eR} = \gamma_{e0}$  is a reference value.

This is a minimax problem or Chebyshev problem of optimal control. It can be reformulated as a Bolza problem of optimal control, in which one minimizes the integral performance index (Ref. 29)

$$J = \int_0^T (\gamma_e - \gamma_{eR})^q dt, \quad (90)$$

for large values of the positive, even exponent  $q$ .

Numerical Data. The computations presented here refer to the Boeing B-727 aircraft powered by three JT8D-17 turbofan engines. It is assumed that: the runway is located at sea-level altitude; the ambient temperature is 100 deg F; the gear is up; the flap setting is  $\delta_F = 15$  deg; the take-off weight is  $W = 180,000$  lb.

The inequality constraints (78) on the angle of attack are enforced with

$$\alpha_* = 16.0 \text{ deg}, \quad (91a)$$

$$\dot{\alpha}_* = 3.0 \text{ deg sec}^{-1} \quad (91b)$$

The following conditions are assumed at the initial point:

$$x_0 = 0 \text{ ft}, \quad (92a)$$

$$h_0 = 50 \text{ ft}, \quad (92b)$$

$$V_0 = 164 \text{ knots} = 276.8 \text{ ft sec}^{-1}, \quad (92c)$$

$$\gamma_0 = 6.989 \text{ deg}, \quad (92d)$$

and at the final point:

$$\gamma_\tau = 6.989 \text{ deg}; \quad (93a)$$

the final time is assumed to be

$$\tau = 40 \text{ sec}. \quad (93b)$$

For the windshear model assumed, this time is about twice the duration of the windshear encounter ( $\Delta t = 18$  sec).

Numerical Results. Numerical results were obtained using the dual sequential gradient-restoration algorithm (DSGRA) of Part 2. They are shown in Fig. 7, which contains three parts: the altitude  $h$  versus the time  $t$  (Fig. 7A); the velocity  $V$  versus the time  $t$  (Fig. 7B); and the angle of attack  $\alpha$  versus the time  $t$  (Fig. 7C). From Fig. 7, the following comments arise:

(a) the path inclination of the optimal trajectory decreases as the windshear intensity increases; for a severe windshear,  $\Delta W_x = 110 \text{ ft sec}^{-1}$ , the optimal trajectory is nearly horizontal in the shear region; in the aftershear region, the optimal trajectory ascends;

(b) the velocity decreases in the shear region and increases in the aftershear region; the point of minimum velocity occurs at the end of the shear; the value of the minimum velocity is nearly independent of the windshear intensity;

(c) the angle of attack exhibits an initial decrease, followed by a gradual, sustained increase; the maximum value of the angle of attack is reached at about the end of the shear; then, the angle of attack decreases gradually in the aftershear region.

## 3.7. ABORT LANDING PROBLEM

For the abort landing problem, we assume that: (i) maximum power setting is employed; namely, the power setting is increased to the maximum value at a constant time rate; afterward, the maximum value is maintained; hence, the only control is the angle of attack; (ii) the constraints (73)-(79) must be satisfied; (iii) the initial conditions are given; and (iv) at the final point, gamma recovery is required, that is,

$$\gamma_\tau = \gamma_{*} \quad (94)$$

where  $\gamma_{*}$  is the path inclination for quasi-steady steepest climb (LAC).

The performance index being minimized is the peak value of the modulus of the difference between the instantaneous altitude and a reference value,

$$I = \max_t |h_R - h|, \quad 0 \leq t \leq \tau; \quad (95)$$

here,  $h_R = h_{*} = 1000$  ft is a constant reference value.

This is a minimax problem or Chebyshev problem of optimal control. It can be reformulated as a Bolza problem of optimal control, in which one minimizes the integral performance index (Ref. 29)

$$J = \int_0^\tau (h_R - h)^q dt, \quad (96)$$

for large values of the positive, even exponent  $q$ .

Numerical Data. The computations presented here refer to the Boeing B-727 aircraft powered by three JT8D-17 turbofan engines. It is assumed that: the runway is located at sea-level altitude; the ambient temperature is 100 deg F; the gear is down; the flap setting is  $\delta_f = 30$  deg; the landing weight is  $W = 150,000$  lb.

The inequality constraints (78) on the angle of attack are enforced with

$$\alpha_{*} = 17.2 \text{ deg}, \quad (97a)$$

$$\dot{\alpha}_{*} = 3.0 \text{ deg sec}^{-1}. \quad (97b)$$

The following conditions are assumed at the initial point:

$$x_0 = 0 \text{ ft}, \quad (98a)$$

$$h_0 = 600 \text{ ft}, \quad (98b)$$

$$V_0 = 142 \text{ knots} = 239.7 \text{ ft sec}^{-1}, \quad (98c)$$

$$\gamma_{e0} = -3.0 \text{ deg}, \quad (98d)$$

and at the final point:

$$\gamma_\tau = 7.431 \text{ deg}; \quad (99a)$$

the final time is assumed to be

$$\tau = 40 \text{ sec}. \quad (99b)$$

For the windshear model assumed, this time is about twice the duration of the windshear encounter ( $\Delta t = 22$  sec).

Numerical Results. Numerical results were obtained using the dual sequential gradient-restoration algorithm (DSGRA) of Part 2. They are shown in Fig. 8, which contains three parts: the altitude  $h$  versus the time  $t$  (Fig. 8A); the velocity  $V$  versus the time  $t$  (Fig. 8B); and the angle of attack  $\alpha$  versus the time  $t$  (Fig. 8C). From Fig. 8, the following comments arise:

(a) the optimal trajectory includes three branches: a descending flight branch, followed by a nearly horizontal flight branch, followed by an ascending flight branch after the aircraft has passed through the shear region; the maximum altitude drop increases with the windshear intensity and the initial altitude;

(b) the velocity decreases in the shear region and increases in the aftershear region; the point of minimum velocity occurs at the end of the shear; the value of the minimum velocity is nearly independent of the windshear intensity;

(c) the angle of attack exhibits an initial decrease, followed by a gradual, sustained increase; the maximum value of the angle of attack is reached at about the end of the shear; then, the angle of attack decreases gradually in the aftershear region.

### 3.8. COMPARISON OF TRAJECTORIES

In this section, we compare three trajectories: the optimal trajectory (OT), the constant pitch trajectory (CPT), and the maximum angle of attack trajectory (MAAT). The comparison is done for both the take-off problem and the abort landing problem.

For the take-off problem, the comparison is shown in Fig. 9 for the windshear intensity  $\Delta W_x = 100$  ft sec<sup>-1</sup>. Clearly, the OT exhibits a monotonic climb behavior, while the CPT nearly touches the ground, and the MAAT crashes.

For the abort landing problem, the comparison is shown in Fig. 10 for the windshear intensity  $\Delta W_x = 120$  ft sec<sup>-1</sup>. Clearly, the minimum altitude of the OT is higher than the minimum altitude of the CPT, which in turn is higher than the minimum altitude of the MAAT. While both the OT and the CPT avoid the ground, the MAAT crashes.

### 3.9. SURVIVAL CAPABILITY

In this section, we analyze the survival capability of an aircraft in a severe windshear. Indicative of this survival capability is the windshear/downdraft combination which results in the minimum altitude being equal to the ground altitude.

To analyze this important problem, we recall the windshear model (86), where  $\lambda$  is a parameter characterizing the intensity of the windshear/downdraft combination. By increasing the value of  $\lambda$ , more intense windshear/downdraft combinations are generated until a critical value  $\lambda_c$  is found such that  $h_{\min} = 0$  for a particular trajectory type.

More precisely, we consider the optimal trajectory (OT), the constant pitch trajectory (CPT), and the maximum angle of attack trajectory (MAAT) in connection with both the take-off problem and the abort landing problem. The results are shown in Tables 1-2, which display the following information: the initial altitude  $h_0$ ; the critical value of the wind intensity parameter  $\lambda_c$ ; the critical value of the wind velocity difference  $\Delta W_{xc}$ ; and the windshear efficiency ratio WER, defined to be

$$WER = (\lambda_c)_{PT} / (\lambda_c)_{OT} = (\Delta W_{xc})_{PT} / (\Delta W_{xc})_{OT} \quad (100)$$

Here, the subscript PT denotes a particular trajectory and the subscript OT denotes the optimal trajectory. It appears that, for both the take-off problem and the abort landing problem, the survival capability of the OT is superior to that of the CPT, which in turn is superior to that of the MAAT.

Table 1. Survival capability in take-off.

Trajectory	$h_0$ (ft)	$\lambda_c$	$\Delta W_{xc}$ (fps)	WER
OT	50	1.195	119.5	1.000
CPT	50	1.018	101.8	0.852
MAAT	50	0.577	57.7	0.483

Table 2. Survival capability in abort landing.

Trajectory	$h_0$ (ft)	$\lambda_c$	$\Delta W_{xc}$ (fps)	WER
OT	600	1.871	187.1	1.000
CPT	600	1.394	139.4	0.745
MAAT	600	0.817	81.7	0.437

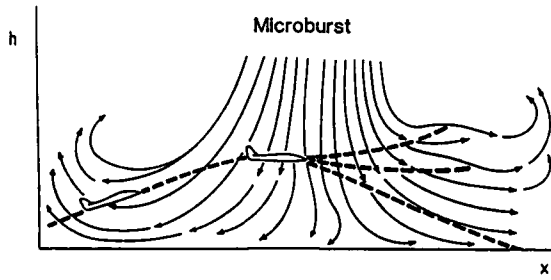


Fig. 1. Downburst configuration.

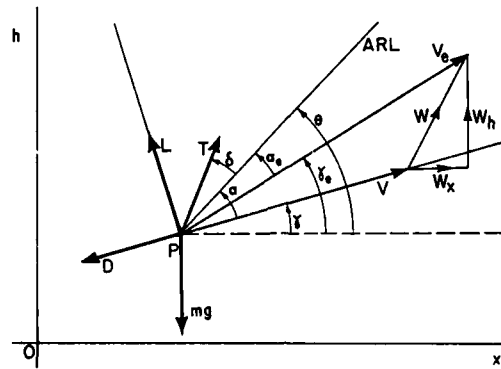


Fig. 2. Coordinate system and force diagram.

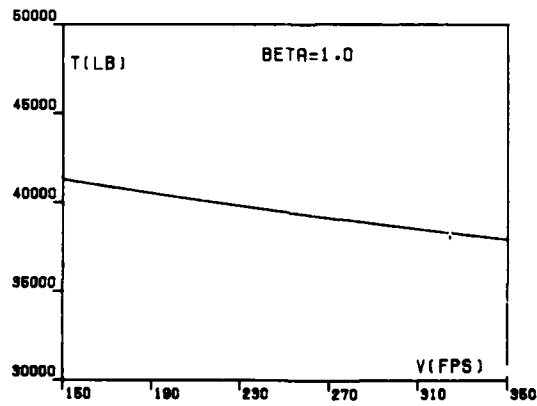


Fig. 3. Thrust  $T_x$  versus velocity  $V$  for the Boeing B-727 aircraft (maximum power setting, sea-level altitude, ambient temperature = 100 deg F).

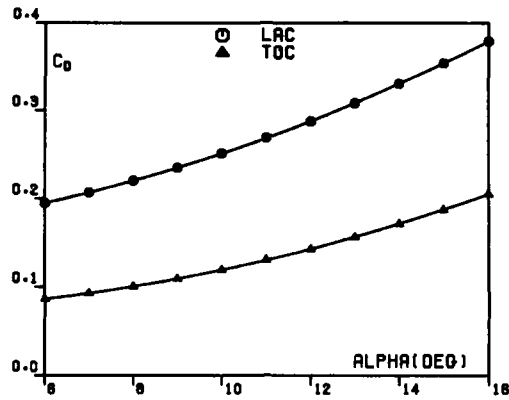


Fig. 4. Drag coefficient  $C_D$  versus angle of attack  $\alpha$  for the Boeing B-727 aircraft (TOC = take-off configuration, LAC = landing configuration).

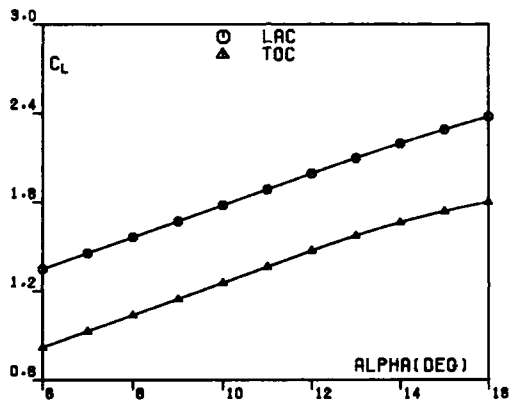


Fig. 5. Lift coefficient  $C_L$  versus angle of attack  $\alpha$  for the Boeing B-727 aircraft (TOC = take-off configuration, LAC = landing configuration).

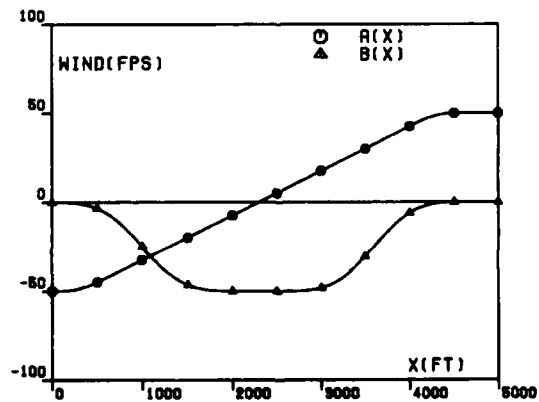


Fig. 6. Wind functions  $A(x)$  and  $B(x)$ .

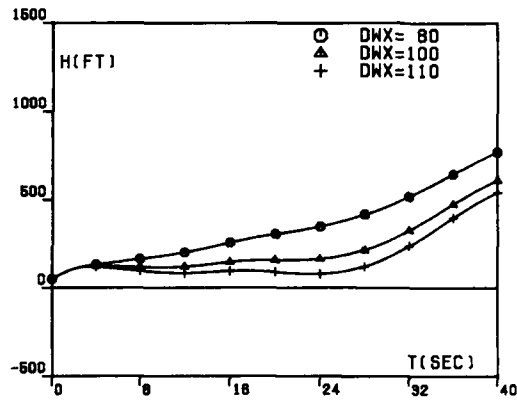


Fig. 7A. Optimal take-off trajectories, altitude  $h$  versus time  $t$ .

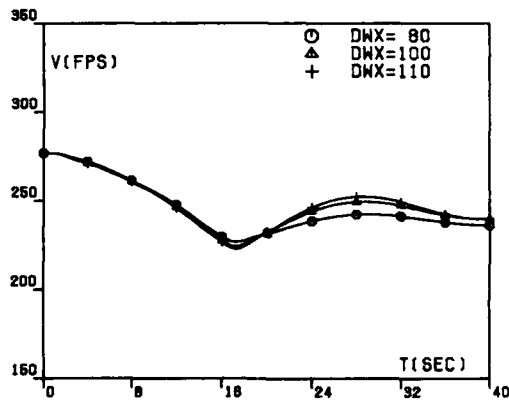


Fig. 7B. Optimal take-off trajectories, velocity  $V$  versus time  $t$ .

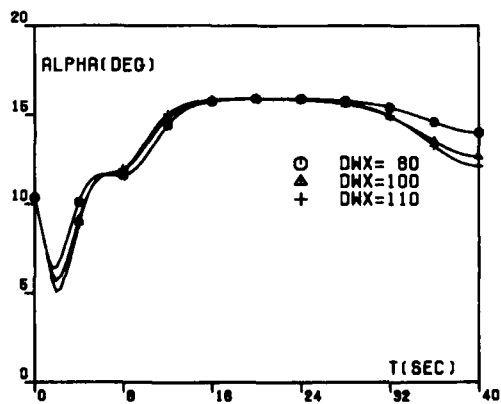


Fig. 7C. Optimal take-off trajectories, angle of attack  $\alpha$  versus time  $t$ .

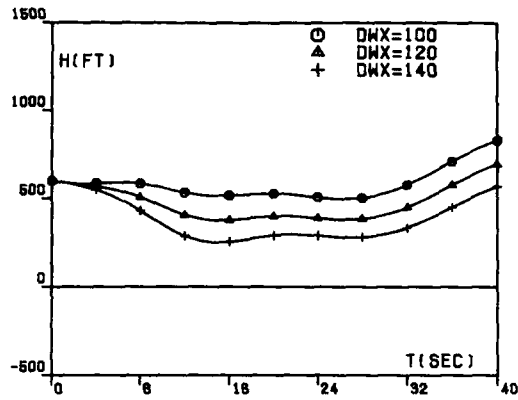


Fig. 8A. Optimal abort landing trajectories, altitude  $h$  versus time  $t$ .

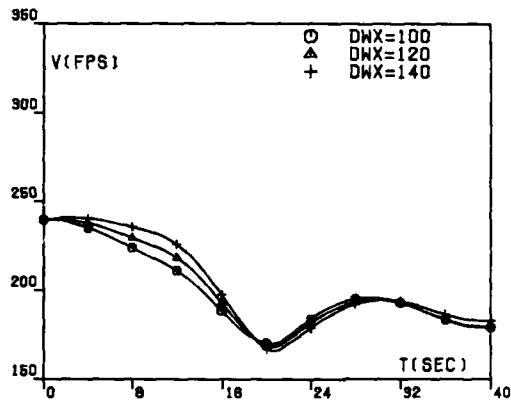


Fig. 8B. Optimal abort landing trajectories, velocity  $V$  versus time  $t$ .

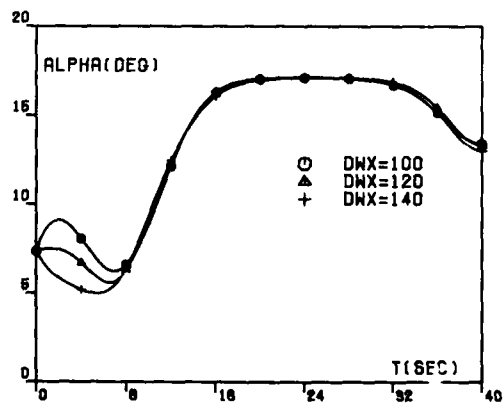


Fig. 8C. Optimal abort landing trajectories, angle of attack  $\alpha$  versus time  $t$ .

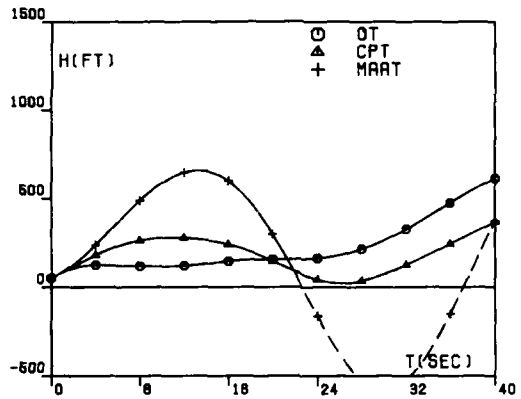


Fig. 9. Comparison of take-off trajectories, altitude  $h$  versus time  $t$  ( $\Delta W_x = 100$  ft/sec).

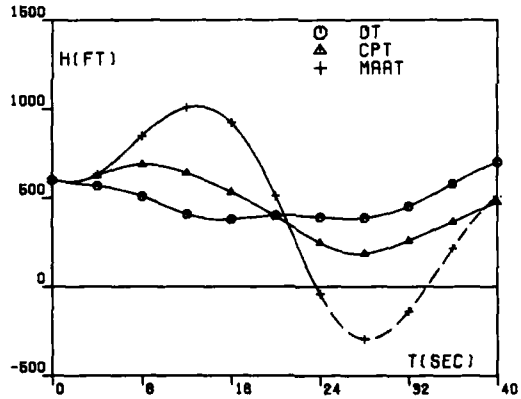


Fig. 10. Comparison of abort landing trajectories, altitude  $h$  versus time  $t$  ( $\Delta W_x = 120$  ft/sec).

## PART 4. OPTIMAL SPACECRAFT TRAJECTORIES FOR COPLANAR AEROASSISTED ORBITAL TRANSFER

## 4.1. OUTLINE

In Part 4, we present the application of the primal sequential gradient-restoration algorithm (PSGRA) to the determination of optimal trajectories for coplanar aeroassisted orbital transfer (AOT).

Section 4.2 contains the notations, and Section 4.3 contains some general considerations relative to aeroassisted orbital transfer. The equations of motion are given in Section 4.4, and the system description is given in Section 4.5.

The performance indexes of interest for AOT maneuvers are discussed in Section 4.6 within the frame of three problems: minimization of the total characteristic velocity; minimization of the time integral of the square of the path inclination; and minimization of the peak heating rate. The solutions of these problems are presented in Section 4.7. It is shown that these solutions are nearly indistinguishable from one another from the point of view of the total characteristic velocity and the peak heating rate.

## 4.2. NOTATIONS

Throughout Part 4, the metric system of physics is employed [the basic units are the meter, the kilogram(mass), and the second]. The following scalar notations are employed:

$C_D$ = drag coefficient;	$S$ = reference surface, $m^2$ ;
$C_{D0}$ = zero-lift drag coefficient;	$t$ = dimensionless time, $0 \leq t \leq 1$ ;
$C_L$ = lift coefficient;	$V$ = velocity, $m \text{ sec}^{-1}$ ;
$D$ = drag, N;	$\gamma$ = path inclination, rad;
$g$ = local acceleration of gravity, $m \text{ sec}^{-2}$ ;	$\mu$ = Earth's gravitational constant, $m^3 \text{ sec}^{-2}$ ;
$h$ = altitude, m;	$\rho$ = air density, $Kg \text{ m}^{-3}$ ;
$H$ = height of the atmosphere, m;	$\tau$ = flight time, sec;
$K$ = induced drag factor;	$\Delta V$ = characteristic velocity, $m \text{ sec}^{-1}$ .
$L$ = lift, N;	Subscripts
$m$ = mass, Kg;	0 = entry into the atmosphere;
$r$ = radial distance from the center of the Earth, m;	1 = exit from the atmosphere;
$r_e$ = radius of the Earth, m;	00 = exit from HEO (high Earth orbit);
$r_a$ = radius of the outer edge of the atmosphere, m;	11 = entry into LEO (low Earth orbit).

## 4.3. AEROASSISTED ORBITAL TRANSFER

Since the initial paper by London (Ref. 71), considerable research has been done on aeroassisted orbital transfer (AOT), especially on the optimization and guidance of flight trajectories. For surveys of the state of the art, see the papers by Walberg (Ref. 69) and Mease (Ref. 86). See also the Special Issue on Hypervelocity Flight of the Journal of the Astronautical Sciences (Ref. 70) and the papers therein (Refs. 86-94).

While most of the work on optimal trajectories has dealt with minimum-fuel transfers (namely, transfers minimizing the total characteristic velocity), the work performed at Rice University under JPL sponsorship has dealt with transfers minimizing alternative performance indexes (for instance, the peak heating rate, the peak dynamic pressure, and the peak altitude drop during the atmospheric part of the AOT maneuver). See Refs. 80-85.

In the following sections, we summarize some of the research done at Rice University on coplanar, aeroassisted orbital transfer from high Earth orbit (HEO) to low Earth orbit (LEO). We employ the following assumptions: (i) the initial and final orbits are circular; (ii) two tangential impulses are employed, one at HEO and one at LEO; (iii) the gravitational field is central and is governed by the inverse square law.

The four key points of the maneuver are these: 00 (HEO exit); 0 (atmospheric entry); 1 (atmospheric exit); 11 (LEO entry). The maneuver starts with a tangential propulsive burn, having characteristic velocity  $\Delta V_{00}$ , at point 00; here, the spacecraft enters into an elliptical transfer orbit, connecting the points 00 and 0. At point 0, the spacecraft enters into the atmosphere; during the atmospheric pass, the velocity of the spacecraft is reduced, due to the aerodynamic drag. At point 1, the spacecraft exits from the atmosphere; then, the spacecraft enters into an elliptical transfer orbit connecting the points 1 and 11. The maneuver ends with a tangential propulsive burn, having characteristic velocity  $\Delta V_{11}$ , at point 11; here, the spacecraft enters into the low Earth orbit, in that the magnitude of  $\Delta V_{11}$  is such that the desired circularization into LEO is achieved.

#### 4.4. EQUATIONS OF MOTION

With reference to the atmospheric portion of the trajectory of an AOT vehicle, the following hypotheses are employed: (a) the flight is made with engine shut-off; hence, the AOT vehicle behaves as a particle of constant mass; (b) Coriolis acceleration terms and transport acceleration terms are neglected; (c) the aerodynamic forces are evaluated using the inertial velocity, rather than the relative velocity; (d) under extreme hypersonic conditions, the dependence of the aerodynamic coefficients on the Mach number and the Reynolds number is disregarded.

Differential System. With the above assumptions, and upon normalizing the flight time to unity, the equations of motion are given by

$$\dot{h} = \tau[V\sin\gamma], \quad (101a)$$

$$\dot{V} = \tau[-D/m - g\sin\gamma], \quad (101b)$$

$$\dot{\gamma} = \tau[L/mV + (V/r - g/V)\cos\gamma]. \quad (101c)$$

In the above equations,

$$r = r_e + h, \quad g = \mu/r^2, \quad (102)$$

$$D = (1/2)C_D\rho SV^2, \quad L = (1/2)C_L\rho SV^2. \quad (103)$$

The density function  $\rho = \rho(h)$  can be found in Ref. 95. In particular, if a parabolic polar is postulated, the relation between the drag coefficient and the lift coefficient is given by

$$C_D = C_{D0} + KC_L^2. \quad (104)$$

Boundary Conditions. At the entry into the atmosphere ( $t = 0$ ) and at the exit from the atmosphere ( $t = 1$ ), certain static and dynamic boundary conditions must be satisfied. Specifically, at atmospheric entry, we have

$$h_0 = H, \quad (105a)$$

$$r_{00}^2 (2V_a^2 - V_0^2) - 2r_{00}r_a V_a^2 + r_a^2 V_0^2 \cos^2 \gamma_0 = 0, \quad (105b)$$

where  $V_a$  is the circular velocity at  $r = r_a$ . In addition, at atmospheric exit, we have

$$h_1 = H, \quad (106a)$$

$$r_{11}^2 (2V_a^2 - V_1^2) - 2r_{11}r_a V_a^2 + r_a^2 V_1^2 \cos^2 \gamma_1 = 0. \quad (106b)$$

Equations (105a) and (106a) reflect the definition of thickness of the atmosphere; Eq. (105b) arises from energy conservation and angular momentum conservation applied to the HEO-to-entry transfer orbit; and Eq. (106b) arises from energy conservation and angular momentum conservation applied to the exit-to-LEO transfer orbit.

Inequality Constraints. To ensure that the vehicle enters into the atmosphere at point 0 and exits from the atmosphere at point 1, the terminal path inclinations  $\gamma_0, \gamma_1$  must satisfy the inequality constraints

$$\gamma_0 \leq 0, \quad (107a)$$

$$\gamma_1 \geq 0. \quad (107b)$$

These inequality constraints can be converted into equality constraints by means of the Valentine transformations

$$\gamma_0 + \eta^2 = 0, \quad (108a)$$

$$\gamma_1 - \zeta^2 = 0, \quad (108b)$$

where  $\eta, \zeta$  denote parameters to be determined.

In addition, to obtain realistic solutions, the presence of upper and lower bounds on the lift coefficient is necessary. Therefore, the two-sided inequality constraint

$$C_{La} \leq C_L \leq C_{Lb} \quad (109)$$

must be satisfied everywhere along the interval of integration. The above inequality constraint can be converted into an equality constraint by means of the trigonometric transformation

$$C_L = (1/2)(C_{La} + C_{Lb}) + (1/2)(C_{Lb} - C_{La})\sin\beta, \quad (110)$$

in which  $\beta(t)$  denotes an auxiliary control variable.

Summary. To sum up, the equations governing the atmospheric pass include the differential system (101)-(104), the boundary conditions (105)-(106), and the inequality constraints (107) and (109), converted into equality constraints by means of the transformations (108) and (110). In this formulation, the independent variable is the dimensionless time  $t, 0 \leq t \leq 1$ . The dependent variables include three state variables  $\{h(t), V(t), \gamma(t)\}$ , one control variable  $\{\beta(t)\}$ , and three parameters  $\{\tau, \eta, \zeta\}$ . After a solution is found for the auxiliary control  $\beta(t)$ , the original control  $C_L(t)$  is recovered via Eq. (110).

#### 4.5. SYSTEM DESCRIPTION

The numerical examples of the subsequent sections refer to a spacecraft characterized as follows: the mass per unit reference surface is  $m/S = 300 \text{ Kg/m}^2$ ; the zero-lift drag coefficient is  $C_{D0} = 0.21$ ;

the induced drag factor is  $K = 1.67$ ; the maximum lift-to-drag ratio is  $E_{\max} = 0.8443$ ; the bounds on the lift coefficient are  $C_{La} = -0.9$  and  $C_{Lb} = +0.9$ .

For the transfer maneuver, the HEO radius is  $r_{00} = 2r_a = 12996$  Km, and the LEO radius is  $r_{11} = r_a + 60$  Km = 6558 Km.

The following physical constants are used in the computation: the radius of the Earth is  $r_e = 6378$  Km; the radius of the outer edge of the atmosphere is  $r_a = 6498$  Km; the height of the atmosphere is  $H = r_a - r_e = 120$  Km; and the Earth's gravitational constant is  $\mu = 398600$  Km<sup>3</sup>/sec<sup>2</sup>.

The atmospheric model assumed is that of the US Standard Atmosphere, 1976 (see Ref. 95). In this model, the values of the density are tabulated at discrete altitudes. For intermediate altitudes, the density is computed by assuming an exponential fit for the function  $\rho(h)$ .

#### 4.6. PERFORMANCE INDEXES

Subject to the previous constraints, different AOT optimization problems can be formulated, depending on the performance index chosen. The resulting optimal control problems are either of the Bolza type [see Problems (P1) and (P2) below] or of the Chebyshev type [see Problem (P3) below]

Problem (P1). It is required to minimize the energy needed for orbital transfer. A measure of this energy is the total characteristic velocity  $\Delta V$ , the sum of the initial characteristic velocity  $\Delta V_{00}$  associated with the propulsive burn from HEO and the final characteristic velocity  $\Delta V_{11}$  associated with the propulsive burn into LEO. Clearly,

$$I = \Delta V = \Delta V_{00} + \Delta V_{11}. \quad (111a)$$

with

$$\Delta V_{00} = V_a \sqrt{(r_a/r_{00})} - V_0 (r_a/r_{00}) \cos \gamma_0, \quad (111b)$$

$$\Delta V_{11} = V_a \sqrt{(r_a/r_{11})} - V_1 (r_a/r_{11}) \cos \gamma_1. \quad (111c)$$

Problem (P2). It is required to minimize the time integral of the square of the path inclination. Here, the performance index is given by

$$I = \int_0^1 \tau \gamma^2 dt. \quad (112)$$

The trajectory obtained by minimizing the performance index (112) is called nearly-grazing trajectory.

Problem (P3). It is required to minimize the peak value of the heating rate at a particular point of the spacecraft, for instance, the stagnation point. The performance index is given by

$$I = \text{PHR} = \max_t (C \sqrt{\rho} V^{3.08}), \quad (113)$$

where  $C$  is a dimensional constant.

This is a minimax problem or Chebyshev problem of optimal control. It can be reformulated as a Bolza problem of optimal control, in which one minimizes the integral performance index (Ref. 29)

$$J = \int_0^1 \tau (C \sqrt{\rho} V^{3.08})^q dt, \quad (114)$$

for large values of the positive exponent  $q$ .

## 4.7. NUMERICAL SOLUTIONS

Problems (P1)-(P3) were solved employing the primal sequential-gradient restoration algorithm (PSGRA) of Part 2 in conjunction with the equations of motion of Section 4.4 and the system data of Section 4.5. Summary results are shown in Tables 3-4. Table 3 presents the values of the performance indexes (I11), (I12), (I13) for all of the solutions of Problems (P1), (P2), (P3). Table 4 presents the components of the total characteristic velocity and the flight time. The following comments are pertinent:

(i) The solutions (P1), (P2), (P3) are nearly indistinguishable from one another from the point of view of the total characteristic velocity and the peak heating rate.

(ii) The total characteristic velocity of the solutions (P1), (P2), (P3) is less than half that of the two-impulse Hohmann transfer,  $\Delta V = 2.194$  Km/sec.

For the nearly-grazing solution (P2), the time history of the state variables and the control variable is shown in Fig. 11, which contains four parts: the altitude  $h$  versus the time  $t$  (Fig. 11A); the velocity  $V$  versus the time  $t$  (Fig. 11B); the path inclination  $\gamma$  versus the time  $t$  (Fig. 11C); and the lift coefficient  $C_L$  versus the time  $t$  (Fig. 11D).

Table 3. Results for coplanar transfer.

	(P1)	(P2)	(P3)	Units
$\Delta V$	1.050	1.050	1.050	Km/sec
$\int_0^1 \tau \gamma^2 dt$	0.1593	0.1591	0.1606	(rad) <sup>2</sup> sec
PHR	31.66	31.66	31.64	W/cm <sup>2</sup>

PHR = Peak heating rate. Note that PHR values are based on a reference heating rate (heating rate at  $h = 40$  Km and  $V = V_a$ ) of  $348.7$  W/cm<sup>2</sup>.

Also note that, should the reference heating rate change, PHR values would change proportionally.

Table 4. Results for coplanar transfer.

	(P1)	(P2)	(P3)	Units
$\Delta V_{00}$	1.024	1.024	1.024	Km/sec
$\Delta V_{11}$	0.026	0.026	0.026	Km/sec
$\Delta V$	1.050	1.050	1.050	Km/sec
$\tau$	1657	1696	1560	sec

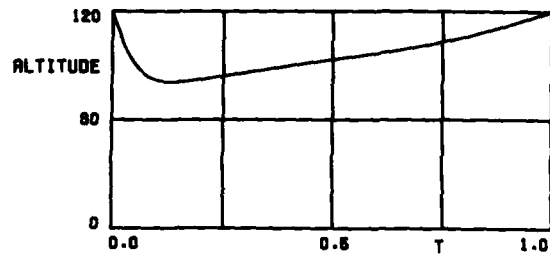


Fig. 11A. Nearly-grazing trajectory,  
altitude  $h(\text{Km})$  versus time  $t$ .

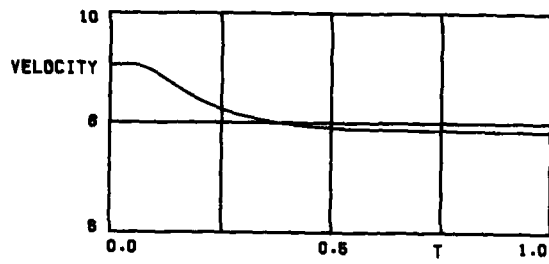


Fig. 11B. Nearly-grazing trajectory,  
velocity  $V(\text{Km/sec})$  versus time  $t$ .

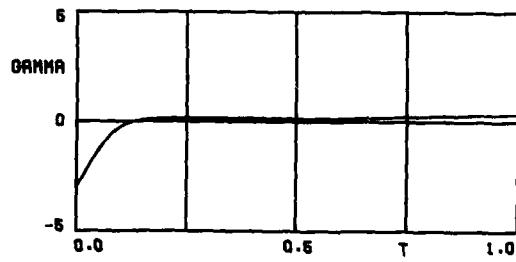


Fig. 11C. Nearly-grazing trajectory,  
path inclination  $\gamma(\text{deg})$  versus time  $t$ .

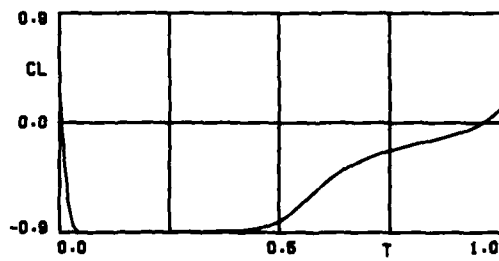


Fig. 11D. Nearly-grazing trajectory,  
lift coefficient  $C_L$  versus time  $t$ .

## PART 5. OPTIMAL SPACECRAFT TRAJECTORIES FOR NONCOPLANAR AEROASSISTED ORBITAL TRANSFER

## 5.1. OUTLINE

In Part 5, we present the application of the primal sequential gradient-restoration algorithm (PSGRA) to the determination of optimal trajectories for noncoplanar aeroassisted orbital transfer (AOT).

Section 5.2 contains the notations, and Section 5.3 contains some general considerations relative to aeroassisted orbital transfer. The equations of motion are given in Section 5.4, and the system description is given in Section 5.5.

The performance indexes of interest for AOT maneuvers are discussed in Section 5.6 within the frame of three problems: minimization of the total characteristic velocity; minimization of the time integral of the square of the path inclination; and minimization of the peak heating rate. The solutions of these problems are presented in Section 5.7. In particular, it is shown that the nearly-grazing solution (namely, the solution minimizing the time integral of the square of the path inclination) constitutes a useful engineering compromise between energy requirements and aerodynamic heating requirements.

## 5.2. NOTATIONS

Throughout Part 5, the metric system of physics is employed [the basic units are the meter, the kilogram(mass), and the second]. The following scalar notations are employed:

$C_D$ = drag coefficient;	$S$ = reference surface, $m^2$ ;
$C_{D0}$ = zero-lift drag coefficient;	$t$ = dimensionless time, $0 \leq t \leq 1$ ;
$C_L$ = lift coefficient;	$V$ = velocity, $m \text{ sec}^{-1}$ ;
$D$ = drag, N;	$\gamma$ = path inclination, rad;
$g$ = local acceleration of gravity, $m \text{ sec}^{-2}$ ;	$\theta$ = longitude, rad;
$h$ = altitude, m;	$\mu$ = Earth's gravitational constant, $m^3 \text{ sec}^{-2}$ ;
$H$ = height of the atmosphere, m;	$\rho$ = air density, $Kg \text{ m}^{-3}$ ;
$i$ = total plane change, rad;	$\sigma$ = angle of bank, rad;
$i_a$ = atmospheric plane change, rad;	$\tau$ = flight time, sec;
$i_s$ = space plane change, rad;	$\phi$ = latitude, rad;
$K$ = induced drag factor;	$\psi$ = heading angle, rad;
$L$ = lift, N;	$\Delta V$ = characteristic velocity, $m \text{ sec}^{-1}$ .
$m$ = mass, Kg;	Subscripts
$r$ = radial distance from the center of the Earth, m;	0 = entry into the atmosphere;
$r_e$ = radius of the Earth, m;	1 = exit from the atmosphere;
$r_a$ = radius of the outer edge of the atmosphere, m;	00 = exit from HEO (high Earth orbit);
	11 = entry into LEO (low Earth orbit).

## 5.3. AEROASSISTED ORBITAL TRANSFER

Noncoplanar orbital transfer is considerably more important than coplanar orbital transfer. Not only the initial motivation for AOT maneuvers was supplied by the plane change problem (Ref. 71), but a large number of the references listed at the end of this paper (Refs. 61-95) deal with the plane change problem.

In the following sections, we summarize some of the research done at Rice University on non-coplanar, aeroassisted orbital transfer from high Earth orbit (HEO) to low Earth orbit (LEO). We employ

the following assumptions: (i) the initial and final orbits are circular; (ii) three impulses are employed: a nontangential impulse at HEO, a tangential impulse at atmospheric exit, and a tangential impulse at LEO; (iii) the plane change is performed partly in space and partly in the atmosphere; and (iv) the gravitational field is central and is governed by the inverse square law.

The four key points of the maneuver are these: 00 (HEO exit); 0 (atmospheric entry); 1 (atmospheric exit); 11 (LEO entry). The maneuver starts with a nontangential propulsive burn, having characteristic velocity  $\Delta V_{00}$ , at point 00. Here, the spacecraft performs the plane change  $i_s$  and enters into an elliptical transfer orbit, connecting the points 00 and 0. At point 0, the spacecraft enters into the atmosphere; after traversing the upper layers of the atmosphere, it exits from the atmosphere at point 1. During the atmospheric pass, the velocity of the spacecraft is reduced, due to the aerodynamic drag; in addition, the plane change  $i_a$  is performed gradually. At point 1, the spacecraft exits from the atmosphere; right at the exit, a tangential propulsive burn takes place, having characteristic velocity  $\Delta V_1$ . Here, the spacecraft enters into an elliptical transfer orbit connecting the points 1 and 11. The maneuver ends with a tangential propulsive burn, having characteristic velocity  $\Delta V_{11}$ , at point 11. Here, the spacecraft enters into the low Earth orbit, in that the magnitude of  $\Delta V_{11}$  is such that the desired circularization into LEO is achieved.

#### 5.4. EQUATIONS OF MOTION

With reference to the atmospheric portion of the trajectory of an AOT vehicle, the following hypotheses are employed: (a) the flight is made with engine shut-off; hence, the AOT vehicle behaves as a particle of constant mass; (b) Coriolis acceleration terms and transport acceleration terms are neglected; (c) the aerodynamic forces are evaluated using the inertial velocity, rather than the relative velocity; (d) under extreme hypersonic conditions, the dependence of the aerodynamic coefficients on the Mach number and the Reynolds number is disregarded.

Differential System. With the above assumptions, and upon normalizing the flight time to unity, the equations of motion are given by

$$\dot{h} = \tau[Vs\sin\gamma], \quad (115a)$$

$$\dot{V} = \tau[-D/m - gs\sin\gamma], \quad (115b)$$

$$\dot{\gamma} = \tau\{(L/mV)\cos\sigma + (V/r - g/V)\cos\gamma\}, \quad (115c)$$

$$\dot{\theta} = \tau[V\cos\gamma\cos\psi/r\cos\phi], \quad (115d)$$

$$\dot{\phi} = \tau[V\cos\gamma\sin\psi/r], \quad (115e)$$

$$\dot{\psi} = \tau\{(L/mV)\sin\sigma/\cos\gamma - (V/r)\cos\gamma\cos\psi\tan\phi\} \quad (115f)$$

In the above equations,

$$r = r_e + h, \quad g = \mu/r^2, \quad (116)$$

$$D = (1/2)C_D\rho SV^2, \quad L = (1/2)C_L\rho SV^2. \quad (117)$$

The density function  $\rho = \rho(h)$  can be found in Ref. 95. In particular, if a parabolic polar is postulated, the relation between the drag coefficient and the lift coefficient is given by

$$C_D = C_{D0} + KC_L^2. \quad (118)$$

Boundary Conditions. At the entry into the atmosphere ( $t = 0$ ) and at the exit from the atmosphere ( $t = 1$ ), certain static and dynamic boundary conditions must be satisfied. Specifically, at atmospheric entry, we have

$$h_0 = H, \quad (119a)$$

$$r_{00}^2(2V_a^2 - V_0^2) - 2r_{00}r_a V_a^2 + r_a^2 V_0^2 \cos^2 \gamma_0 = 0, \quad (119b)$$

$$\theta_0 = 0, \quad (119c)$$

$$\phi_0 = 0, \quad (119d)$$

$$\psi_0 = 0, \quad (119e)$$

where  $V_a$  is the circular velocity at  $r = r_a$ . In addition, at atmospheric exit, we have

$$h_1 = H, \quad (120a)$$

$$r_{11}^2[2V_a^2 - (V_1 + \xi)^2] - 2r_{11}r_a V_a^2 + r_a^2(V_1 + \xi)^2 \cos^2 \gamma_1 = 0, \quad (120b)$$

$$\cos \phi_1 \cos \psi_1 - \cos i_a = 0, \quad (120c)$$

where  $\xi$  is the velocity impulse at point 1. Equations (119a) and (120a) reflect the definition of thickness of the atmosphere; Eq. (119b) arises from energy conservation and angular momentum conservation applied to the HEO-to-entry transfer orbit; Eq. (120b) arises from energy conservation and angular momentum conservation applied to the exit-to-LEO transfer orbit; Eqs. (119c), (119d), (119e) assume a particular type of entry, with the entry velocity contained in the equatorial plane; and Eq. (120c) constitutes a relation between the exit latitude, the exit heading angle, and the atmospheric plane change.

Plane Change Condition. For noncoplanar orbital transfer, the following approximate relation holds between the total plane change, the space plane change, and the atmospheric plane change:

$$i = i_s + i_a, \quad (121)$$

where  $i_s$ ,  $i_a$  are parameters. It must be emphasized that the linear relation (121) is only an approximation. For more precise calculations, Eq. (121) must be replaced by nonlinear equations (Refs. 77 and 85). However, for feasibility studies directed at assessing the relative merits of various optimal trajectories, the simpler linear relation (121) is sufficiently accurate: it predicts the total plane change  $i$  with a precision of the order of 0.5% or better.

Inequality Constraints. To ensure that the vehicle enters into the atmosphere at point 0 and exits from the atmosphere at point 1, the terminal path inclinations  $\gamma_0$ ,  $\gamma_1$  must satisfy the inequality constraints

$$\gamma_0 \leq 0, \quad (122a)$$

$$\gamma_1 \geq 0. \quad (122b)$$

These inequality constraints can be converted into equality constraints by means of the Valentine transformations

$$\gamma_0 + \eta^2 = 0, \quad (123a)$$

$$\gamma_1 - \zeta^2 = 0, \quad (123b)$$

where  $\eta$ ,  $\zeta$  denote parameters to be determined.

In addition, to obtain realistic solutions, the presence of upper and lower bounds on the lift coefficient is necessary. Therefore, the two-sided inequality constraint

$$C_{La} \leq C_L \leq C_{Lb} \quad (124)$$

must be satisfied everywhere along the interval of integration. The above inequality constraint can be converted into an equality constraint by means of the trigonometric transformation

$$C_L = (1/2)(C_{La} + C_{Lb}) + (1/2)(C_{Lb} - C_{La})\sin\beta, \quad (125)$$

in which  $\beta(t)$  denotes an auxiliary control variable.

**Summary.** To sum up, the equations governing the atmospheric pass include the differential system (115)-(118), the boundary conditions (119)-(120), the plane change condition (121), and the inequality constraints (122) and (124), converted into equality constraints by means of the transformations (123) and (125). In this formulation, the independent variable is the dimensionless time  $t$ ,  $0 \leq t \leq 1$ . The dependent variables include six state variables [ $h(t)$ ,  $V(t)$ ,  $\gamma(t)$ ,  $\theta(t)$ ,  $\phi(t)$ ,  $\psi(t)$ ], two control variables [ $\beta(t)$ ,  $\sigma(t)$ ], and six parameters [ $\tau$ ,  $\xi$ ,  $\eta$ ,  $\zeta$ ,  $i_s$ ,  $i_a$ ]. After a solution is found for the auxiliary control  $\beta(t)$ , the original control  $C_L(t)$  is recovered via Eq. (125).

#### 5.5. SYSTEM DESCRIPTION

The numerical examples of the subsequent sections refer to a spacecraft characterized as follows: the mass per unit reference surface is  $m/S = 300 \text{ Kg/m}^2$ ; the zero-lift drag coefficient is  $C_{D0} = 0.10$ ; the induced drag factor is  $K = 1.11$ ; the maximum lift-to-drag ratio is  $E_{\max} = 1.50$ ; the bounds on the lift coefficient are  $C_{La} = -0.9$  and  $C_{Lb} = +0.9$ .

For the transfer maneuver, the HEO radius is  $r_{00} = 2r_a = 12996 \text{ Km}$ , the LEO radius is  $r_{11} = r_a + 60 \text{ Km} = 6558 \text{ Km}$ , and the prescribed plane change is  $i = 30 \text{ deg}$ .

The following physical constants are used in the computation: the radius of the Earth is  $r_e = 6378 \text{ Km}$ ; the radius of the outer edge of the atmosphere is  $r_a = 6498 \text{ Km}$ ; the height of the atmosphere is  $H = r_a - r_e = 120 \text{ Km}$ ; and the Earth's gravitational constant is  $\mu = 398600 \text{ Km}^3/\text{sec}^2$ .

The atmospheric model assumed is that of the US Standard Atmosphere, 1976 (see Ref. 95). In this model, the values of the density are tabulated at discrete altitudes. For intermediate altitudes, the density is computed by assuming an exponential fit for the function  $\rho(h)$ .

#### 5.6. PERFORMANCE INDEXES

Subject to the previous constraints, different AOT optimization problems can be formulated, depending on the performance index chosen. The resulting optimal control problems are either of the Bolza type [see Problems (P1) and (P2) below] or of the Chebyshev type [see Problem (P3) below].

**Problem (P1).** It is required to minimize the energy needed for orbital transfer. A measure of this energy is the total characteristic velocity  $\Delta V$ , the sum of the initial characteristic velocity  $\Delta V_{00}$

associated with the propulsive burn from HEO, the final characteristic velocity  $\Delta V_{11}$  associated with the propulsive burn into LEO, and the intermediate characteristic velocity  $\Delta V_1$  associated with the propulsive burn at atmospheric exit. Clearly,

$$I = \Delta V = \Delta V_{00} + \Delta V_{11} + \Delta V_1, \quad (126a)$$

with

$$\Delta V_{00} = \sqrt{[V_a^2(r_a/r_{00}) + V_0^2(r_a/r_{00})^2 \cos^2 \gamma_0 - 2V_a V_0 (r_a/r_{00})^{3/2} \cos \gamma_0 \cos i_s]}, \quad (126b)$$

$$\Delta V_{11} = V_a \sqrt{r_a/r_{11}} - (V_1 + \epsilon)(r_a/r_{11}) \cos \gamma_1, \quad (126c)$$

$$\Delta V_1 = \epsilon. \quad (126d)$$

Problem (P2) It is required to minimize the time integral of the square of the path inclination. Here, the performance index is given by

$$I = \int_0^1 \tau \gamma^2 dt. \quad (127)$$

The trajectory obtained by minimizing the performance index (127) is called nearly-grazing trajectory.

Problem (P3) It is required to minimize the peak value of the heating rate at a particular point of the spacecraft, for instance, the stagnation point. The performance index is given by

$$I = \text{PHR} = \max_t (C \sqrt{\rho} V^{3.08}), \quad (128)$$

where  $C$  is a dimensional constant.

This is a minimax problem or Chebyshev problem of optimal control. It can be reformulated as a Bolza problem of optimal control, in which one minimizes the integral performance index (Ref. 29)

$$J = \int_0^1 \tau (C \sqrt{\rho} V^{3.08})^q dt, \quad (129)$$

for large values of the positive exponent  $q$ .

## 5.7. NUMERICAL SOLUTIONS

Problems (P1)-(P3) were solved employing the primal sequential-gradient restoration algorithm (PSGRA) of Part 2 in conjunction with the equations of motion of Section 5.4 and the system data of Section 5.5. In computing numerical solutions to Problems (P1), (P2), (P3), the following procedure was adopted: for Problem (P1), the space component  $i_s$  and the atmospheric component  $i_a$  of the prescribed plane change were optimized; for Problems (P2) and (P3), the components of the plane change were kept at the same levels determined for Problem (P1). This was done in order to impart good energy characteristics to the solutions of Problems (P2) and (P3).

Summary results are shown in Tables 5-6. Table 5 presents the values of the performance indexes (126), (127), (128) for all of the solutions of Problems (P1), (P2), (P3). Table 6 presents the components of the total characteristic velocity, the components of the plane change, and the flight time. The following comments are pertinent:

(i) The total characteristic velocities of the solutions (P1), (P2), (P3) are below the total characteristic velocity of the two-impulse Hohmann transfer,  $\Delta V = 3.788$  Km/sec.

(ii) While the solution (P2) requires 2.5% more characteristic velocity than the solution (P1), at the same time it involves less peak heating rate (25%).

Clearly, the nearly-grazing solution (P2) is an interesting engineering compromise between energy requirements and heating requirements. For the solution (P2), the time history of the state variables and the control variables is shown in Fig. 12, which contains eight parts: the altitude  $h$  versus the time  $t$  (Fig. 12A); the velocity  $V$  versus the time  $t$  (Fig. 12B); the path inclination  $\gamma$  versus the time  $t$  (Fig. 12C); the longitude  $\theta$  versus the time  $t$  (Fig. 12D); the latitude  $\phi$  versus the time  $t$  (Fig. 12E); the heading angle  $\psi$  versus the time  $t$  (Fig. 12F); the lift coefficient  $C_L$  versus the time  $t$  (Fig. 12G); and the bank angle  $\sigma$  versus the time  $t$  (Fig. 12H).

Table 5. Results for noncoplanar transfer.

	(P1)	(P2)	(P3)	Units
$\Delta V$	1.919	1.966	2.143	Km/sec
$\int_0^1 \gamma^2 dt$	0.3471	0.2919	0.3685	(rad) <sup>2</sup> sec
PHR	125.6	94.7	71.4	W/cm <sup>2</sup>

PHR = Peak heating rate. Note that PHR values are based on a reference heating rate (heating rate at  $h = 40$  Km and  $V = V_a$ ) of  $348.7$  W/cm<sup>2</sup>.

Also note that, should the reference heating rate change, PHR values would change proportionally.

Table 6. Results for noncoplanar transfer.

	(P1)	(P2)	(P3)	Units
$\Delta V_{00}$	1.837	1.836	1.836	Km/sec
$\Delta V_1$	0.064	0.112	0.289	Km/sec
$\Delta V_{11}$	0.018	0.018	0.018	Km/sec
$\Delta V$	1.919	1.966	2.143	Km/sec
$i_s$	17.51	17.51	17.51	deg
$i_a$	12.49	12.49	12.49	deg
$i$	30.00	30.00	30.00	deg
$\tau$	1379	1187	875	sec

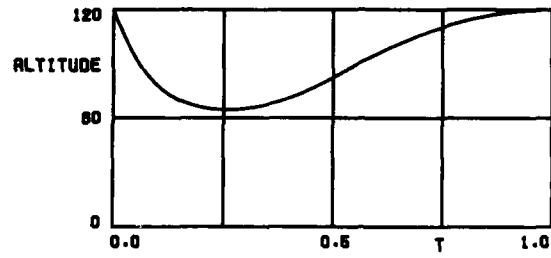


Fig. 12A. Nearly-grazing trajectory,  
altitude  $h$ (Km) versus time  $t$ .

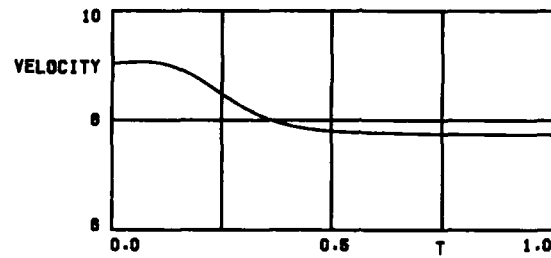


Fig. 12B. Nearly-grazing trajectory,  
velocity  $V$ (Km/sec) versus time  $t$ .

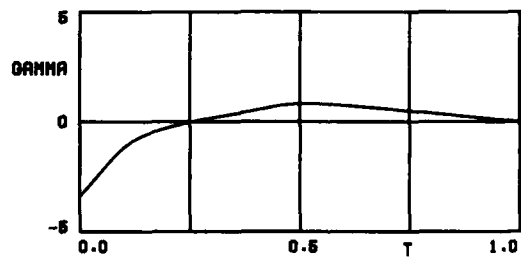


Fig. 12C. Nearly-grazing trajectory,  
path inclination  $\gamma$ (deg) versus time  $t$ .

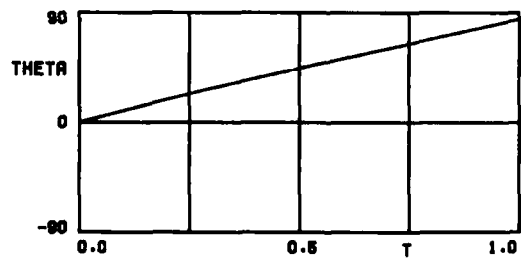


Fig. 12D. Nearly-grazing trajectory,  
longitude  $\theta$ (deg) versus time  $t$ .

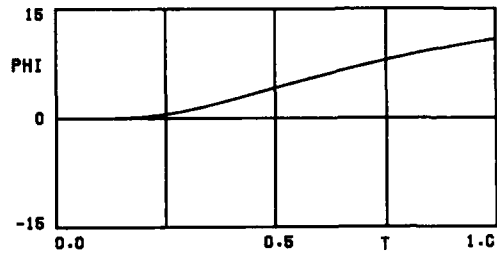


Fig. 12E. Nearly-grazing trajectory,  
latitude  $\phi$ (deg) versus time  $t$ .

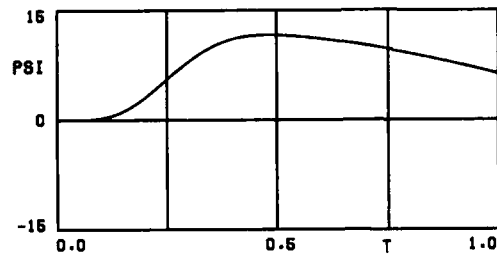


Fig. 12F. Nearly-grazing trajectory,  
heading angle  $\psi$ (deg) versus time  $t$ .

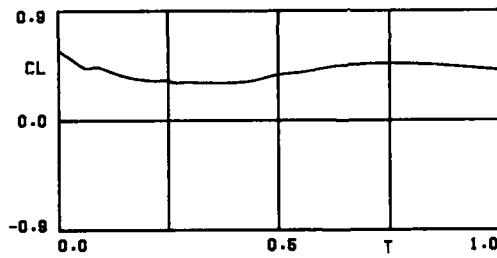


Fig. 12G. Nearly-grazing trajectory,  
lift coefficient  $C_L$  versus time  $t$ .

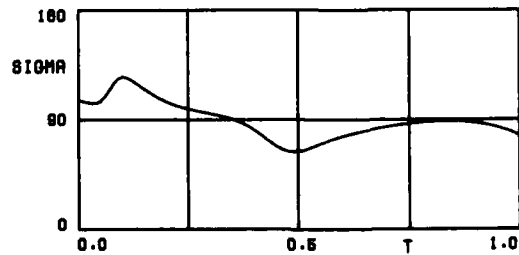


Fig. 12H. Nearly-grazing trajectory,  
bank angle  $\sigma$ (deg) versus time  $t$ .

## PART 6. CONCLUSIONS

One of the most effective first-order algorithms for solving trajectory optimization problems is the sequential gradient-restoration algorithm (SGRA, Refs. 15-24). Originally developed in the primal formulation (PSGRA, Refs. 15-21), this algorithm has been extended to incorporate a dual formulation (DSGRA, Refs. 22-24).

Both the primal formulation and the dual formulation involve a sequence of two-phase cycles, each cycle including a gradient phase and a restoration phase. In turn, each iteration of the gradient phase and the restoration phase requires the solution of an auxiliary minimization problem (AMP). In the primal formulation, the AMP is solved with respect to the variations of the state, the control, and the parameter. In the dual formulation, the AMP is solved with respect to the Lagrange multipliers. A characteristic of the dual formulation is that the AMP's associated with the gradient phase and the restoration phase of SGRA can be reduced to mathematical programming problems involving a finite number of parameters as unknowns. Hence, the algorithmic efficiency of SGRA can be enhanced.

Numerical experience with SGRA has shown that, for nonstiff problems of flight mechanics, the dual formulation is superior to the primal formulation in terms of CPU time and is about equal in accuracy. On the other hand, for stiff problems of flight mechanics, the primal formulation is superior to the dual formulation in both CPU time and accuracy.

In this paper, a complete description of SGRA is given in both its primal form (PSGRA) and its dual form (DSGRA). Then, the application of SGRA to flight mechanics problems is shown via a variety of examples concerning aircraft and spacecraft.

For aircraft trajectories, the dual sequential gradient-restoration algorithm (DSGRA) is applied to compute optimal trajectories in the presence of windshear. Take-off trajectories are optimized by minimizing the peak deviation of the absolute path inclination from a reference value. Abort landing trajectories are optimized by minimizing the peak drop of altitude from a reference value.

For spacecraft trajectories, the primal sequential gradient-restoration algorithm (PSGRA) is applied to compute optimal trajectories for aeroassisted orbital transfer from high Earth orbit (HEO) to low Earth orbit (LEO). Both the coplanar case (problem without plane change) and the noncoplanar case (problem with plane change) are discussed within the frame of three problems: minimization of the total characteristic velocity; minimization of the time integral of the square of the path inclination; and minimization of the peak heating rate.

For spacecraft trajectories, the procedure employed to optimize HEO-to-LEO transfers can be extended to include GEO-to-LEO transfers and LEO-to-LEO transfers (Ref. 92). Here, GEO denotes geosynchronous Earth orbit and LEO denotes low Earth orbit. Note that LEO-to-LEO transfers are of interest for the National Aero-Space Plane (NASP).

To sum up, the sequential gradient-restoration algorithm has shown to be a powerful and versatile algorithm to solve optimal trajectory problems of atmospheric flight mechanics, suborbital flight mechanics, and orbital flight mechanics. While the examples provided belong to the extreme regions of the velocity spectrum (low subsonic flight and hypervelocity flight), the sequential gradient-restoration algorithm can handle equally well optimal trajectory problems of supersonic and hypersonic aircraft as well as optimal trajectory problems for vehicles of the space shuttle type and the Hermes type.

## PART 7. REFERENCES

Calculus of Variations and Optimal Control

1. BLISS, G. A., "Lectures on the Calculus of Variations", University of Chicago Press, Chicago, Illinois, 1946.
2. BOLZA, O., "Lectures on the Calculus of Variations", Dover Publications, New York, New York, 1961.
3. PONTRYAGIN, L. S., BOLTYANSKII, V. G., GAMKRELIDZE, R. V., and MISHCHENKO, E. F., "The Mathematical Theory of Optimal Processes", Interscience Publishers, New York, New York, 1962.
4. LEITMANN, G., Editor, "Optimization Techniques", Academic Press, New York, New York, 1962.
5. MIELE, A., Editor, "Theory of Optimum Aerodynamic Shapes", Academic Press, New York, New York, 1965.
6. HESTENES, M. R., "Calculus of Variations and Optimal Control Theory", John Wiley and Sons, New York, New York, 1966.
7. BRYSON, A. E., and HO, Y. C., "Applied Optimal Control", Blaisdell Publishing Company, Waltham, Massachusetts, 1969.
8. LEITMANN, G., "The Calculus of Variations and Optimal Control", Plenum Press, New York, New York, 1981.

Numerical Algorithms for Optimal Control

9. KELLEY, H. J., "Gradient Theory of Optimal Flight Paths", ARS Journal, Vol. 30, No. 10, pp. 947-954, 1960.
10. KELLEY, H. J., "Method of Gradients", Optimization Techniques, Edited by G. Leitmann, Academic Press, New York, New York, pp. 205-254, 1962.
11. BRYSON, A. E., Jr., and DENHAM, W. F., "Multivariable Terminal Control for Minimum Mean-Square Deviation from a Nominal Path", Raytheon Company, Missile and Space Division, Report No. BR-1333, 1961.
12. BRYSON, A. E., Jr., and DENHAM, W. F., "A Steepest-Ascent Method for Solving Optimum Programming Problems", Journal of Applied Mechanics, Vol. 84, No. 3, pp. 247-257, 1962.
13. DENHAM, W. F., and BRYSON, A. E., Jr., "Optimal Programming Problems with Inequality Constraints, Part 2, Solution by Steepest Ascent", AIAA Journal, Vol. 2, No. 1, pp. 25-34, 1964.
14. SPEYER, J. L., MEHRA, R. K., and BRYSON, A. E., Jr., "The Separate Computation of Arcs for Optimal Flight Paths with State Variable Inequality Constraints", Harvard University, Division of Engineering and Applied Physics, Technical Report No. 256, 1967.
15. MIELE, A., PRITCHARD, R. E., and DAMOULAKIS, J. N., "Sequential Gradient-Restoration Algorithm for Optimal Control Problems", Journal of Optimization Theory and Applications, Vol. 5, No. 4, pp. 235-282, 1970.
16. MIELE, A., and DAMOULAKIS, J. N., "Modifications and Extensions of the Sequential Gradient-Restoration Algorithm for Optimal Control Theory", Journal of the Franklin Institute, Vol. 294, No. 1, pp. 23-42, 1972.
17. MIELE, A., DAMOULAKIS, J. N., CLOUTIER, J. R., and TIETZE, J. L., "Sequential Gradient-Restoration Algorithm for Optimal Control Problems with Nondifferential Constraints", Journal of Optimization Theory and Applications, Vol. 13, No. 2, pp. 218-255, 1974.
18. HEIDEMAN, J. C., and LEVY, A. V., "Sequential Conjugate Gradient-Restoration Algorithm for Optimal Control Problems, Part 1, Theory", Journal of Optimization Theory and Applications, Vol. 15, No. 2, pp. 203-222, 1975.

19. HEIDEMAN, J. C., and LEVY, A. V., "Sequential Conjugate Gradient-Restoration Algorithm for Optimal Control Problems, Part 2, Examples", *Journal of Optimization Theory and Applications*, Vol. 15, No.2, pp. 223-244, 1975.
20. MIELE, A., "Recent Advances in Gradient Algorithms for Optimal Control Problems", *Journal of Optimization Theory and Applications*, Vol. 17, Nos. 5-6, pp. 361-430, 1975.
21. GONZALEZ, S., and MIELE, A., "Sequential Gradient-Restoration Algorithm for Optimal Control Problems with General Boundary Conditions", *Journal of Optimization Theory and Applications*, Vol. 26, No. 3, pp. 395-425, 1978.
22. MIELE, A., and WANG, T., "Primal-Dual Properties of Sequential Gradient-Restoration Algorithms for Optimal Control Problems, Part 1, Basic Problem", *Integral Methods in Science and Engineering*, Edited by F. R. Payne et al, Hemisphere Publishing Corporation, Washington, DC, pp. 577-607, 1986.
23. MIELE, A., and WANG, T., "Primal-Dual Properties of Sequential Gradient-Restoration Algorithms for Optimal Control Problems, Part 2, General Problem", *Journal of Mathematical Analysis and Applications*, Vol. 119, Nos. 1-2, pp. 21-54, 1986.
24. MIELE, A., WANG, T., and BASAPUR, V. K., "Primal and Dual Formulations of Sequential Gradient-Restoration Algorithms for Trajectory Optimization Problems", *Acta Astronautica*, Vol. 13, No. 8, pp. 491-505, 1986.
25. MIELE, A., "Method of Particular Solutions for Linear, Two-Point Boundary-Value Problems", *Journal of Optimization Theory and Applications*, Vol. 2, No. 4, pp. 260-273, 1968.
26. MIELE, A., and IYER, R. R., "General Technique for Solving Nonlinear, Two-Point Boundary-Value Problems via the Method of Particular Solutions", *Journal of Optimization Theory and Applications*, Vol. 5, No. 5, pp. 382-399, 1970.
27. MIELE, A., and IYER, R. R., "Modified Quasilinearization Method for Solving Nonlinear, Two-Point Boundary-Value Problems", *Journal of Mathematical Analysis and Applications*, Vol. 36, No. 3, pp. 674-692, 1971.
28. MIELE, A., NAQVI, S., LEVY, A. V., and IYER, R. R., "Numerical Solution of Nonlinear Equations and Nonlinear, Two-Point Boundary-Value Problems", *Advances in Control Systems*, Edited by C. T. Leondes, Academic Press, New York, New York, Vol. 8, pp. 189-215, 1971.
29. MIELE, A., and WANG, T., "An Elementary Proof of a Functional Analysis Result Having Interest for Minimax Optimal Control of Aeroassisted Orbital Transfer Vehicles", *Rice University, Aero-Astronautics Report No. 182*, 1985.
30. RALSTON, A., "Numerical Integration Methods for the Solution of Ordinary Differential Equations", *Mathematical Methods for Digital Computers*, Edited by A. Ralston and H. S. Wilf, John Wiley and Sons, New York, New York, Vol. 1, pp. 95-109, 1960.

Flight in a Windshear

31. ANONYMOUS, N. N., "Low Altitude Windshear and Its Hazard to Aviation", National Academy Press, Washington, DC, 1983.
32. FRUST, W., "Flight in Low Level Windshear", NASA, Contractor Report No. 3678, 1983.
33. ANONYMOUS, N. N., "Aircraft Accident Report: Pan American World Airways, Clipper 759, Boeing 727-235, N4737, New Orleans International Airport, Kenner, Louisiana, July 9, 1982", Report No. NTSB-AAR-8302, National Transportation Safety Board, Washington, DC, 1983.

34. PSIAKI, M. L., and STENGEL, R. F., "Analysis of Aircraft Control Strategies for Microburst Encounter", Paper No. AIAA-84-0238, AIAA 22nd Aerospace Sciences Meeting, Reno, Nevada, 1984.
35. FROST, W., and BOWLES, R. L., "Windshear Terms in the Equations of Aircraft Motion", *Journal of Aircraft*, Vol. 21, No. 11, pp. 866-872, 1984.
36. ANONYMOUS, N. N., "Flight Path Control in Windshear", Boeing Airliner, pp. 1-12, January-March, 1985.
37. FUJITA, T. T., "The Downburst", Department of Geophysical Sciences, University of Chicago, Chicago, Illinois, 1985.
38. ZHU, S., and ETKIN, B., "Model of the Wind Field in a Downburst", *Journal of Aircraft*, Vol. 22, No. 7, pp. 595-601, 1985.
39. ANONYMOUS, N. N., "Aircraft Accident Report: Delta Airlines, Lockheed L-1011-3851, N726DA, Dallas-Fort Worth International Airport, Texas, August 2, 1985", Report No. NTSB-AAR-8605, National Transportation Safety Board, Washington, DC, 1986.
40. FUJITA, T. T., "DFW Microburst", Department of Geophysical Sciences, University of Chicago, Chicago, Illinois, 1986.
41. BRAY, R. S., "Aircraft Performance and Control in Downburst Windshear", Paper No. SAE-86-1698, Society of Automotive Engineers, Aerospace Technology Conference and Exposition, Long Beach, California, 1986.
42. HAHN, K. W., "Take-Off and Landing in a Downburst", Paper No. ICAS-86-562, 15th Congress of the International Council of the Aeronautical Sciences, London, England, 1986.
43. PSIAKI, M. L., and STENGEL, R. F., "Optimal Flight Paths through Microburst Wind Profiles", *Journal of Aircraft*, Vol. 23, No. 8, pp. 629-635, 1986.
44. IVAN, M., "A Ring-Vortex Downburst Model for Flight Simulation", *Journal of Aircraft*, Vol. 23, No. 3, pp. 232-236, 1986.
45. CHU, P. Y., and BRYSON, A. E., Jr., "Control of Aircraft Landing Approach in Windshear", Paper No. AIAA-87-0632, AIAA 25th Aerospace Sciences Meeting, Reno, Nevada, 1987.
46. GORNEY, J. L., "An Analysis of the Delta 191 Windshear Accident", Paper No. AIAA-87-0626, AIAA 25th Aerospace Sciences Meeting, Reno, Nevada, 1987.
47. WINGROVE, R. C., and BACH, R. E., Jr., "Severe Winds in the DFW Microburst Measured from Two Aircraft", Paper No. AIAA-87-2340, AIAA Guidance, Navigation, and Control Conference, Monterey, California, 1987.
48. ANONYMOUS, N. N., "Windshear Training Aid, Vols. 1 and 2", Federal Aviation Administration, Washington, DC, 1987.
49. MIELE, A., WANG, T., and MELVIN, W. W., "Optimal Take-Off Trajectories in the Presence of Windshear", *Journal of Optimization Theory and Applications*, Vol. 49, No. 1, pp. 1-45, 1986.
50. MIELE, A., WANG, T., and MELVIN, W. W., "Guidance Strategies for Near-Optimum Take-Off Performance in a Windshear", *Journal of Optimization Theory and Applications*, Vol. 50, No. 1, pp. 1-47, 1986.
51. MIELE, A., WANG, T., MELVIN, W. W., and BOWLES, R. L., "Maximum Survival Capability of an Aircraft in a Severe Windshear", *Journal of Optimization Theory and Applications*, Vol. 53, No. 2, pp. 181-217, 1987.
52. MIELE, A., WANG, T., and MELVIN, W. W., "Quasi-Steady Flight to Quasi-Steady Flight Transition in a Windshear: Trajectory Optimization and Guidance", *Journal of Optimization Theory and Applications*,

Vol. 54, No. 2, pp. 203-240, 1987.

53. MIELE, A., WANG, T., TZENG, C. Y., and MELVIN, W. W., "Optimal Abort Landing Trajectories in the Presence of Windshear", *Journal of Optimization Theory and Applications*, Vol. 55, No. 2, pp. 165-202, 1987.
54. MIELE, A., WANG, T., and MELVIN, W. W., "Optimization and Acceleration Guidance of Flight Trajectories in a Windshear", *Journal of Guidance, Control, and Dynamics*, Vol. 10, No. 4, pp. 368-377, 1987.
55. MIELE, A., WANG, T., WANG, H., and MELVIN, W. W., "Optimal Penetration Landing Trajectories in the Presence of Windshear", *Journal of Optimization Theory and Applications*, Vol. 57, No. 1, pp. 1-40, 1988.
56. MIELE, A., WANG, T., and MELVIN, W. W., "Quasi-Steady Flight to Quasi-Steady Flight Transition for Abort Landing in a Windshear: Trajectory Optimization and Guidance", *Journal of Optimization Theory and Applications*, Vol. 58, No. 2, pp. 165-207, 1988.
57. MIELE, A., WANG, T., MELVIN, W. W., and BOWLES, R. L., "Gamma Guidance Schemes for Flight in a Windshear", *Journal of Guidance, Control, and Dynamics*, Vol. 11, No. 4, pp. xxx-xxx, 1988.
58. MIELE, A., and WANG, T., "Optimal Trajectories for Flight in a Windshear: Take-Off, Abort Landing, and Penetration Landing", Paper No. IMACS-88-314, 12th IMACS World Congress on Scientific Computation, Paris, France, 1988.
59. MIELE, A., WANG, T., and MELVIN, W. W., "Penetration Landing Guidance Trajectories in the Presence of Windshear", Paper No. AIAA-88-4069, AIAA Guidance, Navigation, and Control Conference, Minneapolis, Minnesota, 1988.
60. MIELE, A., WANG, T., and MELVIN, W. W., "Optimization and Guidance of Landing Trajectories in a Windshear", Paper No. ICAS-88-332, 16th Congress of the International Council of the Aeronautical Sciences, Jerusalem, Israel, 1988.

#### Hypervelocity Flight

61. SÄNGER, E., and BREDT, I., "A Rocket Drive for Long Range Bombers", Navy Department, Bureau of Aeronautics, Translation No. CGD-32, 1944.
62. ALLEN, H. J., and EGGERS, A. J., "A Study of the Motion and Aerodynamic Heating of Missiles Entering the Earth's Atmosphere at High Supersonic Speeds", NACA, Technical Note No. 4047, 1957.
63. EGGERS, A. J., ALLEN, H. J., and NEICE, S. E., "A Comparative Analysis of the Performance of Long-Range Hypervelocity Vehicles", NACA, Technical Note No. 4046, 1957.
64. CHAPMAN, D. R., "An Approximate Analytical Method for Studying Entry into Planetary Atmospheres", NACA, Technical Note No. 4276, 1958.
65. CHAPMAN, D. R., "An Analysis of the Corridor and Guidance Requirements for Supercircular Entry into Planetary Atmospheres", NASA, Technical Report No. R-55, 1960.
66. MIELE, A., "Flight Mechanics, Vol. 1, Theory of Flight Paths", Chapters 13 and 14, Addison-Wesley Publishing Company, Reading, Massachusetts, 1962.
67. LOH, W. H. T., "Dynamics and Thermodynamics of Planetary Entry", Prentice Hall, Englewood Cliffs, New Jersey, 1963.
68. VINH, H. X., BUSEMANN, A., and CULP, R. D., "Hypersonic and Planetary Entry Flight Mechanics", University of Michigan Press, Ann Arbor, Michigan, 1980.

69. WALBERG, G. D., "A Survey of Aeroassisted Orbit Transfer", *Journal of Spacecraft and Rockets*, Vol. 22, No. 1, pp. 3-18, 1985.
70. MIELE, A., Editor, "Special Issue on Hypervelocity Flight", *Journal of the Astronautical Sciences*, Vol. 36, Nos. 1-2, January-June, 1988.
71. LONDON, H. S., "Change of Satellite Orbit Plane by Aerodynamic Maneuvering", *Journal of the Aerospace Sciences*, Vol. 29, No. 3, pp. 323-332, 1962.
72. PAINE, J. P., "Some Considerations on the Use of Lifting Reentry Vehicles for Synergetic Maneuvers", *Journal of Spacecraft and Rockets*, Vol. 4, No. 5, pp. 698-700, 1967.
73. ROSSLER, M., "Optimal Aerodynamic-Propulsive Maneuvering for the Orbital Plane Change of a Space Vehicle", *Journal of Spacecraft and Rockets*, Vol. 4, No. 12, pp. 1678-1680, 1967.
74. JOOSTEN, B. K., and PIERSON, B. L., "Minimum Fuel Aerodynamic Orbital Plane Change Maneuvers", Paper No. AIAA-81-0167, AIAA 19th Aerospace Sciences Meeting, St. Louis, Missouri, 1981.
75. KECHICHIAN, J. A., CRUZ, M. I., VINH, N. X., and RINDERLE, E. A., "Optimization and Closed-Loop Guidance of Drag Modulated Aeroassisted Orbital Transfer", Paper No. AIAA-83-2093, AIAA Flight Mechanics Conference, Gatlinburg, Tennessee, 1983.
76. CRUZ, M. I., "Trajectory Optimization and Closed-Loop Guidance of Aeroassisted Orbital Transfer", Paper No. AAS-83-413, AAS/AIAA Astrodynamics Conference, Lake Placid, New York, 1983.
77. VINH, N. X., and HANSON, J. M., "Optimal Aeroassisted Return from High Earth Orbit with Plane Change", *Acta Astronautica*, Vol. 12, No. 1, pp. 11-25, 1985.
78. MEASE, K. D., and VINH, N. X., "Minimum-Fuel Aeroassisted Coplanar Orbit Transfer Using Lift Modulation", *Journal of Guidance, Control, and Dynamics*, Vol. 8, No. 1, pp. 134-141, 1985.
79. HULL, D. G., GILTNER, J. M., SPEYER, J. L., and MAPAR, J., "Minimum-Energy-Loss Guidance for Aeroassisted Orbital Plane Change", *Journal of Guidance, Control, and Dynamics*, Vol. 8, No. 4, pp. 487-493, 1985.
80. MIELE, A., and VENKATARAMAN, P., "Optimal Trajectories for Aeroassisted Orbital Transfer", *Acta Astronautica*, Vol. 11, Nos. 7-8, pp. 423-433, 1984.
81. MIELE, A., and BASAPUR, V. K., "Approximate Solutions to Minimax Optimal Control Problems for Aeroassisted Orbital Transfer", *Acta Astronautica*, Vol. 12, No. 10, pp. 809-818, 1985.
82. MIELE, A., and VENKATARAMAN, P., "Minimax Optimal Control and Its Application to the Reentry of a Space Glider", *Recent Advances in the Aerospace Sciences*, Edited by L. Casci, Plenum Publishing Corporation, New York, New York, pp. 21-40, 1985.
83. MIELE, A., BASAPUR, V. K., and MEASE, K. D., "Nearly-Grazing Optimal Trajectories for Aeroassisted Orbital Transfer", *Journal of the Astronautical Sciences*, Vol. 34, No. 1, pp. 3-18, 1986.
84. MIELE, A., BASAPUR, V. K., and LEE, W. Y., "Optimal Trajectories for Aeroassisted, Coplanar Orbital Transfer", *Journal of Optimization Theory and Applications*, Vol. 52, No. 1, pp. 1-24, 1987.
85. MIELE, A., BASAPUR, V. K., and LEE, W. Y., "Optimal Trajectories for Aeroassisted, Noncoplanar Orbital Transfer", *Acta Astronautica*, Vol. 15, Nos. 6-7, pp. 399-411, 1987.
86. MEASE, K. D., "Optimization of Aeroassisted Orbital Transfer: Current Status", *Journal of the Astronautical Sciences*, Vol. 36, Nos. 1-2, pp. 7-33, 1988.
87. CALISE, A. J., "Singular Perturbation Analysis of the Atmospheric Orbital Plane Change Problem", *Journal of the Astronautical Sciences*, Vol. 36, Nos. 1-2, pp. 35-43, 1988.

88. GAMBLE, J. D., CERIMELE, C. J., MOORE, T. E., and HIGGINS, J., "Atmospheric Guidance Concepts for an Aeroassist Flight Experiment", *Journal of the Astronautical Sciences*, Vol. 36, Nos. 1-2, pp. 45-71, 1988.
89. HULL, D. G., McCLENDON, J. R., and SPEYER, J. L., "Aeroassisted Orbital Plane Change Using an Elliptic Drag Polar", *Journal of the Astronautical Sciences*, Vol. 36, Nos. 1-2, pp. 73-87, 1988.
90. HULL, D. G., McCLENDON, J. R., and SPEYER, J. L., "Improved Aeroassisted Plane Change Using Successive Approximation", *Journal of the Astronautical Sciences*, Vol. 36, Nos. 1-2, pp. 89-101, 1988.
91. MEASE, K. D., LEE, J. Y., and VINH, N. X., "Orbital Changes during Hypersonic Aerocruise", *Journal of the Astronautical Sciences*, Vol. 36, Nos. 1-2, pp. 103-137, 1988.
92. MIELE, A., LEE, W. Y., and MEASE, K. D., "Nearly-Grazing Optimal Trajectories for Aeroassisted, Noncoplanar Orbital Transfer", *Journal of the Astronautical Sciences*, Vol. 36, Nos. 1-2, pp. 139-157, 1988.
93. OBERLE, H. J., "Numerical Treatment of Minimax Optimal Control Problems with Application to the Reentry Flight Path Problem", *Journal of the Astronautical Sciences*, Vol. 36, Nos. 1-2, pp. 159-178, 1988.
94. VINH, N. X., and LU, P., "Chebyshev Minimax Problems for Skip Trajectories", *Journal of the Astronautical Sciences*, Vol. 36, Nos. 1-2, pp. 179-197, 1988.
95. NOAA, NASA, and USAF, "US Standard Atmosphere, 1976", US Government Printing Office, Washington, DC, 1976.

COMPARISON OF A MATHEMATICAL ONE-POINT MODEL AND A MULTI-POINT MODEL  
OF AIRCRAFT MOTION IN MOVING AIR<sup>\*)</sup>

by

R. Brockhaus

Technische Universität Braunschweig  
Hans-Sommer-Str. 66  
D-3300 Braunschweig  
Federal Republic of Germany

**Summary**

The steadily growing capacity of computers favours increasingly exact simulation of even complex processes. On the other hand, parameter identification and state estimation require much more precise models than are generally used for the design of feedback systems. In this paper, therefore, a multi-point model of the aircraft motion is proposed in which the different coupling effects between the two sub-processes, "aircraft" and "air flow", can be modelled with much higher accuracy than is obtained by using the ordinary one-point model, where all the force, moment and velocity vectors are referred to the aircraft center of gravity. The modelling of the effects of aircraft rotation, wing down-wash, wind gradients and other unstationary effects should be greatly improved by a multi-point approach, provided that the aerodynamic effects on the aircraft components (wing, fuselage, tail) can be described appropriately. The nonlinear equations of the total process are set up for the one-point and multi-point models and compiled into block-diagrams, from which the physical background of the interrelations between air and aircraft motion can be seen very clearly. The possible improvement in model quality and the additional computer capacity needed are estimated by comparing the two approaches.

**List of Symbols**

All the symbols used are from the ISO-standards /1/ and /2/ with the following additional symbols:

$u_{wx}$ = $\partial u_w / \partial x$	ect.	wind gradient component
$V_A$		vector of relative velocity between aircraft and air (airspeed)
$\Omega_A$		vector of relative rotational velocity between aircraft and air
$p_A, q_A, r_A$		components of $\Omega_A$
$\Omega_K = \Omega^{b_2}$		vector of aircraft rotational velocity relative to the Earth
$p_K, q_K, r_K$		components of $\Omega_K$
$\Omega_w$		vector of air rotational velocity relative to the Earth
$p_w, q_w, r_w$		components of $\Omega_w$
$r$		vector of aircraft position relative to a point fixed relative to Earth
$x_P$		vector of coordinates of point P in aircraft body fixed axes
$Q$		resulting moment vector

<sup>\*)</sup> This article has first been published in the *Zeitschrift für Flugwissenschaften und Weltraumforschung* 11 (1987) p. 174 - 184 under the title "A mathematical multi-point model for aircraft motion in moving air". It is reproduced here with slight modifications.

## 1. Introduction

The complete mathematical model of the aircraft motion is very complex, because it has to describe the reciprocal action of different physical processes, the main ones being:

- the motion of the surrounding air mass,
- the motion of the rigid aircraft,
- the degrees of freedom of the flexible aircraft and their interactions with the airflow,
- unsteady aerodynamic effects,
- the engines.

It is therefore impossible to describe the "aircraft motion" process completely. The model has to be simplified and reduced to a partial one to suit the specific problem. The models used, up to now, for control system design or real-time simulation, have usually treated the aircraft as a one-point mass and referred all the forces and moments to the center of gravity. This approach demands simplifications which are sometimes quite serious, especially with respect to aircraft rotation, wind gradients, downwash flow, engine airstream, ground effect and other unsteady effects on the generation of forces and moments /5/. Since it was mainly linearized equations which were used, the approximations were adequate and remain so for analytical calculations in the future. Linear or non-linear equations based on these assumptions are also still quite suitable for the design of flight control systems because of their inherent insensitivity to parameter uncertainties /8/.

However, this is not true in the case of parameter identification or state estimation and filtering. These methods react very sensitively to model errors and may then produce totally wrong results /16/. The shortcomings of the one-point model appear first in the longitudinal equations, where the modelling of the downwash is very much simplified by the use of time derivative of the state variable  $\alpha$  (which is most awkward in numerical simulation). Secondly, the modelling of the wind gradient effects in the lateral equations is quite difficult and can only be represented very roughly by rotary derivatives. Thirdly, the model of engine flow effects and of the aerodynamic coupling between longitudinal and lateral equations should be improved.

All these problems can be alleviated if the equations of aircraft motion are based on a multi-point approach where the forces and moments are calculated separately for different points of the aircraft, e.g. wing, tailplane and fin, as a function of the local air flow. Such a model is derived in this paper, assuming that adequate models for the aerodynamic effects on the separate aircraft components as wing, fuselage and tailplane, can be found, and it is compared to the one-point approach. Both models show the strong low-frequency coupling between air and aircraft motions. The higher frequency coupling, however, which primarily affects the rotational degrees of freedom, is expressed much more precisely and clearly in the multi-point approach. For simplicity, the aircraft is here considered to be a rigid body and unsteady aerodynamic effects (such as the time delay in flow circulation changes) are neglected. The multi-point approach could, however, be extended to elastic and unsteady effects if needed. To simplify the equations, only two different coordinate systems are used: (local) velocity, force and moment vectors are calculated in the aircraft body axes system, whereas the aircraft flight path, the local wind velocity and the wind gradients are calculated in the aircraft carried Earth axes (inertial) system.

The equations of both models are assembled into a block diagram, from which the physical interrelations of the two subprocesses, "air motion" and "aircraft motion", can be seen very clearly. These block-diagrams permit estimation of the amount of additional computing capacity and they may also be used to set up a modular simulation program.

## 2. Modelling the wind effects on the aircraft (one-point model)

The wind process can be represented by a three-dimensional wind vector field which is changing in space and time according to statistical and deterministic laws. The effects of this wind-field on the aircraft flying through it are primarily generated by the stationary wind and the components of the wind gradient at the instantaneous location of the aircraft. These wind gradients are shown to represent the primary disturbing inputs to the aircraft motion while the coupling between the air and aircraft motions are represented by additional states of the overall process /6/.

### 2.1 Translational effects

The aerodynamic forces acting on the aircraft depend on the aircraft shape, the air density and the relative motion between the aircraft and the surrounding air mass, i.e. on the vector

$$(2.1) \quad \mathbf{V}_A = \mathbf{V}_K - \mathbf{V}_W$$

of the relative velocity between the aircraft ( $\mathbf{V}_K$ ) and the air ( $\mathbf{V}_W$ ) and

$$(2.2) \quad \Omega_A = \Omega_K - \Omega_W$$

the vector of the relative rotational velocity between the aircraft ( $\Omega_K$ ) and the air ( $\Omega_W$ ). To model the aircraft dynamics exactly, the "air motion" process has to be described in addition to the "aircraft motion" process. Figure 1 shows a simplified wind field where the z-component  $w_{Wz}$  is a two-dimensional sinusoidal function of space. The air velocity change "seen" by the aircraft can be described by the following equation:

$$(2.3) \quad \frac{dV_W}{dt} = \frac{\partial V_W}{\partial t} + \frac{\partial V_W}{\partial r} \frac{dr}{dt}$$

The first term  $\partial V_W / \partial t$  is usually neglected because the wind-field can be considered as approximately "frozen" (steady state) as long as the aircraft velocity is high compared to the change of air velocity with time /5/. This assumption is valid, except in extremely low speed flight, because on one hand, the effect of higher frequency wind motion (with frequencies above the aircraft short period modes) cannot be modelled exactly by quasi-steady aerodynamics and, on the other hand, the low frequency wind effects are homogeneous over a large area and change quite slowly with time. This is especially true for quasi-steady air streams and wind shear conditions. Equation 2.3, in Earth axes, is written:

$$(2.4) \quad \begin{bmatrix} \dot{u}_W \\ \dot{v}_W \\ \dot{w}_W \\ \dot{w}_{Wz} \end{bmatrix}_G = \frac{\partial}{\partial t} \begin{bmatrix} u_W \\ v_W \\ w_W \\ w_{Wz} \end{bmatrix}_G + \begin{bmatrix} u_{Wx} & u_{Wy} & u_{Wz} \\ v_{Wx} & v_{Wy} & v_{Wz} \\ w_{Wx} & w_{Wy} & w_{Wz} \end{bmatrix}_G \begin{bmatrix} \cos\gamma \cos\chi \\ \cos\gamma \sin\chi \\ -\sin\gamma \end{bmatrix} V_K$$

This differential equation describes the wind components at the actual aircraft position. The matrix elements

$$(2.5) \quad u_{Wx} = \partial u_{Wx} / \partial x \text{ etc.}$$

are the local wind gradient components. These are the real disturbance input variables to the aircraft. This model eliminates the error usually made by introducing "Taylor's hypothesis", in which the space-distribution of wind velocity is converted into a function of time without considering the flight path vector variations. The components of the wind velocity at the aircraft's position result from the integration of Equation (2.3).

The wind gradient components are a function of the local meteorological situation and contain low frequency deterministic and higher frequency stochastic elements. The model of this wind process cannot be derived here, it has been considered elsewhere, e.g. in /7, 11, 13/. Figure 2 shows the results of wind measurements as a function of height in a region up to 500 m from the ground. It can be seen that the wind velocity can be separated into a lower frequency part (wind shear) with gradients up to 0.2 m/s/m and a higher frequency part, which can best be described by statistical models, such as the Dryden spectrum /7/.

Figure 3 shows the wind vector distribution in the x-z plane of a typical thunderstorm situation where the aircraft encounters rapid changes of wind vector in amplitude and direction. The wind vector acts on the aircraft forces and moments through Equations (2.1) and (2.2) because the latter depend directly on  $V_A$  and  $\Omega_A$ . These are complex, nonlinear functions of air density  $\rho$ , airspeed  $V_A$ , Mach number M, angle of attack  $\alpha$ , sideslip angle  $\beta$  and other variables; for example the aerodynamic X-force is given by the equation

$$(2.6) \quad X^A = \frac{\rho}{2} V_A^2 S C_W (M, \alpha, \dot{\alpha}, \beta, q_A, \eta, \eta_K, \dots)$$

### 2.2 Rotational effects

The wind effect, as described so far, is due to the influence of the local wind vector at the center of gravity of the aircraft, considered as a one point mass, resulting in a variation of  $V_A$ ,  $\alpha$  and  $\beta$ . This can be considered to be the zero order term of a Taylor series of the wind effect. The first order term of this Taylor series turns out to be the effect of a linear wind distribution on the aircraft body, as is shown in Figure 4 for a sinusoidal vertical wind-field. These linear terms, which are described by the local components of the wind gradient, may be introduced into the usual aircraft equations as the effects of a rotating air mass. This leads to a relatively simple model, because the way in which the aerodynamic derivatives depend on the aircraft rates p, q and r is known. The local air rotational velocity vector can be represented by a vector function as follows, where  $M_{bg}$  is the transformation matrix between Earth-fixed and body-fixed coordinates:

$$(2.7) \quad \Omega_{wb} = \begin{bmatrix} p_W \\ q_W \\ r_W \end{bmatrix}_b = M_{bg} \begin{bmatrix} w_{Wy} & -v_{Wz} \\ u_{Wz} & -w_{Wx} \\ v_{Wx} & -u_{Wy} \end{bmatrix}_g$$

This is illustrated by Figure 5, where all the gradients are introduced with positive sign and are defined in aircraft coordinates. Because of the law of continuity, the gradients are not independent of each other. Figure 6 shows two extreme situations; in general, any intermediate state, whose relative amplitude varies with time, may exist. Figure 6 makes clear that a representation of these effects by rate derivatives is an approximation which is only valid in cases corresponding to Figure 6b. A better model will be introduced in Sect. 4.

The three wind gradient components which are not incorporated in Eq. (2.7), the diagonal elements  $u_{wx}$ ,  $v_{wy}$ , and  $w_{wz}$ , result in an inhomogeneous distribution of the airflow in the directions of the aircraft axes, as illustrated in Figure 7. As these effects are probably small and cannot be measured in flight, they are usually neglected.

From the reconstruction of down-draughts in thunderstorms /9/ and from extended flight measurements /13, 14/ maximum wind shear gradients have been calculated and are summarized in Table 1. The differential wind values in Table 1, calculated for an Airbus (length 52 m, overall-height 16 m, minimum speed 70 m/s), give a rough idea of the possible influence of these gradients. Additional estimations should be made for the higher frequency case.

	wind gradient 1/s	differential wind $\Delta V_w$
$u_{wx}$	0,03	1,6 m/s
$u_{wz}, v_{wz}$	0,13	2,1 m/s
$w_{wz}$	0,18	2,9 m/s

Table 1 Effect of wind gradients on differential velocities at aircraft extremities

For more exact models, the Taylor series of wind effects (Figure 4) should be continued with higher order terms, thus further approximating a sinusoidal distribution. This would call for the introduction of the local derivatives of wind gradients and would greatly complicate the model. However, since the corresponding wind model and the effects of nonlinear wind distributions on the aerodynamic forces are hardly known and the elastic modes have been neglected here, the higher order terms are also neglected. The linear model is valid as long as the wavelength of the air motion is 8-12 times larger than the aircraft dimensions. This is true for both the approximation of sinusoidal distribution and the quasi-steady model of aerodynamic force generation /11/. This also means that the wind model must be restricted to frequencies not higher than those of the short period modes of the aircraft.

### 2.3 Block diagram of the wind equations

From the block diagram of Figure 8, it may be seen that the wind equations are characterized by three dynamical states, the three components of the wind vector  $V_{wg}$ . The wind-field, as a physical process, does, of course, contain additional states but no detailed model can be given here (see e.g. /7/). It can also be seen that there is a strong coupling between the two processes (wind and aircraft), given by the feedback of  $V_{kg}$  and  $r$ , which determine the wind vector and its gradients at the aircraft's momentary position /15/.

## 3. The equations of the coupled process (one point model)

### 3.1 The force and moment equations

The most practicable way of writing down the non-linear equations of aircraft motion in moving air, especially for the purpose of numerical simulation, is to write down the forces and moment equations in body axes. For transport aircraft, the earth rotation can be neglected and the earth surface considered as flat, the Earth axes system thus being identical to the inertial space. The force and moment vector equations in body axes are as follows:

$$(3.1) \quad m \left[ \frac{\partial V_K}{\partial t} + \Omega^{bs} \times V_K \right]_b = R_b^A + R_b^F + M_{bg} G$$

$$(3.2) \quad \left[ I \frac{\partial \Omega^{bs}}{\partial t} + \Omega^{bs} \times I \Omega^{bs} \right]_b = Q_b^A + Q_b^F$$

Equations (3.1) and (3.2) both represent the equilibrium at the aircraft center of gravity. Here  $R_b^A$  and  $Q_b^A$  are the resulting vectors of aerodynamic forces and moments in body coordinates and  $R_b^F$  and  $Q_b^F$  are the resulting force and moment vectors of engine thrust.  $I$  is the inertia tensor of the aircraft

$$(3.3) \quad I = \begin{bmatrix} I_x & -I_{xy} & -I_{xz} \\ -I_{xy} & I_y & -I_{yz} \\ -I_{xz} & -I_{yz} & I_z \end{bmatrix}$$

where  $I_{xy}$  and  $I_{yz}$  are zero for symmetrical aircraft.  $\Omega^{bs}$  is the vector of aircraft rotation relative to the Earth expressed in body axes

$$(3.4) \quad \Omega^{bs} = \Omega_{kb} = \begin{bmatrix} p_K \\ q_K \\ r_K \end{bmatrix}_b$$

and  $M_{bg}$  represents the transformation matrix from Earth axes into body axes /2/.

$$(3.5) \quad M_{bg} = M_{gb}^T = \begin{bmatrix} \cos\theta \cos\psi & \cos\theta \sin\psi & -\sin\theta \\ \sin\phi \sin\theta \cos\psi & \sin\phi \sin\theta \sin\psi & \sin\phi \cos\theta \\ -\cos\phi \sin\psi & +\cos\phi \cos\psi & \\ \cos\phi \sin\theta \cos\psi & \cos\phi \sin\theta \sin\psi & \cos\phi \cos\theta \\ +\sin\phi \sin\psi & -\sin\phi \cos\psi & \end{bmatrix}$$

The angular relationships between the two coordinate systems and the velocity vectors are shown in Figure 9. Equation (3.1) reads in detail, after dividing by the aircraft mass

$$(3.6) \quad \begin{bmatrix} \dot{u}_K \\ \dot{v}_K \\ \dot{w}_K \end{bmatrix}_b = \frac{1}{m} \begin{bmatrix} X^A + X^F \\ Y^A + Y^F \\ Z^A + Z^F \end{bmatrix}_b + M_{bg} \begin{bmatrix} 0 \\ 0 \\ g \end{bmatrix} - \begin{bmatrix} q_K w_K - r_K v_K \\ r_K u_K - p_K w_K \\ p_K v_K - q_K u_K \end{bmatrix}_b$$

Integrating this equation gives the three components of the aircraft translational velocity in body coordinates. From these, the polar components of aircraft velocity (flight path velocity  $V_K$ , flight path azimuth  $\chi$  and flight path angle  $\gamma$ ) can be calculated by using the following transformation

$$(3.7) \quad V_{Kg} = \begin{bmatrix} u_K \\ v_K \\ w_K \end{bmatrix} = M_{gk} V_K = \begin{bmatrix} \cos\gamma \cos\chi \\ \cos\gamma \sin\chi \\ -\sin\gamma \end{bmatrix} V_K.$$

The polar components are found to be

$$(3.8) \quad V_K = \sqrt{u_{Kg}^2 + v_{Kg}^2 + w_{Kg}^2}$$

$$(3.9) \quad \chi = \arctan v_{Kg}/u_{Kg}$$

$$(3.10) \quad \gamma = -\arcsin w_{Kg}/V_K$$

The detailed moment equation (3.2) for a symmetrical aircraft is

$$(3.11) \quad \begin{bmatrix} \dot{p}_K \\ \dot{q}_K \\ \dot{r}_K \end{bmatrix}_b = I^{-1} \begin{bmatrix} L^A + L^F \\ M^A + M^F \\ N^A + N^F \end{bmatrix}_b - I^{-1} \begin{bmatrix} q_K r_K (I_z - I_y) - p_K q_K I_{xz} \\ r_K p_K (I_x - I_z) + (p_K^2 - r_K^2) I_{xz} \\ p_K q_K (I_y - I_x) + p_K r_K I_{xz} \end{bmatrix}_b$$

which gives the three components of the aircraft rotation. If the aerodynamic derivatives are given in aerodynamic or experimental coordinates, they have first to be transformed into body coordinates /4/.

### 3.2 The equations for angular and translational position

The differential equation for the Euler angles /1/

$$(3.12) \quad \frac{d\Theta}{dt} = \begin{bmatrix} \dot{\phi} \\ \dot{\theta} \\ \dot{\psi} \end{bmatrix} = M_{\Theta\Omega} \Omega_{kb} = \begin{bmatrix} 1 & \sin\theta \tan\theta & \cos\theta \tan\theta \\ 0 & \cos\theta & -\sin\theta \\ 0 & \sin\theta/\cos\theta & \cos\theta/\cos\theta \end{bmatrix} \begin{bmatrix} p_K \\ q_K \\ r_K \end{bmatrix}_b$$

and the integration of the velocity vector

$$(3.13) \quad \frac{dr}{dt} = \begin{bmatrix} \dot{x} \\ \dot{y} \\ \dot{z} \end{bmatrix}_g = V_{Kg} = \begin{bmatrix} u_K \\ v_K \\ w_K \end{bmatrix}_g$$

give the six additional components of the angular ( $\Theta$ ) and translational position ( $r$ ) relative to the Earth.

### 3.3 The wind equations

The fifth differential vector equation is given by Equation (2.3), for which the local wind gradient components are the input variables (they should be stored as disturbances in a numerical simulation program). A constant wind velocity has to be taken into account by the initial condition  $V_{Wg}(0)$ .

$$(2.3) \quad \frac{dV_{Wg}}{dt} = \frac{\partial V_{Wg}}{\partial t} + \frac{\partial V_{Wg}}{\partial r} \frac{dr}{dt}$$

As derived in Sect. 2, the wind effects are described by three additional algebraic equations for the airspeed vector (see Eq. 2.1) in body axes

$$(3.14) \quad V_{Ab} = M_{bg} (V_{Kg} - V_{Wg})$$

for the vector of relative rotation

$$(2.2) \quad \Omega_{Ab} = \Omega_{Kb} - M_{bg} \Omega_{Wg}$$

and for the wind rotation

$$(2.7) \quad \Omega_{Wg} = M_{bg} \begin{bmatrix} w_{Wy} - v_{Wz} \\ u_{Wz} - w_{Wx} \\ v_{Wx} - u_{Wy} \end{bmatrix}$$

### 3.4 The equations for the vector of the resultant forces and moments

The aircraft motion finally is generated by the aerodynamic and engine forces which can only be written down here in a global way. The vector of resultant aerodynamic forces is

$$(3.15) \quad R^A = f(\rho, M, V_A, \alpha, \beta, \dot{\alpha}, \dot{\beta}, p_A, q_A, r_A, \xi, \zeta, \eta, \eta_K, \dots),$$

the vector of the resultant aerodynamic moment is

$$(3.16) \quad Q^A = g(\rho, M, V_A, I_{\mu}, \alpha, \beta, \dot{\alpha}, \dot{\beta}, p_A, q_A, r_A, \xi, \zeta, \eta, \eta_K, \dots),$$

the vector of the engine thrust force is

$$(3.17) \quad R^F = h(\rho, M, f, \alpha, \dots)$$

and the moment resulting from the engine thrust is

$$(3.18) \quad Q^F = k(\rho, M, f, \alpha, x_p, \dots)$$

where  $f$  is the throttle input and  $x_p$  is the radius vector of the thrust relative to the center of gravity. The first two equations are highly non-linear, multi-dimensional functions which follow from wind-tunnel measurements and aerodynamic calculations; they are usually simplified, especially with respect to unsteady and aeroelastic effects and multi-variable functions. The thrust equations are also quite complex functions which have to be simplified. Time derivatives of  $V_A$ ,  $\alpha$  and  $\beta$  also have to be introduced into Eqs. (3.15) and (3.16). The time-derivative of  $V_A$  in body axes is given by the Euler equation

$$(3.19) \quad \frac{\partial V_{Ab}}{\partial t} = \frac{dV_{Ab}}{dt} - \Omega_{Ab}^* \times V_{Ab}$$

To calculate the right hand term, Equation (2.3) should not itself be integrated, but should be introduced into the differentiated Equation (2.1) as follows:

$$(3.20) \quad \frac{dV_{Ag}}{dt} = \frac{dV_{Kg}}{dt} - \frac{dV_{Wg}}{dt} = M_{gb} (R^A + Q^A)_b + G_g - \frac{\partial V_{Wg}}{\partial r} V_{Kg}$$

The variables  $\dot{V}_A$ ,  $\dot{\beta}$  and  $\dot{\alpha}$  can be calculated from the time derivative  $\partial V_A / \partial t$  in body coordinates, using Equation (3.21) and inverting the matrix on the right hand side:

$$(3.21) \quad \begin{bmatrix} \dot{u} \\ \dot{v} \\ \dot{w} \end{bmatrix}_b = \frac{d}{dt} \begin{bmatrix} V \cos \alpha \cos \beta \\ V \sin \beta \\ V \sin \alpha \cos \beta \end{bmatrix} = \begin{bmatrix} \cos \alpha \cos \beta & -V \cos \alpha \sin \beta & -V \sin \alpha \cos \beta \\ \sin \beta & V \cos \beta & 0 \\ \sin \alpha \cos \beta & -V \sin \alpha \sin \beta & V \cos \alpha \cos \beta \end{bmatrix} \begin{bmatrix} \dot{V} \\ \dot{\beta} \\ \dot{\alpha} \end{bmatrix}$$

Equations (3.19) to (3.21) represent a tremendous computational task to model a small effect. In most cases, only the time derivative of the angle of attack  $\alpha$  is needed because the effects of  $\dot{V}$  and  $\dot{\beta}$  are not well known. The equations should therefore be simplified considerably. In numerical simulations, however,  $\dot{\alpha}$  is usually calculated by numerical differentiation.

### 3.5 The range of validity of the equations

The validity of the equations which have been derived so far is restricted by the simplifications introduced in Sects. 2 and 3:

- aircraft considered as rigid body,
- quasi-steady aerodynamic effects,
- one point model,

and by the simplifications of the wind model introduced in Sect. 2, especially by replacing the gradient effects by wind rotation. The equations may be further simplified by the following assumptions:

- excluding high turn rates ( $p_K$ ,  $q_K$  and  $r_K$  small)
- airspeed vector almost along the aircraft longitudinal axes ( $\alpha$  and  $\beta$  small),

and by simplifying the aerodynamic functions in Eqs. (3.15) and (3.16). Again, the transformation matrices may be simplified by assuming that the flight path velocity vector  $V_K$  is almost along the aircraft longitudinal axes, i.e. assuming that the angles  $\Theta - \gamma$  and  $\chi - \Psi$  are small too /10/.

### 3.6 Discussion of the coupling between air and aircraft motion

The relationships between the whole set of equations are illustrated by the diagrams which follow. They contain all the transformations and feedback effects. Figure 10 contains the force and moment equations - the numbers refer to the equations given in the text. Their inputs are given by the vectors  $\Omega_{WG}$  and  $V_{WG}$ , which are the output vectors of the wind process shown in Figure 8. This part of the overall model will be modified in Sect. 4. Figure 11 shows the four state equations of the aircraft motion with the resultant forces and moments as input vectors and from which the twelve states of translational and rotational motion are integrated. This part of the model remains unchanged in Sect. 4 in which a multi point model is introduced.

(1.) The rigid body motion of the aircraft is governed by twelve state variables (which define the translational and rotational velocity and position components). Three additional state variables (components of the wind velocity) describe the coupling between air and aircraft motions. In the case where  $dV_W/dr = 0$ , the vectors  $V_A$  and  $V_K$  differ only by the constant vector  $V_W(0)$ , and  $\Omega_W$  is zero.

(2.) The choice of state variables in the present paper leads to a very clear modelling of the physical coupling between the two processes and uses a minimum number of transformation matrices. It therefore seems to be advantageous for the analysis of non-linear equations and for numerical simulation purposes.

(3.) The aerodynamic effects on the aircraft are generated exclusively by the air density, by the relative motion between the aircraft and the air, and by the aerodynamic control surfaces. These include the main disturbance and control inputs (in addition to engine thrust and variations of mass distribution). The well-known feedback effects of aircraft motion on the aerodynamic forces are represented by inner feedback loops of the aircraft sub-process.

(4.) If the wind process is modelled by a vector field in space, its effect on the aircraft flying through this field can be described by mathematical vector functions. The wind effect on the airspeed vector is thus represented exactly, eliminating the errors resulting from the use of "Taylor's hypothesis". The wind effect on the non-uniform distribution of forces and moments over the aircraft dimensions is only represented approximately. This, however, has the advantage, that the well-known rotary aerodynamic derivatives can be retained to provide a rough approximation for the wind effects.

(5.) It is shown that the wind does not act as an independent disturbance process on the aircraft but that the two processes are coupled. There are three different feedback effects, which are represented by three external feedback loops connecting the two sub-processes:

(a) The momentary aircraft position  $r(t)$  determines the local wind vector and wind gradient acting on the aircraft.

(b) The flight path velocity vector  $V_K(t)$  influences the instantaneous variation of the wind vector [Eq. (2.3)] and, together with the wind vector, generates the airspeed vector [Eq. (2.2)]. These feedback loops represent the most critical coupling effects between the two sub-processes because both affect the phugoid stability /9/.

(c) The Euler angles  $\Theta(t)$  determine the transformation of the wind gradients from Earth axes into aircraft body axes, and thus affect the unsteady wind effects, especially on the moment equations. As there are very few measurements of wind gradients in Earth coordinates (the gust models are mostly derived from flight tests i.e. from measurements in body axes), practically nothing is known about the importance of this feedback.

#### 4. Presentation of a multi-point model

The previous sections have shown that the quasi-steady concept, where all the force and velocity vectors are referred to the center of gravity (one point model), involves extensive simplifications with respect to the aerodynamic effects of

- the aircraft rotation,
- the downwash from the wing,
- the engine flow,
- the wind gradients,
- the aircraft elastic modes.

A really new way of improving the mathematical model is to calculate the local air velocity vector separately for the different parts of the aircraft (as e.g. wing, body, tailplane and fin), and to determine the local forces and moments from the results. Given the capacity of existing large computers, even a calculation with distributed parameters seems to be possible (e.g. using finite element methods), but this would call for a tremendous amount of calculations and would not be practicable for real time simulations. In this paper, therefore, the force and velocity vectors are concentrated in a few distinct points, thus limiting the computation effort. However, the basic concept of the multi-point model could, if necessary, be generalized later. The velocity vector at a given point on the aircraft is composed of its average value (at the center of gravity)  $V_{CG}$  and the supplementary values  $\Delta V$  generated by the various local effects. It is therefore crucial to distinguish clearly between velocity components of the aircraft ( $V_K$ ) and those of the surrounding airflow ( $V_W$ ), the local airspeed vector  $V_A$  then resulting from the application of Eq. (2.1) to each point. The local forces and moments are calculated separately and are then combined to give the overall force and moment components with respect to the centre of gravity. To facilitate this compilation, all local force, moment and velocity vectors are defined in aircraft body axes.

##### 4.1 The effect of aircraft rotation

First, the supplementary value of airspeed, generated by aircraft rotation alone, is calculated. Figure 12 illustrates the motion of a point P (e.g. the right wing neutral point) with respect to the center of gravity in case of a yawing velocity  $r_K$ . The relative velocity of P in body coordinates is given by:

$$(4.1) \quad \Delta V_K(P, r_K) = \begin{bmatrix} -r_K y_P \\ +r_K x_P \\ 0 \end{bmatrix}$$

where  $x_P$  and  $y_P$  are the coordinates of P in body axes, taken as positive in the coordinate directions. Under a generalized rotation  $\Omega_K$  of the aircraft, the local velocity increment is found to be

$$(4.2) \quad \Delta V_K(P, \Omega_K) = \Omega_K \times \mathbf{x}_P = \begin{bmatrix} q_K z_P - r_K y_P \\ r_K x_P - p_K z_P \\ p_K y_P - q_K x_P \end{bmatrix}$$

The local airspeed vector at point P with aircraft rotation is then

$$(4.3) \quad V_A(P) = V_{Acg} + \Delta V_K(P, \Omega_K)$$

The effect of elastic modes on the relative velocities could be similarly modelled. From these, the local forces and moments can be calculated, as is shown in Section 4.4.

##### 4.2 The effect of wind gradients

Taking the  $x-y$  plane as an example, Figure 13 shows how the wind velocity at a point P is influenced by the wind gradients in body coordinates  $v_{Wx}$  and  $w_{Wx}$ . This is represented by the following expression:

$$(4.4) \quad \Delta V_W(P, v_{Wx}, w_{Wy}) = \begin{bmatrix} 0 \\ +v_{Wx} z_P \\ +w_{Wy} y_P \end{bmatrix}$$

The general three-dimensional case is given by

$$(4.5) \quad \Delta V_W(P) = \frac{\partial V_W}{\partial r} \Big|_b x_P = \begin{bmatrix} u_{Wx} & u_{Wy} & u_{Wz} \\ v_{Wx} & v_{Wy} & v_{Wz} \\ w_{Wx} & w_{Wy} & w_{Wz} \end{bmatrix} \begin{bmatrix} x_P \\ y_P \\ z_P \end{bmatrix}_b$$

where the wind gradient matrix has to be transformed into body coordinates

$$(4.6) \quad \frac{\partial V_W}{\partial r} \Big|_b = M_{bg} \frac{\partial V_W}{\partial r} \Big|_g$$

The local airspeed vector at point P in a general homogeneous wind field is, from Eq.(2.1):

$$(4.7) \quad V_A(P) = V_{Acg} - \Delta V_W(P)$$

#### 4.3 The effect of wing downwash and engine flow

Figure 14 illustrates the generation of a supplementary air velocity vector at the tailplane position due to an air-stream caused by wing downwash and by the engine or airscrew. The downwash roughly induces a positive z-component of  $\Delta V_W$ , whereas the engine flow results in a velocity increment  $V_T$  and e.g. in a negative y-component in positive sideslip conditions. As the calculation of the induced flow is very complex and is highly dependent on the aerodynamic state of the wing (lift, sideslip-angle etc) and the aircraft configuration (relative position of wing and tailplane, flap position etc), no specific equation can be given here. This effect of reciprocal coupling between aircraft and airflow can only be expressed generally, as follows:

$$(4.8) \quad \Delta V_D(P) = f(P, V_A, C_L, \beta, \eta_K, \dots F \dots t)$$

It has to be modelled individually for each aircraft. A downwash change, following a lift, a configuration or wind velocity change moves at the local airspeed  $V_A$  towards the tail. Its effect on the tailplane is therefore subject to a delay time

$$(4.9) \quad \tau = |x_{TP}| / V_A$$

where  $x_{TP}$  is the distance between the wing and tailplane neutral points. The same is true for the effect of  $\beta$ -changes on the fin. This delay has to be greatly simplified in one point models where it is generally represented by the "quasi-steady" derivatives:

$C_{L\dot{\alpha}}$ ,  $C_{D\dot{\alpha}}$ ,  $C_{m\dot{\alpha}}$ ,  $C_{n\dot{\beta}}$  etc.

where e.g. (see / 3 /)

$$(4.10) \quad C_{m\dot{\alpha}} = \frac{\partial C_m}{\partial (\frac{\dot{\alpha}}{V_0})} = - \frac{S_T}{S} \left[ \frac{V_{AT}}{V_A} \right]^2 \left[ \frac{x_{TP}}{l_\mu} \right]^2 C_{A\alpha T} \epsilon$$

with  $V_{AT}$  airspeed at tailplane position  
 $\epsilon$  downwash-angle

It is obvious, that this can be modelled much more precisely in multi-point models, thus making the derivatives mentioned unnecessary.

A second time-dependent effect is due to the fact that the circulation around the wing cannot change abruptly after flow changes but builds up with an approximately first order time lag (Wagner- and Küsaner-effect). This too, can be modelled more precisely in a multi-point model, where a new differential equation can be introduced to represent the dependency on time / 12 /.

Finally, the ground effect can be much better represented by the present model than by the one - point model. The change in the local air velocity vector induced by the aircraft approaching the ground can be calculated for different points of the aircraft. All these effects are examples of the very tight feedback coupling between the aircraft and the surrounding airflow; these cannot be neglected in realistic models of aircraft motion.

#### 4.4 The complete local airspeed vector

All the partial velocity vectors can now be summed according to Eq. (1) to give the complete airspeed vector at the point considered.

$$(4.11) \quad \mathbf{V}_A(P) = \mathbf{V}_{KcG} - \mathbf{V}_{WcG} + \Delta \mathbf{V}_K(P, \Omega_K) - \Delta \mathbf{V}_W(P) - \Delta \mathbf{V}_{WD}(P)$$

The aerodynamic effects at the point P are calculated from this vector.

#### 4.5 The calculation of local forces and moments

From Eqs. (3.15) and (3.16), the aerodynamic forces and moments are functions of airspeed, angle of attack and angle of sideslip. The local values of these three variables can be calculated from the local airspeed vector  $\mathbf{V}_A(P)$  by using the transformation

$$(4.12) \quad \mathbf{V}_{Ab} = \begin{bmatrix} u_A \\ v_A \\ w_A \end{bmatrix}_b = \mathbf{M}_{ba} \mathbf{V}_{Aa} = \begin{bmatrix} \cos\alpha \cos\beta \\ \sin\beta \\ \sin\alpha \cos\beta \end{bmatrix} V_A$$

from which the polar coordinates of  $\mathbf{V}_A$  are found to be

$$(4.13) \quad V_A(P) = \sqrt{u_A^2(P) + v_A^2(P) + w_A^2(P)}$$

$$(4.14) \quad \alpha(P) = \arctan w_A(P)/u_A(P)$$

$$(4.15) \quad \beta(P) = \arcsin v_A(P)/V_A(P)$$

These are the input variables to the aerodynamic forces and moment relationships

$$(4.16) \quad \mathbf{R}^A(P) = \rho/2 S V_A^2(P) \mathbf{C}_R [M(P), \alpha(P), \beta(P), \xi, \zeta, \eta, \eta_K, \dots]$$

$$(4.17) \quad \mathbf{Q}^A(P) = \rho/2 S V_A^2(P) l_\mu \mathbf{C}_Q [M(P), \alpha(P), \beta(P), \xi, \zeta, \eta, \eta_K, \dots]$$

where  $\mathbf{C}$  and  $\mathbf{C}$  are the vectors of the local aerodynamic derivatives (in body coordinates)

$$(4.18) \quad \mathbf{C}_R(P) = \begin{bmatrix} C_x(P) \\ C_y(P) \\ C_z(P) \end{bmatrix}$$

$$(4.19) \quad \mathbf{C}_Q(P) = \begin{bmatrix} C_l(P) \\ C_m(P) \\ C_n(P) \end{bmatrix}$$

They are functions of the local Mach number, angle of attack and angle of sideslip only, together with the respective aerodynamic control surface deflections of aileron, elevator, rudder and flaps, the function of the aircraft rates  $p_A$ ,  $q_A$  and  $r_A$  and of the time derivatives  $\dot{V}_A$ ,  $\dot{\alpha}$  and  $\dot{\beta}$  having been eliminated by the multi-point approach.

#### 4.6 The overall forces and moments

The local forces and moments now have to be referred to the center of gravity so that they can be combined to give overall vectors. This will be illustrated by transforming the forces at the tailplane as shown in Figure 15. Referring it to the center of gravity has no influence on the force vector, so the general relation is:

$$(4.20) \quad \Delta \mathbf{R}_{cG}^A = \begin{bmatrix} X^A(P) \\ Y^A(P) \\ Z^A(P) \end{bmatrix}$$

On the other hand, changing the moment reference point gives, for Figure 15

$$(4.21) \quad \Delta \mathbf{M}_{cG} = \mathbf{M}_{TP} + z_P X_{TP}^A - x_P Z_{TP}^A$$

The general relationship for changing the moment vector reference point is

$$(4.22) \quad \Delta \mathbf{Q}_{cG} = \Delta \mathbf{Q}(P) + \mathbf{x}_P \times \Delta \mathbf{R}(P) \\ = \Delta \mathbf{Q}^A(P) + \begin{bmatrix} y_P Z^A(P) - z_P Y^A(P) \\ z_P X^A(P) - x_P Z^A(P) \\ x_P Y^A(P) - y_P X^A(P) \end{bmatrix}$$

The central force and moment vectors are finally given by

$$(4.23) \quad \mathbf{R}_{CG}^{\Delta} = \sum_P \Delta \mathbf{R}^{\Delta}(P)$$

$$(4.24) \quad \mathbf{Q}_{CG}^{\Delta} = \sum_P \Delta \mathbf{Q}^{\Delta}(P) + \sum_P \mathbf{x}_P \times \Delta \mathbf{R}^{\Delta}(P)$$

#### 4.7 Discussion of the multi-point model

The multi-point model situation is illustrated by the two following block diagrams, in which all the equations are combined with their relative couplings, including all transformations and multiplications. Figure 16 shows the wind equations. Relative to Figure 8 the output  $Q_W$  is replaced by the vector  $dV_W/dr$ . Apart from this, the structure of the equations stays the same including, of course, the feedback of  $V_K$  and  $r$ .

Figure 17 replaces Figure 13 of the one-point model. Using the input vectors  $V_{Wg}$  and  $dV_W/dr$ , the resulting local airspeed  $V_A(P)$  is first calculated for each point. By use of the local aerodynamic relations, the local resultant forces and moments are then derived, introducing the local effects of the control surfaces  $\xi$ ,  $\zeta$ ,  $\eta$ ,  $\eta_K$  and of the engine jetflow. This has to be done for every point considered. Finally, these forces and moments are expressed relative to the center of gravity and are summed to give the resultant central force and moment vectors. These are the inputs to the state equations shown in Figure 14, as is the case for the one point model. The latter therefore remain unchanged. The overall multi-point model in Figure 18 is mainly characterized by the feedback couplings between the wind and aircraft process which have already been discussed in Section 3.

Compared with the one point model, the amount of calculation involved in the aerodynamic equations has been multiplied by the number of points considered. On the other hand, the effects of aircraft rotation, wind gradients, downwash and wing vortex can be modelled much more precisely and the calculation of time derivatives of  $V_A$ ,  $\alpha$  and  $\beta$  is eliminated. Finally, this approach can be easily extended to model further phenomena, such as ground effect or unstationary aerodynamic effects. In the parameter identification of a DO 28 aircraft, for example, the results could be greatly improved by taking the different positions of the instrumentation into consideration and calculating the local airspeed vectors /18/. The major unsolved problem in such a multi point model is the definition of aerodynamic models for the different aircraft components, such as wing, fuselage, fin and tailplane. This is a quite difficult task, because of the various existing interference effects which exist, e.g. between wing and fuselage or between tailplane and fin. A further problem lies in the fact that these models have to be derived mostly from aerodynamic calculations because the aircraft components are rarely tested separately in wind tunnel experiments. The influence of engine flow as a function of angle of attack and angle of sideslip is also rather difficult to describe. The proposed multi-point model, therefore, can only be a stimulation to further investigations, the intention of the paper being mainly to show a promising approach from which more exact models of aircraft motion in moving air can be developed.

#### 5. Conclusions

The non-linear equations of aircraft motion in moving air have been introduced and their interactions illustrated by block diagrams. This mathematical model reflects the fact that the two sub-processes (wind and aircraft motion) are strongly coupled, aircraft forces and moments being generated by the relative motion between the air and the aircraft. The usual one point model is first considered, using the classical approach of overall quasi-steady derivatives. This is developed to provide a multi-point model, in which the effects of aircraft rotation, wind gradients, wing downwash and engine flow can be modelled more precisely by a generalized approach. In this the approximate quasi-steady terms are replaced by the calculation of local velocities and forces. This multi-point approach has great potential for improving the accuracy with which the aircraft motion is simulated - as has already been shown in parameter estimation calculations. It does, however, require the development of better models for generating the local aerodynamic forces and moments and the engine flow. This, and improvement to the modelling of higher frequency wind motion and its effects on the aircraft, calls for further research activities.

#### 6. References

- /1/ -- DIN LN 9300 Flugmechanik, Normenstelle Luftfahrt, 1970.
- /2/ -- ISO 1151 - 1153 Terms and symbols for flight dynamics.  
International Organization for Standardization, 1975

- /3/ G. Schänzer Einfluß von verkoppelten instationären Böenstörungen auf die Flugzeuglängsbewegung. Dissertation, TU Braunschweig 1969.
- /4/ G. Rosenau Umrechnung flugmechanischer Derivative. Z. Flugwiss. Weltraumforsch. 19 (1971) p. 512-517
- /5/ B. Etkin Dynamics of atmospheric flight. J. Wiley, London, 1972.
- /6/ R. Brockhaus Flugregelung I R. Oldenbourg, München 1977
- /7/ G. Schänzer Böenmodelle in der Flugdynamik. Z. Flugwiss. Weltraumforsch. 1 (1977), p. 177-185
- /8/ R. Brockhaus Flugregelung II R. Oldenbourg, München 1979
- /9/ P. Krauspe Beiträge zur Längsbewegung von Flugzeugen in Windacherungen. Dissertation, TU Braunschweig 1983
- /10/ R. Brockhaus Ein Vorschlag für die Wahl der Zustandsvariablen in den Bewegungsgleichungen von Flugzeugen unter Windeinfluß. Z. Flugwiss. Weltraumforsch. 9 (1985) p. 376-382
- /11/ G. Schänzer Abschätzung von stochastischen Böenlasten unter Berücksichtigung instationärer Luftkräfte. Z. Flugwiss. Weltraumforsch. 9 (1985) p. 167-178
- /12/ B. Kaufmann Atmospheric turbulence and unsteady aerodynamics in aircraft simulation. 2nd Int. Symposium on Aviation Safety, Toulouse 1986
- /13/ M. Swolinsky Beiträge zur Modellierung von Scherwind für Gefährdungsuntersuchungen. Dissertation TU Braunschweig 1986
- /14/ M. Swolinsky Wind Shear models for aircraft hazard investigation. 2nd Int. Symposium on Aviation Safety, Toulouse 1986
- /15/ R. Brockhaus A mathematical multi-point model for aircraft motion in moving air. Z. Flugwiss. Weltraumforsch. 11, 1987, p. 174 - 184
- /16/ K.O. Proskawetz Identification of the longitudinal motion of a Dornier DO 28 airplane. IFAC Congress München 1987, Paper Nr. 1053
- /17/ W. Mönnich Ein Zweipunkt - Aerodynamikmodell für die Identifizierung. SFB 212 - Symposium Braunschweig 1987 DFVLR - Mitt. 87 - 22 p. 193 - 208
- /18/ K.O. Proskawetz W. Wang ML - data - compatibility - check of general flight - test - data by use of a nonlinear six degrees of freedom model. IFAC - Symposium Beijing, 1988.

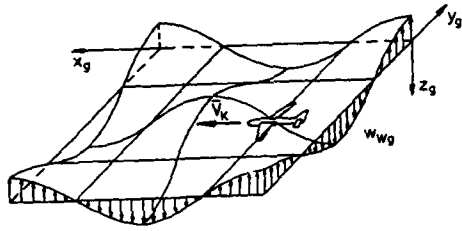


Figure 1 Two-dimensional wind field

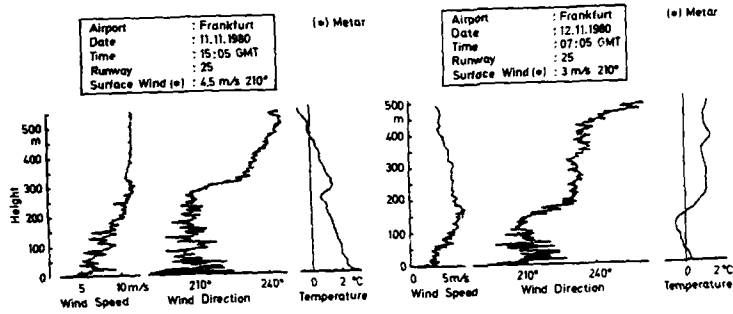


Figure 2 Wind profile from flight measurement as function of height (from / 13 /)

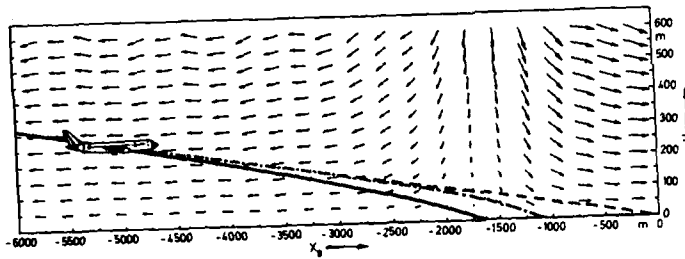


Figure 3 Wind-field in a storm down-draught (from / 13 /)

- uncontrolled flight path
- - - flight path with elevator control
- · - flight path with autopilot and autothrottle

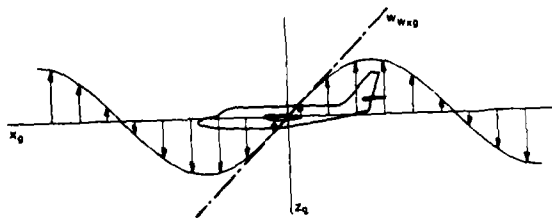


Figure 4 Flight across a sinusoidal wind-field

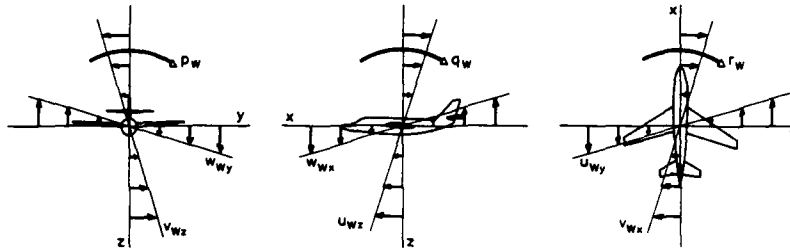


Figure 5 Relation between wind rotational velocity and wind gradients

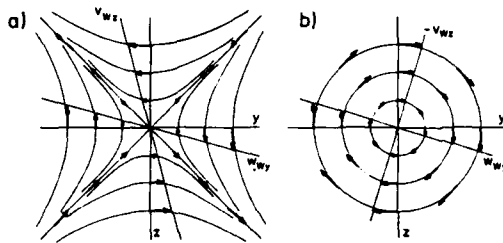


Figure 6 Airflow-fields with different relative wind gradients.  
 a)  $v_{wx} = w_{wy}$       b)  $v_{wz} = -w_{wy}$

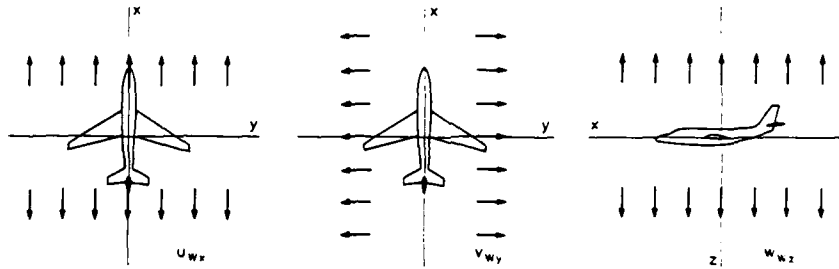


Figure 7. Transverse wind gradients (differential values referred to the velocity at the center of gravity)

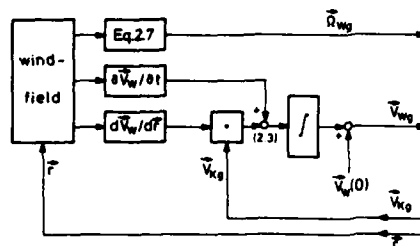


Figure 8. Block diagram of wind equations of the one-point model

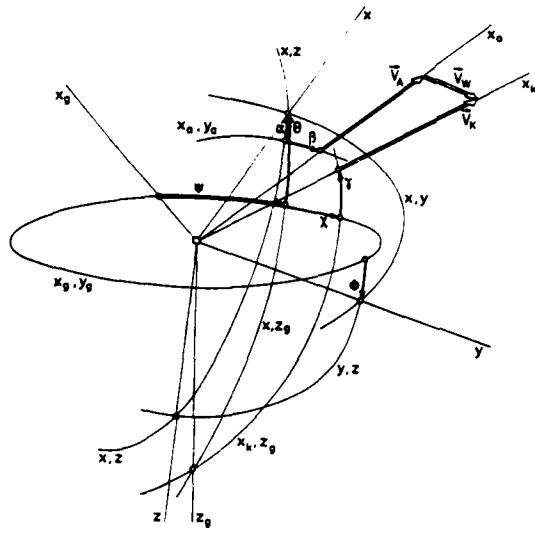


Figure 9. Relation between Earth-fixed and body-fixed coordinate systems.

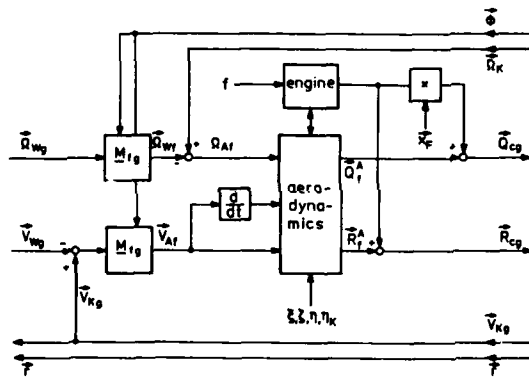


Figure 10. Force and moment equations of the one point model

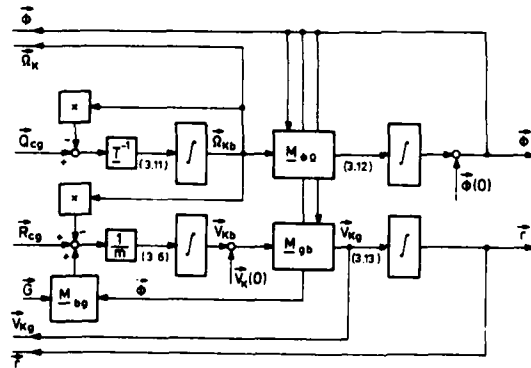


Figure 11. State equations

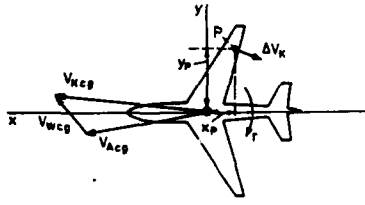


Figure 12. Local differential speed, generated by yawing motion

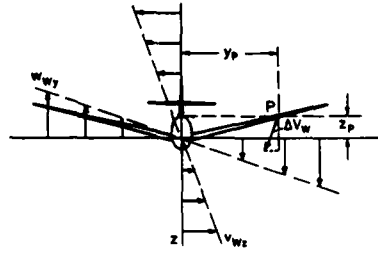


Figure 13. Local differential wind speed generated by a wind gradient

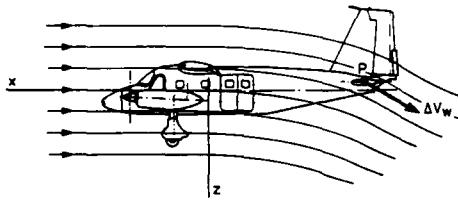


Figure 14. Local differential air-velocity by wing downwash and engine flow

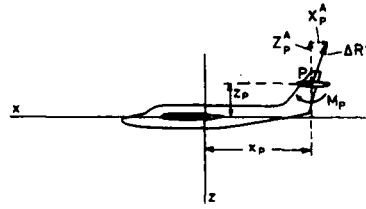


Figure 15. Calculation of the central forces and moments

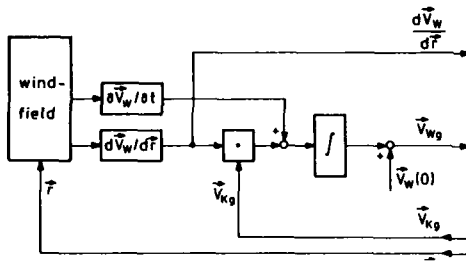


Figure 16. Wind equations of the multi-point model

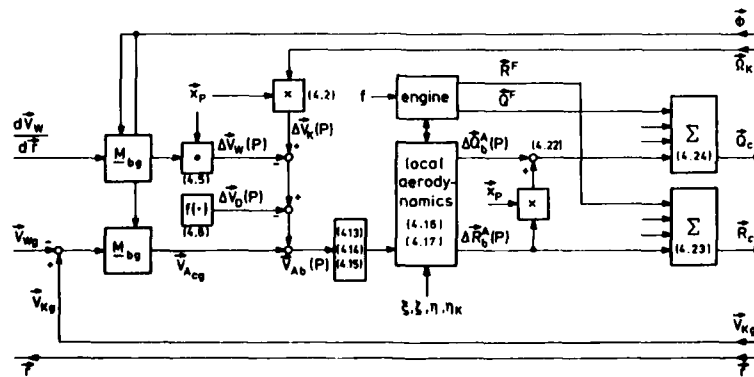


Figure 17. Force and moment equations of the multi-point model



DETERMINATION DES LOIS DE GUIDAGE QUASI-OPTIMALES EN TEMPS REEL  
POUR DES TRAJECTOIRES D'AVIONS DE COMBAT

par  
HUYNE Huu Thanh

Office National d'Etudes et de Recherches Aérospatiales (ONERA)  
29, Avenue de la Division Leclerc - 92320 CHATILLON - France

SUMMARY

COMPUTATION OF SUB-OPTIMAL REAL-TIME GUIDANCE LAWS FOR COMBAT AIRCRAFT TRAJECTORIES

This chapter presents an application of singular perturbation theory (SPT) for the computation of real-time control laws for Combat Aircraft trajectories.

The principle of SPT is first briefly reviewed for solving a multiple-time scale differential equations, then its application to optimization of non-linear systems is presented. The main drawbacks and difficulties which have been encountered in the computation of real-time control laws for aircraft trajectories are described, then various techniques are also pointed out in order to overcome with these problems.

Basing of this SPT, real-time guidance laws, of closed-loop type, have been developed for minimum time to climb in a vertical plane and three-dimensional interception for a combat aircraft. The performances of these sub-optimal guidance laws have been then compared, in numerical simulation using a typical aircraft model, with optimal control laws, of open-loop type, provided by an iterative numerical algorithm, using a generalized projected gradient technique.

A better than 1 % accuracy has been obtained for the performance index (time-to-climb) for vertical climb trajectories. The real-time guidance laws are slightly less accurate for interception trajectories.

The sub-optimal guidance laws can fulfill final conditions on altitude or/and flight path angle and remain valid for a large flight envelope domain. Their computation times are very small and are compatible with real-time on board computer applications.

RESUME

Ce chapitre présente une application de la théorie des systèmes multi-échelles de temps au contrôle en temps réel des trajectoires d'avions de combat.

Après avoir rappelé les principes de la théorie des perturbations singulières dans la résolution des systèmes différentiels multi-échelles de temps, son application à l'optimisation des systèmes non-linéaires est présentée. Les principales difficultés rencontrées dans la détermination des lois de guidage "temps réel" sont ensuite mentionnées, puis différentes techniques utilisées pour les résoudre sont indiquées.

Des lois de guidage "temps réel" en boucle fermée sont ensuite développées pour différents types de trajectoires d'avions de combat : montée en temps minimum, interception dans un plan horizontal, dans un plan vertical et dans l'espace tridimensionnel. Les performances fournies par ces lois sont ensuite évaluées en simulation numérique sur un modèle d'avion type, par comparaison avec les lois optimales en boucle ouverte obtenues par un algorithme numérique de gradient projeté, sans approximation de type multi-échelles de temps.

1 - INTRODUCTION

L'emploi de lois de guidage optimales de trajectoires pour un avion de transport civil ou pour un avion de combat présente un intérêt certain. En effet, l'intégration de ces lois sur un ordinateur embarqué fonctionnant en temps réel devra permettre d'une part de soulager la charge de travail du pilote, dont le rôle se bornera alors à désigner les objectifs à atteindre, et d'autre part d'utiliser au mieux les capacités de manœuvre de l'avion.

Méanmoins la détermination des lois optimales est complexe car elle fait intervenir la résolution de systèmes différentiels non-linéaires avec des conditions aux deux extrémités (Bryson, Ho, 1975). De ce fait, les solutions exactes sont obtenues usuellement par des techniques numériques de programmation non linéaire, de type itérative (gradient par exemple), qui demandent des encombrements mémoires importants et des temps de calcul actuellement incompatibles avec une utilisation en "temps réel".

Pour cette raison, la recherche de lois de guidage sous-optimales, mais avec des temps de calcul moindres, demeure un thème d'investigation intéressant. Parmi les diverses méthodes d'approximation étudiées jusqu'à présent la théorie des perturbations singulières (Wasow, 1965) semble être la plus prometteuse, elle permet d'obtenir des lois de guidage en boucle fermée, de mise en oeuvre numérique relativement simple et de temps de calcul numérique négligeable en comparaison avec les solutions optimales fournies par les algorithmes numériques d'optimisation.

L'objet de ce chapitre est de décrire l'application de cette théorie à la détermination des lois de guidage pour des trajectoires optimales en temps minimum pour un avion de combat.

Il convient de rappeler au préalable le principe, les possibilités et les limites de l'application de la théorie des perturbations singulières à l'optimisation des trajectoires.

Ce chapitre est organisé de la façon suivante.

Le principe et les principaux résultats relatifs à la théorie des perturbations singulières (P.S.) sont d'abord rappelés brièvement. Ensuite l'apport de cette théorie à la résolution d'un problème d'optimisation non linéaire est indiqué, de même que les difficultés rencontrées et les limitations de la méthodes.

La détermination de lois de guidage sous-optimales pour des trajectoires de montée et d'interception utilisant cette théorie des P.S., est ensuite décrite, ainsi que les modifications apportées pour pallier aux inconvénients de la méthode. Des résultats de simulation numériques sont enfin présentés où les performances obtenues par ces lois sous-optimales sont comparées aux solutions optimales fournies par un code numérique d'optimisation de trajectoires utilisant une méthode de gradient projeté.

Les perspectives de l'intérêt de la théorie des P.S. et des lois de guidage ainsi développées sont indiquées en conclusion.

2 - PRINCIPE DE LA THEORIE DES PERTURBATIONS SINGULIERES (Wasow, 1965 ; Smith, 1985)

La théorie des perturbations singulières consiste à résoudre de façon approchée un système non-linéaire mettant en évidence des dynamiques distinctes. Le principe de la méthode est illustré sur un exemple scalaire. Les conditions de validité sont ensuite rappelées, puis le lien avec la théorie des développements asymptotiques est également établi.

2.1 - Résolution d'un système non-linéaire à condition initiale

Soit le système différentiel autonome non-linéaire suivant à résoudre :

$$(1) \quad \begin{cases} \dot{x} = f(x,y) \\ \varepsilon \dot{y} = g(x,y) \end{cases} \quad \text{avec} \quad \begin{cases} x(0, \varepsilon) = x_0 \\ y(0, \varepsilon) = y_0 \end{cases}$$

où les variables  $x(t, \varepsilon)$  et  $y(t, \varepsilon)$  sont des scalaires,  $x_0, y_0$  des constantes initiales,  $\varepsilon$  est un nombre positif infiniment petit comparativement aux autres paramètres du système. Cette formulation fait intervenir de façon explicite deux échelles de temps au système, car la dynamique de la variable  $y$ , donnée par la dérivée  $(1/\varepsilon)g(x,y)$ , est plus grande que celle relative à la variable  $x$ .

La forme (1) est encore dite "singulièrement perturbée" car la dimension du système différentiel est réduite lorsque l'on fait tendre  $\varepsilon$  vers zéro.

2.1.1 - Problème réduit ou extérieur

Pour chercher une solution au problème (1), il est naturel de poser  $\varepsilon = 0$ , de résoudre le nouveau système ainsi obtenu et d'espérer trouver ainsi une approximation raisonnable de la solution du système (1) moyennant certaines conditions.

Le problème obtenu en faisant  $\varepsilon = 0$  est dit problème réduit ou bien encore problème extérieur : on notera  $(\bar{x}, \bar{y})$  la solution extérieure de ce problème (2).

$$(2) \quad \begin{cases} \dot{\bar{x}} = f(\bar{x}, \bar{y}) \\ 0 = g(\bar{x}, \bar{y}) \end{cases} \quad \bar{x}(0) = x_0$$

Comme le système est du premier ordre, il est naturel de ne conserver qu'une seule condition initiale, celle de la variable lente pour laquelle on a conservé la loi d'évolution. Ainsi, on admet une discontinuité sur la variable rapide en  $t = 0$  (figure 1). Le mieux que nous pouvons espérer est donc que  $\bar{x}$  soit une bonne approximation de  $x$  et que  $\bar{y}$  soit une bonne approximation de  $y$  sauf au voisinage de l'origine (exception faite si  $g(x_0, y_0) = 0$ ).

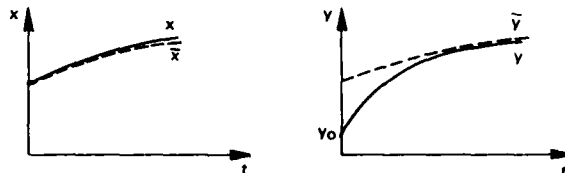


Fig. 1 - Comparaison de la solution réduite et de la solution réelle.

2.1.2 - Couche limite initiale

Il reste donc à étudier le comportement de la variable rapide  $y$  au voisinage de l'origine des temps, ce qui se réalise par une dilatation de l'échelle des temps :  $t = \tau/\varepsilon$ . Il est à noter que l'on retrouve ici la première idée quant à la définition du paramètre  $\varepsilon$ .

Le problème (3) ainsi obtenu est dit problème de la couche limite (initiale car on s'intéresse dans ce cas aux conditions initiales) et sa solution sera notée  $(\hat{x}, \hat{y})$  :

$$(3) \quad \begin{cases} \frac{d\hat{x}}{dt} = cf(\hat{x}, \hat{y}) & \hat{x}(0, \varepsilon) = x_0 \\ \frac{d\hat{y}}{dt} = g(\hat{x}, \hat{y}) & \hat{y}(0, \varepsilon) = y_0 \end{cases}$$

Comme précédemment, une approximation raisonnable de ce problème (3) est obtenue en faisant  $\varepsilon = 0$ . Par suite, il vient :

$$(4) \quad \begin{cases} \hat{x}(t) = x_0 \\ \frac{d\hat{y}}{dt} = g(x_0, \hat{y}) & \hat{y}(0, \varepsilon) = y_0 \end{cases}$$

Le problème de couche limite initiale est, comme pour la solution extérieure, de dimension plus faible que le problème (1), car la solution est obtenue en résolvant l'équation différentielle scalaire relative à la variable rapide, la variable lente  $x$  étant ici figée à sa valeur constante initiale.

Si l'on compare les systèmes (2) et (4), il apparaît que la solution réduite à l'origine  $t = 0$  est un point d'équilibre pour la couche limite initiale. C'est ici que se trouve un point délicat de la méthode. En effet, pour que l'on puisse obtenir une approximation uniformément valable par la solution du problème (1), il faut être assuré de la stabilité de la couche limite initiale par rapport à ce point d'équilibre. Les conditions de validité de cette approche sont données au paragraphe suivant § 2.2.

### 2.1.3 - Solution composite

Pour obtenir une approximation pour  $x$  et  $y$ , valable uniformément sur un large intervalle de temps  $y$  compris l'origine  $t = 0$ , la méthode la plus simple consiste à superposer la solution extérieure et de la couche limite, en rajoutant des constantes de façon à obtenir un raccordement convenable. On obtient ainsi :

$$(5) \quad \begin{cases} x(t) \approx \bar{x}(t) \\ y(t) \approx \hat{y}(t) - \hat{y}(0) + \bar{y}(t) \end{cases}$$

### 2.2 - Théorème de convergence de Tihonov

La validité de la décomposition présentée au précédent paragraphe § 2.1 est fournie par un théorème dû à Tihonov rappelé ci-après (Wasow, 1965 ; Ardena, 1983).

Soient les hypothèses suivantes :

- i) les fonctions  $f$  et  $g$  du problème (1) sont continues sur un certain domaine ouvert  $\Omega$  de l'espace des variables  $x$  et  $y$  ;
- ii) le problème réduit et le problème complet, définis par (2) et (1), ont une solution unique sur l'intervalle de temps  $[0, T]$  ;
- iii) il existe une racine isolée  $\bar{y} = \mu(\bar{x})$  au problème réduit dans  $\Omega$ , c'est-à-dire telle que  $g(\bar{x}, \mu(\bar{x})) = 0$  ;
- iv) cette racine est un point d'équilibre asymptotiquement stable pour la couche limite initiale à l'ordre 0, définie par (4) ;
- v) le point initial  $(x_0, y_0)$  appartient au domaine d'attraction  $(x_0, \mu(x_0))$  associé à la racine  $\bar{y}_0 = \mu(x_0)$ .

Dans ces conditions, Tihonov démontre alors les résultats suivants lorsque que l'on fait tendre le paramètre  $\varepsilon$  vers zéro :

- 1) la solution complète converge uniformément sur  $[0, T]$  vers la solution réduite pour la variable lente

$$\lim_{\varepsilon \rightarrow 0} x(\varepsilon, t) = \bar{x}(t) ;$$

- 2) la solution complète converge uniformément sur tout intervalle  $[t, T]$  contenu dans  $[0, T]$  vers la solution réduite pour la variable rapide :

$$\lim_{\varepsilon \rightarrow 0} y(\varepsilon, t) = \mu(\bar{x}) ;$$

- 3) il y a convergence de la couche limite  $\hat{y}(t)$  vers la valeur d'équilibre  $\bar{y}_0 = \mu(x_0)$  :

$$\lim_{t \rightarrow \infty} \hat{y}(t) = \mu(x_0)$$

D'un point de vue pratique, il convient de noter que la vérification des hypothèses fondamentales iv) et v) de ce théorème n'est pas aisée, notamment dans le cas non-linéaire, car elle fait intervenir des méthodes d'analyse du comportement dynamique des systèmes non-linéaires. D'abord, il peut exister plusieurs racines à l'équation  $g(\bar{x}, \bar{y}) = 0$  et il faut déterminer la racine la "plus" stable. Ensuite, il faudrait déterminer le domaine d'attraction de cette racine, ce qui peut se révéler délicate.

En pratique, on peut seulement donner une condition plus facile à vérifier, mais qui n'est que locale et nécessaire :

$$(6) \quad \left. \frac{\partial g}{\partial y} \right|_{\substack{x=x_0 \\ y=\mu(x_0)}} < 0$$

Il convient de noter que le théorème de Tihonov est valable également pour des systèmes non autonomes et pour le cas général où  $x$  et  $y$  sont des vecteurs de dimension quelconque. Pour obtenir davantage de détails sur la démonstration, les discussions et les généralisations de ce théorème on peut consulter par exemple (Wasow, 1965 ; Ardena 1983).

### 2.3 - Détermination d'une meilleure approximation à l'aide de développements asymptotiques

Si l'on désire une meilleure approximation de la solution que celle fournie par la résolution présentée au § 2.1, il est naturel de chercher une solution par développement asymptotiques dans le paramètre  $\varepsilon$ .

Rappelons qu'un développement asymptotique à l'ordre  $n$  d'une fonction  $f(\varepsilon)$  par rapport à un paramètre  $\varepsilon$  est une expression de la forme :

$$f(\varepsilon) = \sum_{k=0}^n a_k \varepsilon^k + \beta_n(\varepsilon) \varepsilon^n$$

telle que les conditions suivantes soient vérifiées :

$$\lim_{\varepsilon \rightarrow 0} (f(\varepsilon) - \sum_{i=0}^{k-1} a_i \varepsilon^i) \varepsilon^k = a_k$$

$$\text{et } \lim_{\varepsilon \rightarrow 0} \beta_n(\varepsilon) = 0$$

La méthode de développement asymptotique est très utilisée en pratique, elle a permis de résoudre de façon approchée un grand nombre de problèmes physiques, dans des domaines divers comme en mécanique céleste, en mécanique des fluides, etc...

Son application aux systèmes dynamiques à échelles de temps multiples a été également effectuée par de nombreux auteurs. Il existe plusieurs façons d'appliquer la méthode de développement asymptotique aux systèmes à échelles de temps multiples. On peut distinguer, par exemple :

- l'approche dite "des développements asymptotiques raccordés" (Ardena, 1983),
- l'approche dite "multivariable" (Smith, 1985).

La première approche est la plus ancienne et aussi la plus connue. Elle procède, de façon analogue à la démarche précédente, en considérant d'abord deux développements asymptotiques indépendants entre eux : l'un pour la solution "extérieure" ou "réduite", l'autre pour la couche limite initiale. Une solution composite, valable uniformément pour tout l'intervalle  $[0, T]$  est ensuite obtenue en superposant ces deux solutions et en ajoutant en terme dit de raccordement de façon à assurer la vérification des conditions aux limites. Cette approche présente néanmoins les inconvénients suivants :

- le calcul des termes de raccordement n'est toujours pas très simple à effectuer ;
- l'extension au cas multivariable est complexe.

La deuxième approche, dite "multivariable", est plus récente, elle ne présente pas les inconvénients rencontrés par l'approche précédente.

Rappelons brièvement le principe de cette approche "multivariable", due à O'Malley et à Koppensteadt (Smith, 1985).

On cherche, pour chacune des variables  $x$  et  $y$ , un développement asymptotiques défini de la façon suivante :

$$(7) \quad \begin{cases} x(t, \varepsilon) = \bar{x}(t, \varepsilon) + \varepsilon x^1(t, \varepsilon) \\ y(t, \varepsilon) = \bar{y}(t, \varepsilon) + \varepsilon y^1(t, \varepsilon) - \bar{y}(0, \varepsilon) \end{cases}$$

$$\text{avec } \bar{x}(t, \varepsilon) = \sum_{k=0}^n \bar{x}_k(t) \varepsilon^k, \quad x^1(t, \varepsilon) = \sum_{k=0}^n x_k^1(t) \varepsilon^k$$

$$\bar{y}(t, \varepsilon) = \sum_{k=0}^n \bar{y}_k(t) \varepsilon^k, \quad y^1(t, \varepsilon) = \sum_{k=0}^n y_k^1(t) \varepsilon^k$$

où  $\varepsilon$  est l'échelle du temps dilatée au voisinage de l'origine ( $t = \varepsilon \tau$ ).

Pour le développement de la variable  $x$ , le terme  $x^1(t, \varepsilon)$  est multiplié par le paramètre  $\varepsilon$  pour tenir compte du fait que la solution d'ordre 0 pour la variable lente ne contient pas de terme relatif à la couche limite initiale.

Pour définir complètement le problème, on impose en outre les conditions suivantes :

-  $\bar{x}(t, \varepsilon)$  et  $\bar{y}(t, \varepsilon)$ , qui caractérisent la solution "extérieure", doivent satisfaire le système (1) pour tout instant  $t > 0$ , c'est-à-dire :

$$(8) \quad \begin{cases} \frac{d\bar{x}}{dt}(t, \varepsilon) = f(\bar{x}(t, \varepsilon), \bar{y}(t, \varepsilon)) \\ \varepsilon \frac{d\bar{y}}{dt}(t, \varepsilon) = g(\bar{x}(t, \varepsilon), \bar{y}(t, \varepsilon)) \end{cases}$$

- les solutions  $x^i(t, \varepsilon)$  et  $y^i(t, \varepsilon)$ , relatives à la couche limite doivent vérifier les conditions :

$$(9) \quad \lim_{\varepsilon \rightarrow 0} \begin{vmatrix} x^i(t, \varepsilon) \\ y^i(t, \varepsilon) - \bar{y}(0, \varepsilon) \end{vmatrix} = 0$$

En tenant compte des relations (1), (7) et (8), on en déduit les équations différentielles que doivent satisfaire les solutions  $x^i(t, \varepsilon)$  et  $y^i(t, \varepsilon)$  de la couche limite initiale :

$$(10) \quad \begin{cases} \frac{dx^i}{dt}(t, \varepsilon) = \varepsilon [f(x, y) - f(\bar{x}, \bar{y})] \\ \frac{dy^i}{dt}(t, \varepsilon) = [g(x, y) - g(\bar{x}, \bar{y})] \end{cases}$$

A partir des Eq. (7) - (10), on peut déduire que le développement asymptotique à l'ordre  $\varepsilon$  doit satisfaire les mêmes équations (2), (4) que la solution extérieure et la couche limite initiale du précédent paragraphe (§ 2.1). La solution approchée donnée précédemment par (2), (4), (5), constitue ainsi l'approximation à l'ordre  $\varepsilon$  du développement asymptotique défini par (7) - (10).

On peut noter que les équations différentielles relatives aux termes d'ordre supérieur du développement asymptotique (7) sont toutes linéaires, à coefficients fonction du temps. Ces termes peuvent être calculés de proche en proche à partir des formules de récurrence (Smith, 1985).

#### 2.4 - Extension au cas de plusieurs échelles de temps

On peut également généraliser la méthode des perturbations singulières à des problèmes où apparaissent plusieurs échelles de temps :

$$(11) \quad \begin{cases} \frac{dx^0}{dt} = f^0(x^0, x^1, \dots, x^m) & x^0(0) = x_0^0 \\ \varepsilon_j \frac{dx^j}{dt} = f^j(x^0, x^1, \dots, x^m) & x^j(0) = x_0^j \end{cases}$$

avec  $\varepsilon_{j+1}/\varepsilon_j \rightarrow 0$  lorsque  $\varepsilon_j \rightarrow 0$   $j = 1, 2, \dots, m-1$

et où  $x^0, x^1, \dots, x^m$  sont des vecteurs de dimension  $n_0, n_1, \dots, n_m$ .

La procédure est identique à celle effectuée pour deux échelles de temps en prenant la couche limite d'ordre  $j$  comme solution extérieure de la couche limite d'ordre  $(j+1)$ , à chaque couche limite étant affectée une nouvelle dilatation de l'échelle des temps  $\varepsilon_j = \varepsilon/\varepsilon_j$ .

Sous réserve des hypothèses de stabilité pour les équations relatives aux couches limites successives, Tihonov a démontré également la convergence de la solution complète vers la solution extérieure, lorsque tous les  $\varepsilon_j$  tendent vers zéro (Wasow, 1965).

### 3 - APPLICATION A LA DETERMINATION DE LA COMMANDE SOUS-OPTIMALE DES SYSTEMES DIFFERENTIELS NON-LINEAIRES

L'apport de la théorie des perturbations singulières à la détermination de la commande sous-optimale des systèmes régis par des équations différentielles non-linéaires est d'abord décrit brièvement. Les problèmes rencontrés dans les applications, en se limitant à l'optimisation des trajectoires d'avions, sont ensuite présentés, de même que les solutions utilisées pour les résoudre.

#### 3.1 - Définition du problème

Soit le système dynamique, régi par des équations différentielles non-linéaires présentées sous la forme singulièrement perturbée suivante :

$$(12) \quad \begin{cases} \dot{x} = f(x, y, u) & \text{avec } x(0) = x_0 \\ \varepsilon \dot{y} = g(x, y, u) & y(0) = y_0 \end{cases}$$

où  $x, y$  sont des variables d'état à valeurs réelles, de dimensions respectives  $n_1$  et  $n_2$ ,  $u$  est le vecteur des commandes de dimension  $m$ ,  $c$  est un petit paramètre scalaire.

Il s'agit de trouver une loi de commande optimale  $u^*(t)$  permettant de transférer l'état  $(x, y)$  du système (12), d'un état initial donné jusqu'à un certain état final  $(x(t_f), y(t_f))$  de façon à minimiser l'indice de coût intégral suivant :

$$(13) \quad J = \psi(x(t_f), y(t_f)) + \int_0^{t_f} L(x, y, u) dt$$

L'instant final  $t_f$  est libre, mais l'état final doit satisfaire à un vecteur de contraintes, de dimension  $r$  :

$$(14) \quad \sigma(x(t_f), y(t_f)) = 0$$

Pour simplifier, l'exposé suivant sera fait dans le cas particulier suivant des contraintes finales où l'état final est complètement fixé :

$$(15) \quad \begin{cases} x(t_f) = x_f \\ y(t_f) = y_f \end{cases}$$

Pour le cas général des contraintes de la forme (14), le principe de la méthode demeure valable, mais la détermination des constantes d'intégration est plus complexe.

Soulignons enfin que, dans le but de recherche de lois de guidage "temps réel", le problème principal consiste à exprimer, si possible, la commande optimale  $u^*$  sous la forme en "boucle fermée", c'est-à-dire sous la forme d'une fonction de l'état courant  $(x, y)$  du système :

$$(16) \quad u^* = \phi(x, y)$$

Seule cette formulation permet d'adapter efficacement la commande pour tenir compte des écarts par rapport à la trajectoire optimale dus à des perturbations de natures diverses.

### 3.2 - Commande optimale

La solution exacte du problème d'optimisation défini par les Eq. (12), (13), (15) peut être obtenue en utilisant les conditions nécessaires du principe de Pontryagin (Bryson, Ho, 1975).

On définit d'abord le Hamiltonien du système (12), (13) :

$$(17) \quad H = L(x, y, u) + \lambda_x^T f(x, y, u) + \lambda_y^T g(x, y, u)$$

où  $\lambda_x, \lambda_y$  sont les vecteurs adjoints, solutions du système différentiel :

$$(18) \quad \begin{cases} \frac{d\lambda_x}{dt} = -\frac{\partial H}{\partial x} = -\frac{\partial L}{\partial x} - \frac{\partial f^T}{\partial x} \lambda_x - \frac{\partial g^T}{\partial x} \lambda_y \\ \frac{d\lambda_y}{dt} = -\frac{\partial H}{\partial y} = -\frac{\partial L}{\partial y} - \frac{\partial f^T}{\partial y} \lambda_x - \frac{\partial g^T}{\partial y} \lambda_y \end{cases} \quad \text{avec} \quad \begin{cases} \lambda_x(t_f) = v_x \\ \lambda_y(t_f) = v_y \end{cases}$$

où  $v_x$  et  $v_y$  sont des constantes arbitraires à déterminer de façon à obtenir les conditions finales désirées (15) sur l'état.

La commande optimale  $u^*$  doit assurer la minimisation du Hamiltonien dans le sous-espace  $U$  des commandes admissibles (supposé indépendant du temps) :

$$(19) \quad u^* = \underset{u \in U}{\text{Arg Min}} H(x, y, \lambda_x, \lambda_y, u)$$

Il est à noter que le Hamiltonien défini par Eq. (17), (18) est légèrement différent de celui habituellement adopté pour le principe de Pontryagin. On peut vérifier aisément que ces équations peuvent être déduites de la formulation classique de Pontryagin moyennant un changement de variable sur le vecteur adjoint associé à la variable rapide  $y$  (Ardena, 1983).

Les équations (18) montrent ainsi que les vecteurs adjoints  $\lambda_x, \lambda_y$  ont les mêmes dynamiques que les variables d'état  $(x, y)$  du système (12), c'est-à-dire qu'au vecteur de variable lente  $x$  correspond un vecteur adjoint "lent"  $\lambda_x$  et qu'au vecteur de variable rapide  $y$  correspond un vecteur adjoint "rapide".

On suppose que la résolution de (19) permet de mettre la commande optimale sous la forme explicite suivante :

$$(20) \quad u^* = \Phi(x, y, \lambda_x, \lambda_y)$$

Rappelons également une propriété importante qui est souvent utilisée en pratique pour déterminer la commande optimale en "boucle fermée" par la technique des perturbations singulières (voir exemple plus loin § 3.4).

Comme les systèmes considérés sont autonomes, il est facile de montrer que la condition d'optimalité (19) entraîne que le Hamiltonien est constant tout le long de la trajectoire optimale :

$$(21) \quad H(x^*, y^*, \lambda_x^*, \lambda_y^*, u^*) = \text{Cste}$$

Par ailleurs, comme le temps final est libre, on montre qu'il doit être choisi de façon que le Hamiltonien final soit nul, c'est-à-dire :

$$H(x_f^*, y_f^*, \lambda_{x_f}^*, \lambda_{y_f}^*, u_f^*) = 0$$

ce qui implique alors que le Hamiltonien reste identiquement nul tout le long de la trajectoire optimale

$$(22) \quad H(x^*, y^*, \lambda_x^*, \lambda_y^*, u^*) = 0$$

### 3.3 - Application de la théorie des perturbations singulières

Le rappel du principe de Pontryagin met en évidence les difficultés rencontrées pour déterminer la commande optimale en "boucle fermée". D'abord, et surtout, il convient de résoudre un système d'équations différentielles non-linéaires de dimension  $2(n_1 + n_2)$  couplées constituées par les équations d'état (12) et adjoints (18), compte-tenu de la commande optimale (20). Il s'agit là d'un problème aux deux bouts avec des conditions initiales et finales sur l'état. Ensuite l'expression (20) ne fournit pas une véritable commande en boucle fermée, puisqu'elle fait intervenir, outre l'état  $x, y$ , les variables adjointes  $\lambda_x, \lambda_y$ .

En remarquant que le système différentiel (12), (18), (20), à résoudre met en évidence l'existence de deux échelles de temps distinctes, de par sa forme singulièrement perturbée, une résolution approchée est obtenue en appliquant la méthode de développement asymptotique présentée au § 2 précédent.

Une approximation à l'ordre 0 peut être ainsi obtenue en résolvant d'abord le système réduit, en faisant  $\varepsilon = 0$ , puis en effectuant une correction de couches limites, après dilatation du temps. Toutefois, comme les conditions aux limites sont données en partie à l'instant initial, et en partie à l'instant final, il sera nécessaire de considérer deux couches limites pour raccorder les conditions initiales et finales sur le vecteur de variables rapides  $y$ .

L'application de la théorie des perturbations singulières dans la résolution des équations (12), (18), (20) peut être représentée sous la forme équivalente suivante.

En se limitant à l'approximation d'ordre 0, l'optimisation du système initial (12), peut être remplacée par l'optimisation de trois systèmes de dimensions plus réduites :

- la première est relative à la solution extérieure (ou réduite), obtenue en faisant  $\varepsilon = 0$ ,
- la seconde est relative à la correction de couche limite initiale,
- la troisième est relative à la correction de couche limite finale.

La commande composite est ensuite obtenue par superposition des solutions obtenues dans les trois étapes précédentes.

#### 3.1.1 - Solution extérieure (approximation d'ordre 0)

Le problème réduit est défini en faisant  $\varepsilon = 0$  dans les équations d'état et adjointes, et les conditions d'optimalité.

On peut montrer que la commande optimale correspondante est donnée, de façon équivalente, par la résolution du problème d'optimisation de dimension moins élevée où n'intervient plus que le vecteur lent  $x$ , dont l'évolution est régi par le système différentiel :

$$(23) \quad \dot{\bar{x}} = f(\bar{x}, \bar{y}, \bar{u}) \quad \bar{x}(0) = x_0$$

où le symbole  $(\bar{\quad})$  est relatif à la solution extérieure (ou réduite).

Dans cette équation, les variables  $(\bar{y}, \bar{u})$  sont ici les commandes, non indépendantes et reliées entre elles par la relation implicite :

$$(24) \quad g(\bar{x}, \bar{y}, \bar{u}) = 0$$

L'indice de performance à minimiser est identique à l'indice du problème complet, c'est-à-dire défini par (13). L'état final sur le vecteur lent  $x$  est fixé et donné par une partie de la condition (15) :

$$(25) \quad x(t_f) = x_f$$

### 3.3.2 - Couche limite initiale (ordre 0)

La couche limite initiale permet de raccorder la condition initiale sur le vecteur rapide  $y$ . Elle est obtenue en effectuant une dilatation du temps au voisinage de l'instant initial  $t = t_0$ , puis en faisant  $\varepsilon = 0$ . On peut encore montrer que la commande optimale correspondante est donnée, de façon équivalente, par la résolution d'un problème d'optimisation plus simple que le problème original où n'interviennent plus, cette fois-ci, que le vecteur rapide  $y$ . L'évolution de ce vecteur est alors régie par le système différentiel suivant, dans lequel le vecteur lent  $x$  est fixé à sa valeur initiale constante  $x_0$  :

$$(26) \quad \frac{d\hat{y}}{dt} = g(x_0, \hat{y}, \hat{u}) \quad \hat{y}(0) = y_0$$

où le symbole  $\hat{(\cdot)}$  est relatif à la solution de couche limite initiale.

Néanmoins, l'indice de coût du problème simplifié comporte ici un terme de pondération supplémentaire portant sur la dynamique de la variable lente (Kelley, 1972) :

$$(27) \quad \hat{J} = \int_0^{t_f - t_0} [L(x_0, \hat{y}, \hat{u}) + \lambda_{x_0}^T f(x_0, \hat{y}, \hat{u})] dt$$

Le coefficient de pondération  $\lambda_{x_0}$  est la valeur initiale du vecteur adjoint relatif au vecteur lent  $x$ , provenant de la résolution du problème extérieur. La présence de ce terme de pondération portant sur la variable lente, dans l'intégrande du coût (27), permet d'assurer le raccordement de la couche limite initiale à la solution extérieure.

Il est encore à noter que les hypothèses relatives au théorème de Tihonov, présentées au § 2.2., permettent d'assurer l'existence de la solution de ce problème d'optimisation à horizon infini et de la convergence de la couche limite initiale vers la solution extérieure, c'est-à-dire :

$$(28a) \quad \begin{cases} \lim_{t \rightarrow \infty} \hat{y}(t) = \bar{y}^*(x_0) \\ \lim_{t \rightarrow \infty} \hat{u}^*(t) = \bar{u}^*(x_0) \end{cases}$$

où  $\bar{y}^*(x_0), \bar{u}^*(x_0)$  sont les valeurs à l'instant  $t=0$  de la solution extérieure (voir § 3.3).

### 3.3.3 - Couche limite finale

Dans le cas présent où l'on impose également une condition finale sur le vecteur rapide  $y$ , une couche limite finale est nécessaire pour raccorder la condition finale sur la valeur finale  $y_f$ . La démarche est analogue à celle de la couche limite initiale.

L'équation dynamique est obtenue en faisant une dilatation du temps au voisinage de l'instant final ( $\sigma = (t_f - t)$ ), puis en faisant  $\varepsilon = 0$ . Le problème d'optimisation "équivalent" est défini par les équations suivantes :

$$(29) \quad \frac{d\tilde{y}}{d\sigma} = -g(x_f, \tilde{y}, \tilde{u}) \quad \text{avec} \quad \tilde{y}(0) = y_f$$

$$(30) \quad J = - \int_0^{\sigma_f} [L(x_f, \tilde{y}, \tilde{u}) + \lambda_{x_f}^T f(x_f, \tilde{y}, \tilde{u})] d\sigma$$

Ce problème d'optimisation est strictement analogue à celui de la couche limite initiale. Il convient de noter, néanmoins, une différence qui se révèle importante dans la pratique : la convergence vers la solution extérieure est obtenue en intégrant l'équation de la couche limite dans le sens rétrograde, c'est-à-dire en temps inverse, à partir d'un temps final qui n'est pas connu a priori.

Comme pour la couche limite initiale, le théorème de Tihonov fournit les conditions de convergence suivantes pour les quantités relatives à cette couche limite finale :

$$(28b) \quad \begin{cases} \lim_{\sigma \rightarrow \infty} \tilde{y}(\sigma) = y^*(x_f) \\ \lim_{\sigma \rightarrow \infty} \tilde{u}(\sigma) = u^*(x_f) \end{cases}$$

où  $y^*(x_f)$  et  $u^*(x_f)$  sont les valeurs finales de la solution extérieure (§ 3.3.3).

### 3.4. Cas scalaire

Dans le cas où les variables  $x$  et  $y$  du problème complet (12) sont scalaires, l'approximation d'ordre de la théorie des perturbations singulières permet de fournir une solution analytique complète pour le calcul de la commande optimale.

#### 3.4.1 - Solution extérieure

Il est à noter que la résolution du problème réduit (23) fait intervenir le Hamiltonien suivant, où la contrainte courante (24) est prise en compte par l'introduction d'un multiplicateur de Lagrange  $\bar{\lambda}_y$  :

$$(31) \quad H(\bar{x}, \bar{y}, \bar{\lambda}_x, \bar{\lambda}_y, \bar{u}) = L(\bar{x}, \bar{y}, \bar{u}) + \bar{\lambda}_x f(\bar{x}, \bar{y}, \bar{u}) + \bar{\lambda}_y g(\bar{x}, \bar{y}, \bar{u})$$

et que l'équation adjointe qui régit  $\bar{\lambda}_x$  s'écrit :

$$(32) \quad \dot{\bar{\lambda}}_x = - \frac{\partial H}{\partial x} = - \frac{\partial L}{\partial x} - \bar{\lambda}_x \frac{\partial f}{\partial x} - \bar{\lambda}_y \frac{\partial g}{\partial x} \quad \text{avec} \quad \bar{\lambda}_x(t_f) = v_x$$

Les commandes optimales doivent minimiser le Hamiltonien.

En tenant compte de la nullité de la contrainte (24) et de la nullité du Hamiltonien optimal (22), il est possible d'éliminer, dans le scalaire, la variable adjointe  $\bar{\lambda}_x$  de (31) et le multiplicateur  $\bar{\lambda}_y$ , et de se ramener au problème :

$$(33) \quad \bar{y}^*, \bar{u}^* = \underset{\bar{y}, \bar{u}}{\text{Arg Min}} \left\{ L(\bar{x}, \bar{y}, \bar{u}) - \frac{L(x^*, y^*, u^*)}{f(x^*, y^*, u^*)} f(\bar{x}, \bar{y}, \bar{u}) \right\}$$

avec la contrainte  $g(\bar{x}, \bar{y}, \bar{u}) = 0$ .

On peut vérifier que les valeurs optimales de  $\bar{y}^*$  et de  $\bar{u}^*$  sont alors données par :

$$(34) \quad \bar{y}^*, \bar{u}^* = \begin{cases} \underset{\bar{y}, \bar{u}}{\text{Arg Min}} \left\{ \frac{L(\bar{x}, \bar{y}, \bar{u})}{f(\bar{x}, \bar{y}, \bar{u})} \right\} & \text{si } f(\cdot) > 0 \\ \underset{\bar{y}, \bar{u}}{\text{Arg Max}} \left\{ \frac{L(\bar{x}, \bar{y}, \bar{u})}{f(\bar{x}, \bar{y}, \bar{u})} \right\} & \text{si } f(\cdot) < 0 \\ \text{avec } g(\bar{x}, \bar{y}, \bar{u}) = 0 \end{cases}$$

#### 3.4.2 - Couche limite initiale

Le Hamiltonien du problème (26), (27) s'écrit :

$$\hat{H} = L(x_0, \hat{y}, \hat{u}) + \bar{\lambda}_{x_0} f(x_0, \hat{y}, \hat{u}) + \hat{\lambda}_y g(x_0, \hat{y}, \hat{u})$$

La valeur initiale  $\bar{\lambda}_{x_0}$  de la variable adjointe lente est donnée par la relation suivante, obtenue en tenant compte de la nullité du Hamiltonien optimal :

$$(35a) \quad \bar{\lambda}_{x_0} = - \frac{L(x_0, \bar{y}^*(0), \bar{u}^*(0))}{f(x_0, \bar{y}^*(0), \bar{u}^*(0))}$$

En tenant compte de (34), cette variable est uniquement une fonction de la valeur initiale  $x_0$  :

$$(35b) \quad \bar{\lambda}_{x_0} = \bar{\lambda}_{x_0}(x_0)$$

La commande optimale du problème (26), (27) peut être encore obtenue de façon explicite.

En effet, l'intégrale première du Hamiltonien nul permet d'éliminer l'adjoint  $\hat{\lambda}_y$  et d'obtenir la commande optimale par la résolution du problème d'optimisation statique suivant :

$$(36) \quad \hat{u}^* = \begin{cases} \underset{\hat{u}}{\text{Arg Min}} \left\{ \frac{L(x_0, \hat{y}, \hat{u}) + \bar{\lambda}_{x_0} f(x_0, \hat{y}, \hat{u})}{g(x_0, \hat{y}, \hat{u})} \right\} & \text{si } g(\cdot) > 0 \\ \underset{\hat{u}}{\text{Arg Max}} \left\{ \frac{L(x_0, \hat{y}, \hat{u}) + \bar{\lambda}_{x_0} f(x_0, \hat{y}, \hat{u})}{g(x_0, \hat{y}, \hat{u})} \right\} & \text{si } g(\cdot) < 0 \end{cases}$$

#### 3.4.3 - Couche limite finale

La démarche est analogue à celle de la couche limite initiale. On en déduit, de la même façon, une commande optimale  $\bar{u}^*$  en fonction uniquement de la variable d'état à l'instant final  $x_f$  et de la variable rapide  $\bar{y}$ .

### 3.5 - Commande réactualisée en boucle fermée en temps réel

La superposition des solutions obtenues dans la région "extérieure" et dans les couches limite initiale et finale permet d'en déduire une commande composite  $u_{ps}(t)$  uniformément valable tout le long de la trajectoire. En se limitant à l'approximation d'ordre 0, cette commande s'écrit :

$$(37) \quad u_{ps}(t) = \underbrace{\{\hat{u}(x_0, \bar{y}(t)) - \bar{u}(x_0, \bar{y}(x_0))\}}_{\text{C.L. initiale}} + \underbrace{\bar{u}(x, \bar{y}(t))}_{\text{S. extérieure}} + \underbrace{\{\bar{u}(x_f, \bar{y}(t)) - \bar{u}(x_f, \bar{y}(x_f))\}}_{\text{C.L. finale}}$$

Cette commande comprend trois termes : un terme relatif à la solution extérieure et deux termes relatifs aux couches limites initiale et finale. Elle dépend de façon explicite de l'état initial  $(x_0, y_0)$ , de l'état final  $(x_f, y_f)$  et du temps courant  $t$ .

Une commande en "boucle fermée" est obtenue en tenant compte des remarques suivantes :

i) quand on est suffisamment éloigné de la couche limite finale, la commande relative à cette dernière est infiniment petite, on a en effet, d'après (28b) :

$$\left| \bar{u}(x_f, \bar{y}(t)) - \bar{u}(x_f, \bar{y}(x_f)) \right| \leq e^{-\lambda(t-x_f)}$$

$\lambda$  étant un nombre positif fini;

ii) à l'instant initial  $t=0$ , la commande  $u_{ps}(0)$  est uniquement une fonction de l'état initial  $(x_0, y_0)$ . En effet, en supposant que l'on arrive à résoudre complètement de manière analytique les problèmes réduits et de couches limites, ce qui est le cas pour des variables scalaires, la commande (37), compte tenu de la remarque précédente et des Eq. (24), (28a), est de la forme :

$$(38a) \quad u_{ps}(t_0) = \hat{u}(x_0, y_0)$$

iii) la commande de couche limite initiale converge asymptotiquement vers la commande de solution extérieure (voir Eq. (28a)).

En considérant ensuite chaque instant courant  $t$  comme instant initial, on obtient ainsi une commande en "boucle fermée", valable uniformément le long de la trajectoire, à l'exception du voisinage de l'état final (Mehra et Co. auteurs, ... 1979) :

$$(38b) \quad u_{ps}(t) = \hat{u}(x(t), y(t)).$$

La figure (2) illustre cette réactualisation de la commande dans le cas des variables  $x$  et  $y$  scalaires.

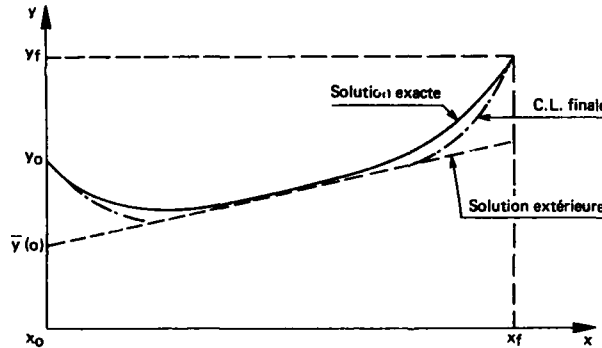


Fig. 2 - Commande composite.

### 3.6 - Extension aux systèmes multivariables

La décomposition d'un problème de commande optimale par un système dynamique à deux échelles de temps, en trois problèmes successifs plus simples :

- couche limite initiale,
- solution extérieure,
- couche limite finale,

est un résultat tout à fait général. Toutefois, on a vu que la commande optimale ne peut pas être facilement explicitée en boucle fermée sur l'état seul, sauf dans le cas où la variable lente et la variable rapide sont toutes les deux scalaires. Dans ce cas, en effet, il est possible d'éliminer les adjoints et d'éviter la résolution du problème aux deux bouts issu de l'application du principe de Pontryagin. Pour traiter le cas général d'un système multivariable, deux approches sont possibles en pratique, supposant l'une et l'autre que la variable lente  $x$  est scalaire, ou encore que le problème réduit puisse être résolu de manière analytique.

### 3.6.1 - Echelles de temps multiples, à séparation "complète"

Le vecteur rapide  $y$  est elle-même décomposée en variables scalaires  $y_i (i=1, \dots, n-1)$  de rapidité croissante.

Les équations sont écrites sous la forme suivante :

$$(39) \quad \begin{cases} \dot{x} &= f(x, y_1, \dots, y_{n-1}, u) \\ \dot{y}_1 &= g_1(x, y_1, \dots, y_{n-1}, u) \\ \dots \\ \dot{y}_{n-1} &= g_{n-1}(x, y_1, \dots, y_{n-1}, u) \end{cases}$$

La démarche précédente (§ 3.4) se généralise directement. Le problème d'optimisation initial d'un système de dimension  $n$  est décomposé en  $n$  problèmes d'optimisation statiques qui peuvent être résolus, de proche en proche, en partant de la variable la plus lente vers la variable la plus rapide.

Comme précédemment, une commande en "boucle fermée", valable uniformément le long de la trajectoire à l'exception du voisinage de l'état final, est donnée par la commande réactualisée fournie par la commande relative à la couche limite initiale la plus rapide.

L'inconvénient de cette démarche est l'hypothèse, pas toujours physiquement justifiée, de la séparation complète des échelles de temps du système. Le principal avantage réside dans l'obtention d'une commande non-linéaire par retour d'état.

### 3.6.2 - Linéarisation de la couche limite

Cette approche permet d'éviter l'hypothèse d'une séparation complète des échelles de temps multiples, et de traiter globalement le cas d'une couche limite comportant plusieurs variables.

Considérons d'abord le cas d'une couche limite initiale. Il est encore possible de résoudre explicitement la détermination de la commande, du moins pour l'approximation à l'ordre 0, en linéarisant les équations de la couche limite autour de la solution nominale définie par la solution extérieure.

La linéarisation de l'équation (26) et de l'indice de coût (27) autour des valeurs d'équilibre  $(x_0, \bar{y}(x_0))$  relatives à la solution extérieure, s'écrit (Bryson, Ho, 1975) :

$$(40) \quad \begin{cases} \frac{d\delta y}{dt} = A \delta y + B \delta u \\ \hat{J} = \int_0^{t \rightarrow \infty} [\delta y^T \delta u^T] \begin{bmatrix} Q & S \\ S^T & R \end{bmatrix} \begin{bmatrix} \delta y \\ \delta u \end{bmatrix} dt \end{cases}$$

$$\text{avec} \quad A = \left. \frac{\partial g}{\partial y} \right|_0, B = \left. \frac{\partial g}{\partial u} \right|_0, Q = \left. \frac{\partial^2 H}{\partial y^2} \right|_0, S = \left. \frac{\partial^2 H}{\partial y \partial u} \right|_0, R = \left. \frac{\partial^2 H}{\partial u^2} \right|_0.$$

$$\delta y = y(t) - \bar{y}(x_0), \delta u = u(t) - \bar{u}(x_0)$$

Les quantités  $A, B, Q, S, R$ , intervenant dans (40) sont des constantes évaluées au point d'équilibre  $(x_0, \bar{y}(x_0))$  relatif à l'instant initial.

La commande optimale  $\delta u^*$  pour la couche limite initiale est donnée par la solution classique du problème linéaire à coût quadratique en horizon infini :

$$(41) \quad \delta u^* = -R^{-1} (B^T P + S^T) \delta y$$

où  $P$  est la solution semi-définie positive de l'équation algébrique de Riccati (Bryson, Ho, 1975) :

$$(42) \quad \begin{aligned} P\hat{A} + \hat{A}^T P + \hat{Q} - PBK^*B^T P &= 0 \\ \text{avec} \quad \hat{A} &= A - BR^{-1}S^T, \hat{Q} = Q - SR^{-1}S^T \end{aligned}$$

L'existence de la solution  $P$  de cette équation est liée directement aux conditions de stabilité asymptotique de la couche limite.

L'avantage de cette démarche, par rapport à la séparation complète des échelles de temps, est qu'elle permet de traiter simultanément plusieurs variables et par suite permet d'éviter les inconvénients dus à une séparation artificielle des dynamiques.

Les inconvénients sont de deux sortes :

- d'une part, l'hypothèse de linéarité impose que les conditions initiales ne soient pas trop éloignées des valeurs d'équilibre de la solution extérieure,

- d'autre part, le calcul de la commande nécessite la résolution d'une équation matricielle algébrique de Riccati, dont la valeur dépend que l'état initial  $x_0$ . Dans le cas d'une réactualisation de la condition initiale, on doit ainsi résoudre cette équation à chaque instant courant  $t$ , ce qui peut conduire à des temps de calcul prohibitifs pour une utilisation en temps réel.

### Cas d'une couche limite finale

La linéarisation procède de façon analogue à celle de la couche limite initiale ; elle en diffère cependant par les points suivants :

- le changement d'échelle de temps est  $\sigma = (t_f - t)/\epsilon$  ;
- le point de linéarisation est le point d'équilibre relatif à l'instant final  $(x_f, \bar{y}(x_f))$  ;
- la convergence est obtenue en temps inverse, et il faut prendre la solution semi-définie négative  $N$  de l'équation de Riccati (42).

On notera enfin qu'il est possible de combiner les deux "recettes" précédentes, en travaillant sur des échelles de temps multiples, correspondant, les unes à des couches limites scalaires, les autres à des couches limites multivariées linéarisables.

### 3.7 - Amélioration de la précision

Pour améliorer la précision de l'approximation d'ordre 0, deux techniques ont été utilisées :

- 1) développement asymptotique à l'ordre 1,
- 2) prise en compte de "pseudo-solution extérieure".

La première méthode utilise la même démarche que la méthode des développements asymptotiques raccordés dont le principe est exposé dans (Ardena, 1983). L'inconvénient est qu'elle met en oeuvre des calculs complexes et il est difficile d'obtenir des solutions analytiques, à l'exception de quelques exemples simples comme l'interception dans un plan horizontal (Visser, Shinar, 1986).

La seconde méthode consiste à remplacer la solution extérieure par une "pseudo-solution extérieure", obtenue en traitant simultanément les équations en  $\bar{x}$  et  $\bar{y}$  du système (39), c'est-à-dire, en supposant que la variable  $y$ , est à la même échelle de temps que la variable lente  $x$  (Calise, Moerder, 1982).

### 3.8 - Problèmes pratiques et solutions

Si l'application de la théorie des perturbations singulières (P.S) à la détermination des lois de commande sous-optimale ne nécessite pas de développement mathématiques complexes, au moins lorsque que l'on se limite à l'approximation d'ordre 0, de nombreuses difficultés ont été rencontrées en pratique et à l'heure actuelle, il n'existe pas encore de méthode "miracle" permettant de résoudre de façon satisfaisante tous les problèmes. Ce paragraphe résume les deux principaux obstacles rencontrés qui font que l'application de cette théorie des P.S. à la commande optimale relève à l'heure actuelle, plus de l'art que la théorie.

#### 3.8.1 - Détermination des échelles de temps

Un travail préliminaire consiste à mettre les équations de la dynamique d'un système différentiel non-linéaire sous la forme singulièrement perturbée, si possible du type (39), c'est-à-dire avec séparation complète des dynamiques.

##### 1) Séparation des dynamiques

Dans le domaine linéaire, le problème est bien maîtrisé et l'on dispose d'un grand nombre de techniques, allant des plus simples (cercles de Gerschgorine et Ovals de Cassini) aux plus sophistiquées (calcul des valeurs propres et des vecteurs propres). Une excellente revue de ces techniques est faite dans (Moreigne, 1984).

Par contre, dans le domaine non-linéaire, les solutions proposées sont souvent complexes et constituent souvent un problème en soi :

i) la première méthode consiste à utiliser les techniques du domaine linéaire en linéarisant les équations autour d'une trajectoire optimale nominale. La méthode a été utilisée dans (Moreigne, 1984). La démarche est complexe et fournit seulement des combinaisons linéaires de variables d'état du système envisagé.

ii) la deuxième approche consiste à rechercher des transformations non-linéaires permettant de séparer les variables lentes et les variables rapides. Le principe est séduisant mais on aboutit à une équation aux dérivées partielles dont la solution est inextricable (Kelley, 1972), à l'exception des cas particulièrement simples dont on connaît déjà la solution a priori (Ardena, Rajan, 1985).

iii) une troisième approche consiste à évaluer simplement la vitesse de variation des diverses variables, par exemple sous la forme (Ardena, Rajan, 1985) :

$$\frac{\dot{x}_i}{\Delta x_i} = \max_{\substack{u \in U \\ x \in D}} \frac{1}{\Delta x_i} f_i(x, u)$$

#### 3.8.2 - Perturbation singulière forcée

Pour mettre en évidence les  $\epsilon^i$ , une solution consiste à effectuer des changements de variables et un changement de l'échelle de temps de façon à faire apparaître ces petits paramètres au premier membre de (39).

Si, dans certains cas simples, comme l'interception dans le plan horizontal, il est possible d'appliquer cette démarche (Visser, Shinar, 1986), le problème est en général non trivial.

Par ailleurs, comme la dynamique est essentiellement non-linéaire, la mise en évidence de ce paramètre  $c$  n'est valable que localement, c'est-à-dire pour une certaine classe de trajectoires et il est à prévoir que la classification entre variables rapides et lentes risque même de changer tout au long d'une même trajectoire.

Pour cette raison, il peut être préférable d'utiliser la démarche appelée "perturbation singulière forcée" (Shinar, Merari, 1980) qui consiste à introduire les paramètres  $c$  de façon tout à fait artificielle. Cela revient à imposer a priori, une hiérarchisation dans la dynamique de comportement du système, qui n'est peut-être pas réaliste, mais est justifiée a posteriori par la qualité des résultats auxquels cette hypothèse conduit.

### 3.8.3 - Conditions finales sur les variables rapides

La mise en oeuvre de la commande optimale "composite" issue de la théorie des P.S. ne permet pas d'obtenir une précision acceptable lorsque les conditions finales portent aussi sur les variables rapides. En effet, comme la couche limite finale converge bien vers la solution extérieure, mais en temps inverse, son utilisation en "temps réel", c'est-à-dire en temps direct conduirait à une erreur insupportable.

Pour pallier à cet inconvénient, il convient de citer les trois solutions suivantes :

- i) la première consiste à changer la décomposition des variables au voisinage de l'instant final de façon à faire apparaître les conditions finales sur les variables lentes seulement.
- ii) la deuxième méthode consiste à adopter une démarche complètement différente. La méthode des P.S. sert à déterminer la loi de commande de couche limite finale. L'arc de trajectoire finale est ensuite intégrée en temps inverse jusqu'à la solution extérieure. Cette portion de trajectoire est enregistrée et utilisée comme profil de guidage à suivre en temps direct. Cette deuxième technique s'applique à toutes sortes de contraintes sur l'état final du type (14) (voir l'application traitée plus loin § 4.2).
- iii) la troisième méthode consiste à commuter sur d'autres lois de commande provenant d'autres décompositions de la dynamique selon une technique de multi-classement (Fossard, Freitas, 1986).

## 4 - APPLICATION AUX LOIS DE GUIDAGE EN "TEMPS REEL" POUR LES TRAJECTOIRES D'AVION A TEMPS MINIMUM

### 4.1 - Pose du problème

#### 4.1.1 - Hypothèses

L'avion est assimilé à un corps ponctuel, de masse constante, évoluant dans un repère inertiel sur une terre plate, de pesanteur constante.

La poussée de l'avion est supposée dirigée le long du vecteur vitesse, sa valeur maximale est une fonction de l'altitude et du nombre de Mach et elle est fournie sous forme de table à deux dimensions  $F_M(h, M)$ .

La polaire est supposée parabolique :

$$(43) \quad C_x = C_{x_0}(M) + k(M)C_z^2$$

où les coefficients  $C_{x_0}$ ,  $k$  sont des fonctions du nombre de Mach. On suppose en outre que l'avion évolue à dérapage nul et les transitoires sur le mouvement d'attitude sont négligées.

De ce fait, les commandes de l'avion sont le taux de poussée  $\delta_z$ , le facteur de charge normal  $n_z$  et l'angle de gîte aérodynamique  $\mu$ . Dans la suite de l'étude, on s'intéresse essentiellement aux trajectoires pour lesquelles le taux de poussée  $\delta_z$  optimal est constamment égal à l'unité, ce qui est généralement le cas des manœuvres d'interception.

#### 4.1.2 - Equations du mouvement

La position et la vitesse de l'avion sont caractérisées par l'altitude  $h$ , les coordonnées horizontales  $x$  et  $y$  de la position relative entre l'avion et une cible (dont la position et la vitesse sont supposées connues par ailleurs) le module de la vitesse  $V$ , ou encore de façon équivalente l'énergie spécifique définie par  $E = h + V^2/2g$  sa pente  $\gamma$  et son azimut  $\chi$  (voir Fig.3).

Dans la suite, on utilise les variables réduites sans dimension définies par :

$$\bar{t} = gt/a_0, \quad \bar{x} = gx/a_0^2, \quad \bar{y} = gy/a_0^2, \quad \bar{h} = gh/a_0^2, \quad \bar{V} = V/a_0, \quad \bar{F}_m = F_m/mg, \quad \bar{E} = gE/a_0^2$$

où  $a_0$  est une vitesse de référence et  $g$  l'accélération de pesanteur.

Les équations réduites sans dimension du mouvement de l'avion sont données par le système différentiel suivant, en omettant le symbole  $(\cdot)$  pour simplifier l'écriture :

$$(44a) \quad \begin{cases} \dot{\bar{x}} = \bar{V} \cos \gamma \cos \chi - \bar{V}_c \\ \dot{\bar{y}} = \bar{V} \cos \gamma \sin \chi \\ \dot{\bar{h}} = \bar{V} \sin \gamma \\ \dot{\bar{E}} = \bar{V} (\delta_z \bar{F}_m - D_0 - D_1 n_z^2) \\ \dot{\chi} = (n_z \sin \mu) / (\bar{V} \cos \gamma) \\ \dot{\gamma} = (1/\bar{V}) (n_z \cos \mu - \cos \gamma) \end{cases} \quad \text{avec} \quad \begin{cases} D_0 = \frac{\rho V_a^2 S C_{x_0}}{2 mg} & D_1 = \frac{2 k mg}{\rho V_a^2 S} \\ n_z = \frac{\rho V_a^2 S C_z}{2 mg} \end{cases}$$

Dans cette équation  $v_c$  désigne la vitesse de la cible, supposée animée d'un mouvement rectiligne uniforme à altitude constante selon l'axe des  $x$ .

En utilisant la vitesse  $V$ , au lieu de l'énergie spécifique  $E$ , on obtient le même système d'équations, mais où l'équation en  $E$  est remplacée par l'équation suivante :

$$(44b) \quad \dot{V} = \delta_z F_m - D_0 - D_1 n_x^2 - \sin \gamma$$

Dans la suite, on considérera uniquement des trajectoires telles que la poussée soit toujours maximale, c'est-à-dire :  $\delta_z = 1$ .

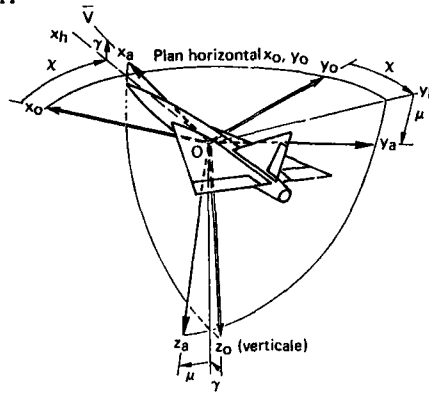


Fig. 3 - Définition des angles  $\gamma, \chi, \mu$ .

4.1.3 - Définition du problème d'optimisation

Le problème consiste à trouver des lois de commande  $n_x$  et  $\mu$  de façon à rejoindre un ensemble de conditions finales spécifiées, à partir d'un état initial complètement défini, en un temps minimum.

La nature du problème dépend des conditions finales imposées. Dans la suite, on s'intéresse aux trajectoires suivantes :

- 1) montée en temps minimum dans un plan vertical : les conditions finales portent uniquement sur les variables  $E, h$  et  $\gamma$ ;
- 2) interception tridimensionnelle : les conditions finales portent uniquement sur la position relative à la cible, c'est-à-dire :

$$(45) \quad x(t_f) = 0, y(t_f) = 0, h(t_f) = h_c,$$

où  $h_c$  est l'altitude de vol de la cible.

La résolution du problème d'optimisation doit prendre en compte des limitations physiques sur les commandes et sur l'état de l'avion :

$$(46) \quad \left\{ \begin{array}{l} C_z \min \leq C_z \leq C_z \max \\ |n_x| \leq n_x \min \\ q = \rho V^2 / 2 \leq q_{\max} \\ M \leq M_{\max} \end{array} \right.$$

Un modèle d'avion de combat typique est utilisé pour les applications numériques. Le domaine de vol de cet avion est présenté sur la figure 4.

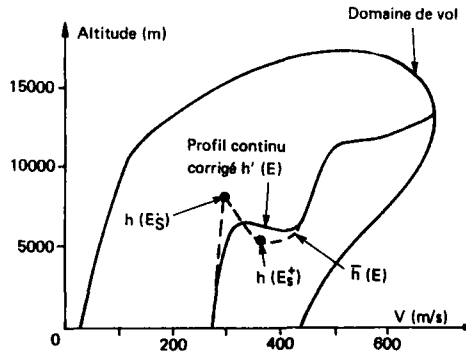


Fig. 4 - Profil continu de montée énergétique.

#### 4.2 - Montée en temps minimum dans un plan vertical

##### 4.2.1 - Equations singulièrement perturbées

Comme la position n'intervient pas dans les conditions finales, et en se limitant au mouvement dans le plan vertical, l'état de l'avion peut être ramené à trois variables : E, h, et  $\gamma$ .

L'étape préliminaire consiste à mettre les équations du mouvement sous la forme singulièrement perturbée, permettant de mettre en évidence la séparation entre différentes échelles de temps du système. La démarche utilisée ici est la méthode des perturbations régulières forcées, déjà mentionnée précédemment. Une étude préliminaire, effectuée avec un modèle linéarisé, utilisant une méthode présentée précédemment (§3.3.1), montre que la dynamique de l'avion peut être décomposée en deux échelles de temps, dans l'ordre de rapidité croissante suivante : énergie E, altitude h et pente  $\gamma$ .

Les équations sont mises sous la forme singulièrement perturbée suivante :

$$(47) \quad \begin{cases} \dot{E} = V(F_m - D_0 - D_1 n_x^2) \\ \dot{h} = V \sin \gamma \\ \dot{\gamma} = (1/V)(n_x - \cos \gamma) \end{cases}$$

à  $\epsilon$  est un "petit" paramètre introduit artificiellement pour séparer l'échelle de temps entre E et (h,  $\gamma$ ).

##### 4.2.2 - Approximation d'ordre 0

###### Solution extérieure

Rappelons qu'elle est obtenue en faisant  $\epsilon = 0$  dans les équations (47). En s'intéressant uniquement aux trajectoires de montée ( $E_f \geq E_0$ ), on obtient les résultats suivants, en désignant par le symbole  $\bar{h}$  la solution obtenue :

$$(48) \quad \begin{cases} \bar{n}_x = 1, \bar{\gamma} = 0 \\ \bar{h}(E) = \underset{h}{\text{Arg Max}} \{V(F_m - D_0 - D_1)\} \\ \bar{\lambda}_E = -\frac{1}{V(F_m - D_0 - D_1)}, \bar{\lambda}_h = 0, \bar{\lambda}_\gamma = 2\bar{\lambda}_E V^2 D_1 \end{cases}$$

Les valeurs de  $\bar{h}(E)$  peuvent être calculées préalablement hors ligne, et enregistrées en fonction de E sous forme de table. Pour le modèle d'avion utilisé, le profil de montée énergétique  $\bar{h}(E)$  est illustré sur la figure (4), avec un modèle d'atmosphère standard.

Une discontinuité apparaît sur ce profil au voisinage de la vitesse du son, c'est une caractéristique bien connue des avions de combat aux performances élevées. Elle est causée par des non-linéarités des coefficients aérodynamiques dans la zone transsonique. Cette discontinuité sera éliminée ultérieurement (voir plus loin §4.2.4).

###### Couche limite sur h et $\gamma$

On traite ici seulement le cas de la couche limite initiale, celui de la couche limite finale s'en déduit de façon similaire (voir §3.3.3).

Les équations de la couche limite initiale sont obtenues en faisant la dilatation de l'échelle de temps à l'origine ( $\tau = Vt$ ), puis en faisant  $\epsilon = 0$ :

$$(49) \quad \begin{cases} \frac{d\hat{h}}{d\tau} = \hat{V} \sin \hat{\gamma} \\ \frac{d\hat{\gamma}}{d\tau} = \frac{1}{\hat{V}} (\hat{n}_x - \cos \hat{\gamma}) \end{cases}$$

où le symbole ( $\hat{\cdot}$ ) est relatif à la couche limite initiale.

Pour obtenir la commande  $\hat{n}_x$  en boucle fermée, on applique la technique de linéarisation décrite précédemment (§3.6.2), le point de linéarisation étant défini par les valeurs de la solution extérieure à l'instant initial  $t_0 = 0$ .

Les éléments des matrices A, B, Q, R, S correspondant au système linéarisé (40) s'écrivent :

$$(50) \quad A = \begin{bmatrix} 0 & \bar{V}_0 \\ 0 & 0 \end{bmatrix}, B = \begin{bmatrix} 0 \\ 1/\bar{V}_0 \end{bmatrix}, Q = \begin{bmatrix} q_1 & 0 \\ 0 & q_2 \end{bmatrix}, S = \begin{bmatrix} s_1 \\ 0 \end{bmatrix}, R = -2\bar{\lambda}_E \bar{V}_0 D_1,$$

$$\text{avec } q_1 = -\bar{\lambda}_E \frac{\partial^2 E}{\partial h^2} \Big|_{E_0}, q_2 = 2\bar{\lambda}_E \bar{V}_0 D_1, s_1 = \frac{4\bar{\lambda}_E D_1}{\bar{V}_0} - 2\bar{\lambda}_E \bar{V}_0 \left( \frac{\partial D_1}{\partial h} \right) \Big|_{E_0}$$

Compte tenu de la forme particulière de ces matrices, la solution algébrique  $P$  de l'équation de Riccati (42) peut être obtenue analytiquement. L'expression de la commande  $\hat{n}_z$  dans la couche limite est, en définitive, donnée par :

$$(51) \quad \hat{n}_z = 1 - \frac{1}{R} (R^T P + S^T) \begin{bmatrix} h - \bar{h} \\ y - \bar{y}_0 \end{bmatrix} = 1 - \frac{1}{R} \left[ \left( \frac{P_2}{\bar{V}_0} + s_1 \right) (h - \bar{h}) + \frac{P_3}{\bar{V}_0} (y - \bar{y}_0) \right]$$

avec  $\bar{y}_0 = 0$  (ordre 0) ,  $\frac{P_2}{\bar{V}_0} = -s_1 + \sqrt{Rq_1} \cdot \left( \frac{P_3}{\bar{V}_0} \right)^2 = R(q_2 + 2p_2 \bar{V}_0) = R(q_2 + 2\bar{V}_0 \sqrt{Rq_1} - 2\bar{V}_0^2 s_1)$  .

#### 4.2.3 - Commande en temps réel à l'ordre 0

Pour obtenir une loi de commande en temps réel, valable tout le long de la trajectoire de montée, on procède de la façon indiquée au paragraphe précédent (§ 3.5). La commande comprend deux parties :

- 1) la première partie est valable tout au long de la trajectoire, sauf au voisinage de l'instant final ;
- 2) la deuxième partie permet d'assurer l'obtention des conditions finales désirées sur les variables rapides, c'est-à-dire l'altitude et/ou la pente.

##### - Commande en couche limite initiale et en solution extérieure

En utilisant la technique de réactualisation décrite plus haut (§ 3.5), la commande est donnée par la loi de couche limite initiale (51), dans laquelle il convient de remplacer la valeur initiale  $E_0$  et par sa valeur courante  $E$ . Il est à noter que la mise en oeuvre de cette loi (51) est relativement simple.

##### - Commande de couche limite finale

Pour tenir compte des conditions finales portant sur l'altitude et/ou sur la pente, en plus de l'énergie finale, la solution adoptée comprend deux étapes :

- 1) la première consiste à calculer la trajectoire permettant de raccorder les conditions finales avec la solution "extérieure". Cette trajectoire est obtenue en intégrant les équations complètes du mouvement à partir des conditions finales, en utilisant la commande de couche limite finale réactualisée, comme pour la couche initiale.

Lorsque l'état final est partiellement fixé, la valeur finale de la variable inconnue ( $h_f$  ou  $y_f$ ) est déterminée en exploitant la relation linéaire liant le vecteur adjoint au vecteur d'état à travers la solution semi-définie négative  $N$  de l'équation de Riccati :

$$(52) \quad \begin{bmatrix} \delta \lambda_{h_f} \\ \delta \lambda_{y_f} \end{bmatrix} = \begin{bmatrix} N \\ N \end{bmatrix} \begin{bmatrix} \delta h_f \\ \delta y_f \end{bmatrix} .$$

La trajectoire ainsi obtenue est ensuite enregistrée sous forme de courbes  $h_d(E)$ ,  $y_d(E)$ .

- 2) en temps direct, la commande  $n_z$  est déterminée de façon à effectuer une "bonne" poursuite de la trajectoire pré-enregistrée. Dans les exemples numériques, la loi retenue pour  $n_z$  est calculée simplement en agissant directement sur la pente au moyen de la formule :

$$(53) \quad n_z = KV(y_d - y) + \cos \gamma$$

où  $y_d$  est la pente désirée à chaque instant, fournie par la trajectoire pré-enregistrée,  $K$  est un gain scalaire choisi de façon à assurer un bon suivi de la pente désirée sans forcer sur le facteur de charge de l'avion.

La commutation sur cette loi peut être effectuée à partir du moment où la solution "extérieure" du profil de montée est atteinte.

#### 4.2.4 - Problème du passage de la zone transsonique

Il a été vu précédemment qu'une discontinuité apparaît sur l'altitude dans le profil de montée énergétique, lors du calcul de la solution "extérieure".

Analytiquement, cette discontinuité peut s'expliquer de la façon suivante. La fonction  $\dot{E}(h, E)$  qu'on désire maximiser (voir (48)), présente au voisinage de  $M = 1$ , deux maximums relatifs correspondant à deux altitudes distinctes. En subsonique, le maximum absolu correspond à l'altitude la plus basse, alors qu'en supersonique, il correspond à l'altitude la plus haute. La discontinuité sur l'altitude apparaît au moment où ces deux maximums sont égaux (voir figure 5).

Pour remédier à cet inconvénient une démarche a été proposée : elle consiste à déterminer une trajectoire permettant de relier les deux points d'équilibre dans un espace à 4 dimensions  $(h, y, \lambda_h, \lambda_y)$ . Cette démarche est de mise en oeuvre complexe car elle nécessite une résolution numérique par programmation non-linéaire (Weston, Cliff, Kelley, 1981).

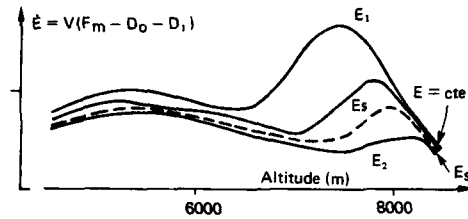


Fig. 5 - Illustration de la discontinuité sur le profil de montée énergétique  $h(E)$ .

La solution proposée ici procède par linéarisation des équations de la couche limite en  $h$  et en  $v$  comme pour une couche limite ordinaire. La trajectoire de transition est obtenue en intégrant les équations complètes du mouvement (47) avec la commande linéarisée (51). Le point de linéarisation est fixé à la valeur d'équilibre stable  $h(E_s)$  pour  $E < E_s$ , il évolue ensuite avec l'énergie  $E$  dès que celle-ci dépasse  $E_s$ . Les conditions initiales, permettant de déterminer l'instant où la transition intervient, ont été obtenues par balayage des valeurs initiales  $(E_0, h(E_0))$  le long du profil de montée, dans la zone subsonique, la pente initiale  $v_0$  étant ajustée de façon à obtenir un "bon" raccordement avec le profil de montée. Un profil continu  $h'(E)$  est ainsi obtenu pour l'altitude (voir figure 4).

#### 4.2.5 - Amélioration de la commande d'ordre 0

On verra dans les exemples numériques que l'approximation à l'ordre 0 est pénalisée par un retard non négligeable pour suivre le profil de montée en énergie  $h'(E)$ . Ce retard provient du fait que l'altitude change de la solution "extérieure", ce qui correspond à une pente  $\gamma$  non nulle, alors que la pente  $\bar{v}$  donnée à l'ordre 0 est nulle.

Pour améliorer cette loi, un développement asymptotique à l'ordre 1 est effectué pour la solution extérieure.

L'utilisation complète du développement à l'ordre 1 est complexe car elle nécessite la détermination de constantes arbitraires qui ne pourrait être obtenue qu'à travers des calculs complexes (Ardema, 1976 ; Moreigne, 1984).

Pour tenir compte de l'apport de l'ordre 1, la démarche proposée ici est d'utiliser toujours la commande de couche limite initiale à l'ordre 0 donnée par (51), mais la valeur nominale relative à la pente  $\bar{v} = 0$  est remplacée par son approximation à l'ordre 1 :  $\bar{v}_1 = \frac{1}{\bar{v}_0} \frac{dh}{dt}$ .

Ce terme peut encore s'écrire, en faisant apparaître la variation de  $h$  en fonction de l'énergie

$$(54) \quad \bar{v}_1 = \frac{1}{\bar{v}_0} \frac{dh}{dE} \cdot \dot{E} = \frac{dh'}{dE} \cdot (F_m - D_0 - D_1)$$

Ce dernier terme peut être calculé aisément à partir du profil de montée donnée par la figure 4.

### 4.3 - Interception tridimensionnelle

#### 4.3.1 - Equations singulièrement perturbées

Comme mentionné au précédent paragraphe, la première étape consiste à mettre en évidence des échelles de temps différentes.

Pour des trajectoires d'interception dans l'espace tridimensionnel, diverses décompositions ont été retenues, permettant de déduire des lois de commandes sous-optimales de mise en oeuvre simple.

Il n'existe aucun moyen théorique permettant de démontrer la validité ou non d'une décomposition par rapport à une autre. La seule manière de vérifier la validité et par suite l'intérêt d'une loi de commande en temps réel par rapport à une autre, est la comparaison avec la solution optimale, en boucle ouverte, fournie par des algorithmes numériques d'optimisation.

Dans la suite, on retiendra la décomposition suivante, en partant de la dynamique la plus lente vers la plus rapide :  $(x, y); E; X; (h, \gamma)$ .

D'autres décompositions ont été également envisagées par divers auteurs. Le lecteur intéressé pourra consulter par exemple (Mehra, 1979 ; Calise, Noerder, 1982 ; Rajan, Ardema, 1985 ; Shinar, Well, Jarmark, 1986).

Dans la suite la résolution est décrite pour la décomposition utilisant l'énergie spécifique  $E$  comme variable d'état. La solution relative à  $\dot{c}$  de la vitesse comme variable d'état est mentionnée plus loin (§4.3.5).

Les équations (44a) sont mises sous la forme singulière perturbée suivante, en introduisant les au premier membre de façon artificielle pour séparer les dynamiques entre les différentes variables :

$$(55) \quad \begin{cases} \dot{x} = V \cos \gamma \cos \chi - V_c \\ \dot{y} = V \cos \gamma \sin \chi \\ c\dot{E} = V(F_m - D_0 - D_1 n_x^2) \\ c^2\dot{\chi} = (n_x \sin \mu)/(V \cos \gamma) \\ c^3\dot{h} = V \sin \gamma \\ c^3\dot{y} = (1/V)(n_x \cos \mu - \cos \gamma) \end{cases}$$

sous cette forme, on a ainsi forcé la séparation de la dynamique en quatre échelles de temps, conformément à la décomposition retenue, c'est-à-dire dans le sens de rapidité croissante suivant : position horizontale  $(x,y)$ , énergie  $E$ , azimut  $\chi$ , altitude et pente  $h, \gamma$ .

#### 4.3.2 - Résolution de la solution à l'ordre 0

A partir de cette formulation (55), l'application de la théorie de la commande optimale des systèmes singulièrement perturbés, conduit à résoudre le problème complet en quatre étapes successives, en partant de la solution extérieure, relative à la variable lente, vers la couche limite la plus rapide.

La solution obtenue pour chacune de ces étapes est résumée dans la suite (pour obtenir plus de détails, voir (Do khac, Buyah, 1988)).

##### . Solution extérieure (on réduite)

La trajectoire est définie par un point dans le domaine de vol  $(h, V)$  de l'avion. Elle correspond à un vol horizontal, rectiligne, à la vitesse maximale de l'avion  $\bar{V}_0 = V_{max}$ . l'altitude correspondante est notée  $h_0$  (voir figure 6).

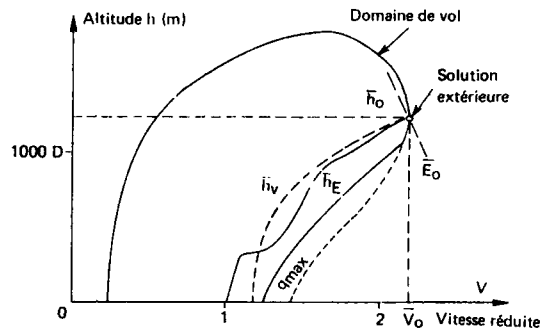


Fig. 6 - Profil de montée en énergie  $h_E(E)$  et en vitesse  $h_V(V)$  pour l'interception.

C'est une trajectoire de collision dans un vertical défini par un azimut nominal  $\bar{\chi}_0$  selon la figure 7.

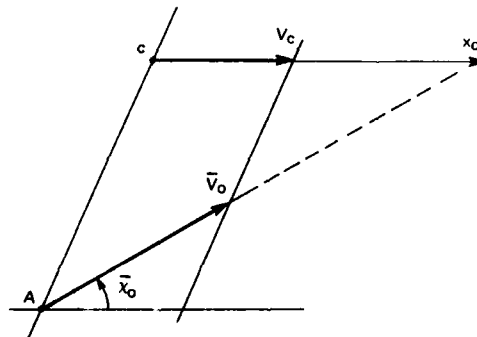


Fig. 7 - Solution extérieure (projection horizontale).

Première couche limite initiale (énergie)

Cette "couche limite" permet, à partir de l'énergie initiale de l'avion, d'atteindre l'énergie correspondante à la solution extérieure, définie par  $\bar{E}_0 = \bar{h}_0 + \bar{V}_0^2 / 2$ .

La trajectoire s'effectue dans un plan vertical, selon un profil, désigné dans la suite par "montée énergétique (en interception)". Ce profil est défini dans le plan (h,V), ou de façon équivalente (h,E), par :

$$(56) \quad \bar{h}_E(E) = \underset{h}{\text{Arg Max}} \left\{ \frac{V(F_m - D_0 - D_1)}{\bar{V}_0 - V} \right\}_{E_{\text{courant}}} \quad (\text{avec } E \leq \bar{E}_0)$$

Il est à noter que ce profil est identique au profil de "montée énergétique" en interception dans un plan vertical (Huynh, Moreigne, 1985). La figure 6 présente, non pas le profil original donné par (56), mais un profil lissé, déduit de ce dernier par un lissage polynomial classique. Ce lissage permet de supprimer la discontinuité qui se trouvait dans la zone transsonique avec le profil d'origine.

Deuxième couche limite initiale (azimut  $\chi$ )

Cette couche limite permet de raccorder l'azimut initial de l'avion à l'azimut du plan nominal, défini par  $\bar{\chi}_0$  (figure 7), dans lequel s'effectue l'interception.

La trajectoire est ici un virage horizontal en suivant un certain profil d'altitude  $\bar{h}_\chi(E, \chi)$  qui est, en principe, différent du profil de "montée énergétique"  $\bar{h}_E(E)$ .

Ce profil  $\bar{h}_\chi(E, \chi)$  dépend de l'énergie E et de l'écart  $\Delta\chi = \chi - \bar{\chi}_0$  entre l'azimut réel de l'avion et l'azimut nominal  $\bar{\chi}_0$  de la solution extérieure, il est défini par la résolution de (57) :

$$(57) \quad \bar{h}_\chi(E, \chi) = \underset{h}{\text{Arg Min}} \left\{ H_\chi(h, \chi) \right\}_{E, \chi_{\text{courant}}}$$

avec

$$H_\chi(h, \chi) = \left| \frac{\bar{V}_0 - V \cos(\chi - \bar{\chi}_0)}{\bar{V}_0 - V_c \cos \bar{\chi}_0} + \bar{\lambda}_{E_0} V (F_m - D_0 - D_1) \right|$$

$$\bar{\lambda}_{E_0} = \left\{ - \frac{\bar{V}_0 - V}{V(\bar{V}_0 - V_c \cos \bar{\chi}_0)(F_m - D_0 - D_1)} \right\} \bar{h}_E$$

On peut vérifier que ce profil de "virage" tend vers le profil de "montée énergétique" précédent  $\bar{h}_E(E)$  (donnée par (56)) quand l'azimut  $\chi$  tend vers l'azimut nominal  $\bar{\chi}_0$  :

$$\lim_{\chi \rightarrow \bar{\chi}_0} \bar{h}_\chi(E, \chi) = \bar{h}_E(E)$$

Les commandes optimales, notées par  $\bar{\mu}_\chi$  et  $\bar{\nu}_\chi$  pour cette couche limite sont données par :

$$(58) \quad \left\{ \begin{array}{l} \text{tg } \bar{\mu}_\chi = \text{signe}(\chi - \bar{\chi}_0) \cdot \sqrt{\frac{H_\chi(h, \chi)}{-\bar{\lambda}_{E_0}(V D_1) \bar{h}_\chi}} \\ \bar{\nu}_\chi = \frac{1}{\cos \bar{\mu}_\chi} \end{array} \right.$$

La quantité sous le radical est donnée par (57).

Troisième couche limite initiale (altitude h et pente  $\nu$ )

Cette couche limite permet de rejoindre, à partir de l'altitude et la pente initiale  $(h_0, \nu_0)$ , l'altitude et la pente relative à la solution "extérieure", c'est-à-dire le profil  $\bar{h}_\chi(E_0, \chi_0)$  de la couche limite précédente.

Pour obtenir une commande en boucle fermée, les équations de la couche limite sont linéarisées selon la technique indiquée précédemment (§ 3.6.2).

La commande, pour cette couche limite, est de la forme suivante :

$$(59) \quad \begin{bmatrix} \hat{\mu} \\ \hat{\nu} \end{bmatrix} = \begin{bmatrix} \bar{\mu}_\chi \\ \bar{\nu}_\chi \end{bmatrix} + \begin{bmatrix} k_1 & k_2 \\ k_3 & k_4 \end{bmatrix} \cdot \begin{bmatrix} \hat{h} - \bar{h}_{\chi_0} \\ \hat{\nu} - \bar{\nu}_{\chi_0} \end{bmatrix}$$

où  $(k_1, k_2, k_3, k_4)$  sont les gains du retour d'état, obtenus par résolution de l'équation matricielle de Riccati (42), de dimension deux dans le cas présent.

Couches limites finales

Pour l'interception tridimensionnelle, les conditions finales, portant sur les variables rapides, font intervenir uniquement l'altitude et par suite, pour résoudre complètement le problème, il reste à compléter les solutions précédentes par le calcul de la couche limite finale sur l'altitude et la pente. Pour cela, la démarche est analogue à celle de la couche limite initiale. (voir plus haut).

#### Loi de commande en boucle fermée à l'ordre 0

Une loi de commande en boucle fermée, valable uniformément le long de la trajectoire, est obtenue en procédant de la même façon que pour la trajectoire de montée en temps minimum.

Elle comprend deux parties :

1) la première partie, valable tout le long de la trajectoire, sauf au voisinage de l'instant final, est donnée par la commande de couche limite initiale (59), en utilisant la méthode de réactualisation mentionnée précédemment (§ 3.5).

2) la deuxième partie, valable au voisinage de l'instant final, peut être obtenue par la technique du suivi de trajectoire nominale comme pour la montée (§ 4.2.3.). En fait, on adopte ici une loi de commande de nature différente (voir ci-après § 4.3.3).

#### 4.3.3 - Améliorations de l'approximation d'ordre 0

Pour améliorer les performances de cette loi de commande en boucle fermée, fournie par l'approximation d'ordre 0, des modifications ont été apportées à cette structure sur les trois points suivants :

- loi de commande finale,
- prise en compte des trajectoires de courte portée,
- amélioration de la pente nominale d'ordre 0.

#### Commande finale

Au lieu d'utiliser la commande donnée par la solution de couche limite en altitude et en pente selon la théorie des P.S. décrite plus haut, on applique pour la phase finale d'interception la commande permettant de réaliser une trajectoire de collision tridimensionnelle. La géométrie d'une telle trajectoire est indiquée sur la figure (8). L'instant de commutation sur cette loi de commande est obtenu par intégration au préalable des équations du mouvement en temps inverse et par le raccordement de l'énergie sur le profil de montée  $h_E$  de la solution extérieure.

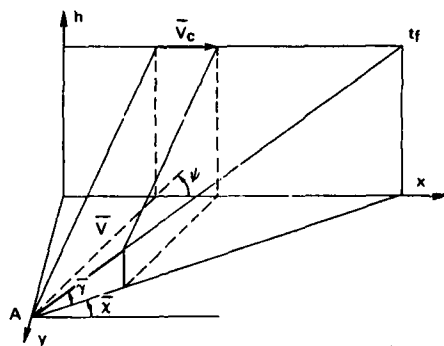


Fig. 8 - Géométrie d'une trajectoire de collision tridimensionnelle  $V_c \sin \psi = V \cos \gamma \sin (\psi - \gamma)$ .

L'emploi de cette commande de trajectoire de collision présente l'avantage, par rapport à la solution fournie par les P.S., d'une meilleure réalisation de conditions finales d'interception (voir résultats numériques plus loin § 4.4).

#### Prise en compte des trajectoires d'interception de courte portée

Pour pouvoir calculer l'arc de trajectoire finale par la méthode retenue ici, il convient de définir complètement l'état final, c'est-à-dire les valeurs finales des variables  $x, y, E, X, h$  et  $\gamma$ . Les conditions finales sur  $x, y$  et  $h$  sont fournies par les conditions d'interception (45).

En principe, les valeurs finales des autres variables  $E, X$  et  $\gamma$  sont fournies par la solution extérieure, c'est-à-dire  $E_0, X_0$  et  $\gamma_0 = 0$  (voir § 4.3.2). Or ces valeurs correspondent aux trajectoires d'interception de portée suffisamment longue pour que l'avion ait le temps d'atteindre la solution extérieure, c'est-à-dire la vitesse maximale de croisière.

Pour prendre en compte des trajectoires de durée moyenne, les conditions finales  $E_f, X_f$  et  $\gamma_f$  sont calculées, de façon hors ligne, en supposant que l'énergie  $E$  est une variable lente, à la même échelle de temps que les coordonnées horizontales  $x, y$ , et en cherchant à résoudre la solution extérieure de ce nouveau problème d'optimisation singulièrement perturbé. On peut alors démontrer que cette solution est encore une trajectoire de collision horizontale, l'altitude étant donnée, à chaque instant, par le profil de montée énergétique  $h_E(E)$  donnée par (56). (voir § 4.3.2).

Les conditions finales  $E_f$  et  $\chi_f$  sont alors fournies par les relations suivantes :

$$(60a) \quad \left\{ \begin{array}{l} x_f - x_0 = -x_0 = \int_{E_0}^{E_f} \frac{V \cos \chi - V_c}{V(F_m - D_0 - D_1) \bar{h}_E} dE = \phi_x(E_f, \chi_f) \\ y_f - y_0 = -y_0 = \int_{E_0}^{E_f} \frac{V \sin \chi - V_c}{V(F_m - D_0 - D_1) \bar{h}_E} dE = \phi_y(E_f, \chi_f) \end{array} \right.$$

La pente finale  $\chi_f$  est fournie par la condition finale d'interception de type collision :

$$(60b) \quad \cos \chi_f = \frac{V_c}{V_f}$$

#### Amélioration de la pente nominale d'ordre 0

Une amélioration de la pente nominale  $\bar{V}_X$ , intervenant dans la commande (59), est obtenue en opérant comme pour les trajectoires de montée dans le plan vertical, en modifiant la valeur nominale utilisée. En effet, l'approximation d'ordre 0 fournit  $\bar{V}_X = 0$ , alors que le profil de "montée énergétique"  $\bar{h}_E(E)$  donnée sur la figure (6), nécessite une pente non nulle.

Dans la suite, il convient de remplacer cette pente nulle par son approximation à l'ordre 1, donnée par :

$$\bar{V}_1 = \frac{1}{\bar{V}} \cdot \frac{d\bar{h}_E}{dt}$$

que l'on peut encore écrire sous la forme suivante :

$$(61) \quad \bar{V}_1 = \frac{1}{\bar{V}} \cdot \frac{d\bar{h}_E}{dE} \cdot \dot{E} = \frac{d\bar{h}_E}{dE} (F_m - D_0 - D_1)$$

Cette dernière quantité peut être calculée aisément à partir du profil de "montée énergétique"  $\bar{h}_E(E)$ .

#### 4.3.4 Résumé de la commande en temps réel

Une loi de commande sous-optimale, uniformément valable dans un large domaine de vol pour des trajectoires d'interception tridimensionnelle, est ainsi obtenue en se basant sur la théorie des P.S., avec quelques aménagements dans le but d'améliorer la réalisation des conditions finales et le domaine d'utilisation.

Le calcul de cette loi de commande en boucle fermée nécessite les étapes suivantes de calculs :

- 1) Profil d'altitude  $\bar{h}_E$  de la solution extérieure (Eq. (56)).
- 2) Valeurs finales de  $E_f, \chi_f, \chi_f$  (Eq. (60)).
- 3) Profil d'altitude  $\bar{h}_X$  relative à la première couche limite initiale (Eq. 57).
- 4) Valeurs "nominales" des commandes  $\bar{u}_x$  et  $\bar{u}_y$ , données par (Eq. (58)).
- 5) Commande en boucle fermée donnée par (Eq. (59), (61)).
- 6) La commutation de la commande précédente vers la commande finale peut être effectuée très simplement en remplaçant les valeurs nominales intervenant dans (Eq. (58) (59)) par des valeurs  $\bar{V}, \bar{X}$  provenant de la trajectoire de collision tridimensionnelle illustrée par la figure (8).

#### 4.3.5 - Solution avec l'utilisation de vitesse

En utilisant comme variable d'état la vitesse  $V$ , au lieu de l'énergie spécifique  $E$ , et en adoptant la même décomposition dynamique pour ce vecteur d'état, on peut déduire de façon analogue une loi de commande en boucle fermée.

Cette nouvelle commande se présente de la même forme que celle provenant de la "solution avec  $E$ " (c'est-à-dire utilisant  $E$  comme variable d'état), la différence se situe uniquement au niveau des profils d'altitude  $\bar{h}_V(V)$  et  $\bar{h}_{X_V}(V)$  relatifs aux couches limites en  $V$  et en  $\chi$ .

Le profil d'altitude  $\bar{h}_V(V)$  est également représenté sur la figure 6, après lissage comme pour  $\bar{h}_E(E)$ . on note une légère différence par rapport au profil  $\bar{h}_E(E)$  relatif à la "solution avec  $E$ ". Pour obtenir davantage de détails, le lecteur pourra consulter (Do Khac, Huynh, 1988).

#### 4.3.6 - Cas particuliers de l'interception dans le plan vertical et dans le plan horizontal

Il convient de noter que les commandes en boucle fermée développées pour l'interception tridimensionnelle sont également valables pour des trajectoires d'interception soit dans un plan vertical, soit encore dans un plan horizontal.

Dans ces cas particuliers, on peut noter les simplifications suivantes par rapport à la solution complète (les remarques concernant la "décomposition en  $E$ ", celles relatives à la "décomposition en  $V$ " sont analogues) :

1) Interception dans un plan vertical

- la deuxième couche limite en  $\chi$  n'existe pas et le profil  $\bar{h}_\chi$  est alors identique au profil de montée puisqu'il n'y a pas de virage à effectuer ;
- la commande (59) est simplifiée, il ne reste plus que le terme en  $n_2$  puisque la commande en roulis  $\mu$  est alors identiquement nulle ;

2) Interception dans un plan horizontal

- comme l'altitude est fixée, la première couche limite en énergie n'existe pas, et la solution de la couche limite en  $\chi$  est également simplifiée, puisque l'altitude  $\bar{h}_\chi$  est alors constante ;
- la commande (59) est également simplifiée, il ne reste plus que l'un des deux termes en  $n_2$  ou en  $\mu$ , puisque l'on a la relation suivante entre ces deux commandes  $n_2 = 1/\cos \mu$ .

4.4 - Résultats de simulation numérique

Avant d'évaluer les performances fournies par les lois de commande en temps réel, une validation de l'approche de linéarisation de la couche limite a été effectuée au préalable en la comparant avec une loi non-linéaire, par retour d'état, obtenue en séparant les variables  $h$  et  $\gamma$ .

Les performances des lois de commande en "boucle fermée" de mise en œuvre simple, sont ensuite comparées avec des lois de commande fournies par un code numérique d'optimisation fonctionnelle utilisant un algorithme de gradient projeté appliqué au problème original, non singulièrement perturbé. Il est à noter que les solutions optimales ainsi obtenues sont seulement de type "boucle ouverte", donc nettement moins intéressantes que les solutions en "boucle fermée".

Pour accélérer la convergence de l'algorithme numérique, son initialisation est fournie par la trajectoire donnée par la commande en "boucle fermée" dérivée de la théorie des perturbations singulières.

Les simulations numériques ont été effectuées sur un ordinateur CYBER 170-750 de l'ONERA.

4.4.1 - Validation de la commande linéarisée

Pour vérifier la qualité de convergence vers la solution "extérieure", les équations non-linéaires de la couche limite initiale (49) ont été intégrées avec deux lois de commande, l'une donnée par (51), l'autre non-linéaire, obtenue par séparation complète des variables  $h$  et  $\gamma$  (Calise, 1982). Plusieurs calculs ont été effectués en faisant varier d'une part le point d'équilibre, défini par l'énergie  $E_{0, \gamma}$  et d'autre part les écarts initiaux sur l'altitude et sur la pente par rapport aux valeurs d'équilibre ( $h(E_0, \gamma_0)$ ).

Pour un niveau d'énergie très élevé ( $E > 22000$  m), les réponses des deux lois sont équivalentes, la convergence vers l'équilibre est satisfaisante (pas d'oscillation). Pour des niveaux d'énergie plus faibles, la loi linéarisée (51) fournit toujours des résultats satisfaisants, alors que la loi non-linéaire induit une convergence vers l'équilibre avec des oscillations (voir figure 9). (Ruynh, Moreigne, 1985).

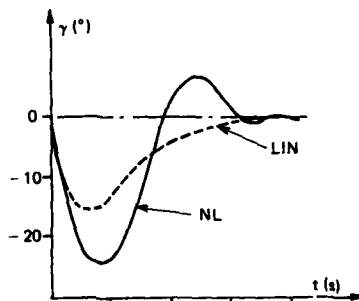
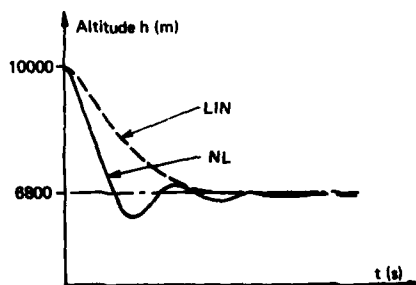


Fig. 9 - Comparaison entre commande non-linéaire (NL) et commande linéarisée (LIN).



La loi linéarisée fournit, par ailleurs, un comportement satisfaisant pour de larges écarts initiaux en altitude (jusqu'à  $\Delta h_0 = 8000$  m) et en pente (jusqu'à  $\pm 60^\circ$ ).

#### 4.4.2 - Trajectoires de montée dans le plan vertical

##### - Comparaison entre la loi d'ordre 0 (PS0) et la loi d'ordre 1 (PS1)

On désigne par loi d'ordre 1 (PS1) la solution obtenue en remplaçant dans (51), la pente nominale  $\bar{\gamma} = 0$  par son approximation à l'ordre 1, donnée par (54).

La figure 10 présente la comparaison entre ces deux lois dans le cas où seule l'énergie finale est fixée. Il est à noter que la loi PS1 permet d'obtenir un gain pouvant atteindre 10 % sur le temps de vol par rapport à la loi d'ordre 0 PS0 (voir tableau 1). D'autre part, cette dernière loi ne permet pas d'obtenir un raccordement satisfaisant avec la couche limite finale car elle ne converge pas rapidement vers la solution "extérieure" (voir figure 10).

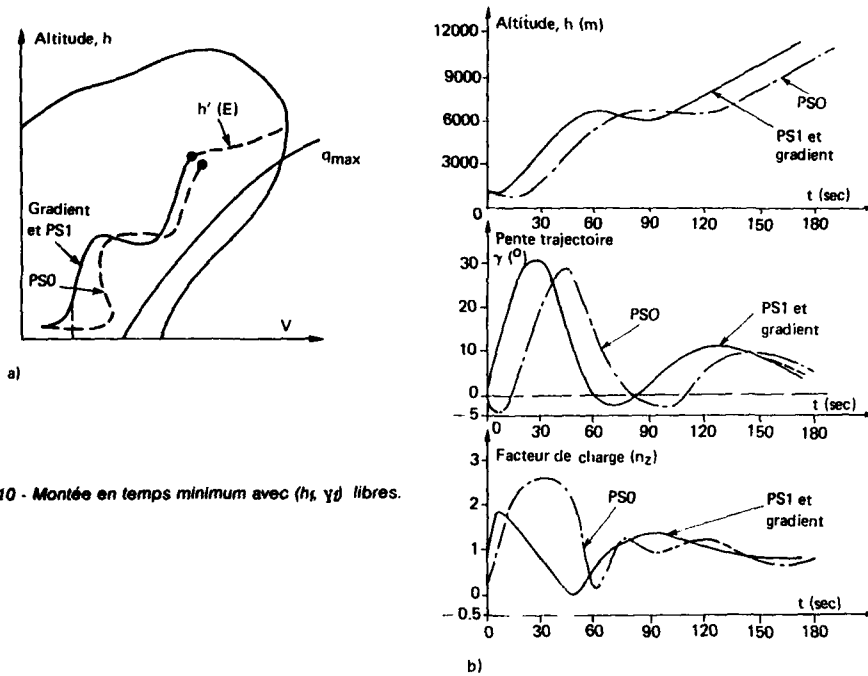


Fig. 10 - Montée en temps minimum avec  $(h_f, \gamma_f)$  libres.

Conditions finales désirées	$E_f = 25\ 000$ m $h_f, \gamma_f$ libres			$E_f = 25\ 000$ m $h_f = 14\ 000$ m $\gamma_f$ libre			$E_f = 25\ 000$ m $h_f = 14\ 000$ m $\gamma_f = 0^\circ$		
	$t_f$ (s)	$h_f$ (m)	$\gamma_f$ (°)	$t_f$ (s)	$h_f$ (m)	$\gamma_f$ (°)	$t_f$ (s)	$h_f$ (m)	$\gamma_f$ (°)
Loi d'ordre 0 (PS0)	186,1	10 810	4,9	Contraintes finales non satisfaites					
Loi d'ordre 1 (PS1)	172,4	11 520	3,4	180	14 000	12,9	181	14 000	0,16
Gradient (solution exacte)	171,7	11 600	3,6	178	14 008	8,9	180	14 000	0,13
Figures n°	10			11					

(\*) L'énergie finale désirée est toujours réalisée, car elle sert de condition d'arrêt pour l'intégration des équations du mouvement.

Tableau 1 : Comparaison de différentes solutions pour montée en temps minimum  
Conditions initiales :  $E_0 = 3030$  m ( $V_0 = 200$  m/s),  $h_0 = 1000$  m,  $\gamma_0 = 0^\circ$ .

Passage de la vitesse du son et prise en compte des contraintes finales

Des trajectoires de montée avec passage de  $M = 1$  ont été effectuées avec la loi d'ordre 1 (PS1), avec contraintes finales sur l'altitude et/ou sur la pente. Les résultats sont résumés sur le tableau 1 (voir figure 11). Le passage du son a été bien effectué, la méthode proposée pour traiter la discontinuité s'est révélée efficace, puisque les écarts par rapport aux solutions exactes sont inférieures à 1 % pour l'indice de coût et les conditions finales sont bien réalisées. La démarche proposée est satisfaisante, du moins pour des pentes finales faibles.

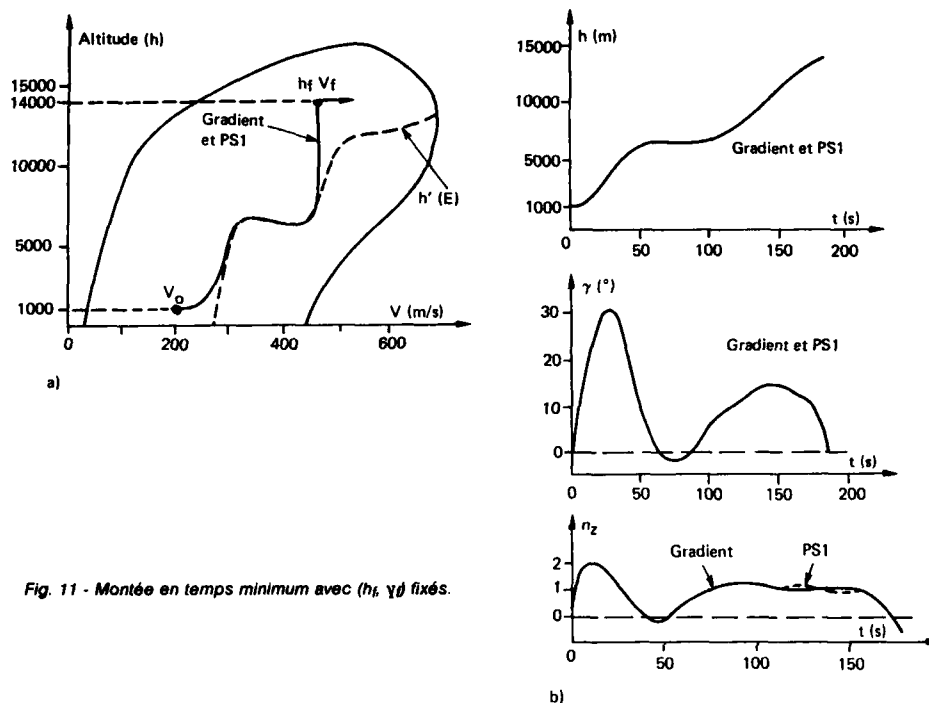


Fig. 11 - Montée en temps minimum avec  $(h_f, \gamma_f)$  fixés.

4.4.3 - Trajectoires d'interception (Do Khac, Huynh, 1988)

Les calculs envisagés correspondent à une interception à haute altitude où la cible évolue à vitesse constante égale à  $V_c = 200$  m/s à l'altitude 1200 m.

Deux lois de commande ont été évaluées en simulation numérique : la première provenant de la formulation utilisant l'énergie spécifique  $E$  comme variable d'état (§ 4.3.2 à 4.3.4), la seconde provenant de celle utilisant la vitesse  $V$  comme variable d'état (§ 4.3.5). Ces deux lois sont désignées respectivement par les symboles SPE et SPV.

Diverses conditions initiales d'interception ont été envisagées pour l'avion intercepteur, avec des angles de dépointage, définis par la différence d'azimut entre l'avion et la cible  $(\chi - \chi_c)$ , variant de 0 à 180 degrés.

Le tableau (2) présente, pour chaque cas de calcul, le temps final, correspondant à la distance minimale de passage à la cible, la distance correspondante  $d_f$ , ainsi que la pente finale  $\gamma_f$  de la trajectoire.

Dans tous les calculs effectués, les solutions fournies par les lois en "boucle fermée" sont analogues aux trajectoires optimales fournies par le code numérique d'optimisation de gradient projeté.

Quand l'avion intercepteur est initialement à altitude élevée, la manoeuvre consiste d'abord à virer tout en descendant, ou à descendre dans le cas d'une manoeuvre dans le plan vertical, dans les basses couches de l'atmosphère pour mieux tirer parti d'un bilan plus favorable de poussée-trainée pour mieux tourner et mieux accélérer, puis à remonter ensuite pour intercepter la cible en fin de vol. Dans tous les cas, la trajectoire tend vers une trajectoire d'interception plane (voir figures 13, 14).

Dans le cas n° 5 à l'intercepteur est initialement en régime subsonique, les solutions sous-optimales et optimales sont encore analogues. Durant la première phase, l'avion effectue un virage à 90° à altitude de 2000 m, il monte ensuite à pente quasi-constante tout en franchissant le mur du son, la pente augmente ensuite plus fortement jusqu'à l'interception finale (voir figure 15 et tableau 2).

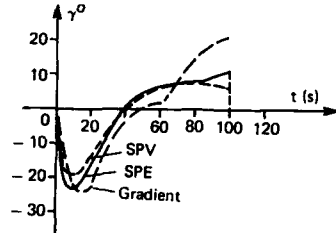
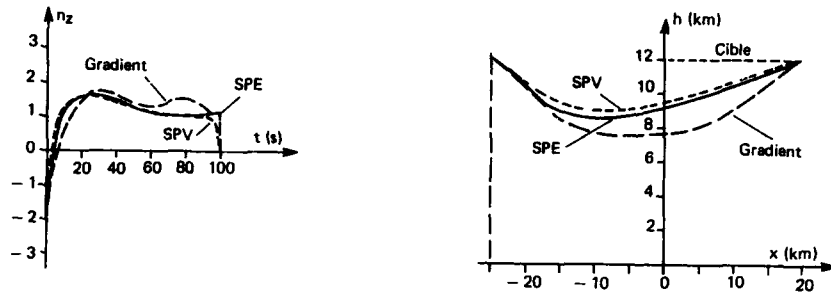


Fig. 12 - Interception dans un plan vertical.

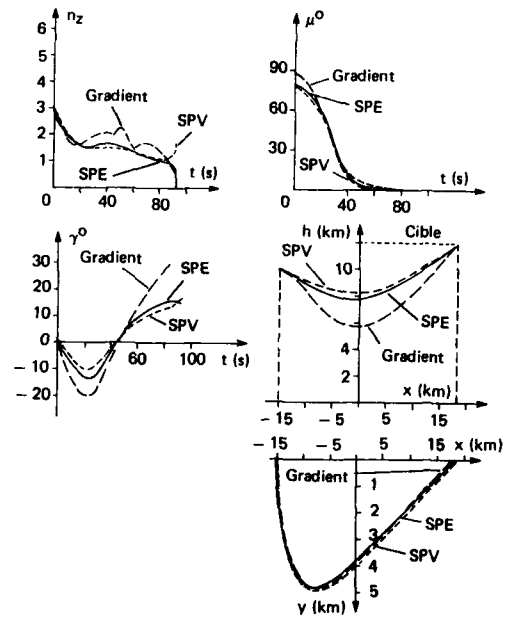


Fig. 13 - Interception tridimensionnelle avec dépointage de 90°.

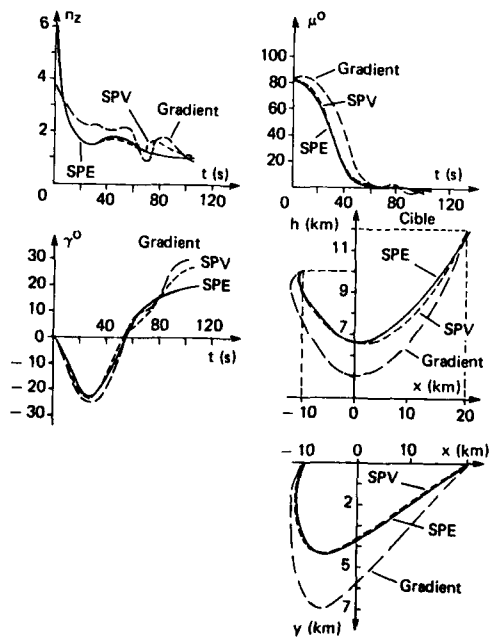


Fig. 14 - Interception tridimensionnelle avec dépointage de 180°.

On note que, dans tous calculs envisagés, les lois en "boucle fermée" permettent de réaliser les conditions finales d'interception de façon tout à fait satisfaisante, la distance minimale de passage à la cible est comparable à la solution optimale numérique pour un grand nombre de cas de calcul, dans tous les cas, elle est inférieure à 60 m.

Les deux solutions SPE et SPV ont fourni des résultats comparables en ce qui concerne l'indice de performance, c'est-à-dire la durée de l'interception.

La précision, en ce qui concerne cette durée de l'interception, par rapport à la solution optimale en boucle ouverte, varie entre 0,1 % et 3,7 % selon les calculs envisagés.

En notant que l'altitude de vol, obtenue par l'algorithme numérique d'optimisation, est toujours inférieure à celle fournie par les lois en boucle fermée, une amélioration des performances de ces dernières pourrait être obtenue en affinant le profil d'altitude de la solution extérieure  $h_g(E)$  ou  $h_v(V)$ .

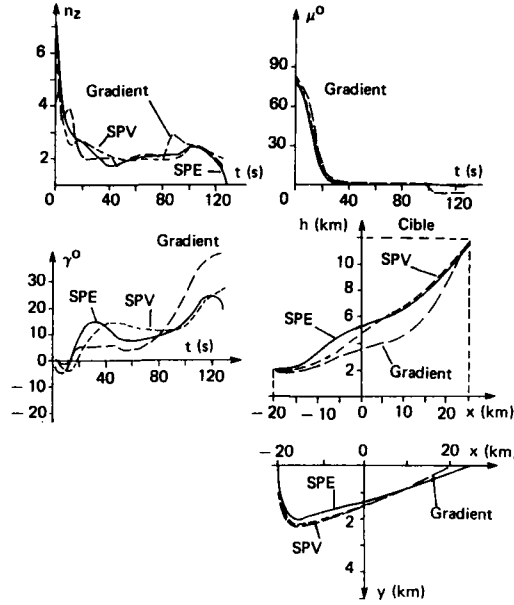


Fig. 15 - Interception tridimensionnelle à basse altitude.

Cible		Altitude = 12000 m ; Vitesse $V_c = 200$ m/s																
Type d'interception		Plan Vertical			Tri-dimensionnel													
		Haute altitude						Basse Altitude										
Conditions Initiales Intercepteur	$\Delta x_0$ (m)	25000	25000	15000	10000	20000												
	$\Delta y_0$ (m)	0	5000	0	0	0												
	$h_0$ (m)	12000	10000	10000	10000	2000												
	$V_0$ (m/s)	313	300	300	300	300												
	$X_0$ ( $^\circ$ )	0	0	-90	-179	-90												
$Y_0$ ( $^\circ$ )	0	0	0	0	0													
Paramètres Finaux		$t_f$ (s)	$d_f$ (m)	$\gamma_f$ ( $^\circ$ )	$t_f$ (s)	$d_f$ (m)	$\gamma_f$ ( $^\circ$ )	$t_f$ (s)	$d_f$ (m)	$\gamma_f$ ( $^\circ$ )	$t_f$ (s)	$d_f$ (m)	$\gamma_f$ ( $^\circ$ )	$t_f$ (s)	$d_f$ (m)	$\gamma_f$ ( $^\circ$ )		
Loi optimale (gradient)		96.5	3	22	102	5	20.5	88	33	32	105.4	9.7	31	123.5	7	40		
Loi SPE		98.5	34	10.8	104.6	49	5.8	89.7	33	16.9	107.2	57	17.3	127.7	17	24.8		
Loi SPV		99.1	11	14.3	103.6	14	11.3	91.3	27	14.6	105.5	27	25	128.1	8	26.3		
Cas N°		1 Figure 12			2			3 Figure 13			4 Figure 14			5 Figure 15				

Tableau 2 - Comparaison entre lois de commande sous-optimales en boucle fermée et loi optimale en boucle ouverte

## 5 - CONCLUSION

Ce chapitre a d'abord rappelé le principe de la théorie des perturbations singulières (P.S.) par la résolution approchée d'un système différentiel "multi-échelles de temps", mis sous la forme "singulièrement perturbée", c'est-à-dire faisant apparaître un petit paramètre de perturbation.

L'extension de cette théorie à l'optimisation des systèmes différentiels non-linéaires, à échelles de temps multiples, permet de remplacer l'optimisation du système initial (de dimension  $n$ ), par une suite de sous-problèmes d'optimisation de systèmes de dimensions plus réduite. Moyennant certaines hypothèses concernant la séparation des dynamiques et des conditions de convergence, la résolution de chacun de ces sous-problèmes, en principe plus simple que le problème complet, permet d'obtenir une solution approchée de celui-ci par composition des solutions des différents sous-problèmes.

En pratique cette théorie permet d'obtenir une loi de commande sous-optimale qui présente deux avantages importants par rapport à la commande optimale exacte qui ne pourrait être obtenue dans le cas général, que par une méthode numérique itérative de programmation non-linéaire :

- d'une part, elle peut être exprimée en boucle fermée, c'est-à-dire en fonction de l'état instantané du système, elle permet donc de mieux prendre en compte des perturbations diverses ;
- d'autre part, elle est de mise en oeuvre numérique beaucoup plus simple, et par suite est susceptible d'être utilisée sur un ordinateur embarqué fonctionnant en "temps réel".

Deux types de difficultés ont néanmoins été rencontrés dans l'application de cette théorie des P.S. à l'optimisation des trajectoires d'avions :

i) Détermination des échelles de temps

Cette étape est nécessaire à l'application, et au succès, de cette théorie. Pour des systèmes non-linéaires, aucune méthode fiable n'est encore disponible, au stade actuel, et dans la pratique on a souvent recours à une démarche empirique, basée sur l'expérience.

ii) Conditions finales sur des variables rapides

Cette théorie ne permet pas d'obtenir, au moins dans un contexte d'utilisation en "temps réel", une précision satisfaisante pour des conditions finales portant sur les variables "rapides". Diverses techniques ont été proposées pour résoudre ce problème.

La méthode précédente a été ensuite appliquée aux trajectoires en temps minimum pour un avion de combat : montée dans un plan vertical et interception tridimensionnelle d'une cible à haute altitude.

Des aménagements ont été apportés à la méthode de base et ont permis d'obtenir des lois de commande "en boucle fermée" valables pour un large domaine de vol de l'avion et permettant de satisfaire des conditions finales pouvant porter sur des variables "rapides".

Ces lois en "boucle fermée" ont été ensuite comparées aux lois optimales de type "boucle ouverte", fournies par un code numérique d'optimisation de trajectoires utilisant un algorithme de gradient projeté.

Les lois "boucle fermée" fournissent des évolutions, en ce qui concerne la nature des trajectoires, comparables aux solutions optimales. Les conditions finales sont généralement bien satisfaites et sont de même ordre de grandeur que les solutions obtenues avec le code numérique d'optimisation.

Une précision meilleure que 1 % a été obtenue, pour des trajectoires de montée dans le plan vertical, pour l'indice de performance (la durée du vol).

La précision est moins bonne pour des trajectoires d'interception, elle dépend des conditions initiales de l'avion intercepteur et du dépointage initial (différence entre l'azimut du vecteur vitesse de l'avion et celui de la cible) par rapport à la cible. Une amélioration des lois de commande en interception pourrait être obtenue en procédant comme pour la montée, c'est-à-dire en cherchant à améliorer le calcul des profils de montée de la solution "extérieure".

Dans tous les cas, la mise en oeuvre numérique de ces lois sous-optimales en "temps réel" est simple, son implantation sur un ordinateur embarqué fonctionnant en temps réel pourrait être faite aisément.

REMERCIEMENTS

Les résultats présentés dans ce chapitre ont été en grande partie obtenus dans le cadre de conventions de la DRET (Direction des Recherches, Etudes et Techniques) à laquelle nous tenons à exprimer nos remerciements.

## REFERENCES

- 1965 Yasny W.  
Asymptotic expansions for ordinary differential equations.  
Interscience Publishers, J. Wiley and sons, New-York (1965).
- 1972 Kelley H.J.  
Aircraft maneuver optimization by reduced-order approximation.  
Advances in Control and Dynamic System, Vol IX,  
C.T. Leondes ed., Academic Press, N.Y., 1972
- 1975 Bryson A.E., Ho Y.C.  
"Applied optimal control". John Wiley and sons, ed., 1975
- 1976 Ardema H.D.  
Solution of the minimum time-to-climb problem by matched asymptotic expansions.  
AIAA Journal, Vol. 14, July 1976, p.843-850
- 1979 Nehra R.K., Washburn, R.B., Saia S., Carroll J.V.  
A study of the application of singular perturbation theory  
NASA CR 3167 (1979)
- 1980 Shinar J., Merari A.  
Aircraft performance optimization by forced singular perturbation.  
12th ICAS, 12-17 oct. 1980, Munich, Germany (1980).
- 1981 Weston A.R., Cliff E.M., Kelley H.J. (1981)  
Altitude transitions in energy climb.  
8ème Congrès IFAC, Kyoto.
- 1982 Calise A.J., Hoerder D.D.  
Singular perturbation techniques for real-time aircraft trajectory, optimization and control.  
NASA CR 3597 (1982)
- 1983 Ardema H.D.  
Singular perturbations and control.  
CIMS Courses and Lectures n° 280  
Springer-Verlag-Wien-New-York (1983)
- 1984 Moreigne O.  
Contribution à la modélisation et à la synthèse des systèmes à échelles de temps multiples.  
Application au calcul en temps réel d'une commande quasi-optimale pour les trajectoires  
d'avions de combat.  
Thèse Docteur-Ingénieur à l'IDN (1984).
- 1985 Ardema H.D., Rajan W.  
Separation of time scales in aircraft trajectory optimization.  
J. Guid., Contr., Dynamics, Vol. 8, N° 2, p. 275-278 (1985).  
Ardema H.D., Rajan W.  
Slow and fast state variables for three-dimensional flight dynamics.  
J. Guid., Contr., Dynamics, Vol. 8, N° 4, p. 532-535 (1985).  
Muvah H.T., Moreigne O.  
"Quasi-optimal on line guidance laws for military aircraft".  
AIAA paper, n° 85-1977-CP, guidance and control conference,  
Snowmass, Co., 1985 ; ONERA TP-1985-91  
Rajan W., Ardema H.D.  
Interception in three dimensions : an energy formulation  
J. Guidance, Control, and dynamics, Vol. 8, n° 9, p. 23-30, Jan. Feb. 1985  
Singular perturbation theory. An introduction with application - Cambridge University Press -  
New-York 1985.

- 1986 Amasson C., Donath T., Mainguy A.M.  
Optimisation itérative de trajectoires soumises à des contraintes et application à la mise à poste de satellites géostationnaires.  
  
L'Automatique pour l'Aéronautique. Colloque SMAI, mars 1986, Paris  
Cepadues-Editions (1986).
- Fossard A.J., Freitas A.  
Applications des techniques de perturbations singulières à l'optimisation des trajectoires d'avion  
  
L'Automatique pour l'Aéronautique. Colloque SMAI, mars 1986, Paris  
Cepadues-Editions (1986).
- Shinar J., Well K.H., Järmark B.  
Near-optimal feedback control for three-dimensionnal interceptions.  
  
ICAS paper n° 86-5.1.3. (1986).
- Visser N.G., Shinar J.  
First-order corrections in optimal feedback control of singularly perturbed non linear systems.  
  
IEEE. Trans. Aut. Contr. Vol. AC-31, n° 5, p. 387-393 (1986)
- 1988 Do Khac M., Huynh H.T.  
Real-time guidance laws for three-dimensionnal interception  
16th - ICAS - Jerusalem, Aug. 28 - Sept. 2, 1988.

**PART II**

**Flight in Critical Atmospheric Conditions**

## CRITICAL ASPECTS OF TRAJECTORY PREDICTION:

## FLIGHT IN NON-UNIFORM WIND

by

Bernard Etkin  
University Professor Emeritus  
Institute for Aerospace Studies, University of Toronto  
Toronto, Canada.

and

David Alexander Etkin  
Meteorologist  
Canadian Climate Centre, Atmospheric Environment Service  
Downsview, Ontario, Canada.

Notation

$F_B (C_x B y_B z_B)$	Frame of reference attached to vehicle.
$F_E (O x_E y_E z_E)$	Frame of reference attached to Earth.
$\{I_x, I_y, I_z, I_{xz}\}$	Moments and product of inertia in frame $F_B$ .
$L_{BE} = [l_{ij}]$	Matrix of direction cosines.
$[L M N]^T$	Aerodynamic moment vector.
$m$	Mass of vehicle.
$\{p_g q_g r_{1g} r_{2g}\}$	Wind gradient inputs.
$\vec{v} = [u v w]^T$	Airspeed vector; the velocity of the airplane mass centre relative to the local air mass.
$\vec{v}^E = [u^E v^E w^E]^T$	Groundspeed vector; the velocity of the airplane mass centre relative to $F_E$ .
$\vec{W} = [W_x W_y W_z]^T$	Wind vector; velocity of the air relative to $F_E$ .
$[X Y Z]^T$	Aerodynamic force vector.
$\{\alpha, \beta\}$	Angles of attack and sideslip.
$\{\Delta\delta_a, \Delta\delta_e, \Delta\delta_r\}$	Aileron, elevator, and rudder angles.
$\vec{\nabla} = [\frac{\partial}{\partial x} \frac{\partial}{\partial y} \frac{\partial}{\partial z}]^T$	Gradient operator.
$\vec{\omega} = [p q r]^T$	Angular velocity vector of vehicle relative to $F_E$ .
$\{\phi, \theta, \psi\}$	Euler angles of $F_B$ relative to $F_E$ .

1. The Atmosphere

The layer of gas that envelops the Earth is very thin, of the order of 1% of the Earth's diameter. This layer, the atmosphere, is host to a multitude of complex phenomena — chemical, thermal, electromagnetic, optical and fluid-dynamic, all of which are coupled, and on which life on Earth depends. Our interest here is confined to the motion of the air — i.e., the wind (horizontal and vertical) and its attendant turbulence.

The atmosphere can be viewed as a giant heat engine, converting radiant solar energy into kinetic and potential energy of the air mass. Radiation reaching the earth from the sun distributes thermal energy unequally due to the increasing angle of incidence from the equator to the poles. This results in a pole-to-equator zonal temperature gradient, a form of potential energy. The system tries to reduce this gradient through a complicated process of energy transfer. Firstly the zonal isotherms (approximately East-West lines) are deformed into large-scale thermal eddies which transport warm air northward and cold air southward, converting zonal available potential energy (ZAPE) into eddy available potential energy (EAPE). The EAPE is then converted into eddy kinetic energy (EKE) through vertical motions in the eddies.

The ZAPE creates winds that increase with height (vertical wind shear) up to the tropopause, resulting in the jet stream; the EAPE deforms the flow from zonal to a

meandering wave form, and the EKE produces the large scale wind fields associated with the systems that dominate our weather on a weekly time scale. These are the synoptic scale features. This large scale wind pattern is further complicated by the irregularity of the Earth's surface and by the Earth's rotation. The oceans, continents, mountain ranges and polar ice caps distort the circulation pattern, 'steering' the highs and lows of the pressure pattern; the Earth's rotation, with its attendant Coriolis force, is responsible for the circulation around the highs and lows. Smaller scale features such as glaciers, valleys and mountain passes can dominate the local wind fields, at times producing winds as strong as those measured in the jet stream. On the microscale, meteorological phenomena such as thunderstorms, tornadoes, waterspouts, cold air funnels and dust devils can be very significant and, although relatively short-lived, very dangerous. Among these, the downburst at ground level [1, 2], which can occur with or without precipitation, is perhaps the most dangerous for aviation. Figure 1, taken from Ref. 3, shows the scales of atmospheric phenomena, from waves of planetary size down to millimetres, and Fig. 2 illustrates the downburst phenomenon [4].

Figure 3, from Ref. 5, shows the three main peaks in the spectrum of the wind; the one at a period of about 100 hours corresponds to synoptic scale highs and lows in the pressure; that at about 24 hours corresponds to the diurnal fluctuation, and the third peak, at a period in the order of one minute, corresponds to the type of gustiness typically seen ruffling a field of wheat on a summer day. It is this latter peak that is associated with the "turbulence" felt by airplanes. Small-scale turbulence is often associated with many larger scale wind features, such as both high and low level jets, all convective phenomena, mountain waves, and the wakes of mountains and cliffs. Local microscale turbulence also occurs in the boundary layer at the ground, and in the wakes of man-made objects such as buildings. Small-scale turbulence is usually a result of strong local shear, i.e., a strong spatial gradient in the velocity vector.

## 2. The Influence of Wind on Flight

Next to reduced visibility and failure of electrical or mechanical equipment, it is wind that presents the greatest hazard to aviation. Because of en-route winds, airplanes have lost their way; because of sudden gusts, airplanes have suffered catastrophic structural failures; because of continuous turbulence, there have been many injuries to passengers and crew and much damage to vehicles; because of low-level wind shear there have been many loss-of-life accidents during landing and take-off [6]. A discussion of all these effects on flight would lead us well beyond the scope of this volume, which is restricted to aircraft trajectories. For this purpose we interpret 'trajectory' to mean primarily the 'flight path', i.e., the locus of the airplane's mass centre in an Earth-fixed coordinate system. A secondary aspect of 'trajectory' can be considered to be the vehicle attitude, as given by  $\theta$  (pitch angle) and  $\phi$  (roll angle). Not only do these angles influence flight path indirectly through the direction of the lift vector, but they must themselves not exceed certain limits when the airplane is near the ground.

Although turbulence during cruising flight far from the ground can exert important influences on structural loading and fatigue, ride qualities, controllability, and pilot workload [7, 8], it is a relatively insignificant factor insofar as flight path is concerned. The random deviations in the trajectory produced in practical controlled flight at altitude are negligible compared to the space available. On the other hand, when flying close to the ground, as in low-level terrain-following, or during landing and take-off, flight path deviations resulting from turbulence may indeed be a significant factor, even in the presence of tight control [9].

That being said, it is nevertheless the mean wind that has the greatest effect on trajectory [11]. By "mean wind" we mean the time-average taken at a fixed point, over an interval of a few minutes — a time long enough for an airplane to travel a distance several times as long as the integral scale of the turbulence. This scale length at cruising heights is of the order of 300-800 m, so at a cruising speed of 300 m/s, 3 minutes can be considered a very long time, the distance traversed being of the order 60-180 scale lengths.

We further note that when considering en-route cruising at altitude, the task of accounting for wind analytically amounts merely to adding the instantaneous wind vector to the instantaneous airspeed vector to arrive at the groundspeed vector:

$$\vec{V}^E = \vec{V} + \vec{W} \quad (1)$$

No other change is needed to the aerodynamic or dynamic models of the vehicle system used for flight in still air. In fact, modern navigation aids enable airplanes cruising at altitude to follow predetermined Earth-fixed paths, with the wind appearing simply as a disturbance that is automatically or manually compensated for. Thus the en-route effect of wind on trajectory has now become a trivial problem. It is principally noticed in the influence of head-winds and tail-winds on block time and fuel consumption.

This leads us finally to the residual issue — the influence of wind, wind shear, and turbulence on flight close to the ground. A natural subdivision into major classes of flight condition occurs in that landing and take-off are low-speed transients whereas terrain-following is a high speed quasi-stochastic process. Within each of these classes there is a further subdivision into the response to mean wind, and the response to turbulence [7]. The distinction between the last two is sometimes blurred, in that when

carrying out simulations the wind model used to provide inputs to the system equations will ordinarily combine the mean wind with a single realization of the turbulence to produce a total wind. This tends to conceal somewhat the true random nature of turbulence, which is only brought out by statistical-type analyses.

In the following, we describe a system model suitable for the computation of transient and statistical responses. It is constructed from the particular viewpoint of flight simulation, but of course can be used for other classes of computation, e.g., open-loop, or where an analytical model of a human or automatic control system is used to close the loop.

### 3. The System Model

The model is subdivided into four parts, viz:

- dynamics
- kinematics and transformations
- aerodynamics
- wind

These are discussed separately in the following and are displayed in diagrammatic form in Fig. 4. It is believed that the particular choice made herein for coordinate systems and variables will lead to the most efficient computation for flight simulators in which variable wind is incorporated. (See also Refs. 12, 21).

#### 3.1 Dynamics

The equations of motion of the vehicle are written essentially as in Ref. 13 with the following assumptions:

- the vehicle is a rigid body
- it has a plane of inertial and aerodynamic symmetry,  $Cx_Bz_B$
- axes fixed to Earth are an inertial frame of reference (the stationary flat-Earth approximation)

Two reference frames are used — the conventional body-fixed axes  $F_B$  ( $Cx_By_Bz_B$ ) with origin at the mass centre  $C$ ; and Earth-fixed axes  $F_E$  ( $ox_Ey_Ez_E$ ). The latter would for convenience have the origin at ground level,  $oz_E$  vertically downward, and  $ox_E$  pointing in some convenient direction, for example, that of the runway, or of the mean wind, or North.

The force equations are written in  $F_E$ , viz:

$$\begin{aligned} X_E &= m \dot{u}_E^E \\ Y_E &= m \dot{v}_E^E \\ mg + Z_E &= m \dot{w}_E^E \end{aligned} \quad (2)$$

Here ( $X_E, Y_E, Z_E$ ) are the components of the resultant aerodynamic force acting on the airplane (including thrust and control forces) projected onto the axes of frame  $F_E$ ;  $\dot{V}_E^E = [u^E \ v^E \ w^E]^T$  is the groundspeed vector, i.e., vehicle velocity relative to  $F_E$  with the directions of the components unspecified, and  $\dot{V}_E^E = [u_E^E \ v_E^E \ w_E^E]^T$  is the groundspeed vector with components given in the frame  $F_E$ .

When the LHS of (2) is input, the equations are readily integrated to yield the groundspeed components.

The moment equations are written in  $F_B$ , viz:

$$\begin{aligned} L &= I_x \dot{p} - I_{zx}(\dot{r} + pq) - (I_y - I_z)qr \\ M &= I_y \dot{q} - I_{zx}(r^2 - p^2) - (I_z - I_x)rp \\ N &= I_z \dot{r} - I_{zx}(\dot{p} - qr) - (I_x - I_y)pq \end{aligned} \quad (3)$$

Here ( $L, M, N$ ) are the aerodynamic moments acting about the vehicle m.c., including those produced by the propulsion system and the control surfaces, ( $I_x, I_y, I_z, I_{zx}$ ) are the usual moments and products of inertia in the frame  $F_B$ , and ( $p, q, r$ ) are the components of the vehicle angular velocity  $\dot{\omega}$  relative to inertial space, which is of course also the angular velocity of  $F_B$  wrt  $F_E$ . The components ( $L, M, N$ ) and ( $p, q, r$ ) are in the directions of the axes of  $F_B$ . No subscripts or superscripts are normally used for these latter symbols.

When the LHS of (3) are input, together with initial values of (p, q, r) (usually zero), the equations are readily integrated to yield  $\vec{\delta}$ .

### 3.2 Kinematics and Transformations

The outputs from (2) are the groundspeed components, which are then readily integrated to yield the desired trajectory, i.e.,

$$\begin{aligned}\Delta x_E &= \int_0^t u_E^g dt \\ \Delta y_E &= \int_0^t v_E^g dt \\ \Delta z_E &= \int_0^t w_E^g dt\end{aligned}\quad (4)$$

Since the aerodynamic forces are calculated using the airspeed components in frame  $F_B$ , we require the components of  $\vec{V}$  in that frame. The airspeed vector is given by (1) and is transformed to  $F_B$  by the matrix of direction cosines,

$$L_{BE} = [l_{ij}]$$

i.e.,

$$\vec{V}_B = L_{BE}(\vec{V}_E^g - \vec{W}_E^g) \quad (5)$$

From the components of  $\vec{V}_B = [u \ v \ w]^T$ , the airspeed and the aerodynamic angles are given by:

$$\begin{aligned}V &= [u^2 + v^2 + w^2]^{1/2} \\ \alpha &= \tan^{-1}(w/u) \\ \beta &= \sin^{-1}(v/V)\end{aligned}\quad (6)$$

The aerodynamic force vector is calculated in frame  $F_B$ , but is needed in frame  $F_E$  for the computation of (2). The transformation is simple, being given by

$$\begin{bmatrix} X_E \\ Y_E \\ Z_E \end{bmatrix} = L_{EB} \begin{bmatrix} X_B \\ Y_B \\ Z_B \end{bmatrix} \quad (7)$$

where

$$L_{EB} = L_{BE}^T \quad (8)$$

The components of the matrix  $L_{BE}$  can be expressed in terms of the conventional Euler angles by (4.5.4) of Ref. 13, viz:

$$L_{BE} = \begin{bmatrix} (\cos\theta \cos\phi) & (\cos\theta \sin\phi) & (-\sin\theta) \\ (\sin\theta \sin\phi \cos\phi - \cos\theta \sin\phi) & (\sin\theta \sin\phi \sin\phi + \cos\theta \cos\phi) & (\sin\theta \cos\theta) \\ (\cos\theta \sin\theta \cos\phi + \sin\theta \sin\phi) & (\cos\theta \sin\theta \sin\phi - \sin\theta \cos\phi) & (\cos\theta \cos\theta) \end{bmatrix} \quad (9)$$

However, because of the trigonometric functions it contains it is not efficient to compute  $L_{BE}$  from this equation except when the angles are small, in which case it reduces to a simple algebraic relation. An alternative for computing  $L_{BE}$  is obtained from (4.6.7) of Ref. 13, i.e.,

$$\dot{L}_{BE} = -\tilde{\omega} L_{BE} \quad (10)$$

where

$$\tilde{\omega} = \begin{bmatrix} 0 & -r & q \\ r & 0 & -p \\ -q & p & 0 \end{bmatrix} \quad (11)$$

Equation (10) is a set of nine ordinary differential equations that can readily be solved for the nine  $i_{ij}$ . For example, the first one reads

$$\dot{i}_{11} = -r i_{21} + q i_{31} \quad (12)$$

and the others are similar. Since there are only 3 independent  $i_{ij}$  in view of six nonlinear algebraic relations among them (see (4.4,8) of Ref. 13), it is not in fact necessary to solve all 9 of the ordinary differential equations. If we denote  $L_{BE} = [i_1 \ i_2 \ i_3]$ , then  $i_k$  are the orthogonal unit vectors of frame  $F_E$ , and an efficient algorithm is to solve six of the nine differential equations of (10) for the components of  $i_1$  and  $i_2$  and then calculate  $i_3$  from the relation

$$\vec{i}_3 = \vec{i}_1 \times \vec{i}_2 \quad (13)$$

If the Euler angles themselves are needed as an output, for example to drive instrumentation or a motion base, they can be updated as frequently as needed from the following relations:

$$\begin{aligned} \theta &= -\sin^{-1} i_{13} \\ \phi &= \tan^{-1}(i_{23}/i_{33}) \\ \psi &= \tan^{-1}(i_{12}/i_{11}) \end{aligned} \quad (14)$$

Because of unsteady aerodynamic terms such as  $Z_w \dot{w}$  and  $M_w \dot{w}$  (or  $Z_{\dot{\alpha}}$  and  $M_{\dot{\alpha}}$ ) which usually appear in the aerodynamic model, we need expressions for  $\dot{w}$  and  $\dot{v}$  (or  $\dot{\alpha}$  and  $\dot{\beta}$ ). It is almost always good enough to approximate the true derivatives [from (6)] by

$$\begin{aligned} \dot{\alpha} &= \frac{\dot{w}}{V} \\ \dot{\beta} &= \frac{\dot{v}}{V} \end{aligned} \quad (15)$$

From (5) we get

$$\begin{bmatrix} \dot{u} \\ \dot{v} \\ \dot{w} \end{bmatrix} = L_{BE}(\dot{V}_E - \dot{W}_E) + L_{BE}\left(\frac{d\vec{V}_E}{dt} - \frac{d\vec{W}_E}{dt}\right) \quad (16)$$

and hence we need the second and third component of the RHS of (16) to calculate  $\dot{v}$  and  $\dot{w}$ . Now  $L_{BE}$  is given by (3), and  $\vec{V}_E$ ,  $\vec{W}_E$ ,  $L_{BE}$  are all known at any computing step. This leaves the last two derivatives on the RHS to be found. The first of these is given from (2) as

$$\frac{d\vec{V}_E}{dt} = \frac{1}{m} \begin{bmatrix} X_E \\ Y_E \\ Z_E + mg \end{bmatrix} \quad (17)$$

The derivative  $d\vec{W}_E/dt$  of (16) must be recognized as a convective derivative. That is,  $\vec{W}_E$  is given as a function of position and time in  $F_E$  and the value of  $\vec{W}_E$  changes at the airplane c.g., even when  $\vec{W}_E$  is constant at any given point in space if there is wind shear, i.e., if there is a gradient in  $\vec{W}_E$ . The gradient is expressed by the square matrix

$$\vec{v}_E \vec{w}_E^T = \begin{bmatrix} \frac{\partial}{\partial x_E} \\ \frac{\partial}{\partial y_E} \\ \frac{\partial}{\partial z_E} \end{bmatrix} [w_{x_E} \ w_{y_E} \ w_{z_E}] = \begin{bmatrix} \frac{\partial w_{x_E}}{\partial x_E} & \frac{\partial w_{y_E}}{\partial x_E} & \frac{\partial w_{z_E}}{\partial x_E} \\ \frac{\partial w_{x_E}}{\partial y_E} & \frac{\partial w_{y_E}}{\partial y_E} & \frac{\partial w_{z_E}}{\partial y_E} \\ \frac{\partial w_{x_E}}{\partial z_E} & \frac{\partial w_{y_E}}{\partial z_E} & \frac{\partial w_{z_E}}{\partial z_E} \end{bmatrix} \quad (18)$$

in which  $\vec{v}$  is the gradient operator. The derivative of  $\vec{W}_E$  is then given by

$$\frac{d\dot{W}_E}{dt} = \frac{\partial}{\partial t} \dot{W}_E + (\dot{\phi}_E \dot{W}_E^T)^T \dot{\phi}_E = \frac{\partial}{\partial t} \dot{W}_E + (\dot{\phi}_E \dot{W}_E^T)^T \begin{bmatrix} \dot{x}_E \\ \dot{y}_E \\ \dot{z}_E \end{bmatrix}$$

$$= \begin{bmatrix} \frac{\partial W_{xE}}{\partial t} + \frac{\partial W_{xE}}{\partial x_E} \dot{x}_E + \frac{\partial W_{xE}}{\partial y_E} \dot{y}_E + \frac{\partial W_{xE}}{\partial z_E} \dot{z}_E \\ \frac{\partial W_{yE}}{\partial t} + \frac{\partial W_{yE}}{\partial x_E} \dot{x}_E + \frac{\partial W_{yE}}{\partial y_E} \dot{y}_E + \frac{\partial W_{yE}}{\partial z_E} \dot{z}_E \\ \frac{\partial W_{zE}}{\partial t} + \frac{\partial W_{zE}}{\partial x_E} \dot{x}_E + \frac{\partial W_{zE}}{\partial y_E} \dot{y}_E + \frac{\partial W_{zE}}{\partial z_E} \dot{z}_E \end{bmatrix} \quad (19)$$

Thus all the ingredients needed for calculating  $\dot{W}$  and  $\dot{V}$  or  $\dot{\alpha}$  and  $\dot{\beta}$  are at hand. In the wind models commonly used, all the  $\partial/\partial t$  terms in (19) are neglected.

One final transformation is needed. If substantial wind gradients are present, and if the aerodynamic model can accommodate them, then it is necessary to calculate these gradients in the frame  $F_B$ . The required transformation is

$$\dot{V}_B \dot{W}_B^T = L_{BE} \dot{V}_E \dot{W}_E^T L_{EB} \quad (20)$$

Although this appears to be a complex transformation, it is much simplified when the gradient in  $F_E$  has few terms. Thus if the case considered is for example landing or take-off through vertical wind shear, the only term that is non-zero on the RHS of (18) is  $\partial W_{xE}/\partial z_E$ . The computation of (20) is then much simplified. In any event, one needs only four of the nine elements of  $\dot{V}_B \dot{W}_B^T$  [see (21)].

### 3.3 Aerodynamics

The aerodynamic model is a sum of three parts:

- (1) The basic power-on force and moment in still air, which is assumed to be given in terms of the airspeed vector  $\dot{V}_E$ , the angular velocity  $\dot{\delta}$ , and the thrust coefficient  $C_T$ . The airspeed vector is characterized by its components (u, v, w) or by its magnitude and two angles, i.e., (V,  $\alpha$ ,  $\beta$ ).  
The basic forces also depend on configuration — i.e., on the position of landing gear, flaps, etc. Changes in configuration can be included when needed, as in landing and take-off transients.  
An additional input to aerodynamic forces and moments that is almost always present are unsteady flow variables such as  $\dot{\alpha}$  or  $\dot{\beta}$ . Unsteady effects cannot normally be ignored, and computing them in the presence of variable wind unfortunately adds significant computation effort, as noted in Section 3.2.
- (2) The additional moments and forces resulting from actuation of the aerodynamic controls — elevator, aileron, rudder, etc.
- (3) The additional forces and moments resulting from the presence of the wind. These are introduced in two parts. First, the wind vector  $\dot{W}$  modifies the airspeed vector  $\dot{V}$  by virtue of (1), i.e.,

$$\dot{V} = \dot{V}^E - \dot{W}$$

In this way  $\alpha$  and  $\beta$  are modified by the presence of wind. Second, it must be noted that  $\dot{W}$  is wind at the vehicle c.g. and that the variation of wind over the length and span of the airplane must be taken into account in some situations. In the "linear-field" model, discussed further below, this variation is expressed in terms of certain equivalent rotations, denoted ( $P, q, r, \dot{P}, \dot{q}, \dot{r}$ ), which then appear as outputs of the wind model and inputs to the aerodynamic model.

From a fundamental viewpoint, an aerodynamic model adequate for trajectory calculation is the "quasi-static linear-field" model (QSLFM) (see Ref. 7). In this model, the wind velocity vector is assumed to vary linearly over the length and span of the airplane, and the unsteady terms in the aerodynamic force except for  $\dot{\alpha}$  and  $\dot{\beta}$  are

neglected. This is in sharp contradistinction to problems of flutter and structural loading due to gusts, in which unsteady aerodynamics plays a fundamental role. The two assumptions, quasi-static and linear-field, are compatible in that both are violated at about the same wave number in sinusoidal wind.

Unfortunately, no general formulation can be given for aerodynamic forces and moments when the angles  $\alpha$  and  $\beta$  are large, i.e., when there is separated flow over the airplane. In the case of small perturbations, i.e., when variations in  $(V, \alpha, \beta)$  are small, and when  $(p, q, r)$  are small, then the classical formulation of aerodynamic forces and moments in terms of aerodynamic derivatives is valid (see for example Ref. 13). Fortunately, this is so for many problems in flight dynamics. When representation by derivatives is not adequate, then individual mathematical models of forces and moments as functions of  $\alpha$  and  $\beta$  must be constructed. The airspeed inputs  $(u, v, w)$  already contain the wind effect on  $(V, \alpha, \beta)$  as noted previously. We have now to add the gradient effects. It is shown in Ref. 7 that there are four significant wind gradients that can produce aerodynamic forces and moments worth including. These are

$$\begin{aligned} p_g &= \partial W_{z_B} / \partial y_B & r_{1g} &= -\partial W_{x_B} / \partial y_B \\ q_g &= -\partial W_{z_B} / \partial x_B & r_{2g} &= \partial W_{y_B} / \partial x_B \end{aligned} \quad (21)$$

Thus the effective relative rates of roll and pitch are  $(p-p_g)$  and  $(q-q_g)$  respectively, and the aerodynamic moments associated with, for example,  $L_p$  and  $M_q$  are correspondingly modified. The atmospheric yaw rate is considered in two parts,  $r_{1g}$  and  $r_{2g}$ , as shown above. This is because  $r_{1g}$  and  $r_{2g}$  can both affect swept wings, but only  $r_{2g}$  affects the vertical tail (see Ref. 7). Thus the derivatives which multiply them must be correspondingly calculated. In the case of small perturbations, then, one would calculate the perturbation aerodynamic forces and moments resulting from motion and wind with equations such as the following. In these we have assumed no cross-coupling between longitudinal and lateral aerodynamics but this assumption is of course not essential to the method of analysis.

$$\begin{bmatrix} \Delta X_B \\ \Delta Z_B \\ \Delta M \end{bmatrix} = \begin{bmatrix} X_u & X_w & X_q \\ Z_u & Z_w & Z_q \\ M_u & M_w & M_q \end{bmatrix} \begin{bmatrix} u \\ w \\ q-q_g \end{bmatrix} + \begin{bmatrix} 0 \\ Z_w \\ M_w \end{bmatrix} \dot{w} \quad (22)$$

$$\begin{bmatrix} \Delta Y_B \\ \Delta L \\ \Delta N \end{bmatrix} = \begin{bmatrix} Y_v & Y_p & Y_r \\ L_v & L_p & L_r \\ N_v & N_p & N_r \end{bmatrix} \begin{bmatrix} v \\ p \\ r \end{bmatrix} - \begin{bmatrix} Y_{r_1} & Y_{r_2} \\ L_{r_1} & L_{r_2} \\ N_{r_1} & N_{r_2} \end{bmatrix} \begin{bmatrix} p_g \\ r_{1g} \\ r_{2g} \end{bmatrix} + \begin{bmatrix} Y_{\dot{v}} \\ L_{\dot{v}} \\ N_{\dot{v}} \end{bmatrix} \dot{v} \quad (23)$$

$(V, \alpha, \beta)$  could be used instead of  $(u, v, w)$  if desired. (We note again, for comparison with the equations given in Ref. 7 that the wind effects on  $(u, v, w)$  have already been included, so that there are no terms  $(u_g, v_g, w_g)$  in (22) and (23)). Finally the addition of control forces and moments completes the aerodynamic model. These might typically look like

$$\begin{bmatrix} \Delta X_B \\ \Delta Z_B \\ \Delta M \end{bmatrix} = \begin{bmatrix} 0 \\ Z_{\delta} \\ M_{\delta} \end{bmatrix} \Delta \delta_e$$

$$\begin{bmatrix} \Delta Y_B \\ \Delta L \\ \Delta N \end{bmatrix} = \begin{bmatrix} 0 & Y_{\delta_r} \\ L_{\delta_a} & L_{\delta_r} \\ N_{\delta_a} & N_{\delta_r} \end{bmatrix} \begin{bmatrix} \Delta \delta_a \\ \Delta \delta_r \end{bmatrix} \quad (24)$$

where  $[\Delta \delta_a, \Delta \delta_e, \Delta \delta_r]$  are the aileron, elevator and rudder angles.

1.3.4 The Wind ModelMean Wind (See Refs. 2, 7, 9, 14, 15, 24, 25, 26)

A model for the mean wind consists of a prescription of  $\vec{W}_E(\vec{r}_E)$ , i.e., of the wind vector  $\vec{W}_E$  relative to Earth, expressed as a function of the position vector  $\vec{r}_E = [x_E \ y_E \ z_E]^T$ . It is usual to omit any explicit dependence of  $\vec{W}$  on time, since temporal changes in the wind at a fixed point are slow relative to the perceived rate of change that comes from the motion of the aircraft penetrating a spatially variable wind at a relatively high speed. As indicated by the subscripts, the components of  $\vec{W}$  and  $\vec{r}$  would normally be given in the Earth-fixed reference frame  $F_E$ . When needed in the body-fixed frame  $F_B$  for aerodynamic calculations, the transformation  $L_{BB}^E \vec{W}_E$  is used, as in (5). When  $\vec{W}_E(\vec{r}_E)$  is given, then the gradient  $\vec{v}_E \vec{W}_E$  is either explicit or implicit. One common situation is landing or take-off through the planetary boundary layer (see Ref. 9). A suitable model for that case, with  $O_E$  at ground level and  $Ox_E$  pointing downwind, is (Ref. 7)

$$\vec{W}_E = \begin{bmatrix} W_{ref} (z_E/z_{Eref})^\alpha \\ 0 \\ 0 \end{bmatrix} \quad (25)$$

Here  $\{W_{ref}, -z_{Eref}\}$  are the reference wind speed and the height at which it occurs. The exponent  $\alpha$  of the power law depends on the roughness of the upwind terrain, and typically varies from about 0.1 for a smooth surface to 0.4 for an urban centre. With the above wind the gradient (or wind shear) matrix is given by

$$\vec{v}_E \vec{W}_E^T = \begin{bmatrix} 0 & 0 & 0 \\ 0 & 0 & 0 \\ \alpha \frac{W_{xE}}{z_E} & 0 & 0 \end{bmatrix} \quad (26)$$

The fact that  $\alpha W_{xE}/z_E \rightarrow \infty$  as  $z_E \rightarrow 0$  at first glance seems unsuitable. However the airplane mass-centre is always a finite distance above the runway, so this term becomes large, but not  $\infty$ . If desired, the model can be further adjusted by displacing the origin slightly downwards.

Another interesting case for the mean wind is the downburst, which has been responsible for numerous airline accidents. A number of models have been proposed for this wind field. A useful three dimensional model with some adjustable parameters is that of Ref. 10. (See also Refs. 14, 20.)

Turbulence (See Refs. 5, 7, 8, 9, 15...19, 22, 23, 26)

When a particular trajectory is to be calculated or simulated, as opposed to a statistical analysis of many trajectories, then the turbulence must be simulated as an appropriate random function of time for input to the system equations. There are seven inputs needed, to be added to those of the mean wind:

$$(\Delta W_x, \Delta W_y, \Delta W_z, P_g, q_g, r_{1g}, r_{2g})$$

although many problems can be solved approximately with only the first three of these. There have been numerous methods proposed in the literature for generating suitable turbulence inputs. When the flight path is in the planetary boundary layer and the turbulence is anisotropic, the turbulence modelling needs to be more sophisticated than for flight at altitude. For then the three turbulence intensities ( $\sigma_{W_{xE}}, \sigma_{W_{yE}}, \sigma_{W_{zE}}$ ) are not equal, they vary with height, the significant scale lengths also vary with height, and there is moreover a non-vanishing cross-correlation between  $W_{xE}$  and  $W_{yE}$ . For the planetary boundary layer, one would of necessity choose to generate the turbulent velocities in the frame  $F_E$  for the above reasons. At altitudes outside the boundary layer, where the turbulence is approximately isotropic, and hence very much simpler, the velocities could be generated in the frame  $F_B$ , and some transformation calculations can be avoided.

The turbulent wind inputs, like those of the mean wind, are treated as functions of  $\vec{r}_E$ , although they are often converted to time series through the relation  $\vec{r}_E = \vec{v}_{ref} t$  with  $\vec{v}_{ref}$  as a constant.

Insofar as statistical analysis of trajectories is concerned, the specific analytical formulation required is outside the scope of this paper. It is however given in Ref. 7. The theory is complicated, and the computations are heavy, especially for

trajectories in the planetary boundary layer, such as in landing. Some studies have been made of landing trajectories that show that turbulence combined with shear can produce operationally important deviations from the glide slope (Refs. 9, 22, 23).

#### References

1. Fujita, T. T., "Downbursts and Microbursts - An Aviation Hazard", Proc. 19th Conf. on Radar Meteorology, American Meteorological Society, Boston, pp. 94-101, 1980.
2. Frost, W., Chang, H. P., Elmore, K. L., and McCarthy, J., "Microburst Wind Shear Models from Joint Airport Weather Studies (JAWS)", U.S. FAA Washington, FM-85-19.
3. Dutton, J. A., The Ceaseless Wind, McGraw-Hill Book Co., New York, 1976.
4. Etkin, B. and Zhu, S., "Model of the Wind Field in a Downburst", AIAA Jour. of Aircraft, Vol. 22, No. 7, July 1985.
5. Lumley, J. L. and Panofsky, H. A., The Structure of Atmospheric Turbulence, John Wiley & Sons, New York, 1964.
6. Etkin, B. and Zhu, S., "Control Logic for Landing-Abort Autopilot Mode", University of Toronto, UTIAS Report No. 258, Oct. 1981.
7. Etkin, B., "Turbulent Wind and Its Effect on Flight", AIAA Jour. of Aircraft, Vol. 18, No. 5, May 1981.
8. Houbolt, J. C., "Atmospheric Turbulence", AIAA Jour., Vol. 11, No. 4, April 1973.
9. Zhu, S., "Automatic Landing Through the Turbulent Planetary Boundary Layer", University of Toronto, UTIAS Report No. 289, Nov. 1985.
11. Psiaki, M. L. and Stengel, R. F., "Optimal Flight Paths Through Microburst Wind Profiles", AIAA Jour. of Aircraft, Vol. 23, No. 8, Aug. 1986.
12. Frost, W. and Bowles, R. L., "Wind Shear Terms in the Equations of Motion", AIAA Jour. of Aircraft, Vol. 21, No. 11, Nov. 1984.
13. Etkin, B., Dynamics of Atmospheric Flight, John Wiley & Sons, New York, 1972.
14. Ivan, M., "A Ring-Vortex Downburst Model for Flight Simulations", AIAA Jour. of Aircraft, Vol. 23, No. 3, March 1986.
15. Campbell, C. W., "A Spatial Model of Wind Shear and Turbulence for Flight Simulation", NASA-TP-2313, May 1984.
16. Reeves, P. M., Campbell, G. S., Granzer, V. M., Joppa, R. G., "Development and Application of a non-Gaussian Atmospheric Turbulence Model for Use in Flight Simulators", NASA CR 2451, 1974.
17. Tatom, F. B., Smith, S. R., Fichtel, G. H., "Simulation of Atmospheric Turbulent Gust and Gust Gradients", AIAA-81-0300, AIAA 19th Aerospace Sciences Meeting, January 12-15, 1981, St. Louis, Missouri.
18. Van de Moesdijk, G. A. J., "The Description of Patchy Atmospheric Turbulence Based on a non-Gaussian Simulation Technique", Delft University Report VTH-192, Feb. 1975.
19. Van de Moesdijk, G. A. J., "Non-Gaussian Structure of the Simulated Turbulent Environment in Piloted Flight Simulation", Delft University Report M-304, 1978.
20. Etkin, B., "Comment on (Ref. 14)", AIAA Jour. of Aircraft, Vol. 23, No. 9, Sept. 1986.
21. Etkin, B., "Comment on (Ref. 12)", AIAA Jour. of Aircraft, Vol. 24, No. 7, July 1987.
22. Holley, W. E. and Bryson, A. E. Jr., "Wind Modelling and Lateral Control for Automatic Landing", AIAA Jour. of Spacecraft & Rockets, Vol. 14, No. 2, Feb. 1977.
23. Reid, L. D., "Correlation Model for Turbulence along the Glide Path", AIAA Jour. of Aircraft, Vol. 15, No. 1, Jan. 1978.
24. Markov, A. B., "The Landing Approach in Variable Winds: Curved Glide Path Geometries and Worst-Case Wind Modelling", University of Toronto, UTIAS Report No. 254, Dec. 1981.
25. Cavalcanti, S. G., "Critical Conditions for the Automatic Control of Landing from Decision Height in Variable Winds", University of Toronto, UTIAS Report No. 284, Oct. 1984.
26. Etkin, B. and Teunissen, H. W., "A Method for the Estimation of Flight Path Perturbations During Steep Descents of V/STOL Aircraft", CASI Trans., Vol. 2, Sept. 1974.

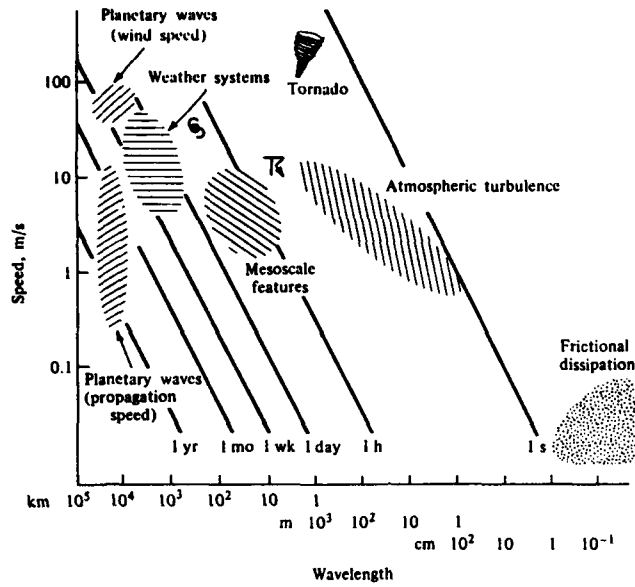


Fig. 1 Scales of atmospheric phenomena. For many of these phenomena, it is possible to choose different length or speed scales, thus giving quite different time scales. (From "The Ceaseless Wind" by John A. Dutton; McGraw-Hill, 1976).

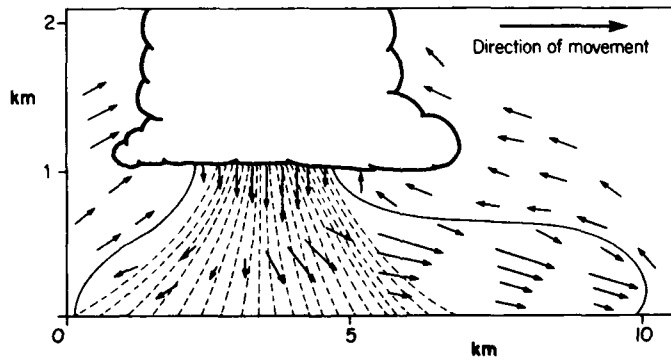


Fig. 2 Section through a thunderstorm in the mature stage (from Byers, M. R., Braham, R. R., "The Thunderstorm", G.P.O. Washington, D.C., 1949).

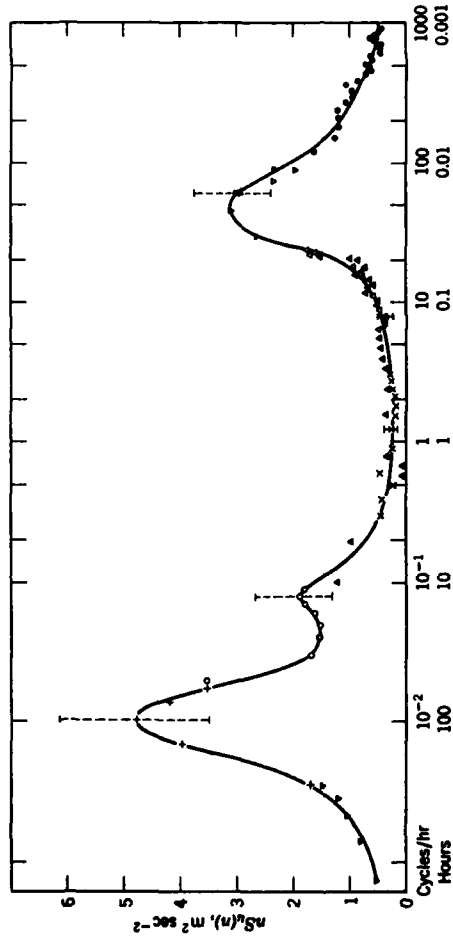


Fig. 3 Schematic spectrum of wind speed near the ground estimated from a study of Van der Hoven (1957).

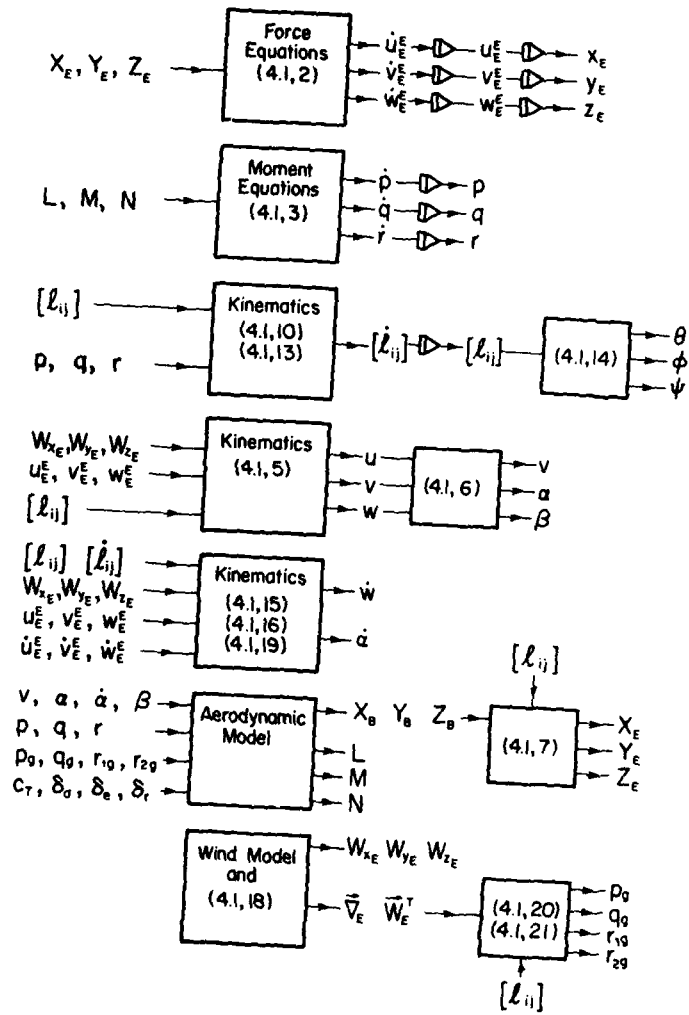


Fig. 4 Block diagram of analytical model.

## EFFECT OF WIND AND WIND VARIATION <sup>\*)</sup> ON AIRCRAFT FLIGHT - PATHS

HAHN, K.-U.; HEINTSCH, T. ; KAUFMANN, B.  
SCHÄNZER, G. ; SWOLINSKY, M.

Institute of Flight Guidance and Control,  
Technical University of Braunschweig,  
Hans-Sommer-Str. 66, 3300 Braunschweig, FRG

### 1. Symbols

D	Drag
E	Energy
$F_x, F_z$	Forces
g	Constant of gravitation
H	Height, altitude
$\dot{H}$	Rate of climb
$H_E$	Energy height
$H_{E\lim}$	Hazard limit
$\Delta H_E$	Energy height error
$I_{yy}$	Moment of inertia
j	$\sqrt{-1}$
L	Lift
$L_w$	Integral scale for the vertical turbulence component
MA	Aerodynamic momentum
MF	Thrust momentum
$M_y$	Momentum
m	Mass of aircraft
S	Reference wing area
$S(\omega)$	Power spectrum
s	Flight-path coordinate
T	Thrust, Time coefficient
$T_K$	KÜSSNER time coefficient
$u_{Kk}$	Value of the flight-path speed vector
$u_{Wg}$	Horizontal wind component
V	Airspeed
$V_K$	Flight path-velocity
$V_W$	Wind velocity
$V_{Wmean}$	Mean wind velocity
$V_{Wturb}$	Turbulence velocity
$v_{Wg}$	Cross-wind
$V_{stall}$	Stall speed
$v_{Wg}$	Vertical wind component
W	Aircraft weight
x, y, z	Coordinates
$z_a$	Normalized force
$z_T$	Normalized force
$\alpha$	Aircraft angle of attack
$\alpha_W$	Wind angle of attack
$\gamma$	Flight path angle
$\gamma_a$	Aerodynamic path angle
$\Delta$	Difference
$\sigma$	Thrust inclination angle
$\rho$	Density
$\omega$	Cyclical frequency, Spatial frequency
$\Psi$	Cross-wind correction angle
$\Omega$	Angular velocity components
$\Theta$	Pitch attitude angle
( $\cdot$ )	Time derivative
( $\underline{\quad}$ )	Vector
( $\wedge$ )	LAPLACE transformation

#### Subscripts:

nom	Nominal value
ref	Reference value
min	Minimum value

<sup>\*)</sup> This research is supported by the Deutsche Forschungsgemeinschaft.

## 2. Introduction

Wind and its variation may crucially restrict flight safety during take-off, approach and go-around (SCHÄNZER, Nov. 1986). For the period between 1964 and 1975 the FAA identified 25 accidents caused by low level wind shear (ZHU, ETKIN, 1985). Wind shear can be caused by meteorological phenomena, orographic effects or wake vortices and any combinations (SWOLINSKY, Nov. 1986). The most dangerous wind field is found in thunderstorms. But even in less severe conditions wind is an important factor, especially in the case of a limited flight performance caused by an engine failure (KÖNIG, KRAUSPE, 1981; HAHN, Nov. 1986; SCHÄNZER et al., 1987).

Although a number of investigations have dealt with the flight in a disturbed atmosphere, the studies of the effect of wind and wind variation on the aircraft's flight-path are not finished at all, but we are at the beginning of the application of the acquired knowledge (SCHLICKENMAIER, 1986; ICAO, 1987). From simulator tests we can gather, that in most cases wind shear accidents and incidents result from the fact, that the wind shear phenomenon was not understood by the pilot, due to his training condition and the aircraft's cockpit instrumentation (SCHÄNZER, 1983). Therefore the pilot was not able to react to the wind situation in an adequate manner. The first step to overcome the wind shear problem is to understand its physical phenomena. This paper tries to clarify some physical background under consideration of the safety aspects during flight.

## 3. Aircraft in wind fields

### 3.1 Equations of motion

For systematic analytical investigations a mathematical model of the aircraft is needed (ETKIN, 1972; KRAUSPE, KLENNER, 1979). The main important aircraft response with respect to take-off and landing will be the motion in the aircraft's vertical axis. Therefore, a simplified aircraft model using only the aircraft's symmetrical plane is sufficient (SCHÄNZER, 1984). Wind effects in the lateral motion of the aircraft will increase the pilot's workload by producing side forces and rolling moments. Crosswinds have to be compensated by an angle of lead according to the sketch in Fig. 1. But normally, the energy situation of an aircraft is less affected by such occurrences in the horizontal plane and the lateral aircraft motion is well controlled by the pilot. The alternating effect between the pilot's workload in the longitudinal and lateral motion is still the object of research.

Fig. 2 shows the vector diagram of speed and Fig. 3 the forces in that plane. The aerodynamic forces are lift  $L$  and drag  $D$ . Other forces which take effect are thrust  $T$  and aircraft weight  $W$ . To satisfy the balance of forces of an unsteady aircraft motion, the d'ALEMBERT forces must be defined. Stipulating a rigid aircraft body the problem can be reduced to the solution of the vehicle mass centre. With the flight-path vector and the angular velocity vector

$$\underline{v}_k = \begin{bmatrix} u_{kk} \\ 0 \\ 0 \end{bmatrix}, \quad \underline{\Omega} = \begin{bmatrix} 0 \\ \dot{\gamma} \\ 0 \end{bmatrix} \quad (1, 2)$$

and stipulating a constant aircraft mass  $m$ , the resulting force equations are in the flight-path fixed coordinate system:

$$F_x: \quad m \cdot \dot{u}_{kk} = L \cdot \sin \alpha_w - D \cdot \cos \alpha_w - W \cdot \sin \gamma + T \cdot \cos(\alpha - \alpha_w + \sigma) \quad (3)$$

$$F_z: \quad -m \cdot \dot{\gamma} \cdot u_{kk} = -L \cdot \cos \alpha_w - D \cdot \sin \alpha_w + W \cdot \cos \gamma - T \cdot \sin(\alpha - \alpha_w + \sigma) \quad (4)$$

For a constant moment of inertia the moment equation in the aircraft symmetrical plane is

$$M_y: \quad I_{yy} \cdot \dot{\theta} = M^A + M^F \quad (5)$$

$M^A$  is the resulting aerodynamic moment and  $M^F$  the thrust moment, both related to the centre of gravity. The eq. (3, 4, 5) are the non-linear differential equations of motion of an aircraft, which can be solved by numerical integration with the help of a computer. The effect of wind and its variation is latent but completely included. The flight-path speed is the superposition of airspeed  $\underline{v}$  and wind  $\underline{v}_w$  (Fig. 2)

$$\underline{v}_k = \underline{v} + \underline{v}_w \quad (6)$$

The wind angle  $\alpha_w$  (MEWES, 1962) depends directly on the horizontal and vertical wind component (see Fig. 2):

$$\sin \alpha_w = \frac{w_{wg}}{v} \cdot \cos \gamma - \frac{u_{wg}}{v} \cdot \sin \gamma \quad (7)$$

The wind angle is part of the flight-path angle

$$\gamma = \gamma_a + \alpha_w \quad (8)$$

for a given air-path angle  $\gamma_a$  as a result of the aircraft's flight performance capability. With eq. (6) and eq. (8) it is clear that the aircraft trajectory is the result of the aircraft's motion, relative to the air mass plus the movement of the air mass relative to the ground. Its components in the symmetrical plane can be calculated by

the flight-path speed and angle.

$$\dot{H} = V_K \cdot \sin \gamma \quad (9)$$

$$\dot{x}_g = V_K \cdot \cos \gamma \quad (10)$$

$\dot{H}$  is the vertical speed and  $\dot{x}_g$  is the ground speed.

### 3.2 Short scale wind variations

The influence of wind velocities on the aircraft motion can be roughly separated into two main parts. The flight performance description of an aircraft depends on the low frequency part of the wind vector, the wind shear component. Only this low frequency part of the wind has important influence on the energy relation of the aircraft. The research work with regard to the flying qualities of the aircraft must consider the high frequency wind components, the gusts and turbulence. Again the boundary between these activities is not well defined; it depends on the aircraft and atmospheric characteristics such as flight velocity, altitude, geometry, wing load, etc. To verify the assumptions about the influence of the wind vector on the aircraft motion is the aim of the following chapters, which demonstrates the frequency dependent aircraft reaction due to a vertical wind perturbation, using a simple heave motion model.

#### 3.2.1 Influence of atmospheric turbulence on the aircraft motion

The integration of the turbulence velocity in the equations of motion is solved by the eq. (6) (see chapt. 3.1), where  $\underline{V}_W$  is the sum of mean wind velocity and turbulence velocity:

$$\underline{V}_W = \underline{V}_{W_{mean}} + \underline{V}_{W_{turb}} \quad (11)$$

The main parameter of the aircraft trajectory is the flight-path deviation in vertical and lateral direction. The influence of vertical wind components on the vertical flight-path deviation shall demonstrate the frequency dependent aircraft reaction. To make some simple qualitative considerations possible, a lot of simplifications are necessary. Only the vertical motion of the aircraft will be taken into account; the other degrees of freedom are frozen. After linearizing the equation of motion, the normalized forces in vertical direction are:

$$\delta \ddot{y} = Z_\alpha \cdot \delta \alpha - Z_\gamma \cdot \delta \gamma \quad (12)$$

with

$$Z_\alpha = \frac{\rho \cdot V_{ref}^2 \cdot S}{m \cdot V_{Kref}} \quad (13)$$

and

$$Z_\gamma = \frac{\rho}{V_{Kref}} \cdot \sin \gamma_{ref} \quad (14)$$

with flight-path angle  $\gamma$  and angle of attack  $\alpha$ . Supposing a horizontal reference condition  $Z_\gamma$  is zero. Using the angle relation:

$$\delta \alpha + \delta \gamma - \delta \Theta = \delta \alpha_W \quad (15)$$

with wind angle of attack  $\alpha_W$  and pitch angle  $\Theta$  the vertical acceleration is described by

$$\delta \ddot{y} = -Z_\alpha \delta \gamma + Z_\alpha \delta \alpha_W \quad (16)$$

The LAPLACE transformation provides the transfer function for the vertical acceleration due to the wind angle of attack:

$$F(s) = \frac{\hat{\delta y}}{\hat{\delta \alpha}_W} = \frac{s}{1 + T \cdot s} \quad (17)$$

with  $s$  as LAPLACE operator and  $T=1/Z_\alpha$ .

In the high frequency range this transfer function should be completed with the influence of unsteady lift effects. The lift response to changing angles of attack is delayed by increasing frequencies. As demonstrated in SCHÄNZER (1985) and KAUFMANN (1986), this effect can be approximated by a first order lag system. The time coefficient  $T_K$  depends on the aircraft characteristics. Adding this effect of unsteady aerodynamic, the transfer function has the following form:

$$F(s) = \frac{\hat{z}}{\hat{w}} = \frac{s}{1 + T \cdot s} \cdot \frac{1}{1 + T_K \cdot s} \quad (18)$$

Referring to the power density spectrum of the atmospheric turbulence (HAHN, KAUFMANN, SWOLINSKY, 1988) it is possible to calculate the power density spectrum of the vertical acceleration and the vertical flight-path deviation. For linear systems and normal distributed random processes the power density spectrum of the flight path deviation can be calculated using the power density spectrum of the input and the transfer function:

$$S_y(\omega) = F(j\omega) \cdot F(-j\omega) \cdot S_{ww}(\omega) \quad (19)$$

The result of this approximation is shown in Fig. 4. The picture contains from top to bottom:

- the DRYDEN power density spectrum as the input signal with the coefficient  $V/L_W$
- the transfer function of the vertical acceleration due to the wind angle of attack based on the simplified heave motion
- the output power density spectrum of the vertical acceleration
- the output power density spectrum of the vertical flight-path deviation.

The last picture demonstrates the influence of vertical turbulence components on the aircraft trajectory. In the high frequency domain the influence of the wind angle of attack on the trajectory is negligible. The mass inertia of the aircraft, the decreasing intensity of the turbulence and the unsteady lift effects are alleviating the amplitude of the flight-path deviation. For low frequencies, the wind shear area of the spectrum, the flight-path is influenced by vertical wind disturbances. In this low frequency area the aircraft follows the changing wind velocity and alters the flight-path. Energy is transferred between wind and aircraft and causes the acceleration or deceleration of the aircraft. In the high frequency range of the spectrum the inertia of the aircraft avoids flight-path deviations. The aircraft accelerations are large, but only for a short time. The integral of these accelerations is small and the influence on the flight-path is negligible.

The discussed solution was calculated for the simplified heave motion. The aircraft has three degrees of freedom in the longitudinal motion. Especially the pitch motion of the aircraft has influence on the behaviour. Fig. 5 shows the transfer function of the flight-path deviation for the complete longitudinal motion. The eigenmotions of the aircraft, phugoid and short period motion, are important frequencies for the separation of effects. If the frequency of the wind perturbation is less than the phugoid frequency, the change of aircraft trajectory is directly proportional to the wind angle of attack. That means, low frequency wind perturbations directly change aircraft trajectory. If the range of frequency is above the short period motion, the inertia of the aircraft avoids large changes of trajectory.

Based on this knowledge, the conclusion is that only large scale wind variations have an important effect on the aircraft trajectory; the influence of high frequency turbulence is negligible.

The influence of short scale perturbations on the aircraft flying qualities is discussed for example in ETKIN (1980), ETKIN (1961), SCHÄNZER (1985), KAUFMANN (1986).

### 3.2.2 Influence of gusts on the aircraft motion

The discussion of the influence of gust effects on the aircraft trajectory is difficult. As demonstrated in chapter 3.2.1, the aircraft reaction due to changes in the wind angle of attack depends on the frequency of the perturbation. In case of gust effects, this frequency can have a wide range, depending on the shape of the gust and the relative speed of encountering it. As gust effects are limited in the geometric dimensions, the influence on aircraft trajectory is also limited. A final classification of the influence of gust effects is not possible. The main effect on the trajectory is not the gust itself but the initialized eigenmotion of the aircraft, especially the phugoid and the dutch roll motion. But with a pilot in the loop or an activated autopilot system, the perturbations are controlled.

The main conclusion of these considerations is that only the large scale perturbations should be taken into account in aircraft trajectory estimations and calculations. Atmospheric turbulence and gust effects have important influence on the flying qualities of aircrafts, the pilots workload or the design of gust alleviation systems. For the aircraft trajectory discussion in the following chapters it is permitted to neglect the influence of these short scale perturbations.

### 3.3 Energy situation

The most important physical effects of the wind in flight become clear by a look at the aircraft's energy situation (KÖNIG et al., 1980). The total flight-path energy can be determined by

$$E_K = \frac{1}{2} \cdot m \cdot V_K^2 + m \cdot g \cdot H, \quad (20)$$

where  $V_K$  is the flight-path speed,  $H$  is the altitude,  $g$  the geographical acceleration and  $m$  the aircraft mass. Related to the aircraft's weight  $W=m \cdot g$  we get the actual energy height from the equation above

$$H_{EK} = \frac{V_K^2}{2 \cdot g} + H \quad (21)$$

and from that the time derivative

$$\dot{H}_{EK} = \frac{V_K \cdot \dot{V}_K}{g} + \dot{H} \quad (22)$$

known as the total flight-path energy rate or specific excess power (SEP). The two terms in eq. (22) represent the kinetic and the potential flight-path energy rate.

Fig. 6 shows a landing approach with fixed controls starting in a constant headwind decreasing to zero (tailwind shear). It can be seen, that the airspeed does not decrease to the same extent as the headwind due to the slowly self-adjusting flight-path velocity. The phugoid mode is stimulated by the rapid wind change which leads to an oscillatory exchange between the portion of the kinetic and the potential energy rate. Large excursions of altitude arise even after the aircraft has left the shear layer. The deviations are not acceptable in any circumstances. From Fig. 6 we can gather that the total energy rate remains nearly constant within the shear layer and shows only small variations after passing that area. Therefore a wind shear warning system based exclusively on the display of the specific excess power cannot give sufficient information about the wind shear hazard (KÖNIG et al., 1980).

Another energy definition can be made using the airspeed. The substitution of  $V_K$  in the equations (20, 21, 22) by  $V$  leads to the total air path energy rate

$$\dot{H}_{EA} = \frac{V \cdot \dot{V}}{g} + \dot{H} \quad (23)$$

This equation normally is used in the total energy vertical speed indicator of glider planes. The result of eq. (23) is compared with eq. (22) in Fig. 7. It can be seen, that a wind shear display based on the total air path energy rate is able to detect the shear situation. The required total energy rates  $\dot{H}_{EK, req}$  and  $\dot{H}_{EA, req}$  to compensate the wind shear are also plotted in Fig. 7. Note that the difference  $\Delta H_E$  between the required total energy rate and the actual total energy rate is quite the same and independent from the reference coordinate system. So only regarding the energy height differences, there is a free option using the airspeed or the flight-path speed for the energy definition.

To obtain a complete compensation of the wind, the pilot has to maintain a constant airspeed  $V_{nom}$  and the required glide slope  $\gamma_{nom}$ . Applying these conditions a relation can be expanded for the calculation of the required change in thrust  $\Delta T$ . From eq. (3) we get after linearisation the non-dimensional equation (KÖNIG, 1982)

$$\frac{\Delta T}{W} = \frac{\dot{u}_{WG}}{g} + \frac{\Delta u_{WG}}{V_{nom}} \cdot \gamma_{nom} + \frac{\Delta w_{WG}}{V_{nom}} \quad (24)$$

In the above equation  $\dot{u}_{WG}$  is the horizontal wind acceleration,  $\Delta u_{WG}$  is the horizontal and  $\Delta w_{WG}$  is the vertical wind difference calculated by the actual wind minus the wind where the computation is started and the aircraft is trimmed. If there is no variation in wind the aircraft will continue its steady flight with constant thrust. The required thrust variation for a descending flight in a headwind shear profile is given on principle in Fig. 8. From eq. (23) it is possible to calculate the energy height error

$$\Delta H_E = H_E - H_{E, nom} \quad (25)$$

representing a useful criterion for the severity of the wind's effect on the aircraft. The balance of power for steady flight is (HAHN, 1987)

$$V_K \cdot \Delta T + W \cdot \Delta \dot{H}_E \stackrel{!}{=} 0 \quad (26)$$

$\Delta T$  is the difference of thrust to compensate the difference in the specific excess power  $\Delta \dot{H}_E = \partial \Delta H_E / \partial t$  caused by the change in wind. An increase in specific excess power requires a reduction of thrust to maintain steady flight. The flight-path speed along the path  $s$  is

$$V_K = \frac{\partial s}{\partial t} \quad (27)$$

With the equations (26) and (27) the energy height error becomes

$$\Delta H_E = - \int \frac{\Delta T}{W} \partial s \quad (28)$$

Applying the equation (24) we get (SWOLINSKY, 1986):

$$\Delta H_E = - \int \left( \frac{\dot{u}_{WG}}{g} + \frac{\Delta u_{WG}}{V_{nom}} \cdot \gamma_{nom} + \frac{\Delta w_{WG}}{V_{nom}} \right) \partial s \quad (29)$$

In the above equation only the nominal approach speed and the nominal flight-path slope is needed to determine the energy height error in a given wind field. The hazard limit, defined by the maximum allowable energy height loss, is based on the fact that the aircraft is not allowed to sink below a specific obstacle surface and the airspeed must be higher than the stall speed (KÖNIG, 1982; HAHN, 1987):

$$\Delta H_{E_{lim}} = H_{E_{min}}(H_{min}, V_{min}) - H_{E_{nom}}(H_{nom}, V_{nom}) \quad (30)$$

If the hazard limit defined by eq. (30) is not reached, the aircraft can increase its height at the expense of airspeed to avoid an obstacle contact. On the other hand, an impact on ground can happen with a proper airspeed even if the energy height error is not critical. So, another important safety aspect is the flight-path deviation.

#### 3.4 Typical aircraft response to wind shear

Wind shear causes deviation from the trimmed aircraft state of flight. Due to the aircraft's inertia the flight-path speed  $V_K$  is nearly constant during the first encounter of wind shear. Therefore, the varying wind changes first the aerodynamic flow field (airspeed, angle of attack). After the occurrence of an airspeed difference as a result of the wind shear, the static stability of the airplane supported by the pilot's behaviour to keep the airspeed constant, will accelerate (tailwind shear) respectively decelerate (headwind shear) the aircraft relative to the ground.

From Fig. 7 we can gather, that the variation of the specific excess power is

$$\Delta \dot{H}_{EK} \approx 0 \quad (31)$$

With eq.(22) the deviation of the vertical speed is

$$\Delta \dot{H} = - \frac{V_K \cdot \dot{V}_K}{g} \quad (32)$$

which results in a height error

$$\Delta H = - \frac{V_K \cdot \Delta V_K}{g} \quad (33)$$

For a changing horizontal wind component  $u_{wg}$  eq. (6) becomes with  $w_{wg}=0$  (see also Fig. 2)

$$V_K \approx V + u_{wg} \quad (34)$$

So if the airspeed variation is small, the mean flight-path deviation caused by the wind

$$\Delta H \approx - \frac{(V + u_{wg}) \cdot \Delta u_{wg}}{g} \quad (35)$$

directly depends on the amount of the wind difference.

Some typical flight-paths through a discrete linear shear layer are given in Fig. 9 and Fig. 10. In the case of a landing in a headwind shear (Fig. 9) only a relatively harmless airspeed deviation appears which takes the aircraft above the glide path. This situation can be classified as *uncritical* because a go-around will always be possible. The approach in tailwind shear produces a significant deviation from the initial state of flight. When the aircraft encounters the shear layer, its flight-path angle becomes steeper, and so the aircraft is self-inducing a more and more intensifying wind shear. It can be seen, that the flight-path deviation in the shear layer itself is small. The greater glide path deviation, caused by the dynamic response of the aircraft, appears outside the shear layer.

The same is true for the take-off in a tailwind shear (Fig. 10). But there is an important difference between the take-off and the landing. While approaching, the energy height error can be compensated by thrust control. Contrary to landing, during take-off the aircraft is flying near its maximum performance capability. Therefore, the compensation of the flight-path deviation is attainable only by shifting kinetic to potential energy. But at least the wind shear will lead to a height deficit during the take-off phase, as illustrated in Fig. 10.

From Fig. 8 we gather, that a tail- or headwind shear affects the flight-path oscillation (phugoid) in a different way. The influence of horizontal and vertical shear gradients on the phugoid is analyzed by KRAUSPE (1983). A fundamental result of this investigation was, that the aircraft response in wind shear is nearly independent of aircraft characteristics. The major parameters of influence are airspeed and lift to drag ratio. It should be noted, that the earth-fixed wind shear can extensively modify the phugoid stability (Fig. 11). The flight-paths in wind fields with constant shear can be approximated by simple analytical functions (Fig. 12), when the phugoid eigenvalues are known. The accuracy of the results is very acceptable for the relevant time period of 20 seconds after the wind shear encounter.

#### 4. Large scale wind variation

##### 4.1 Downburst

The most adverse wind situations are produced by thunderstorms. There the disadvantageous combination of downdraft and tailwind shear can be found in the core of a downburst. But it can be said, that the reasons for the approach accidents cannot exclusively be found in the wind field of the downburst's core. The critical situation results from the fact, that the aircraft's thrust setting for the approach will be done before it reaches the downburst (HAHN, 1987). Fig. 13 shows the landing in a downburst based roughly on the conditions of the B727 approach accident in New York in 1975. The flight-path with fixed aircraft controls (indicated by a dot-dash line) is very close to that of the accident flight. So we can assume that the pilot reacted much too late and not efficiently. Some flights are simulated passing this downburst. An activated autopilot (Fig. 13, dotted lines) tries to position the aircraft on the nominal glide path. The flight-path deviation is small, but the energy height error leads to significant airspeed errors. When the hazard limit is reached, the airspeed is very close to the stall speed. The aircraft does not reach the runway. So, even if the pilot is able to maintain the nominal glide path, the hazard limit is reached. A comparison of the energy height error calculated by the simple equation (29) with those of non-linear simulations along the individual flight-paths with fixed aircraft controls or autopilot demonstrates only small differences. So it can be said, that eq. (29) is a simple but powerful method for the estimation of the wind effect on the aircraft's energy situation.

With Fig. 13 it becomes also clear that a safe landing will only be possible with an additional supply of energy by thrust control. Fig. 14 illustrates an approach in the same downburst with a conventional modern automatic flight control system (autopilot and autothrottle). Airspeed and flight-path deviations are acceptably small. The thrust setting DF (actual thrust related to the maximum thrust) adjusted by the autothrottle never reaches its maximum. A touch-down on the runway will be possible.

The accuracy of automatic flight control systems can be improved by advanced control laws under consideration of wind effects (STENGEL, 1986; KÖNIG, 1982). Generally it can be said, that during landing in a downburst the flight performance is normally not the limiting factor. The problem is, that in a manual approach the pilot needs sufficient information about the required thrust setting caused by the actual wind situation. As discussed before, the total energy and the rate of total energy defined in the airpath fixed coordinate system are the most important parameters for a perfect detection of wind effects acting on the aircraft. So these parameters can be used for a cockpit display concept. The total energy rate can be displayed with an additional pointer in the vertical speed indicator, and the total energy error may be displayed in a modified "fast-slow-indicator" of the flight director display (KÖNIG et al., 1980). This concept has been tested in a moving cockpit simulator by a joint team of Bodensee Gerätetechnik, Deutsche Forschungs- und Versuchsanstalt für Luft- und Raumfahrt (DFVLR) and the Technical University of Braunschweig. The simulated wide body aircraft was flown by fourteen airline pilots. With the display of energy and energy rate most of the pilots, even those of less experience, were able to carry out a hard but safe landing or to initiate a go-around as shown in Fig. 15 (SCHÄNZER, 1983). The research on this field was sponsored by the German Ministry of Transportation (BMV, March 1983).

As mentioned above, the aircraft is flying near its maximum performance capability during take-off. Therefore, if the wind gradients in a downburst are strong enough, a take-off accident can become inevitable. Fig. 16 shows such a take-off accident of a B727 in Denver in August 7th, 1975. The reconstructed wind gradients are  $u_{wx}=0.03 \text{ s}^{-1}$  and  $w_{wh}=0.18 \text{ s}^{-1}$  (KRAUSPE, 1983). The simulation is done with fixed controls and it starts at a distance of  $\Delta x_z=-350\text{m}$  before the centre of the downburst comparable to the Denver accident. Although all engines are running, the aircraft is not able to climb. The energy height loss increases from the beginning and the aircraft is permanently losing airspeed. The stall speed is reached shortly before crossing the hazard limit. The reconstructed flight-path of the Denver accident is similar to the flight-path with fixed aircraft controls. So it can be assumed again, that the pilot's inputs are not very efficient. But it must be realized, that a take-off under these wind conditions can be assumed as impossible.

Downbursts with gradients less than those of the above Denver accident can be crossed by a simple escape manoeuvre (HAHN, 1987). As gathered from Fig. 16 a realistic pilot behaviour in downbursts comes close to simulations with fixed aircraft controls. Such a simulation carried out in the Philadelphia downburst (June 23rd, 1976;  $u_{wx}=0.02 \text{ s}^{-1}$  and  $w_{wx}=0.165 \text{ s}^{-1}$ ) is illustrated in Fig. 17. The take-off climb begins at a distance of  $\Delta x_z=-1000\text{m}$  before the centre of the downburst. Airspeed and energy height error are rapidly decreasing and the hazard limit is nearly reached when the aircraft has a ground impact. A practicable escape manoeuvre is the level flight at a low height to pass the core of the downburst before starting the climb (Fig. 17). The main important advantage of this flight procedure results from the smaller vertical wind close to the ground. During the climbing flight with fixed controls the downdraft increases with height.

In principle the go-around can be assumed as a combination of approach and take-off climb. By taking the above discussed results into consideration, the following conclusions can be drawn: Regarding the energy situation in most of the downbursts approaching is possible provided that the pilot or the automatic flight control system reacts in the required manner. Initiating the go-around, the above described flight level procedure is to prefer for crossing the core before climbing to higher altitudes.

##### 4.2 Low-level jet

The low level jet is characterized by a jet like wind profile with low altitude wind maxima (Fig. 18). In some cases an intensive variation of wind direction with height can be observed (see SWOLINSKY, 1986). Especially the nocturnal low level jet can be assumed as a phenomenon of far-reaching horizontal homogeneity, i.e. wind speed and direction, acting on an aircraft, are dependent only on the distance of the aircraft from the ground. Passing a low level jet during landing approach, an energy height excess is building up in the region of increasing headwind, which leads to positive flight-path deviations. After passing the windspeed maximum, the decreasing headwind produces an energy deficit and leads the actual flight-path beneath the nominal glide path. Fig. 19 and Fig. 20 show these effects for a simulated landing approach with fixed controls respectively for manual flight, using a flight simulator. The model parameters of the wind profile have been derived from measurements, which have to

be classified as a worst case low level jet. In both cases the flight-path deviation are similar, but for simulation of manual approach the pilot succeeded in intercepting the aircraft a few meters above the ground. Systematic investigations show, that the height of the maximum headwind and the headwind difference between maximum wind and value and reference wind speed near the ground (e.g.  $H_{ref}=10\text{m}$ ) are the most influential parameters. Flight path deviations, respectively, aircraft hazard are increasing with increasing headwind difference in connection with decreasing height of the maximum headwind.

#### 4.3 Orographical effects on the streamlines flow

The wind flow, especially in the lower boundary layer, is influenced by the orographic shape of the surface (Hahn et al., 1988), as it can be seen in Fig. 21. The figure shows the streamlines of a wind flow over a flat hill. The main effects caused by the disturbance of the flow field are an updraft at the windward-side and a downdraft at the lee-side of the hill. Further it can be seen that the streamlines are not exactly parallel to the surface contour. The hill causes a contraction of the streamlines at the top of the hill, which leads to an increase in the wind speed according to the law of continuity.

In the case of higher wind speeds, the occurrence of flow separation depending on the hill slopes on the luv- and lee-side is possible (MERONEY, 1979). This may lead to a vortex flow in the lee of the hill with additional, partly strong up- and downwinds as it is illustrated in Fig. 22 (EICHENBERGER, 1962).

Based on the above mentioned phenomena, a wind model was developed to investigate the influence of the hill flow on the take-off flight-path of a starting aircraft by simulation (HAHN, 1986). As a result, Fig. 23 shows the simulated net path of a take-off climb of a two-engine aircraft under the condition of an engine failure during the start, together with the calculated wind along the flight-path (wind model without vortex flow). Compared with a take-off in the boundary layer, without the influence of the hill (broken line), the decrease of the flight-path angle can be seen; resulting in a loss of height about 40 meters at the top of the hill. The difference between the two flight-paths is a degree for the influence of the hill flow. In this case the net flight-path does not reach the minimum height of 10.7 m above the highest obstacle.

By order of the Bundesministerium für Verkehr, about 40 test flights were carried out measuring the wind flow in the lee of a flat hill (Weidacher Höhe) near Stuttgart airport to investigate the influence of the measured wind speeds on the trajectory of a starting aircraft by simulation (SCHÄNZER et al., 1987). As an example, a typical measurement flight-path together with the horizontal and vertical velocities along the flight-path is presented in Fig. 24. To get the most realistic results with the simulation, the measurement flight-path had to be near the expected simulation flight-path.

The analysis of the measured data shows large varieties in the wind speed courses as well as in the mean wind velocities. The flow of the horizontal wind component partly confirms the theory of the developed wind models with increasing headwind speed to the top of the hill. In some other cases a nearly constant wind course or even a decrease in headwind can be noticed. These unexpected phenomena can not be explained yet.

Another estimation of the influence of the hill can be realized by comparing the mean horizontal wind speed in the lee of the hill and the mean wind speed in the undisturbed flow. For this comparison, the reported wind (a horizontal reference wind) measured at the Stuttgart airport was chosen, which additionally is the basis for the calculation of the allowed take-off weight.

In most cases (about 80%) an increase of the wind speed in the lee of the hill can be noticed (SCHÄNZER et al., 1987). The vertical wind speed courses show, in almost all cases, the above mentioned downdraft in the lee of the hill. The measured downwind speeds with mean wind speed values of up to 0.6 m/s are greater than the expected values received from the wind model.

As a special phenomenon a vortex flow in the lee of the hill was found, which can be seen in Fig. 25 (HEINTSCH, 1987). Detailed investigations of the hill characteristics (SCHÄNZER et al., 1987), however, lead to the conclusion that a flow separation is not probable in this case so that the vortex flow is not a constant, but a temporary phenomenon.

With regard to the measured wind data the simulations were carried out for a start of a two engine-aircraft with an engine failure during the start. The determination of the aircraft's maximum allowable take-off weight to reach a minimum net height of 10.7 m above the highest obstacle in the start sector was performed according to the flight manual of the investigated aircraft. In the calculation half the reported wind is taken into account. The influence of the wind on the aircraft motion can be seen directly in the simulation results comparing the simulated flight-path (measured wind data) with the cross reference flight-path (half the reported wind). A typical simulated case is presented in Fig. 26. The differences between the simulated and the reference flight-path correspond to the differences between the actual wind situation and the reference reported wind.

A statistical analysis of the simulation results showed that in most cases a more or less clear loss of height of the simulated flight-path with respect to the reference flight-path can be noticed caused by the downdraft as well as by changes in the horizontal wind velocities (horizontal wind shear). In Fig. 27 the frequency of the height above the obstacle (see Fig. 26) is presented. The values vary in a range from 2 m up to 80 m. In 55% of the 40 investigated cases the cross reference height of 35 m according to the net height of 10.7 m, which can be seen as the minimum limit for a sure take-off, was not reached (SCHÄNZER et al., 1987).



- Meroney, R.N. WECS site screening by physical modeling.  
Proceedings Conference and Workshop on Wind Energy Characteristics and Wind Energy Siting DEO and AMS, Oregon, USA, 1979.
- Mewes, E. Flugmechanische Bezeichnungen bei bewegter Luft.  
Zeitschrift für Flugwissenschaft und Weltraumforschung, Heft 3, 1962.
- Schänzer, G. Abschätzung von stochastischen Böenlasten unter Berücksichtigung instationärer Luftkräfte.  
Z. f. Flugwiss. u. Weltraumforsch. 9, Heft 3, S. 167-178, 1985.
- Schänzer, G. Influence of Windshear on Flight Safety.  
62nd Symposium of the Flight Mechanics Panel, AGARD, Athen, Greece, 1983.
- Schänzer, G. Influence of Wind Shear, Downdraft and Turbulence on Flight Safety.  
2nd International Symposium on Aviation Safety, Toulouse, Nov. 1986.
- Schänzer, G. Einführung in die Flugphysik.  
Vorlesungsscript am Institut für Flugführung der TU Braunschweig, 1984.
- Schänzer, G. Heintsch, T. Hoyer, H. Tetzlaff, G. Untersuchung der Scherwindverhältnisse an der Weidacher Höhe.  
Gutachten, Braunschweig, July 1987.
- Schlickemaier, H. Integrated Wind Shear Program.  
2nd International Symposium on Aviation Safety, Toulouse, Nov. 1986.
- Stengel, R.F. Optimal Control Laws for Microburst Encounter.  
15th ICAS-Congress, ICAS-86-5.6.3, London, 1986.
- Swolinsky, M. Beiträge zur Modellierung von Scherwind für Gefährdungsuntersuchungen.  
Thesis, Techn. Univ. Braunschweig, 1986.
- Swolinsky, M. Wind Shear Models for Aircraft Hazard Investigation.  
2nd International Symposium on Aviation Safety, Toulouse, Nov. 1986.
- Zhu, S. Model of the Wind Field in a Downburst.  
Journal of Aircraft, Vol. 22, No. 7, July 1985.
- Etkin, B. Wind Shear.  
ICAO Circular 186-AN/122, Organization, Montreal, 1987.

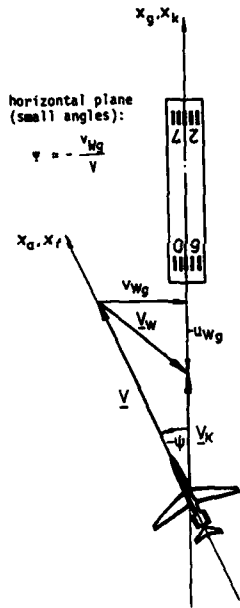


Fig. 1 Crosswind compensation (aircraft horizontal plane)

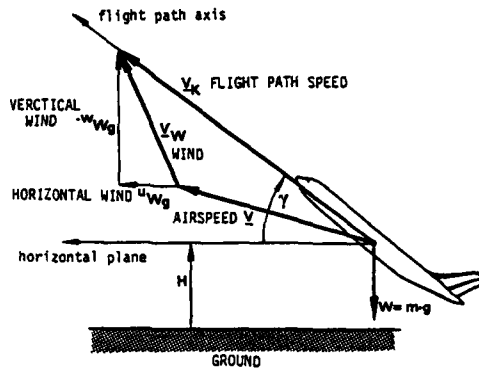


Fig. 2 Vector diagram of speeds in the aircraft symmetrical plane

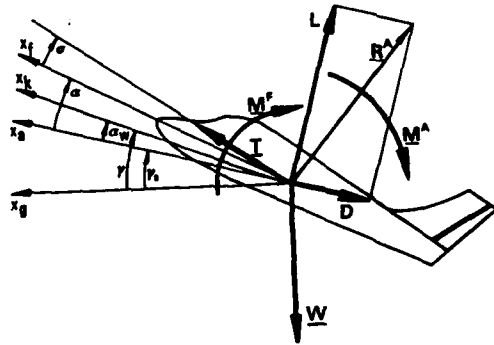


Fig. 3 Angles definitions, forces and moments

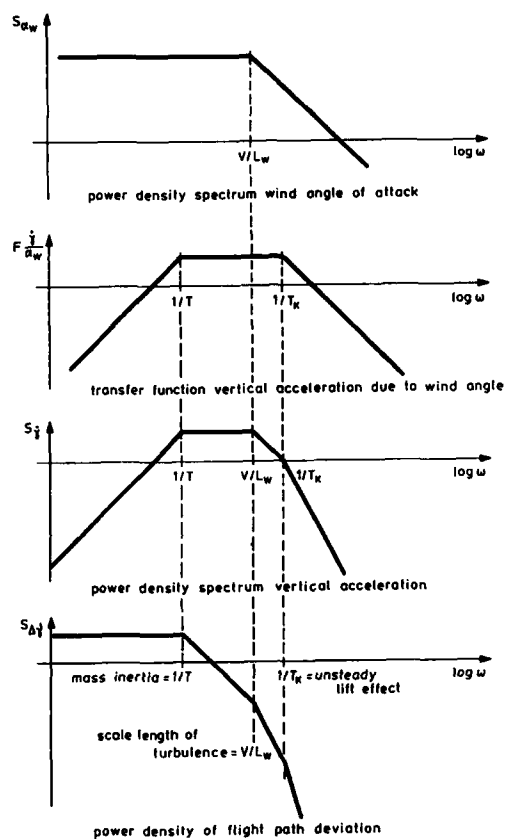


Fig. 4 Vertical flight-path deviation due to vertical turbulence

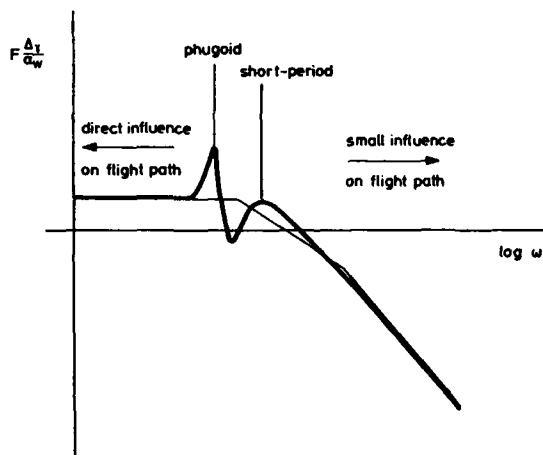


Fig. 5 Flight-path transfer function of complete longitudinal motion

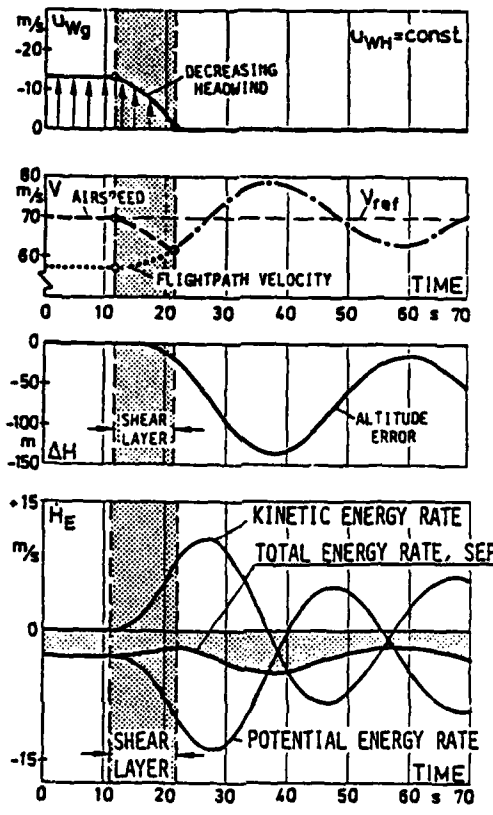


Fig. 6 Effect of tailwind shear on velocities, altitude and energy deviation (KÖNIG et al., 1980)

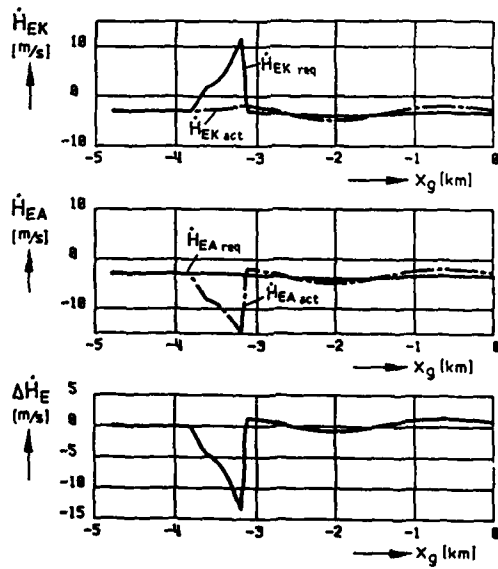


Fig. 7 Comparison of the specific flight-path ( $\dot{H}_{EK}$ ) and air-path energy rate ( $\dot{H}_{EA}$ ) in a tailwind shear (KÖNIG, 1982)

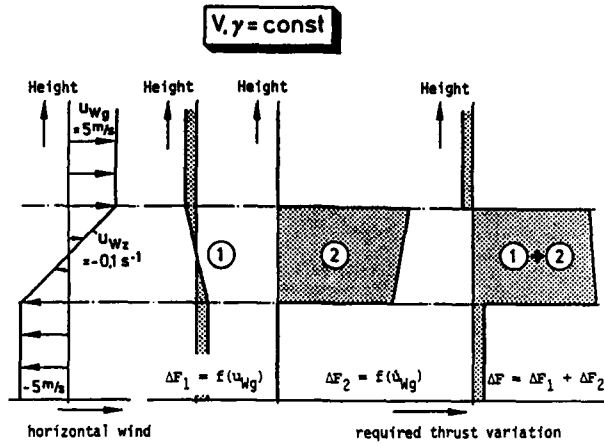


Fig. 8 Required thrust in a wind field of a changing wind component (KRAUSPE, 1983)

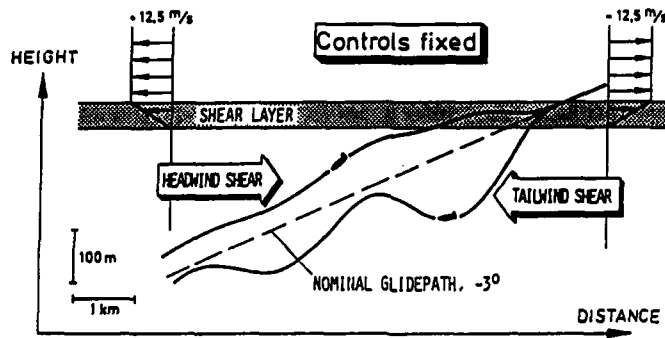


Fig. 9 Landing approaches with controls fixed in a headwind respectively tailwind shear (KÖNIG et al., 1980)

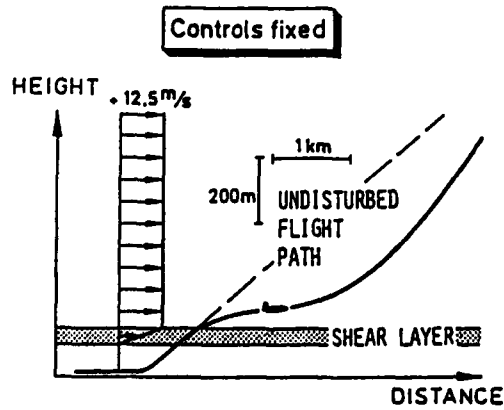


Fig. 10 Take-off flight-path with controls fixed in a tailwind shear (KÖNIG et al., 1980)

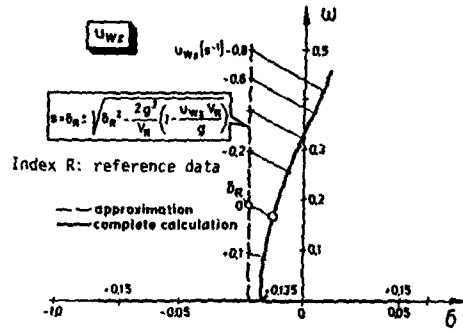


Fig. 11 Eigenvalues of the phugoid mode as a function of a constant vertical wind shear gradient  $u_{wz}$  (KRAUSPE, 1983)

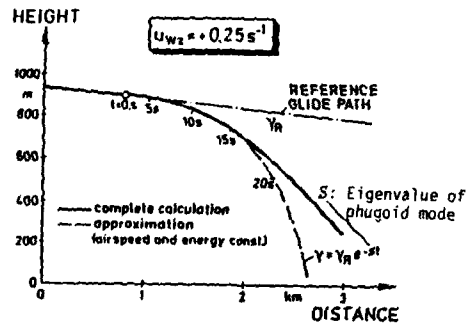
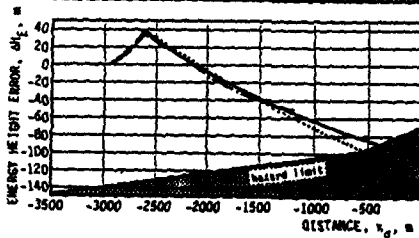
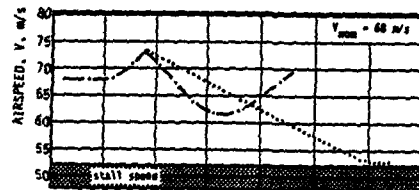
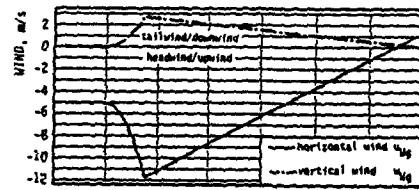
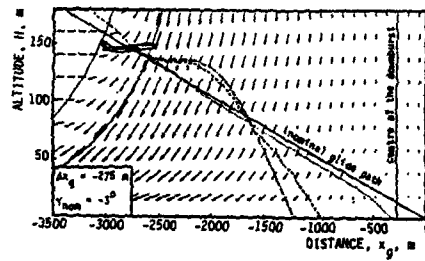


Fig. 12 Flight-path of an aircraft with fixed controls in a constant vertical wind shear gradient (KRAUSPE, 1983)



- calculation by equation (17)
- - - fixed aircraft controls
- ..... autopilot
- - - - - reconstructed accident flight path

Fig. 13 Landing approach paths in a downburst (HANN, 1987)

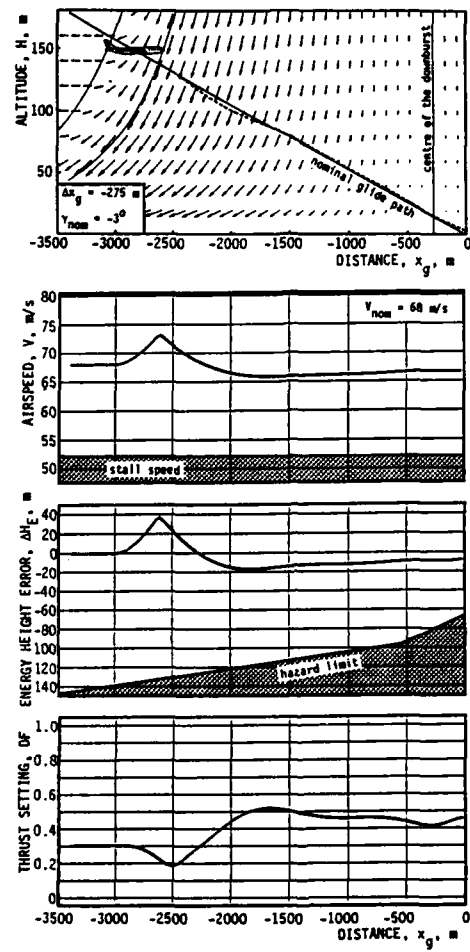


Fig. 14 Landing in a downburst with automatic controls (HAHN, 1987)



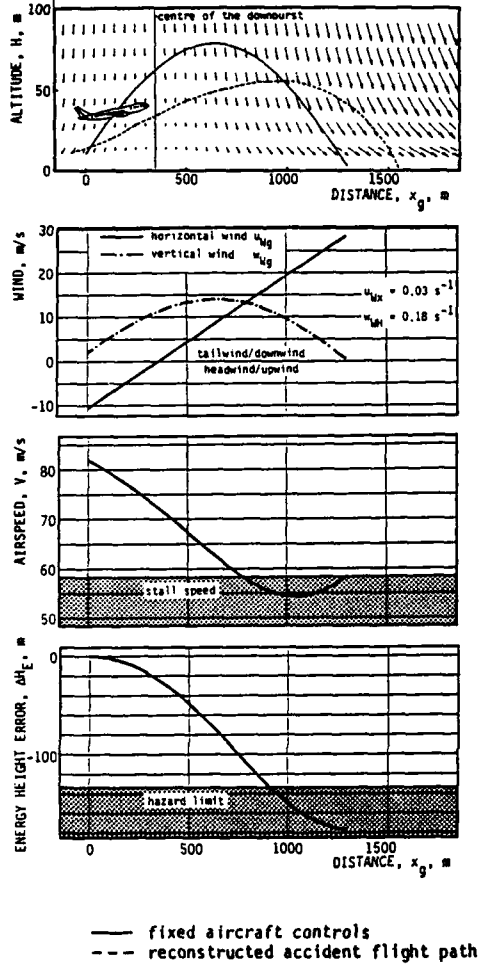


Fig. 16 Take-off in the core of a downburst  
(HAHN, 1987)

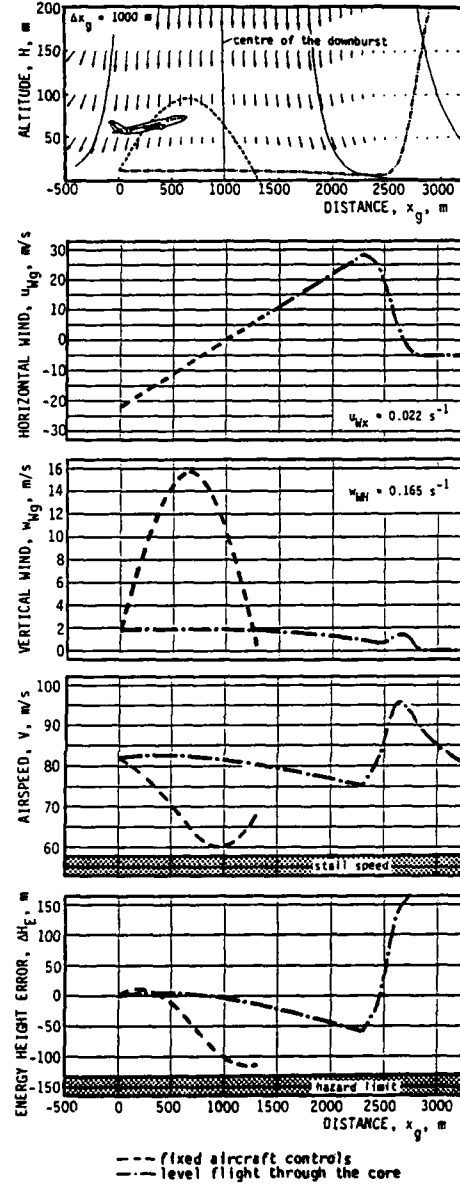


Fig. 17 Escape manoeuvre in a downburst (HAHN, 1987)

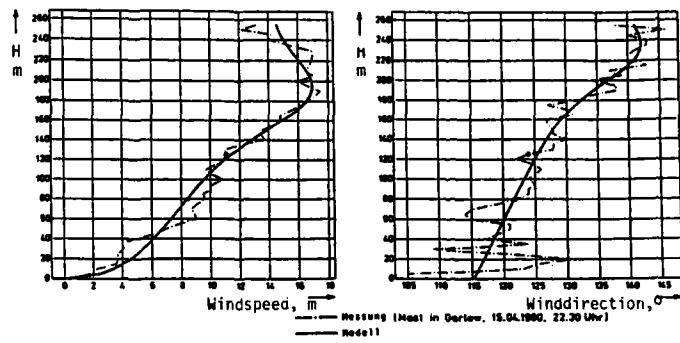


Fig. 18 Example for a measured low level jet

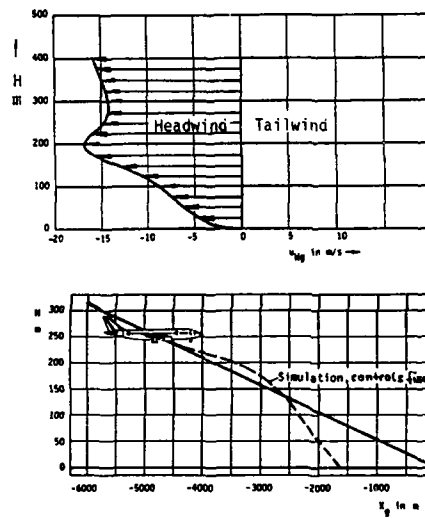


Fig. 19 Simulated landing approach in a low level jet (controls fixed)

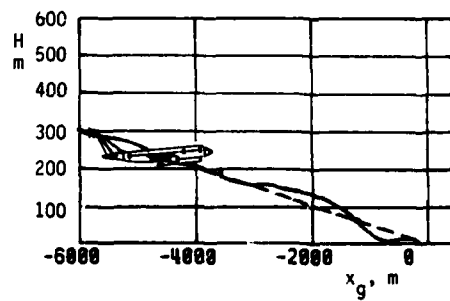


Fig. 20 Simulated landing approach in a low level jet (manual)

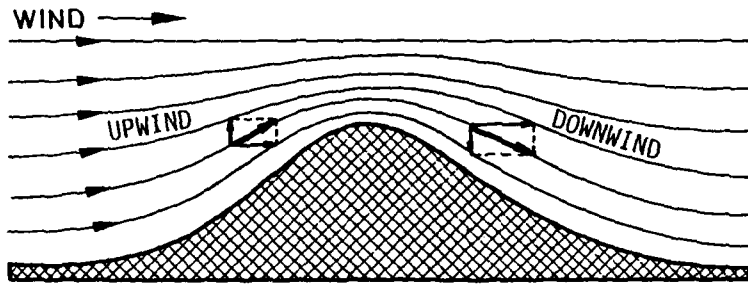


Fig. 21 Streamlines of a flow over flat hill



Fig. 22 Vortex flow in the lee of a mountain

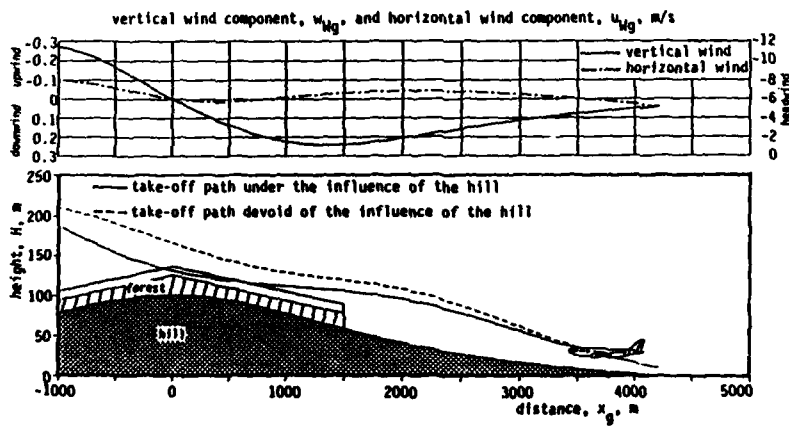


Fig. 23 Take-off path over a hill model

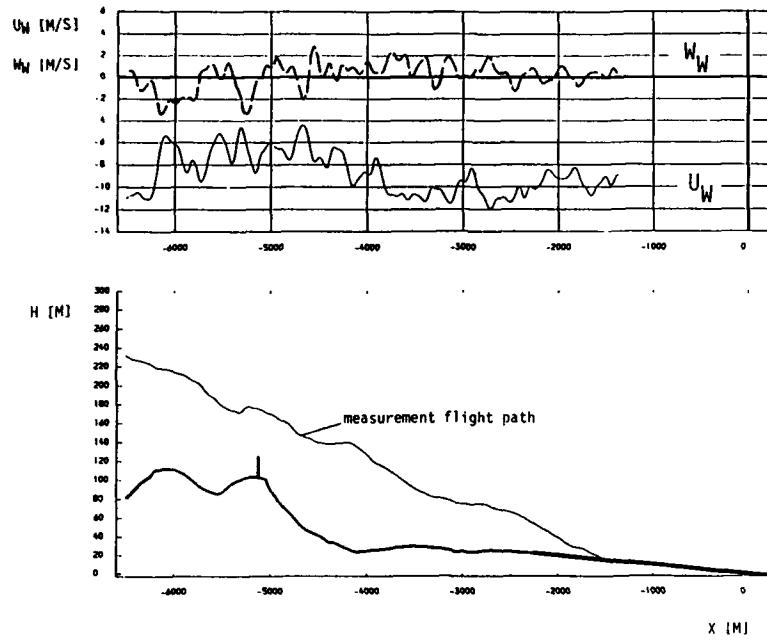


Fig. 24 Measurement flight-path over the hill with measured data

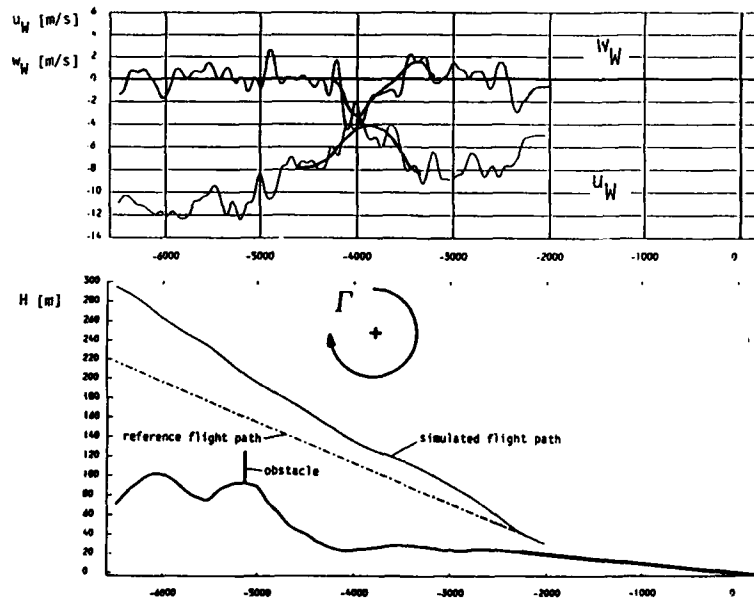


Fig. 25 Measured vortex flow on the lee-side of the hill

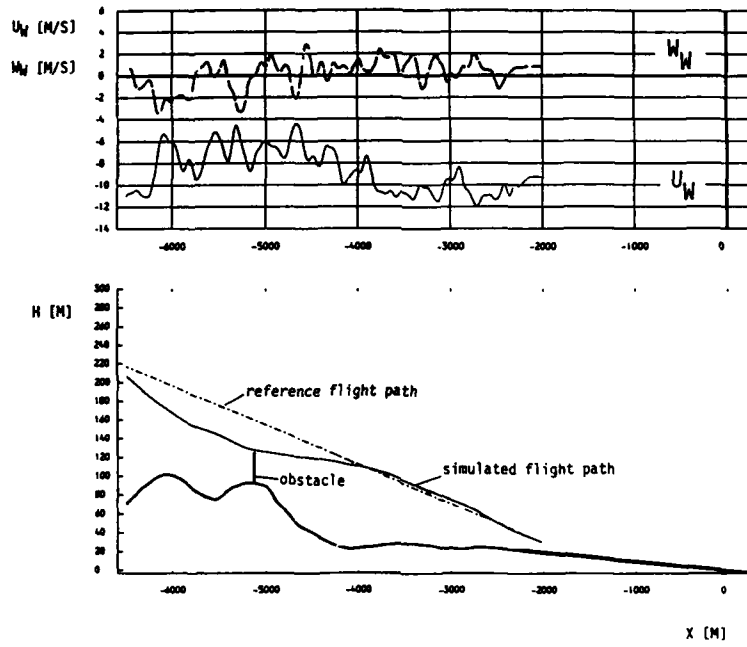


Fig. 26 Reference flight-path and simulated flight-path over the hill

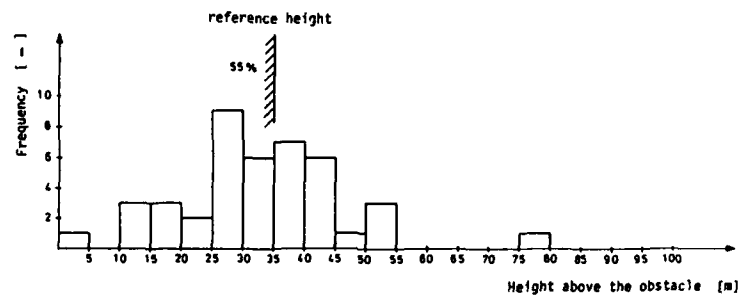


Fig. 27 Frequency of the height above the obstacle

## AIRCRAFT FLIGHT IN WIND-SHEAR

by

**D. McLean**  
Westland Professor of Aeronautics  
University of Southampton  
United Kingdom

### SUMMARY

A brief account of wind-shear and some representations is given before discussing the effects of wind-shear on aircraft motion. A procedure for estimating the vertical and horizontal velocity components of a wind-shear microburst, based on observer theory is developed, and a brief discussion of flying in wind-shear concludes the paper.

### INTRODUCTION

The value of any aircraft to its user depends upon how effectively it can be made to proceed in the time allowed on a precisely-controllable path between its point of departure and its intended destination. Deviation from the required path can be caused by any form of disturbance. There is particular concern with atmospheric disturbances because their forms and times of occurrence are both random and, therefore, difficult to predict so that they may be effectively countered. One form of atmospheric disturbance which is particularly dangerous is the wind-shear, a change in the wind's vector in a very short period of time.

The air through which an aircraft flies is never still. As a consequence, whenever an aircraft flies in this disturbed air, its motion is erratic. The nature of those disturbances to the air is influenced by a number of factors, but it is customary to consider turbulence, which occurs above that region of space where the atmosphere behaves as a boundary layer, as belonging to either of these classes:

- a. convective turbulence, which occurs in and around clouds. This class includes thunderstorms particularly.
- b. clear air turbulence (CAT). Below the cloudbase, direct convection heats the air and causes motion which, together with the many small eddies arising as a result of surface heating, are often regarded as mild CAT. Above a cluster of cumulus clouds a regular, short broken motion can persist, particularly when the change in the velocity with height is large. More virulent C.A.T. is usually to be found near mountains. And, depending upon the meteorological conditions, flights near the tropopause can often be turbulent. The most virulent turbulence of all, however, is caused by thunderstorms and squall lines, especially when the same area is simultaneously being subjected to rain, hail, sleet, or snow.

Another violent atmospheric phenomenon, which can be encountered in flight, is the microburst, a severe downburst of air. Microbursts are associated with considerable changes in the direction and/or velocity of the wind as the height changes. They exist for only very brief periods. Such severe changes in the nature of the wind over restricted ranges of height are caused by convection and they are often referred to as "wind-shears". Rising, or falling, columns of air, ringed by toroids of extreme vorticity, are produced by the convection and it is this phenomenon which is called the microburst. A fuller account is presented below.

Because the mechanisms of turbulence are so varied and involved, it has been found that the only effective methods of analysing dynamic problems in which turbulence is involved are statistical methods. However, large gusts, which are reasonably well defined by a particular deterministic function, do occur, but at random times. To assess the effect an aircraft encountering such gusts, it is common practice to employ a discrete gust as a testing function. Even though its time of occurrence may be random, a wind-shear, once it has occurred, can be effectively regarded, as a deterministic phenomenon. Models of wind-shear are not entirely descriptive of the phenomenon which they are meant to represent, but they can represent the significant characteristics sufficiently well to permit an analysis to be carried out with adequate accuracy for engineering purposes.

### WINDSHEAR AND MICROBURSTS

It has been indicated earlier that wind-shear is a change in the wind vector in a relatively short amount of space. One of the consequences of such an atmospheric phenomenon is a rapid change in the airflow over the aerodynamic surfaces of an aircraft.

Such rapid changes of airflow can be hazardous, particularly to aircraft flying at low altitudes and at low speeds. It is a particularly difficult phenomenon to detect, since the effects of wind-shear are transitory, and its nature and occurrence are random. The form of wind-shear which is of particular concern is the microburst, in which a large mass of air is propelled downwards in a jet from some convective cloud system, or, perhaps, from a rapid build-up of small weather cells.

A physical account of how such a microburst forms, acts, and decays is given in ref (1). Thunderstorms, being highly variable and dynamic atmospheric occurrences, translate rapidly across the ground. As they travel, they grow and then decay. A thunderstorm results from the rapid growth and expansion in the vertical of a cumulus cloud. In its initial stages, such a storm comprises an updraft of warm, moist air, with a velocity as great as 15m/s. In the updraft, moisture droplets are lifted up until the temperature of the atmosphere causes freezing to occur. These droplets next grow into super-cooled raindrops. However, the size of these raindrops is soon too large to be supported by the updraft, at which stage they fall, dragging air with them, which produces a strong downdraft. This stage is the most mature stage of any storm. The downdraft is strengthened by drier outside air becoming entrained, and then cooled, as the raindrops evaporate. This reinforcing of the downdraft causes both the wind to become stronger and also sudden, heavy precipitation, typified by a sudden downpour. As the thunderstorm abates, the downdraft becomes even more extensive and cuts off the downdraft from its inflow of warm, moist air. As a result, the storm begins to subside, the precipitation to lessen and then stop, and, soon after, the clouds begin to disperse. In the area separating the inflow and outflow, which is usually called the gust front, and which can extend for 20km, wind-shear may occur at low altitudes.

Since aircraft do not normally have sufficient specific excess power to counter the force of such a downwardly-propelled air mass, the microburst is particularly dangerous. In such an atmospheric condition, within a period of one minute or less, an aircraft can be subjected to, say, a headwind, followed by a downdraft, and then succeeded by a tailwind. There has been observed in the performance of pilots flying in such conditions a consistent pattern of response; when an updraft is first experienced, the pilot lowers the nose of the aircraft and reduces thrust. Then follows a headwind, with a consequent increase in the airspeed of the aircraft, causing the pilot to further reduce thrust. From the microburst, there is next experienced a strong, downdraft and tailwind, but the pilot's actions, already taken, have set the scene for further difficulty, since the thrust has been reduced and the nose lowered. In general, the performance of untrained pilots in wind-shear situations is rarely adequate, manifesting itself (usually), in a failure to maintain the appropriate airspeed and the correct flight path.

Notwithstanding the evident importance for flight safety of the phenomenon of wind-shear, standard representations for use in analytical studies are unsatisfactory, although Frost<sup>(2)</sup> has recently provided a number of new models for consideration. Two important vortex models (3, 4) have also been suggested. Yet, there are but two official forms, one defined by the FAA, and the other by the ARB in the U.K. Both are represented in Figure 1. The ARB profile is logarithmic and, at the lower heights, its gradient becomes progressively steeper than that of the FAA profile. In Figure 1  $V_w$  represents the wind velocity;  $V_R$  is a reference velocity, taken as the velocity of the wind measured at a reference height of 25ft (7.6m). Neither profile is adequate for studying the microburst situation. The problem of how to adequately represent such a situation remains unsolved.

In any wind-shear encounter it is the phugoid mode, the slow period response of the aircraft, which is most important because it depends upon the interchange between the kinetic and the potential energy of the aircraft in the vertical plane. It is known that the phugoid mode is usually oscillatory and very lightly damped. In some cases it can be unstable. Significantly, the time involved in a microburst encounter is often about the same as the period of the phugoid mode, thereby making possible a resonant response, in which the interchange energy is amplified. Such amplification leads to a greater deviation from the intended flight path than would have occurred with a well-damped mode.

One form of representation of wind-shear<sup>(5)</sup>, which takes these facts into account, is represented in Figure 2. It must be "tuned" to accord with the flying characteristics of the aircraft being studied. In Figure 2, the square wave oscillation represents a head/tailwind combination: at the mid-point of the square wave, a (1-cos) downdraft is introduced. The period of the square wave is adjusted to be the same as the period of the phugoid motion of the aircraft being investigated. Although the profile in Figure 2 has been presented as a function of time, it is intended to represent a physical phenomenon in which the velocity changes with height. There is an implicit assumption that during the period of the wind-shear encounter the aircraft will be climbing or landing, i.e. changing its height.

Another method of representation is to use any record of a wind-shear which may have been obtained, either from meteorological studies or from flight records. A number of records are now available; the most celebrated was obtained from a reconstruction of the available data relating to the disastrous crash of a Boeing 727 which occurred on 24th June 1975 at J F Kennedy Airport, New York, U.S.A. The reconstructed data is shown in Figure 3, together with the aircraft trajectory. 00 seconds (2006 GMT) denotes the time when the aircraft reached the outburst centre. Note how the characteristic "ballooning" of the aircraft's path started 15 seconds before this point, and how some 11.5 seconds after its occurrence the severe downdraft caused the aircraft to crash some 2000 feet (600m) short of the runway. Resolution of this wind-shear into vertical and horizontal components results in the profiles for  $u_g$  and  $w_g$  shown in Figure 4. These can be used, with appropriate amplitude scaling, in wind-shear studies.

#### EFFECT OF WIND-SHEAR ON AIRCRAFT MOTION

The small perturbation motion of an aircraft affected by an atmospheric disturbance can be represented by the vector differential equation:-

$$\dot{x} = Ax + Bu + Ed_g \quad (1)$$

where  $x \in R^n$ ,  $u \in R^m$ , and  $d_g \in R^s$ .

The coefficient matrix,  $A$ , is of order  $n \times n$ ; the control driving matrix,  $B$ , is of order  $n \times m$ , and the disturbance driving matrix,  $E$ , is of order  $n \times s$ .

Such equations as eq. (1) are habitually used in studies concerned with flight control systems. But the small perturbation approach is generally only justified when the wind field is uniform<sup>(6)</sup>. For a non-uniform wind field there is normally a continuously changing equilibrium flight condition (about which the small perturbation motion is supposed to occur) which manifests itself physically in there being observable changes in the equilibrium flight path angle, lift, and side forces with time. However, consideration of the hazardous flight problem indicates that the primary effect of wind-shear relates to longitudinal motion, particularly in the low-speed regimes of landing or take-off, so that these time-varying changes in  $\gamma$ ,  $L$  and  $Y$  can be neglected as a first approximation. Consequently, eq. (1) can be taken as a reasonable representation. Since  $d_g$  is unknown it would be useful to measure it accurately in flight so that the pilot, or a control system, could generate a suitable control input,  $u$ , to counter its effects. One method of obtaining,  $d_g$ , is to use an observer. If the control action,  $u$ , is taken as inappropriate, for example, a pilot continues to fly the aircraft in an appropriate way for a normal landing, without allowing for the effects of wind-shear, then the aircraft's trajectory is normally represented by the "ballooning" curve shown in Figure 4, with its attendant disaster at ground contact. It is evidently necessary to provide a good estimate of  $d_g$ , the vector whose elements are the velocity components of the wind-shear. It has been pointed out in the Introduction to this paper that once it has occurred a wind-shear can be effectively regarded as a deterministic phenomenon, and consequently it can be reconstructed from a knowledge of the output vector of the aircraft, composed of a few of the state variables representing the aircraft's motion, and of the control inputs if they are being applied. The most convenient form of reconstruction is a Luenberger observer. A number of algorithms are available to permit such a design, but one method which provides a convenient technique is to design an observer making use of linear optimal control theory.

#### OPTIMAL OBSERVER

Suppose that the dynamics of some aircraft are defined by state and output equations viz.

$$\dot{x} = Ax + Bu \quad (2)$$

$$y = Cx \quad (3)$$

It is intended to design an observer to provide an estimated state vector,  $x_k$ , which will be close to the original state vector,  $x$ , but requires as its inputs only the control vector,  $u$ , and another vector,  $w$ , which is related to the output vector,  $y$ , of the aircraft i.e.

$$\dot{x}_k = Fx_k + Gu + w \quad (4)$$

The forcing vector,  $w$ , is chosen to be

$$w = \Delta K(y - y_k) \quad (5)$$

where

$$y_k = \Delta Cx_k \quad (6)$$

Therefore,

$$\dot{x}_k = (F - KC)x_k + Gu + KCx \quad (7)$$

However, from eq. (2),

$$Bu = \dot{\hat{x}} - Ax \quad (8)$$

and if

$$G \stackrel{\Delta}{=} B \quad (9)$$

then

$$\dot{\hat{x}}_E = (F - KC)x_E + x - (A - KC)x \quad (10)$$

i.e.

$$\dot{\hat{x}} - \dot{\hat{x}}_E = (A - KC)x - (F - KC)x_E \quad (11)$$

By choosing the coefficient matrix,  $F$ , of the observer to be identical to that of the aircraft namely

$$F \stackrel{\Delta}{=} A \quad (12)$$

and by defining any difference between the actual state estimated and vector as an error vector,  $e$ , it can easily be shown that

$$\dot{e} = (A - KC)e \quad (12)$$

Provided that  $\lambda(A-KC) < 0$  then, as  $t$  tends to infinity, the error vector,  $e$ , will tend to zero and the observer's vector,  $\hat{x}_E$ , will correspond to the state vector,  $x$ , of the aircraft. To secure this desirable condition requires only that the matrix,  $K$ , be determined.

As a first step, let  $K$  be chosen to be a stabilizing matrix. Imagine that the observer dynamics are defined by eq. (13) rather than eq. (4), that is to say, that

$$\dot{\hat{x}}_E = F\hat{x}_E + Gu + Ky \quad (13)$$

Letting  $G \stackrel{\Delta}{=} B$  (as before) results in

$$\dot{\hat{x}} - \dot{\hat{x}}_E = Ax - F\hat{x}_E - KCx = (A - KC)x - F\hat{x}_E \quad (14)$$

If  $F$  is chosen to be  $(A-KC)$ , and

$$e \stackrel{\Delta}{=} x - \hat{x}_E \quad (15)$$

then

$$\dot{e} = (A - KC)e = De \quad (16)$$

Suppose that we have a system defined by an equation

$$\dot{e} = Me + Nv \quad (17)$$

then if we chose as a performance index

$$J = \frac{1}{2} \int_0^{\infty} (e'Qe + v'Gu) dt \quad (18)$$

then minimizing eq. (18) subject to eq. (17) will result in a control law

$$v = He \quad (19)$$

Hence

$$\dot{e} = (M + NH)e \quad (20)$$

If it can be arranged that

$$\lambda(A - KC) = \lambda(M + NH) = \lambda(D) \quad (21)$$

then the optimal closed loop observer will be the required observer provided that

$$\begin{aligned} M &= A \\ N &= C \\ \text{and } H &= -K \end{aligned} \quad (22)$$

A block diagram representing the optimal closed-loop observer is shown in Figure 5.

The optimal observer provides an estimate,  $\hat{x}_E$ , of the state vector; what is wanted is the wind-shear vector,  $d_E$ .

However, if a "model" equation is constructed with the following dynamics

$$\dot{\mathbf{x}}_m = D\mathbf{x}_g + B\mathbf{u} + K\mathbf{y} \quad (23)$$

then

$$(\dot{\mathbf{x}}_g - \dot{\mathbf{x}}_m) = E\mathbf{d}_g \quad (24)$$

If eq. (1) was re-written in its elemental form it is evident from eq. (24) that

$$\dot{u}_g - \dot{u}_m = -X_u u_g - X_w w_g \quad (25)$$

$$\dot{w}_g - \dot{w}_m = Z_u u_g - Z_w w_g \quad (26)$$

It can easily be shown that:

$$X_w(\dot{w}_g - \dot{w}_m) - Z_w(u_g - u_m) = (X_u Z_w - Z_u Z_w) u_g \quad (27)$$

$$Z_u(u_g - u_m) - X_u(\dot{w}_g - \dot{w}_m) = (X_u Z_w - Z_u Z_w) w_g \quad (28)$$

Equations (27) and (28) can be very easily synthesized and a suitable block diagram representation is shown as Figure 6. In that figure the output signals have been denoted as  $\hat{u}_g$  and  $\hat{w}_g$  which are identically equal to  $u_g$  and  $w_g$ , the required wind-shear components, when the values of the stability derivatives used in the synthesis viz  $Z_u$ ,  $Z_w$ ,  $X_u$ ,  $X_w$  are exact; otherwise  $\hat{u}_g$  and  $\hat{w}_g$  are subject to error.

The effectiveness of the estimation scheme can be judged from Figure 7, in which are shown the estimated horizontal and vertical components obtained from the simulation of a Jetstar aircraft landing when encountering the JFK wind-shear of Figure 3.

#### FLYING IN WIND-SHEAR

A number of operational techniques have been recommended<sup>(7)</sup> for flying in hazardous wind-shear conditions. For example, it is considered by some that pilots should allow the airspeed to fall to stick shaker speed while gaining height by pitching up, although the Airworthiness and Performance Committee of the ALPA considers that it is best to achieve the speed for best angle of climb i.e. minimum drag speed. It is the view of that committee that sacrificing all the available energy of the aircraft down to stick shaker speed while increasing at the same time the aircraft's drag (thereby reducing the aircraft's climb capability) is unsafe. Whatever technique is adopted requires a recognition on the part of the pilot that he is countering the effects of a wind-shear. The provision of an airborne detection system is advantageous for a number of reasons, including the fact that the aircraft does not depend on any ground-based system at each airport. With such a system the pilot can monitor quantitatively how the longitudinal and vertical components of the wind-shear are changing, and with that indication, even if it gives only a few seconds warning, will allow a pilot to attempt to bank away or to go around.

The technique proposed in this paper avoids the need for an accurate measurement of ground speed and is particularly suitable for general aviation aircraft, such as business jets. It will provide an indication on the runway if a wind-shear is present if the aircraft is in motion, but the accuracy of the estimation is not as great. Nevertheless, in common with any measurement system, it has a disadvantage that in providing a measurement the aircraft must have entered the wind-shear field. The use of automatic feedback control systems using the estimated wind-shear components to achieve a proper automatic recovery is feasible<sup>(8)</sup> in some situations, but in low speed regimes the need to avoid stall would make the design of such control systems difficult and, since wind-shear encounters are likely to be rare, not economically attractive.

## REFERENCES

1. Etkin, B.  
The Turbulent Wind and Its Effect on Flight - AIAA Wright Brothers Lecture, 1980  
UTIAS Review No. 44, Aug. 1980, Institute of Aero. Studies, University of Toronto, Canada.
2. Frost, W.  
Flight in Low Level Wind Shear  
NASA CR-3678, 1983.
3. Markov, B.  
The Landing Approach in Variable Winds: Curved Glidepath Geometries and Worst Case Wind Modelling.  
UTIAS Rept. 254, Dec. 1981, Toronto, Canada.
4. Woodfield, A.A.  
Wind-Shear Topics at RAE Flight Systems Department  
RAE TM FS132, 1985.
5. Frost, W., B.S. Turkel and J. MacCarthy.  
Simulation of Phugoid Excitation Due to Hazardous Wind Shear.  
Proc. 20th AIAA Aerospace Sciences Meeting, Jan. 1982, Orlando, Florida, USA.
6. Etkin, B.  
Dynamics of Atmospheric Flight.  
J. Wiley, 1972, NY.
7. Higgins, P.R. and Paterson, D.H.  
More About Wind-Shear Hazards.  
Boeing Airliner, Jan. 1979, p.3.
8. Psiaki, M.L. and R.F. Stengel.  
Analysis of Aircraft Control Strategies for Microburst Encounter.  
J. Guid. Cont. and Dyn. 8(5), 1985, 553-559.

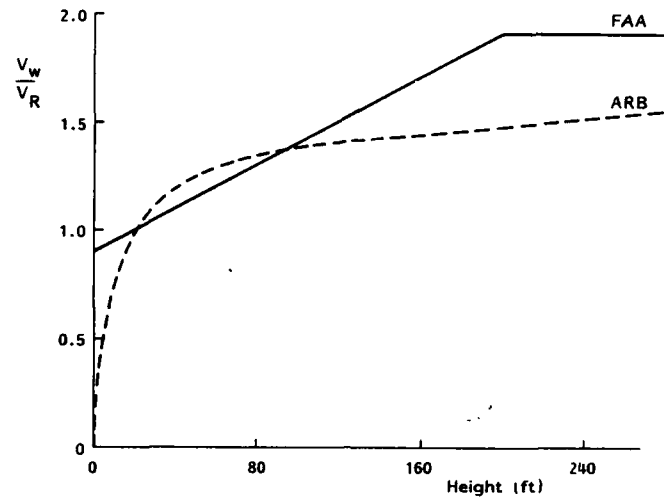


FIG. 1 REGULATORY WIND - SHEAR PROFILE

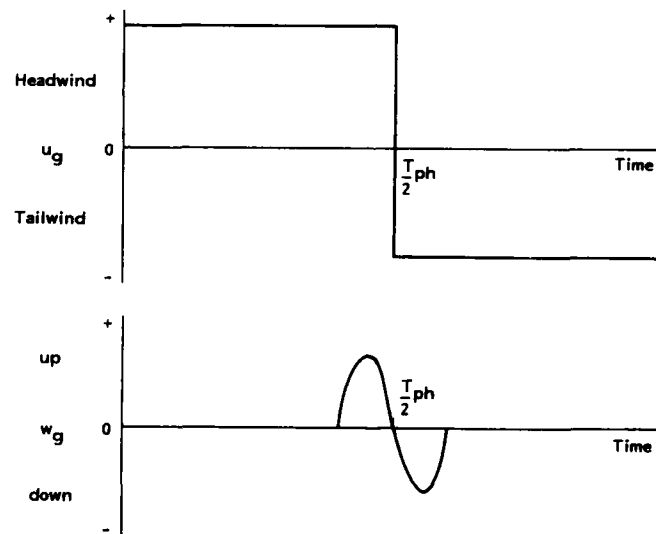


FIG. 2 WIND-SHEAR TEST PROFILE

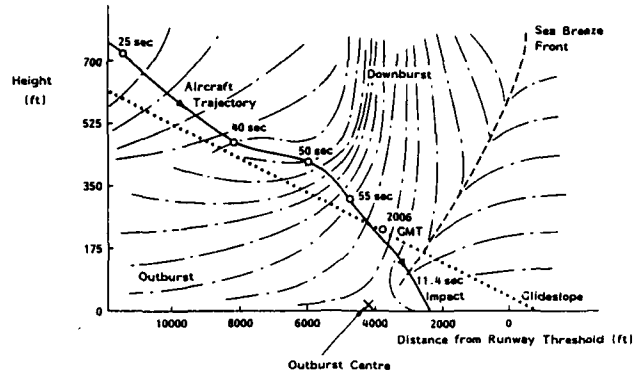


FIG. 3 WIND SHEAR REPRESENTATION AT JFK AIRPORT ON JUNE 24, 1975

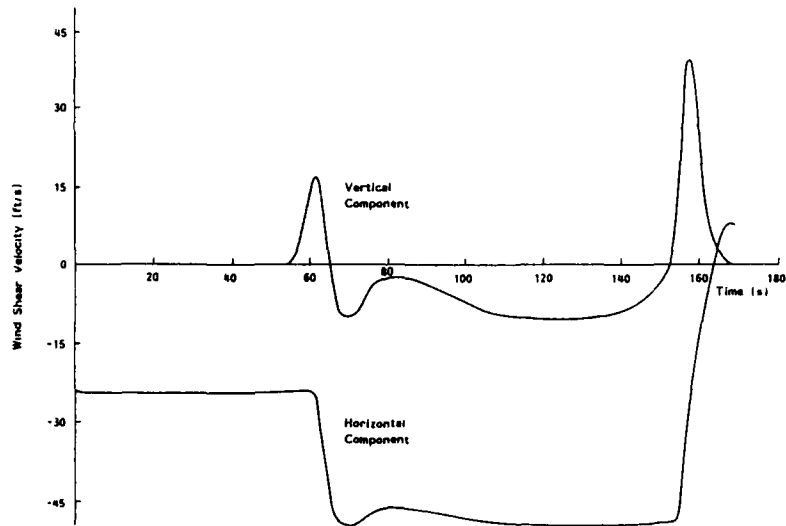


FIG. 4 RECORDED WIND SHEAR COMPONENTS AT JFK JUNE 1975



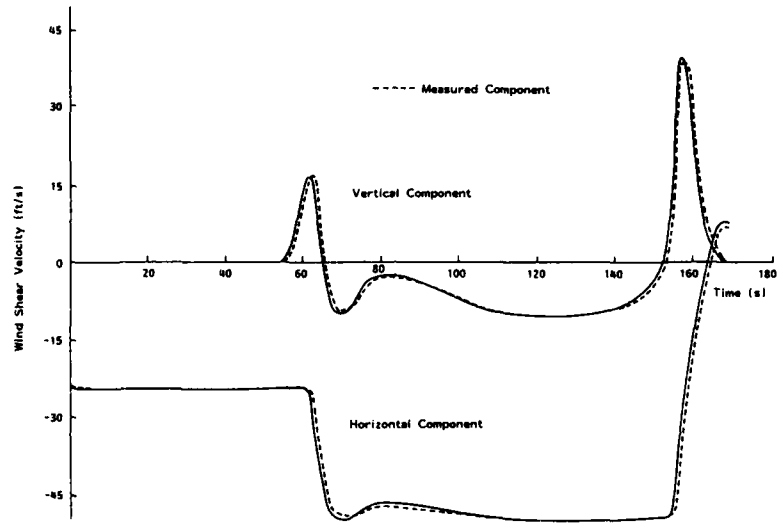


FIG. 7 ESTIMATED WIND SHEAR COMPONENTS.

## HOW TO FLY WINDSHEAR

by

Paul Camus -- Group Manager Flight Controls  
Airbus Industrie  
1 rond-point M.Bellonte  
31707 Blagnac Cedex  
France

Aviation safety history is a long fight against severe environmental constraint. Modern aircraft are able to face safely most of them but one still remain a potential killer, that is what is generally described as a windshear situation.

What can be done, necessarily fall either in how to timely detect such a situation in order to avoid it or/and what tools could be given to the crew to better escape should they are trapped in.

Latest state of build-in equipment, 3-D Navigation, Electronic displays and Flight Control, provide now all necessary tools to develop an efficient in-board detection and protection system. Such system will be described altogether with a review of some fundamental criteria to be considered when assessing their efficiency.

In the recent years a big emphasis has been put on windshear since a few fatal accidents have focused the attention of the people on a very old phenomenon known by the flying crews.

Due to the increasing air traffic leading to a higher exposure into bad weather conditions the attention of the air transportation community has been driven to look more carefully into the complexity of the "windshear" phenomenon and into the way to survive it.

Thanks in particular to the work and publications of Professor T. T. FUJITA from the University of Chicago, the Aviation Community is now able to better understand these short, violent and almost unpredictable "Microbursts" which may end up in fatal accident.

In general the term "Windshear" defines a variety of atmospheric conditions characterized by a sudden change in air mass direction and/or velocity. Amongst the shears an airplane may encounter, the microburst is one of the most threatening since this sudden strong downdraft close to the ground induces outburst winds as high as 150 kt. All this phenomenon is limited in a small horizontal scale leaving little room for a rapid manoeuvre where survival may be a matter of seconds. The case of Delta 191 in Dallas is a typical example of this violent case where within one minute the burst developed to an hazardous situation (ref. figure 1). A scan of the flight recorder shows the behaviour of the main parameters in this case (ref. figure 2).

It is clear to everybody that the best to survive such cases is to AVOID it. Of course the Airbus Industrie recommendation is to apply this very simple rule : "AVOID, AVOID, AVOID".

However the avoidance procedure will be based on a reliable and quick information process given to the crew to be in a position either to stay on ground before take off or to initiate an early go-around during the approach. Despite strong efforts in the USA to develop and install ground facilities to detect the windshear, most of the places where convective weather situations may be encountered leading to violent wind bursts will remain for a long time with only visual information and pilot reports. This means that for the time being the only available solution remains an equipment installed on board of the aircraft.

One could consider to have an advisory airborne system to alert the crew in advance for early avoidance. Unfortunately no simple system yet exists and the today on board weather radar is not able to do the job properly.

Therefore the only remaining possibility is to have a redundant and integrated airborne system combined with operational procedures to help the crew in flying through the windshear.

Since 1972, Airbus Industrie has considered as a necessity to implement on its newly designed aircraft means to help the pilot in coping with the windshear. With the support of the new technologies Airbus Industrie has been permanently improving or bringing additional information to further enhance the capacity of the pilot to safely fly through the burst (ref. fig. 3).

Based on the standard equation of flight, it is possible to work on two parameters : THRUST and LIFT.

It is clear that the use of the maximum rated thrust as soon as possible helps in recovery as well as pitch attitude increase in order to increase the lift, thus increasing potential energy. Since the success is a matter of seconds, Airbus Industrie has implemented :

- an automatic thrust increase which is available in automatic and manual modes and
- a pitch guidance which will give a good cue to the pilot to maintain an attitude avoiding to sacrifice altitude.

#### SPEED REFERENCE SYSTEM

This system has been developed to guide the pilot in pitch during take-off and go-around. The system works basically as a speed control system however it includes protections which are activated in case of windshear.

The prevailing order is defined by increasing pitch toward 18° thus increasing the lift. However, in case of extreme condition the pitch order may be superseded by the control of the speed slightly above the stick shaker level by the pilot himself. Simulation has shown that following the SRS order it was possible to maintain the altitude for a fair period of time which should save the airplane in most of the shears.

The first point on which it was possible to easily implement a solution was the automatic increase of thrust in case of excessive angle of attack. This apply mainly during the approach where the windshear will generally lead to an increase of angle of attack and if it is severe enough the effect of full thrust as soon as possible will improve the safety. The system reacts automatically when the angle of attack exceeds a predetermined value. Should this occur, the recommended procedure during approach is to make a go-around.

If the measured rate of change of airspeed and ground speed exceeds a preset threshold, the system will react with a phase advance. The nose up change which accompanies the power increase brings an additional safety factor by trending to higher angle of attack.

The system will not react to a pure vertical draft as quickly as to an horizontal shear. However, it is worth noticing that at low level (below 500 ft) the probability of getting a pure vertical draft is very low since the proximity of the ground will deviate the flow and turn it to horizontal out draft. In the case of Delta 191, the main wind component was a strong tailwind in the last 400 ft.

With the installation of the Cathod Ray Tube (CRT), Airbus Industrie has introduced some information giving a clear synthesis of the situation such as the speed trend and the position of the actual speed compared to reference speeds such as 1.3 Vs and 1.1 Vs.

An important effort has been made in matter of rationalization of the information presented to the crew (ref. Figure 6).

#### SPEED TREND INFORMATION AND SPEED MARGIN

On the Cathod Ray Tube of the primary flight display, it has been possible to present with an arrow where will be the speed in the next 10 seconds. Eventhough no rule has been defined, one will notice by the jerk of the arrow and particularly its size that an abnormality is raising which may on the ground lead naturally to the take-off abort. In flight it will give a good indication and help in an early response.

In addition the permanent display of the stick shaker speed will give the pilot the best support to fly the airplane at the maximum possible lift should the case occur.

#### FLIGHT PATH VECTOR

One important tool, which is not used as it should, is the flight path vector which could be monitored by the non flying pilot. The "Bird" is generated by the inertial reference system which is independent from the other parameters and shows the direction of the flight path. It is obvious that, when the "Bird" is below the horizon, the path is converging towards the ground. Such a synthesis from the basic parameters as presented on conventional aircraft is not easy in particular in critical phase.

On the A320 a further step will be implemented with the happening of the "fly thru computer".

The basic pitch control law is working up to a certain angle of attack where it is replaced by an angle of attack control law (ref. Figures 9 and 10) which covers the high lift zone : an increasingly positive stability is introduced so that a maximum angle of attack corresponding to the stall protection is achieved with the full stick deflection. At that point the wing is delivering all its lift allowing a fair margin to the stall with good capability in roll. In the same zone the high angle of attack floor protection will activate automatically the thrust to the maximum rated level, where it will be latched.

In case of windshear :

The pitch control law is based on load factor demand and therefore try to maintain the flight under IG condition, thus fighting the shear.

If the shear becomes too severe the maximum rated thrust will be automatically applied in all phases of flight and the pitch demand will be somehow optimized.

In extreme condition, since the airplane will be stall protected, the procedure is to pull the stick right back. This last action will demand the maximum possible lift from the airplane while the pilot knows that the airplane will not stall.

#### Procedure

In addition to the airborne installation, Airbus Industrie insists on the following procedures since a strong windshear can be considered as an emergency situation where immediate and simple action is the only solution. Airbus Industrie believes that when survival is a matter of seconds, there is no parameter to be precisely flown. Nothing else but trading speed for altitude, which means pulling up, would help in a case such as the one of CO 426 (ref. Figure 8).

1 - AVOID : if windshear is expected or announced, delay take-off or landing.

2 - If caught in the shear : keep the nose up to at least maintain altitude, and trigger the go levers in case of flexible thrust take-off or approach.

The information and displays available in the Airbus Industrie aircraft family will help the crew in identification and guidance :

- maximum rated thrust is automatically applied through the GO AROUND lever or the protection
- pitch guidance is provided through the Speed Reference System
- stick shaker speed is continuously displayed (valid from A310 on).

The recovery technique for the A320 is further simplified :

PULL the STICK FULL BACKWARDS which provides automatically the maximum rated thrust and lift.

Airbus Industrie is presently working on training program to give the airlines information and recovery technics. This effort is consistent with the present program developed by the FAA and Airbus Industrie participates at the FAA audit on this subject. In addition we are developing information to be introduced in the *Flight Crew Operating Manual* to give the crew the performance capability of the airplane under prevailing weather conditions and weight.

In summary the Airbus Industrie goal is to give the crew information and guidances (ref. Figure 11) which complement and do not supersede the data available from the ground and the crew experience in matter of weather knowledge. Our aim is to help in case of recovery from severe windshear keeping in mind that avoidance is the target. Airbus Industrie will continue to work on this essential objective which is FLIGHT SAFETY.

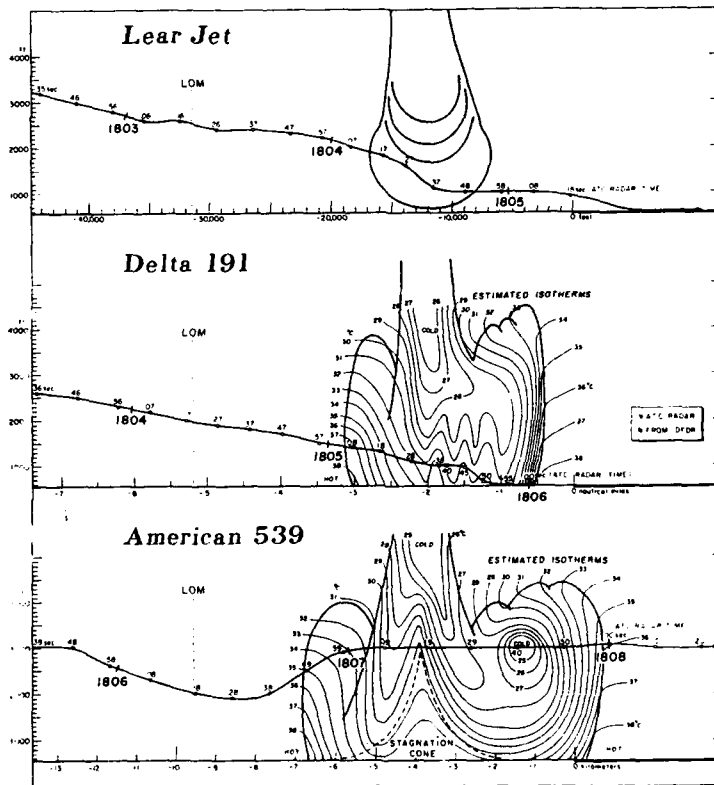


Figure 1

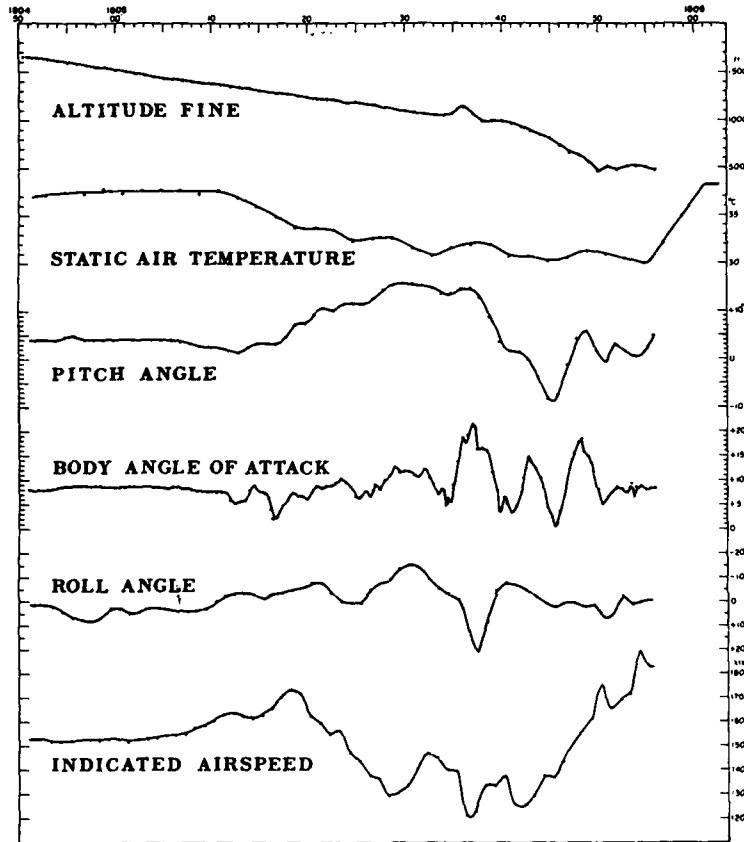


Figure 2

## Airbus Industrie efforts against windshear since 1972

	A300	A310 & A300-600	A320
Angle of attack protection	X	X	X
Speed reference system	X	X	X
Beam deviation on ILS	X	X	X
Stick shaker speed and speed Trend information		X	X
Wind speed and direction info		X	X
Flight path vector		X	X
Visual warning		X	X
Stall protection	Stick shaker	Stick shaker	Full protection against stall
High Angle of Attack Control			X

Figure 3

## Excessive angle of attack protection

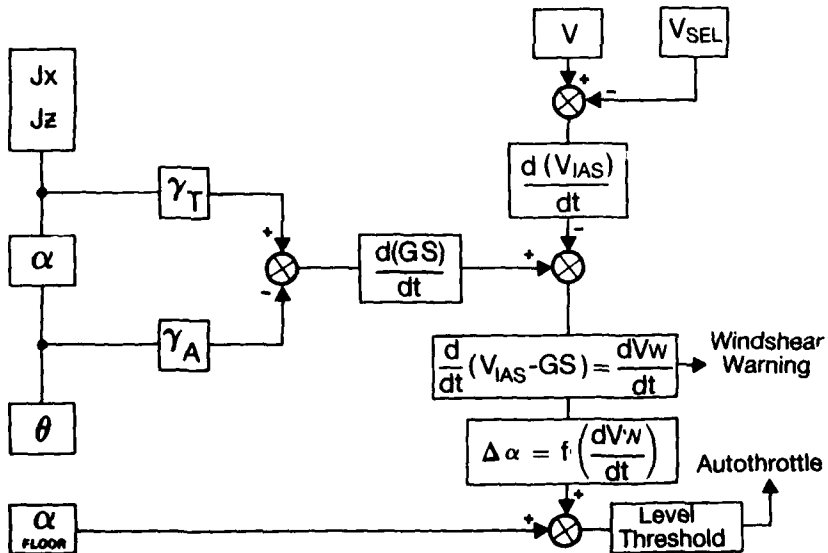


Figure 4

**A300 S.R.S.**

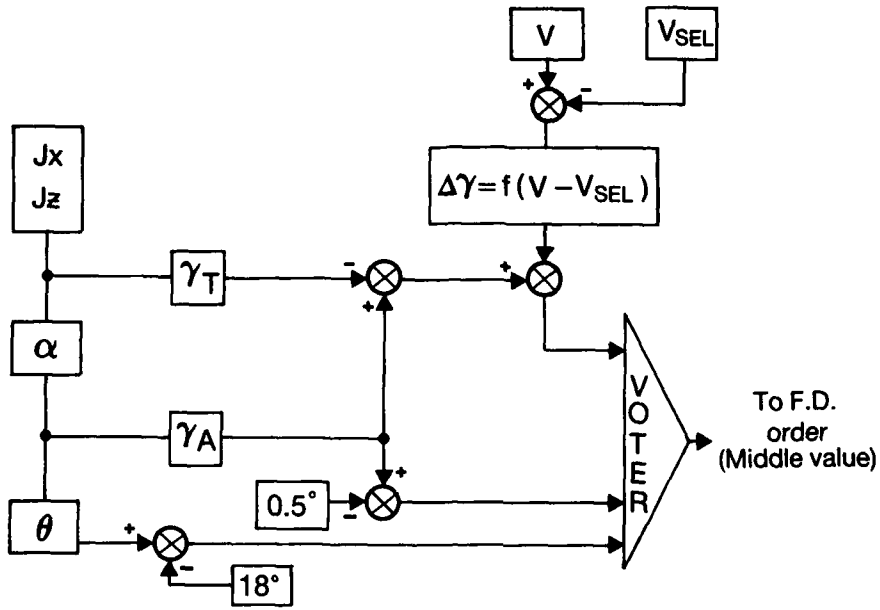


Figure 5a

**A310 S.R.S.**

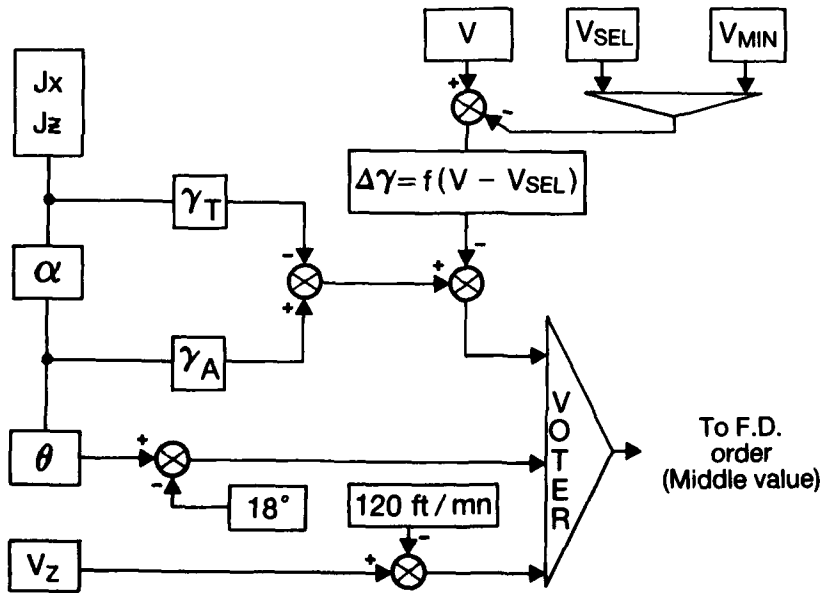


Figure 5b

## Windshear - rationalization of indication

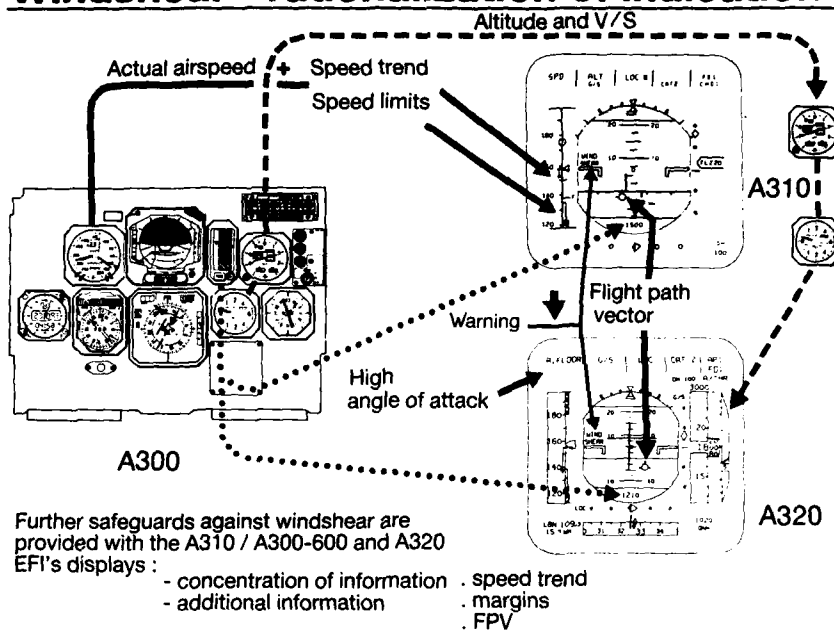


Figure 6

## Primary information given by the FPV (« bird »)

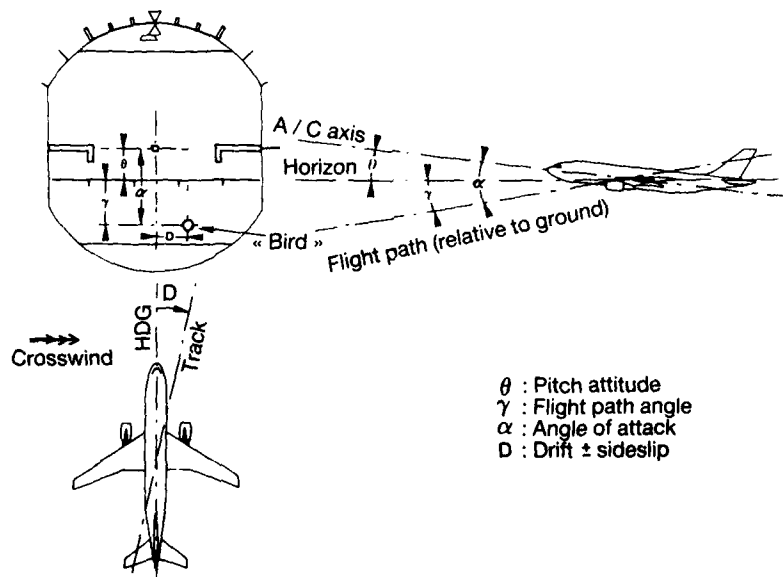


Figure 7



## A320 Protection : Stall and wind shear

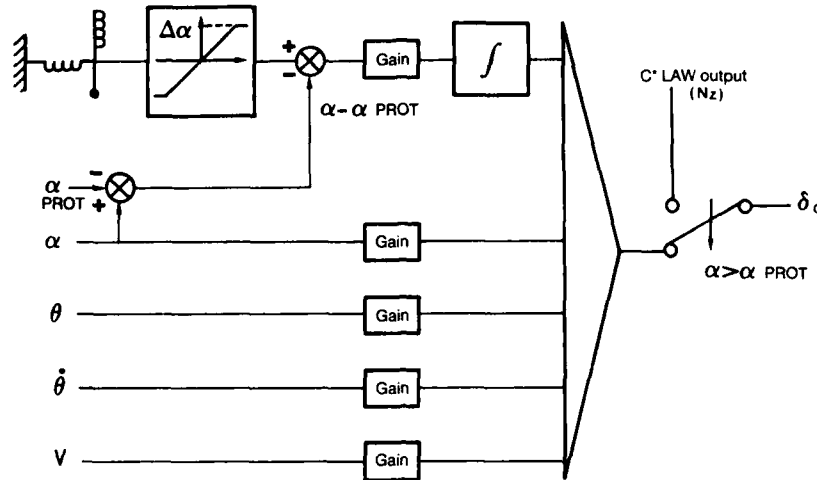


Figure 10

	Detection Alert	Guidance	Procedure
A300	<ul style="list-style-type: none"> <li>- Raw data</li> <li>- Beam deviation</li> <li>- Autothrottle activation</li> </ul>	<ul style="list-style-type: none"> <li>- Speed reference system (pitch bar)</li> </ul>	<ul style="list-style-type: none"> <li>- Max thrust</li> <li>- Stay at or above stick shaker speed</li> <li>- Monitor ground speed</li> </ul>
A310	<p>Same +</p> <ul style="list-style-type: none"> <li>- Speed trend</li> <li>- Speed margin</li> <li>- Flight path vector</li> <li>- Warning in PFD</li> </ul>	Same	<p>Same +</p> <ul style="list-style-type: none"> <li>- Visual speed cues</li> <li>- Flight path vector monitoring by PNF</li> </ul>
A320	<p>Same +</p> <ul style="list-style-type: none"> <li>- Indication on FMA</li> </ul>	<p>Same</p> <p>*Note : pitch law will try to maintain the flight path</p>	<ul style="list-style-type: none"> <li>- Full stick aft</li> </ul>

Figure 11

## WIND MODELS FOR FLIGHT SIMULATION \*)

HAHN, K.-U. ; HEINTSCH, T. ; KAUFMANN, B.  
SCHÄNZER, G. ; SWOLINSKY, M.

Institute of Flight Guidance and Control,  
Technical University of Braunschweig,  
Hans-Sommer-Str. 66, 3300 Braunschweig, FRG

### 1. Symbols

A	Lift
$c_p$	Specific heat at constant pressure
E	Energy
F	Thrust
$f_i$	Sensor parameter
G	Aircraft weight
g	Constant of gravitation
H	Height, altitude
$\dot{H}$	Rate of climb
$\ddot{H}$	vertical acceleration
$H_E$	Energy height
$H_{hill}$	Height of the hill
$\Delta H_E$	Energy height error
INS	Inertial Navigation System
k	Von Karman's constant
$L_u, L_w$	Integral scale for the longitudinal and vertical turbulence component
m	Exponent of power law
m	Mass of aircraft
n	Load factor
$p_a$	Static pressure
q	Dynamic pressure
q	Angular velocity around the aircraft y-axis
r	Angular velocity around the aircraft z-axis
$\vec{R}$	Vector of the distance between flight log and inertial navigation system
R	Gas constant, Radius
Ri	Richardson number
$R_T$	Roughness factor
S	Reference wing area, Shape factor
$S(\Omega)$	Power spectrum
$T_c$	Time constant of the complementary filter
$T_t$	Total temperature
u, v, w	Components of flow
$u_{wg}, v_{wg}, w_{wg}$	Wind components in the geographical coordinate system
$u_{wrep}$	Reported wind at the aerodrome
$u^*$	Friction velocity
V	Airspeed
$V_k$	Flight path velocity
$V_w$	Wind velocity
$V_{stall}$	Stall speed
$w_{wg}$	Vertical wind component
W	Drag
x	Spatial coordinate
$x_g, z_g$	Earth fixed coordinates
$x_p, z_p$	Potential flow coordinates
$z_0$	Surface roughness height
$\alpha$	Aircraft angle of attack
$\alpha_f$	Flight log angle of attack
$\alpha_n$	Reference angle of attack
$\beta$	Aircraft angle of sideslip
$\beta_f$	Flight log angle of sideslip
$\chi_w$	Wind azimuth
$\gamma$	Flight path angle
$\sigma$	Standard deviation
$\epsilon$	Ratio of specific heat
$\Theta$	Pitch attitude angle
$\Phi$	Bank angle
$\Psi$	True heading, Streamline
$\Omega$	Spatial frequency, Speed of rotation
Ref	Reference

\*) This research is supported by the Deutsche Forschungsgemeinschaft.

## 2. Introduction

Variable wind conditions may considerably influence flight-path and speed of an aircraft. Especially strong wind shear and downdraft may initiate flight path deviations, which may restrict flight safety during take-off, go-around and landing approach.

Investigations of aircraft response on wind and turbulence by means of flight simulation require suitable wind and turbulence models. The specification of these models is a sufficient mathematical description of the wind velocity field on one hand and a simple mathematical structure on the other hand to work at adequate expense under condition of real time simulation.

There are a number of analytical and numerical dynamic wind models in the area of meteorology, describing the temporal development of thunderstorm downburst, cold fronts and low level jet by extensive simulation programs. Because of the mathematical expense and the insufficient horizontal and vertical resolution, these models are unsuitable for application in flight simulation. In take-off and landing approach of transport aircraft the essential shear layer is passed in only a few minutes. Thus, the modeling task can concentrate on quasi-stationary engineering models. In general the turbulent wind profiles are composed of large scale trend and turbulent fluctuations with stationary mean (Fig. 1). In some cases gusts are considered as a third category of atmospheric disturbances. The aircraft response on large scale wind variations is quite different compared with the response on turbulence or short scale gusts. Variations of the mean wind influence the energy status of the aircraft producing flight path and airspeed deviations. Atmospheric turbulence is effecting the acceleration terms of the aircraft influencing airframe loads, structural fatigue, pilot's workload, passenger comfort and handling qualities of the aircraft. Hence, for the prediction of the aircraft trajectories under wind influence the knowledge of the mean wind variations is sufficient for most of the problems. An essential prerequisite for the identification of the model parameters is the availability of suitable wind measuring data which may originate from different measuring systems.

## 3. Wind determination

The wind at a certain point can be regarded as a vector with a value, the wind speed, and a direction, the wind direction. In this paper, the components of the wind vector are defined in the following earth fixed coordinate system (see Fig. 2): a horizontal wind blowing from south to north represents a positive  $x_g$ -component  $u_{w_g}$ , a horizontal wind from west to east a positive  $y_g$ -component  $v_{w_g}$  and a downdraft indicates a positive vertical wind component  $w_{w_g}$  (VÖRSMANN, 1984).

The influence of wind on aircraft trajectories can be investigated either in reality by flight tests or as mentioned above by flight simulation with measured wind data or with wind data generated by a wind model. The advantages of the simulation are the lower costs of the procedure, together with the ability to investigate even hazardous flight situations without a risk for the pilot and the aircraft. Furtheron the simulations can be repeated easily to investigate for example the pilot's reaction on certain situations. The quality of the simulation with a wind model essentially depends on the quality of the wind model in comparison with real wind data.

So the determination of wind by measurement is necessary both for the design and valuation of wind models.

Concerning the principle of measurement there are basically two different kinds, the ground based systems, measuring the wind from the surface and the on board determination, measuring the wind on board an aircraft.

### 3.1 Principles of wind measurement

#### 3.1.1 Ground based systems

The ground based systems can be separated into two different groups regarding the procedure of measurement: systems to determine the wind locally at a certain point and systems to determine the wind in a greater distance (remote sensing systems).

The first group represents an easy way to measure the value and the direction of the wind by means of a relative simple equipment like e.g. a cup anemometer or a propeller anemometer combined with a wind direction vane. The system gives information about the mean horizontal wind at a certain point. A determination of the vertical wind component as well as variations in the wind speed or direction over a horizontal or vertical distance is not possible. Therefore the system is not qualified to carry out measurements of whole wind fields as a basis for wind models with wind variations, which are important especially in the lower boundary layer. As a solution to this problem the local wind speeds are to be measured at some certain points so that the wind field can be determined by interpolating between the measured wind speeds. A typical example for this principle is the profile measurement from towers, booms or masts in the boundary layer. With the help of the vertical stepwise installed sensors changes in the wind speed and direction in different heights can be determined. Measurements over a longer time period can additionally give informations about the large scale wind variations in a constant height. Using this principle of measurement it must be considered, that the tower used for supporting the sensors can interfere with the flow, thus introducing errors in the measured data. These errors may be reduced to acceptable levels by calibrating the measurement equipment (LENSCHOW, 1984).

The main virtues of the above described sensors are simplicity, ruggedness and dependability. The disadvantages of the rotating devices are long response times, so that they are not able to analyse turbulent phenomena of higher frequencies. Better results are available with fast response wind sensors like the hot-wire anemometer.

To avoid the problems of interference between the tower and the flow it is possible to employ systems basing on the remote sensing technique, which allow additionally to carry out measurements in any direction within the current range of the instrument without disturbing the variable being measured. The systems are based on the principle of transmitting acoustic or electromagnetic radiation measuring the reflected radiation signals.

Examples for developed instruments are the lidar, radar and sodar systems using light, radio and sound waves as transmitting medium.

In general the remote sensing systems are able to determine the wind speed components in a limited range. For the principle of measurement is based on averaging the wind speeds over a certain spatial volume it is not possible to resolve higher frequencies in the measured wind speeds. The problems of resolution in connection with the limited range of measurement combined with ground based systems lead to another measuring principle determining the wind on board an aircraft.

### 3.1.2 On-board determination

The theory and realization of an on board measurement system should be presented at the example of the DORNIER DO 28 research aircraft of the Technical University of Braunschweig. For the investigation of the influence of wind and wind shear on flight safety of aeroplanes the Institute of Flight Guidance and Control of the TU Braunschweig developed and implemented an on-line wind measuring system on board a DO 28 aircraft. This purpose was supported by the German Society for the Advancement of Scientific Research within the research program "Sicherheit im Luftverkehr" (safety in air traffic).

#### Principle of measurement

In contrast to the ground based systems the wind cannot be measured directly on board an aircraft. The indirect way to determine the vector of the wind velocity  $\underline{V}_W$  is to take the difference between the flight path velocity  $\underline{V}_K$  (the velocity of the aircraft relative to the earth) and the true airspeed  $\underline{V}$  (the velocity of the aeroplane relative to the air). For obtaining a high precision of the relative small wind vector compared to the large aircraft speeds an accurate measurement of the flight path velocity and the true airspeed is necessary. The determination of the wind vector components in the earth fixed coordinate system (see Fig. 2) is described by the following set of equations (VÖRSMANN, SWOLINSKY, 1980, LENSCHOW, 1972). The general equation to determine the wind vector is

$$\underline{V}_W = \underline{V}_K - \underline{V} \quad (1)$$

Written with the components in the earth fixed system eq. (1) leads to

$$\begin{bmatrix} u_W \\ v_W \\ w_W \end{bmatrix}_g = \begin{bmatrix} u_K \\ v_K \\ w_K \end{bmatrix}_g - \begin{bmatrix} u \\ v \\ w \end{bmatrix}_g \quad (2)$$

In Fig. 3 the three velocities  $\underline{V}_W$ ,  $\underline{V}_K$  and  $\underline{V}$  are illustrated together with different coordinate systems, which are necessary to explain the relations between the velocities.

The flight path velocity  $\underline{V}_K$  can be measured in the flight path coordinate system ( $x_K$ -axis) as well as in the earth fixed system ( $x_g$ -axis). The advantage of the earth fixed determination of the  $\underline{V}_K$  is, that there is no coordinate transformation necessary, while the flight path fixed  $\underline{V}_K$  vector must be transformed in the earth fixed system (angles  $\chi$  and  $\gamma$ ).

The true airspeed is defined in the aerodynamic coordinate system ( $x_a$ -axis) (see Fig. 3). To get the components of  $\underline{V}$  in the geographic coordinate system, a transformation from the aerodynamic into the aircraft fixed ( $x_f$ -axis) system (angles  $\alpha$  and  $\beta$ ) and from the aircraft fixed into the geographic system (angles  $\Theta$ ,  $\Phi$  and  $\Upsilon$ ) is necessary. The complete transformation leads to the following three equations for the true airspeed components (VÖRSMANN, 1984):

$$u_g = V \cdot \left[ \cos\alpha \cdot \cos\beta \cdot \cos\Theta \cdot \cos\Upsilon + \sin\beta \cdot (\sin\Theta \cdot \sin\Theta \cdot \cos\Upsilon - \cos\Theta \cdot \sin\Upsilon) + \sin\alpha \cdot \cos\beta \cdot (\cos\Theta \cdot \sin\Theta \cdot \cos\Upsilon + \sin\Theta \cdot \sin\Upsilon) \right] \quad (3)$$

$$v_g = V \cdot \left[ \cos\alpha \cdot \cos\beta \cdot \cos\Theta \cdot \sin\Upsilon + \sin\beta \cdot (\sin\Theta \cdot \sin\Theta \cdot \sin\Upsilon + \cos\Theta \cdot \cos\Upsilon) + \sin\alpha \cdot \cos\beta \cdot (\cos\Theta \cdot \sin\Theta \cdot \sin\Upsilon - \sin\Theta \cdot \cos\Upsilon) \right] \quad (4)$$

$$w_g = V \cdot \left[ -\cos\alpha \cdot \cos\beta \cdot \sin\Theta + \sin\beta \cdot \sin\Theta \cdot \cos\Theta + \sin\alpha \cdot \cos\beta \cdot \cos\Theta \cdot \cos\Theta \right] \quad (5)$$

As an example the two dimensional problem in the aircraft symmetrical plane is given in Fig. 4. For this case the angles  $\beta$ ,  $\Phi$  and  $\Upsilon$  are equal zero, so that the components in the eq. 3-5 can be determined by

$$u_g = V \cdot (\cos\alpha \cdot \cos\Theta + \sin\alpha \cdot \sin\Theta) \quad (6)$$

$$v_g = 0 \quad (7)$$

$$w_g = V \cdot (-\cos\alpha \cdot \sin\Theta + \sin\alpha \cdot \cos\Theta) \quad (8)$$

The horizontal and vertical components (eq. 6 and 8) can also be written as

$$u_g = V \cos(\Theta - \alpha) \quad (9)$$

$$w_g = V \sin(\Theta - \alpha) \quad (10)$$

which corresponds to Fig. 4.

The calculation of the wind vector components according to equations 2-5 presumes that the required angles and velocities are measured at the same position. In practice the flight path data (flight path velocity, EULER angles  $\Theta$ ,  $\Phi$ ,  $\Psi$ ) can be determined by an INS or a laser navigation platform, which is positioned near the aircraft's centre of gravity (see Fig. 5). The aerodynamic data (amount of the true airspeed, angle of attack, sideslip angle) however have to be measured outside the aircraft influenced flow for example with a flight log on a nose boom, as it can be seen in Fig. 5. In the case of angular movement of the aircraft another velocity vector has to be considered. It is described by the aircraft's speed of rotation  $\Omega$  and the vector of the distance  $R$  between the location of the navigation platform and the location of the sensor measuring the aerodynamic data.

With this correction the wind vector at the location of the platform  $\underline{V}_{WP}$  can be determined by the flight path velocity at the platform  $\underline{V}_{KP}$ , the true airspeed at the location of the aerodynamic data sensor (flight log)  $\underline{V}_T$  and the vector  $\underline{R}_T$  from the flight log to the platform as well as the aircraft's rotation speed  $\Omega$ .

$$\underline{V}_{WP} = \underline{V}_{KP} - \underline{V}_T + \Omega \times \underline{R}_T \quad (11)$$

The correction of the additional velocity  $\Omega \times \underline{R}_T$  induced by the aircraft's rotation is most important, when for example a Doppler Laser is used measuring the true airspeed nearly 100m before the aircraft. In this case a rotation speed of  $\dot{\Theta} = 0.1 \text{ rad/s}$  would lead to an additional vertical velocity component of 10 m/s.

The principles of measurement concerning the true airspeed  $\underline{V}_T$  are given by WUEST (WUEST, 1980). Detailed investigations of the determination of the flight path velocity  $\underline{V}_{KP}$  by an INS are made by WINTER and STIELER (WINTER et al., 1987).

Besides the correction of the true airspeed vector (see eq. (11)) another correction has to be considered concerning the angle of attack and the angle of sideslip. In the case of an aircraft rotation the angles  $\alpha$  and  $\beta$  in the eq. 3 to 5 have to be determined by

$$\alpha = \alpha_f + \frac{g \cdot R}{V} \quad (12)$$

$$\beta = \beta_f - \frac{r \cdot R}{V} \quad (13)$$

with  $\alpha$  and  $\beta$  as the angles at the reference point (location at the INS),  $\alpha_f$  and  $\beta_f$  as the angles measured with the aerodynamic data sensor and R as the distance from the aerodynamic data sensor to the reference point.

The equations (3) to (5) determining the true airspeed components contain numerous nonlinear SINE- and COSINE functions, so that it is difficult to estimate the effects of sensor errors on the resulting error of the wind component. As a simplification a linear error model is used to determine the wind component error caused by a known sensor error. For example the measured wind speed component  $u_{Wgm}$  consists of the true value  $u_{Wg}$  and its error  $\Delta u_{Wg}$

$$u_{Wgm} = u_{Wg} + \Delta u_{Wg} \quad (14)$$

The linear error model for this case is

$$\Delta u_{Wg} = \frac{\delta u_{Wg}}{\delta f_i} \cdot \Delta f_i \quad (15)$$

with  $\delta u_{Wg} / \delta f_i$  as the partial derivatives of the concerning signal inputs and  $\Delta f_i$  as the signal errors.

The complete equation for the total error  $\Delta u_{Wg}$  reads as follows:

$$\begin{aligned} \Delta u_{Wg} = & \frac{\delta u_{Wg}}{\delta \alpha} \cdot \Delta \alpha + \frac{\delta u_{Wg}}{\delta \beta} \cdot \Delta \beta + \frac{\delta u_{Wg}}{\delta \Theta} \cdot \Delta \Theta + \frac{\delta u_{Wg}}{\delta \Phi} \cdot \Delta \Phi + \frac{\delta u_{Wg}}{\delta \Psi} \cdot \Delta \Psi \\ & + \frac{\delta u_{Wg}}{\delta V} \cdot \Delta V + \frac{\delta u_{Wg}}{\delta u_{Kg}} \cdot \Delta u_{Kg} + \frac{\delta u_{Wg}}{\delta v_{Kg}} \cdot \Delta v_{Kg} + \frac{\delta u_{Wg}}{\delta H} \cdot \Delta H \end{aligned} \quad (16)$$

The equations for the v and w components correspond to eq. (16). The determination of the partial derivatives lead to very complex expressions, which can however be approximated neglecting second order terms. The results are listed in Tab. 1. In this table the index R stands for values of the error free reference state.

On the basis of Tab. 1 the following general statements can be made (VÖRSMANN, 1984)

1. The wind component errors, which are caused by angular parameters, are directly proportional to the true airspeed of the aircraft. Therefore errors in wind speed and wind direction increase with true airspeed
2. The errors of the horizontal wind components  $u_{wg}$  and  $v_{wg}$  caused by errors in true airspeed and angular parameters are a function of the SINE or the COSINE of the true heading, while the error of the vertical wind component is of course independent from the true heading.
3. For the errors depending on the true heading there is a  $\pm 90^\circ$  phase shift between the  $u_{wg}$  and  $v_{wg}$  component. However, the maximum amplitude of the error is the same for both components.
4. The wind component errors are not a function of the wind speed or wind direction.

The following two examples illustrate these dependencies for level flight ( $\gamma_R = \Theta_R = 0^\circ$ ). As reference values an angle of attack of  $\alpha_R = 4.85^\circ$  and a cruising speed of  $V_R = 80 \text{ m/s}$  are assumed. As a function of true heading Fig. 6 shows the error in the  $u_{wg}$  component, which results from sensor errors with an assumed magnitude of one degree respectively  $1 \text{ m/s}$ . For the same amount of sensor errors Fig. 7 illustrates the error in the  $w_{wg}$  component as a function of true airspeed. It can be seen that errors in the vertical wind component are caused only by an error in the vertical speed and errors in the angle of attack and pitch. The other failure gradients are equal zero because of the reference values for  $\gamma$  and  $\Theta$ .

Most of the parameters, which are required for the wind vector determination can be measured directly except the true airspeed and the vertical speed of the aircraft. The vertical speed of the aircraft can be measured easily with a variometer, which differentiates the static pressure. The problem of this method is the long response time of the instrument caused by the differentiation. A high frequent wind determination however needs a high frequent vertical speed information. This real time signal information can be derived synthetically by means of a complementary filter (see Fig. 8) (VÖRSMANN, 1984). The input for the high frequency information is the output signal of the vertical accelerometer  $\ddot{H}_b$ , which is integrated to get a vertical speed signal. This signal possesses an excellent dynamic response but also a long term instability. Therefore the low frequency information is gathered by the above mentioned differentiation of the barometric altimeter signal  $H_B$ . The determination of the vertical speed is described by the equation

$$\dot{H} = H_B \cdot \frac{s}{T_c s + 1} + \ddot{H}_b \cdot \frac{T_c}{T_c s + 1} \quad (17)$$

In case of error-free sensor signals for  $H_B$  and  $\ddot{H}_b$  this filter produces an ideal vertical speed signal. As already mentioned above the determination of the true airspeed is not explained in this paper. Detailed informations are given by WUEST (WUEST, 1980).

By knowledge of the accuracy of all parameters required for the calculation of the wind components the error of the measured wind vector can be derived by using the GAUSSIAN law of error propagation. Some values are given for a special research aircraft and a transportation aircraft in Tab. 2. The accuracies, which are available with special research aircrafts reach values between  $0.5 \text{ m/s}$  and  $0.7 \text{ m/s}$  in the horizontal wind component. The lower value is achieved during tail- or headwind situations while the higher value applies to wind measurements during prevailing crosswinds. For the vertical wind component a precision of  $0.3 \text{ m/s}$  can be stated. The accuracy of the calculated wind direction turns out to be a hyperbolic function of the horizontal wind speed (see Fig. 9). The mentioned accuracies include offsets, which may be due to constant sensor biases. Higher frequency variations of the wind speed and wind direction can be determined more precisely (factor 5 to 10).

To achieve these accuracies it is necessary to calibrate the equipment before a test flight. To control the measurement system it is possible to compare the on board measured data with data determined by ground based system (see chapt. 3.1.1), which additionally might decrease the offset failure.

During a wind measurement campaign those comparisons between a research aircraft and a ground based system were made in a tower fly-by. On the tower a platform was installed supporting an anemometer on a slant lift to measure the wind speed and direction. As an example Fig. 10 shows the wind profiles measured with the research aircraft DO 28 and the tower. It can be seen that tower and aircraft data display a good correspondence. The aircraft measured curves additionally show a high resolution of the signals. Deviations between the measurements like difference in wind direction above  $160 \text{ m}$  height are not necessarily system errors. They may be caused by the time difference of the two measurements and the spatial difference of up to  $4 \text{ km}$  between aircraft and tower for the same altitude sample. In comparison to the measurement with a special research aircraft, the accuracies which are available using the data coming from the sensors of a transportation aircraft reach only half the value, so that deviations of  $1 \text{ m/s}$  to  $1.5 \text{ m/s}$  in the horizontal wind component and  $0.5 \text{ m/s}$  to  $0.7 \text{ m/s}$  in the vertical wind component have to be considered (SWOLINSKY, KRAUSPE, 1984).

#### 4. Wind and turbulence characterization and modeling

The introduction of this paper has already mentioned the typical separation of wind and turbulence effects. The high frequency part of the wind vector, the turbulence, is characterized as a fluctuation with a stationary mean value. The mean value itself is the deterministic low frequency part of the wind vector. After discussion of the wind determination it is helpful to characterize these two main parts of the wind vector. As demonstrated in HAHN et al., 1988, the influence of wind and turbulence on the aircraft motion is completely different. The main influence on the aircraft trajectory is caused by low frequency wind effects. The turbulent components are producing only indirect effects due to the increased pilot's workload.

#### 4.1 Short scale gusts and turbulence

A realistic aircraft flight simulation requires the consideration of the influence of atmospheric turbulence and gust effects in the simulation model of an aircraft even if it is not the primary influence on aircraft trajectories. The wind velocity in general means the deterministic mean wind velocity as well as stochastic effects like turbulence and gusts. The proper definition of the boundary between the low frequency mean wind velocity and the high frequency turbulence is not possible. To reply this question seems to be a philosophical problem depending on the actual application. The same problem appears in the description of gusts. For a glider a special gust may be a medium frequency disturbance. Encountering the same gust with a supersonic aircraft appears like a high frequency shock. The first item in the short scale range of wind perturbations shall be the atmospheric turbulence.

#### 4.1.1 Atmospheric turbulence

The atmospheric motion is always characterized by a typical mean wind direction, caused by the differences of barometric pressure. This motion consists of the mean wind and an overlaid flow in all three geometric directions. The reason of this turbulent flow components is the instability of the atmospheric flow. Phenomena like

- wind gradients caused by surface friction
- jet streams, frontal shear flows, lee-effects of hills
- convection like thermic, convective cells, thunderstorm activities
- wake turbulence produced by trailing vortices of aircrafts

and other effects are the source of wind shear in the atmosphere. This changing of flow velocity with the location and with time produces due to the friction turbulent flow components in three dimensions. The description of these effects is given by the NAVIER-STOKES equations, but due to the complexity, non-linearity and cross-coupling of these differential equations there is no complete solution possible today. A lot of theoretical investigations were made to understand the turbulence mechanism (HINZE, 1959). Some assumptions can be summarized for all these models:

- turbulence is a three-dimensional effect
- turbulence is based on friction effects
- turbulence can be described by vortices of different scale
- there is an energy transfer necessary to replace the dissipative energy in the small scale range of the turbulence.

Most of the turbulence models are based on the assumption of isotropy and stationarity. The isotropy of the atmosphere can be assumed for altitudes above ca. 300-500 m. This altitude depends on the stability conditions of the atmosphere, the ground roughness and other parameters. Below this height the influence of the boundary layer and the restrictions in the vertical flow direction due to the ground causes anisotropic conditions.

KRAICHNAN, 1962, has developed a model for the energy transfer, using a cascade model. The energy is transmitted from large scale to short scale vortices and dissipates in the high frequency range in kind of heat. This cascade model provides also the influence of the ground on the turbulence parameters. With decreasing altitude, the maximum scale of the vortices is limited to the actual height.

As demonstrated the characterization of turbulence depends on the scale, i.e. the frequency range. Especially the power density spectrum description is a tool to separate different ranges of turbulence (Fig. 1f). Based on theory and measurement, the knowledge about the inertial subrange is sufficient. The power density depends on the spatial frequency with a power coefficient of  $-5/3$  in this range (KOLMOGOROW, 1941; ONSAGER, 1945; WEIZSÄCKER, 1948). Measurements provided a power factor between 1.2 and 2.2 (PRITCHARD, 1965).

More problems appear in the high frequency range of the spectrum, when friction effects are increasing and the negative slope of the power density spectrum is enhanced. HEISENBERG, 1948, calculated a power factor of  $-7$  for this range. This large negative slope ensures that the derivatives of the turbulence velocities and the variances of the turbulence accelerations are existing. In the low frequency range the power density spectrum seems to be constant, but there must be a limitation, because the maximum scale of turbulence fields in the atmosphere is limited. Another limitation using the vortex model is given by the altitude, as the maximum scale is limited to the altitude.

The purpose of the aircraft simulation deals with turbulence as a perturbation effect. The available computation time for the turbulence model, for example in a realtime aircraft simulation is only a few milliseconds. Therefore several simplified theories are necessary to handle turbulence effects in aircraft simulation problems. One of these simple approximations was given by DRYDEN, 1943. He proposed an exponential function for the autocorrelation function of a turbulence component:

$$R(x) = \sigma_w^2 \cdot e^{-\frac{x}{L_w}} \quad (14)$$

Fig. 11 shows this autocorrelation function together with a measured one. The DRYDEN approximation has the advantage that the realization and calculation in simulation purposes is very simple. Using the FOURIER transformation it is possible to transfer between the autocorrelation function and the power density spectrum.

$$S(\Omega) = \int_{-\infty}^{\infty} R(x) \cdot e^{-j\Omega x} dx \quad (15)$$

The equivalent power density spectrum of the DRYDEN approximation is

$$S(\Omega) = 2 \cdot \sigma_w^2 \cdot L_w \cdot \frac{1}{1 + L_w^2 \cdot \Omega^2} \quad (16)$$

with the scale length  $L_w$ , the variance  $\sigma_w^2$  and the spatial frequency  $\Omega$ . This equation describes the power density of the components along the flight-path. Investigations have shown, that there is a different spectrum for the perpendicular direction.

$$S_{\perp}(\Omega) = \sigma_w^2 \cdot L_w \cdot \frac{1 + 3 \cdot L_w^2 \cdot \Omega^2}{(1 + L_w^2 \cdot \Omega^2)^2} \quad (17)$$

The reason is the selection of a special direction of observing, if the turbulence component is measured along the flight-path. This turbulence component is more correlated than the perpendicular ones.

Other spectra are proposed by v.KARMAN, 1938. These spectra are more complicated, as they connect the horizontal part of the power density spectrum in the large scale range with the  $-5/3$  inertial subrange. This requires more complex computational models. The difference between the v.KARMAN and the DRYDEN model is small compared to the uncertainty of the turbulence models at all, so that the DRYDEN spectrum is the basis of the following description of a simulation model for atmospheric turbulence.

This DRYDEN power spectrum is based on two important parameters:

- the variance of the turbulence velocity  $\sigma_w^2$
- the scale length of the turbulence velocity  $L_w$ .

In a simulation program, the time is the independent variable. This requires a transformation between the time and the spatial coordinates, because a parameter like the scale length is a spatial parameter which must be transformed in a time coefficient. Using the TAYLOR Hypothesis (TAYLOR, 1938) of a frozen atmosphere the DRYDEN power spectrum can be transformed in the following time dependent form:

$$S(\omega) = 2 \cdot \sigma_w^2 \cdot T_w \cdot \frac{1}{1 + T_w^2 \cdot \omega^2} \quad (17)$$

This DRYDEN power density spectrum can be used for simulation purposes. The valid range of frequencies is limited. For low frequencies a DRYDEN power spectrum provides constant power density. Following our assumption this low frequency part of atmospheric motion shall be described by special low frequency models. Other reasons for the low frequency limitations were discussed above. Due to this assumption the DRYDEN model must be limited in the low frequency area. On the other hand the very high frequency part of the DRYDEN model is limited. The DRYDEN spectrum provides unrealistic infinite variance of the turbulence velocity derivatives. This result is unrealistic. There must be a second crack in the high frequency part of the power density spectrum, which pays regard to the dissipative effects. The discussion of the turbulence description has demonstrated, that the available models have limitations in the valid range of frequencies and uncertainties in the question of accuracy. An engineering model for aircraft simulation purposes shall be discussed in the following chapter, based on the DRYDEN approximation, containing the uncertainties and limited accuracy.

#### 4.1.2 Turbulence model for digital simulation

In a digital aircraft simulation program the simple DRYDEN power spectrum yields the basic requirements of a turbulence simulation model. It is more important to use realistic values for the parameters scale length and standard deviation. Fig. 13 shows the structure of a turbulence simulation model for calculation of vertical turbulence velocities in earth-fixed axes. The turbulence velocities are generated in earth-fixed axes, because the parameters standard deviation and scale length for horizontal and vertical turbulence are different in the boundary layer of the ground.

The inputs of the turbulence calculation model are:

- mean wind velocity
- stability of the atmosphere
- height above ground
- the terrain roughness

The mean wind velocity is provided by the low frequency wind models, discussed in chapter 4.2 and includes the calculation of the boundary layer etc. This mean wind velocity causes the intensity of the turbulent fluctuations. The second important influence is based on the atmospheric stability. If a test volume of air is climbing in the atmosphere, the atmospheric temperature change with altitude determines whether the climbing air volume is warmer or colder than the surrounding atmosphere. Depending on this relative temperature, the test volume will continue the climbing motion, if it is warmer or will fall down again, if it is colder than the surrounding atmosphere. The RICHARDSON number  $Ri$  describes this effect of atmospheric stability.

$$Ri = \frac{g}{T_i} \cdot \frac{\left( \frac{\partial T_i}{\partial H} + \frac{g}{c_p} \right)}{\left( \frac{\partial V_W}{\partial H} \right)^2} \quad (18)$$

with  $g$  as gravity constant,  $\partial T_i / \partial H$  as actual temperature gradient with altitude,  $c_p$  as specific heat at constant pressure and  $\partial V_W / \partial H$  as vertical gradient of the mean wind velocity. The RICHARDSON number means:

- $Ri > 0$ : stable atmospheric conditions
- $Ri = 0$ : indifferent atmospheric conditions
- $Ri < 0$ : unstable atmospheric conditions

Fig. 14 shows a typical example of the influence of atmospheric stability on the turbulence conditions. The figure shows the altitude dependent profile of the wind velocity, the wind direction and the temperature, measured during landing approach (SWOLINSKY, KRAUSPE, 1984). Close to the ground the turbulence effects are visible in the wind velocity diagram. Above the temperature inversion, the turbulence components are nearly disappearing due to the damping effect of increased atmospheric stability.

The height above ground has influence on isotropy of the turbulence. Below altitudes of ca. 500m, the atmospheric conditions are more anisotropic as the vortex scales are more and more limited by the surface of the earth. The terrain roughness has influence on the standard deviation of the turbulent motions.

The calculation of the standard deviation of the horizontal turbulence components depends on the mean wind velocity, the atmospheric stability and the terrain roughness. Fig. 15 shows an approximation of this dependence, based on measurements by HOUBOLD, 1973. The value of the standard deviation is corrected by the influence of the terrain roughness, using a roughness factor  $R_T$ :

$$\sigma_{Wrough} = R_T \cdot \sigma_{Wwater} \quad (19)$$

Some values of this factor are given in the following schedule:

terrain structure	$R_T$
water	1.0
field	1.1
forest	1.15
flat mountains	1.3
high mountains	1.4

The influence of the altitude is involved by the mean wind velocity, which depends on the altitude. Other information about estimation of standard deviation is given by PRITCHARD et al., 1965. The standard deviation of the vertical turbulence component depends on the altitude. Below 200-300m, a reduction of the vertical component appears due to the limitation of vertical motions.

The other basic parameter of the turbulence spectrum is the scale length, which pays regard to the frequency dependent influences. This scale length depends on the height above ground and the atmospheric stability (Fig. 16, PRITCHARD et al., 1965). The atmospheric stability is again damping the turbulence effects. Stable conditions have large scale lengths, i.e. low energy of high frequency components. The other important effect is the reduction of scale length below ca. 300m. This means more energy in the high frequency components of the turbulence close to the ground and has influence on the aircraft reaction, as the acceleration due to the turbulence is increasing close to the ground. On the other hand, the reduction of standard deviation is compensating parts of these effects.

For small heights above ground it is necessary to pay regard to the differences between horizontal and vertical turbulence components. Due to the influence of the ground the turbulence components in horizontal and vertical

direction are different. Very close to the ground the vertical component is nearly zero. The parameters standard deviation and scale length must be calculated depending on the horizontal parameters and the height above ground. Fig. 17 shows the relation of scale length for horizontal and vertical turbulence. The calculation of standard deviation of vertical turbulence is based on a similar dependence.

After this calculations both parameters standard deviation and scale length for horizontal and vertical turbulence components are known and it is possible to use a normal distributed white noise random signal of a digital random noise generator to produce the time stepped turbulence signal with a DRYDEN power density spectrum. The TAYLOR Hypothesis is used to transform the space dependent scale length in a time dependent parameter. The velocity components are produced in earth-fixed axes because of the dependence of the parameters standard deviation and scale length on horizontal and vertical direction.

This simulation model provides the basic effects of atmospheric turbulence. But there is still a lot of lack in the knowledge about turbulence mechanism and engineering models. The main effect of the turbulence on the aircraft motion shall be discussed in HAHN et al., 1988.

#### 4.1.3 Gusts

The description of turbulence was solved using the tools for random processes. The definition of gusts is a mixture of stochastic and deterministic items. The gust itself is a deterministic effect, but the appearance of a discrete gust is a random process. The key to the engineering model of gusts is again the question about the physical source.

Atmospheric turbulence is a random process which has no special alignment in horizontal or vertical direction, it is approximately an isotropic phenomenon. The appearance of gusts on the other hand is caused for example by thermic effects. If the sun heats the air close to the ground a bubble of warm air will separate and move through the atmosphere in vertical direction. This is a deterministic effect. But if an aircraft encounters this bubble of climbing air, the appearance of the gust seems to be a stochastic effect. Other phenomena are wakes due to hills or mountains or temperature inversions (ETKIN, 1980).

A well known mathematical model of a gust is the 1-cos-model, which is the basis of the FAR Part 23 and the MIL 8785 specifications. Other models like the gust step or the short ramp gust are based on theoretical considerations. The advantages in mathematical description, especially paying regard to the LAPLACE transformation, are evident.

The mathematical description of these models is simple and shall not be discussed in detail. The gust models are used in the structural design to calculate the maximum load of the wing for example. For the design of automatic control system, the gust models represent the maximum perturbations. For more detailed modelling, there are approximations for thermal effects, which are more complicated.

Concluding the short scale effects means, that the influence on aircraft trajectory is small due to the inertia of the aircraft, which provides a lag effect in turbulence reactions.

#### 4.2 Large scale wind variations

In the planetary boundary layer wind shear can exist under a broad variety of weather conditions. In addition to the ordinary planetary boundary layer wind shear, shown in Fig. 1, there are three basic wind conditions which may influence aircraft flight path during take-off and landing (Fig. 18): downburst and microburst cells in connection with thunderstorm activities, or high cumulus clouds, fast moving cold or warm fronts, and the low level jet.

##### 4.2.1. Boundary layer wind shear

In general the planetary boundary layer is divided into two different horizontal layers (Fig. 19). The surface layer (the so called PRANDTL-layer) is the lower portion of the atmospheric friction layer. The PRANDTL-layer extends up to 50-100 m above the surface and describes a region of approximately constant shearing stress and only small variation in wind direction. Above this layer there is a region of transition from the disturbed flow near the surface to the frictionless free atmosphere. This height is considerably variable; it can go up to more than 1000 m. There are a number of models for the mean wind profile valid for the PRANDTL-layer.

The most widely used profile for this layer is the PRANDTL's logarithmic wind profile (Fig. 20, curve a). In this case the wind speed with respect of height is a function of roughness length  $z_0$  and friction velocity  $u_*$  (eq. (18)).

$$v_w = \frac{u_*}{k} \cdot \ln \frac{H}{z_0} \quad (18)$$

As the logarithmic law is valid only for adiabatic atmospheric conditions many other models have been developed for the case of non-adiabatic conditions. Most of them are applications of the MONIN-OBUKHOV similarity theory with different universal functions. The well known logarithmic-linear profile is a simple form of this approach. In this case a linear with height varying term is added to PRANDTL's adiabatic profile, depending on stability of the atmosphere (Fig. 21).

One of the most simple and for flight simulation widely used empirical wind model is described by the power law (Fig. 20, curve b). The expression  $V_{Ref}$  in eq. (19) refers to the wind speed at reference altitude  $H_{Ref}$ .

$$V_W = V_{W,Ref} \left( \frac{H}{H_{Ref}} \right)^m \quad (19)$$

The exponent  $m$  depends on surface roughness and stability of the atmosphere. Fig. 22 illustrates that the power law gives a good approximation of measured wind profiles up to some hundred meters of height. Furthermore this figure demonstrates that the neglect of wind direction change, as considered for the PRANDTL-layer, is not generally valid for the whole boundary layer. In principle the wind direction is changing clockwise on northern hemisphere from the rotating surface of the earth to the boundary layer. The change of direction is extremely variable, making any quantitative investigations rather difficult.

The first theoretical study of wind veering for laminar flow condition led to the well known EKMAN-spiral. But it gives only a quantitative description of direction change with respect of height. A simple approximation for the turbulent flow type has been published by PRANDTL (PRANDTL, 1965). This approach seems to be suitable for application in flight simulation. In eq. (20) the deviation from the wind direction of free atmosphere depends on thickness of the boundary layer  $H_G$  and the difference between direction of geostrophic and surface wind  $\Delta X_{W,G}$  (see Fig. 23):

$$\tan \Delta X_W = \left( 1 - \frac{H}{H_G} \right) \cdot \tan \Delta X_{W,G} \quad (20)$$

The determination of the angle  $\Delta X_{W,G}$ , given in eq. (21), is a function of the power law exponent  $m$ :

$$\tan \Delta X_{W,G} = \sqrt{m \cdot (m+2)} \quad (21)$$

In the case of missing information about the direction of geostrophic wind and the height of the boundary layer, a simple derivation of PRANDTL's law (eq. (20)) can be made for fitting measured wind direction profiles:

$$X_W = X_{W,u} + \arctan \left( \frac{H - H_u}{H_1 - H_u} \right) \cdot \tan \Delta X_W \quad (22)$$

with

$$\Delta X_W = X_{W,1} - X_{W,u} \quad (22a)$$

$\Delta X_W$  is the veering angle between wind direction at height  $H_u$  and  $H_1$ .

Some examples for the comparison between model and measurement are illustrated in Fig. 22.

#### 4.2.2 Inhomogeneity effects on the wind profile

The shape of wind profiles can be influenced by meteorological and orographic conditions like inhomogeneity of the atmosphere and the terrain, which cannot be pointed out in detail in this paper. An illustration of the influence of temperature inversion on wind speed and wind direction is given in Fig. 24. This effects can be modeled by partial variation of the parameter of the power law or by use of the low-level-jet model, described below. The second example (Fig. 25) describes the influence of vortex-effects on boundary layer wind profiles. The vortices may be caused by lee-effects of obstacles like mountain ridges, buildings or by wake vortices of aircraft. A mathematical description of the tangential velocity in a spreaded vortex (SCHLICHTING, 1982) is shown in eq. (23).

$$U_T(r,t) = \frac{\Gamma_0}{2 \cdot \pi \cdot r} \left( 1 - e^{-\frac{r^2}{4 \cdot \nu \cdot t}} \right) \quad (23)$$

It depends on circulation  $\Gamma_0$ , the distance  $r$  from the core of vortex, the dynamic viscosity  $\nu$  and the time since formation of the vortex. Superposing a velocity field of the vortex and a boundary layer wind speed profile the wind velocity like the example of measurement in Fig. 25 can be produced (Fig. 26).

#### 4.2.3 Low level jet

The term "low level jet" is used to describe wind phenomena of the lower part of the boundary layer, characterizing jet like wind profiles with a low altitude wind maximum. This kind of wind profiles has been observed in connection with specific local terrains, thermal effects in mountain valley regions, frontal activities, and the nocturnal boundary layer. Usually the nocturnal low level jet is to be found in the time between late afternoon and morning under clear nocturnal sky when a strong radiation temperature inversion develops. Because of the strong stability in the inversion layer friction disappears and the unbalanced CORIOLIS and pressure gradient forces produce an acceleration of wind speed. BLACKEDAR (BLACKEDAR, 1957) describes the evolution of low level jet as a non-stationary process, where the vector difference between the actual wind and the geostrophic wind is rotating nearly circular around the geostrophic wind (inertial oscillation, see Fig. 27). In the northern part of Germany the low level jet can be found approximately in 10% of all nights. Fig. 28 shows a typical low level jet sample recorded during a wind shear measuring project by means of a LUFTHANSA AIRBUS A 300. Investigations in the plains of northern Germany, carried out by two 300 m high meteorological towers (KOTTMEIER, 1982), show a cycle period of 14.5 hours for the inertial oscillation. During take-off and landing approach the critical zone of wind shear is passed in only one or two minutes. In this case the temporal evolution

is not relevant and modeling can concentrate on quasi-stationary engineering models. Velocity profiles like low level jet wind profiles have been observed in fluid dynamic research of free jet and wall jet (REICHARDT, 1951). As a rough low level jet approximation (SWOLINSKY, 1986) a superposition of a boundary layer profile and a plane free jet velocity profile is used (see Fig. 29 and eq. (24)).

Describing the wind direction with respect to height a proceeding similar to the magnitude of wind speed is used, i.e. the superposition of a suitable function to the direction profile of the boundary layer (eq. (5)) is intended. The principle procedure is illustrated in Fig. 30 and eq. (25).

For a large number of data records a comparison of measured data with modeled low level jet has been carried out (SWOLINSKY, 1986). The examples of tower (Fig. 31) and aircraft data (Fig. 32) are in good agreement with the model.

#### 4.2.4 Frontal wind shear

During the passage of fast moving cold or warm fronts considerable wind shears may develop due to changes of wind direction ahead and behind the frontal line. Especially strong fronts with sharp transition zones may effect aircraft operation. Fig. 33 illustrates the principle development of meteorological parameters like wind speed, wind direction, temperature, and atmospheric pressure during the passage of a frontal system (cyclone). In the range of the warm front warm air displaces the cold air by sliding upon the cold air situated ahead the front line. The maximal change of wind direction is about 90 degrees. In the following cold front zone cold air is flowing beneath the warm air ahead to the front line. The wind direction changes of about 135 degrees. A wind speed change of about 15 m/s and a vertical wind speed of 4 m/s (updraft) can be observed. In principle similar conditions as described for cold fronts are to be found in gust fronts in connection with a thunderstorm outflow.

A mathematical description of the local velocity field in the front line region can be generated by superposition of vortex induced flow velocities. The principle proceeding is shown in Fig. 34.

Another approach is based on a fluid dynamic description of stream surface bifurcations. Local solutions in the vicinity of stream surface bifurcation lines, obtained by HORNUNG et al., 1984, can be adapted and modified for the problem of modeling frontal wind shear. An example for a simulated frontal velocity field is shown in Fig. 35. The lower part of this figure illustrates magnitude and direction of the wind vector along a 3°-glide slope, compared with measured data (ELLIS et al., 1978).

#### 4.2.5 Thunderstorm outflows

The thunderstorm, with typical effects like strong downdraft, flash lights, and hail showers, is well known to be dangerous to aviation. Fig. 36 shows a typical thunderstorm outflow of cold air, the so called downburst. Near to the ground the vertical air flow changes to a horizontal outflow with increasing distance to the cell. The outer boundary of the horizontal wind shear can extend to a range of up to 20 km. A number of fatal and near-fatal accidents in the last 20 years, which have been attributed to the thunderstorm wind phenomena, initiated world wide research activities in hazard investigations and downburst modeling. As dynamic meteorological models are in general too extensive to be used in real time flight simulations more simple basic modeling techniques are used. One method is the construction of wind components from measured data by interpolation between the grid points (BARR et al., 1974). The second technique for the generation of downburst wind fields is based on relatively simple fluid dynamic approaches. Some of them are presented below.

ETKIN and ZHU (SHANGXIANG et al., 1983) have developed a 3-dimensional downburst model using circular doublet sheets of variable intensity (Fig. 37) while WOODFIELD and WOOD (WOODFIELD et al., 1983) suggest two ring vortices (Fig. 38). Another 3-dimensional, axially symmetric downburst model, suggested by BRAY (BRAY, 1985), is illustrated in Fig. 39.

As the downburst produces a flow like a vertically downward directed jet, which spreads out horizontally as it approaches the ground, KRAUSPE (KRAUSPE, 1983) uses steady jet flow toward a stagnation point.

Each of this models describes more or less the flow field of the pure core of the downburst. A critical point is the flow field in the vicinity of the core because of the occurrence of severe wind shear in this area. However, there is insufficient information about the flow field in this region. The stagnation point model, shown in a vertical cross section through the centre of the downburst model in Fig. 40, has been complemented by zones of vicinity and transition flow. Experimental results show that the flow field in these zones may be very complex, which could not be taken in account in this model up to now.

For the modeling of a downburst wind field including the mean flow of the gust front, Fig. 41 shows the result of the superposition of 24 spreaded vortices in combination to the same number of image vortices (SWOLINSKY, 1986). The centre of vortices are positioned along a stream line of the downburst cell (2-dimensional model). In the case of a 3-dimensional mode, ring vortices are used instead of flat vortices (see Fig. 42 resp. BAUSCHAT, 1988). The real time capability for flight simulation was verified using a prior VAX-computer for the aircraft and wind model with sample rate of 20 Hz.

Each model has its advantage for the approximation of measured wind fields and may be chosen with respect to the specific problem.

#### 4.2.6 Model of the flow over a flat hill

There are two essential effects caused by a hill:

1. The hill induces a downwind at its lee side. This fact leads to a reduced flight path angle compared

with the case of no obstacle influence on the atmospheric flow conditions.

2. During a normal take-off in a boundary layer the headwind rises with the height above the ground. While flying along a hill shape the ground level also ascends. Therefore the height rises more slowly and so does the headwind. But a smaller headwind leads to a smaller flight path angle.

An additional effect is caused by the change in surface roughness. Normally in the area surrounding a runway you will find grass and fields. Therefore the surface roughness is small. On hills normally there are woodlands and forests with higher surface roughness. This means the windspeed near to the ground will slow down from runway to hill. Thus the above described influence of a smaller headwind is intensified.

The model of flow over a flat hill is based on the potential flow around a symmetrical cylinder, on which the atmospheric boundary layer described by eq. (18) is superimposed to implement the effect of friction (HAHN, Nov. 1986). The friction velocity  $u^*$  in eq. (18) is calculated by a given reference wind  $u_{Wref}$  at a reference height  $H_{ref}$ :

$$u^* = \frac{k \cdot u_{Wref}}{\ln\left(\frac{H_{ref}}{z_0}\right)} \quad (24)$$

For the determination of the friction velocity the reported wind is chosen. The reported wind is defined as the official measured wind at the aerodrome. It is an average of the horizontal wind which is normally determined every fifteen minutes. So  $u_{Wref} = u_{Wrep}$  and  $H_{ref}$  is the height, where the reported wind is measured.

The flow over a flat hill is represented by the potential flow around a symmetrical cylinder. Thus every streamline can be taken as a solid wall devoid of any influence on the configuration of flow (see Fig. 43). So every streamline can be chosen as a hill's shape. The flow stream function around a symmetrical cylinder is

$$\Psi(x_p, z_p) = u_{p\infty} \cdot \left( z_p - \frac{R^2 \cdot z_p}{x_p^2 + z_p^2} \right) \quad (25)$$

In the above equation  $x_p$  and  $z_p$  define the coordinate system of the potential flow with its origin in the cylinder axis (see Fig. 43).  $R$  is the radius of the cylinder and  $u_{p\infty}$  is the undisturbed flow velocity far away of the cylinder. For each position the velocity of the potential flow  $V_p$  can be computed. Stipulating that the potential flow at the position, where the reference wind profile is defined, has to be equal to the boundary layer of eq. (18) for each streamline a factor can be determined to describe the influence of the friction

$$f(\Psi) = \frac{u_w(x_g, ref, H)}{u_p(x_g, ref, H)} \quad (26)$$

In the above equation  $u_p$  is the horizontal component of the potential flow velocity. The factor  $f(\Psi)$  is assumed as constant for each streamline. The velocity in consideration of the boundary layer is defined as the wind  $V_w$

$$V_w(x_g, H) = f(\Psi) \cdot V_p(x_g, H). \quad (27)$$

The inclination  $\chi$  of the streamline can be calculated by

$$\tan \chi(x_g, H) = \frac{w_p(x_g, H)}{u_p(x_g, H)} \quad (28)$$

where  $w_p$  is the vertical component of the potential flow velocity. The components of the wind over the flat hill then become:

$$\text{horizontal wind: } u_{wg}(x_g, H) = V_w(x_g, H) \cdot \cos \chi \quad (29)$$

$$\text{vertical wind: } w_{wg}(x_g, H) = V_w(x_g, H) \cdot \sin \chi \quad (30)$$

For drawing comparisons computations with a finite difference technique are used to solve the equation of the non compressible steady turbulent boundary layer (KNORR, 1982). From Fig. 44 we can gather that the simple model of the above described flow over a hill is a good approximation.

The shape of the hill model can be described by a shape factor

$$S = \frac{H_{hill}}{R} \quad (31)$$

It can vary between  $0 \leq S \leq 1$  (Fig. 45). For  $S=1$  the hill has the shape of an arc of a circle and for  $S=0$  we have a horizontal plane.

The change of surface roughness is realized by a variation of the reference wind profile defined by eq. ???. As a simplification it can be assumed that the surface roughness changes linearly from runway to hill. When a discontinuity in surface roughness occurs, the wind will change its profile with a time delay to the shape

belonging to the new roughness (FROST et al., 1977). This delay can be taken into account by choosing a higher surface roughness for the area around the runway than it will be in reality. The resulting wind profiles and streamlines simulated by the described model are shown in Fig. 46.

### Summary

Wind shear, downdraft and turbulence can endanger take-off and landing approach. The effects of wind results in a modified dynamic response of the aircraft as well as in flight performance variation. In each case flight path deviation can occur, more or less controlled by the pilot. For the analysis of the aircraft's behaviour in changing wind field, a mathematical model of the aircraft is used including the wind effects. It can be said, that gusts and turbulence will have more influence on the pilot's work load and his reaction to this short scale wind disturbances. Large scale wind variations can produce significant flight paths respectively safety problems. An important aspect for the flight safety is the energy situation of an aircraft affected by wind. Therefore this is chosen as a useful criterion for the determination of the influences of the wind and wind variation.

### 9. References:

- Badner, J. Low-Level Wind Shear: A Critical Review.  
NOAA Techn. Memorandum NWS FCST - 23. National Oceanic and Atmospheric Administration, Silver Spring, Md., Apr. 1979.
- Barr, M.M. et al. Wind Models for Flight Simulator Certification of Landing and Approach Guidance and Control Systems.  
FAA-RD-74-206. Dec. 1974.
- Bauschat, M. Entwicklung eines dreidimensionalen, mathematischen Gewittermodells zur Untersuchung des Flugverhaltens in Gewitterstürmen.  
Diplomarbeit am Institut für Flugführung der TU Braunschweig, Januar 1988.
- Blackadar, A.K. Boundary Layer Wind Maxima and their Significance for the Growth of Nocturnal Inversions.  
Bull. Am. Meteorol. Soc. 83, 283-290, 1957
- Bray, R.S. A Method for Three-Dimensional Modelling of Wind-Shear Environments for Flight Simulator Applications.  
NASA TM 85969, 1985
- Brockhaus, R. Wüst, P. Open Loop Compensation of Wind Shear Effects in Low Level Flight.  
AGARD Conference Proceedings CP 240 "Guidance and Control Design Considerations for Low Altitude and Terminal Area Flight".  
Dayton, Ohio 1977.
- Counihan, J. Adiabatic Atmospheric Boundary Layers  
A Review and Analysis of Data from the Period 1880-1972.  
Atmosph. Environment, Vol. 9, S. 871-905, Pergamon Press 1975.
- Delage, Y. A Numerical Study of the Nocturnal Atmospheric Boundary Layer.  
Quart. J. R. Met. Soc. 100 (1974), 351-364.
- Dryden, H.L. A Review of Statistical Theory of Turbulence.  
Quarterly of Applied Mathematics 1, 7 - 42 (1943).
- Eichenberger, W. Flugwetterkunde.  
Schweizer Druck- und Verlagshaus AG, Zürich, 2. Auflage, 1962.
- Ellis, D.W. Keenan, M.G. Development of Wind Shear Models and Determination of Wind Shear Hazards.  
FAA-Report No. FAA-RD-79-119, Jan. 1978.
- England, J. Ulbricht, H. Flugmeteorologie.  
Transpress VEB Verlag für Verkehrswesen, Berlin 1980.
- Etkin, B. The Turbulent Wind and its Effects on Flight.  
The AIAA Wright Brothers Lecture, 1980, UTIAS Review No. 44.
- Fiedler, F. Die Grenzschicht der Atmosphäre: Struktureller Aufbau.  
in: Promet 4, Heft 1, 1974, S. 1-3.
- Frost, W. Maus, J.R. Simpson, W.R. A Boundary Layer Approach to the Analysis of Atmospheric Motion over a Surface Obstruction.  
NASA Constructor Report CR-2182, 1973.
- Hahn, K.U. Take-off Flight Paths along a Lee Side of a Flat Mountain Ridge under Flight Safety Aspects.  
2nd International Symposium on Aviation Safety, Toulouse, Nov. 1986.

- Hahn, K.U.  
Heintach, T.  
Kaufmann, B.  
Schänzer, G.  
Swolinsky, M.
- Wind Models for Flight Simulation.  
AGARDograph No. 301, 1988.
- Heintach, T.
- Windmessung mit dem Forschungsflugzeug DO 128 im Leebereich von Hügeln.  
DFG Abschlußbericht, Braunschweig, 1987.
- Heisenberg, W.
- Zur statistischen Theorie der Turbulenz.  
Zeitschrift für Physik, pg. 628, 1948.
- Hinze, J.O.
- Turbulence  
Mac Graw-Hill, New York, 1959.
- Hornung, H.  
Perry, A.E.
- Some Aspects of Three-Dimensional Separation. Part I: Streamsurface Bifurcations.  
Z. f. Flugwiss. u. Weltraumforsch. 8 (1984), Heft 2.
- Houbold, J.C.
- Atmospheric Turbulence.  
(Dryden Research Lecture), AIAA Journal Vol. 11, No. 4, April 1973.
- Karman, Th. V.
- On the Statistical Theory of Isotropic Turbulence.  
Proc. Roy. Soc. (a) 164 (1938).
- Kaufmann, B.
- Atmospheric Turbulence and Unsteady Aerodynamics in Aircraft Simulation.  
2nd International Symposium on Aviation Safety, Toulouse, Nov. 1986.
- Knorr, W.
- Einfluß verschiedener Hügelumströmungen auf dem Steigflug von Flugzeugen.  
Studienarbeit am Institut für Flugführung der TU Braunschweig, 1982.
- König, R.
- Erhöhung der Flugsicherheit bei Scherwindanflügen durch Modifikation von Schubregelungssystemen und bestehender Cockpit-Instrumentierung.  
Jahrestagung der DGLR, Stuttgart, 5. - 7. Oktober 1982, Vortrag Nr. 82 - 033 und Wissenschaftliche Berichte 1982, SFB 58 "Flugführung", TU Braunschweig u. DFVLR.
- König, R.  
Krauspe, P.  
Schänzer, G.
- Procedures to Improve Flight Safety in Wind Shear Conditions.  
Proceedings of the 12th Congress of the Aeronautical Sciences.  
Munich, Germany, Oct. 1980.
- Kolmogoroff, A.N.
- The Local Structure of Turbulence in Incompressible Viscous Fluids for Very Large REYNOLDS Numbers.  
C.R. (Doklady) Acad. Sci. U.R.S.S., N.S. 30(4) 301 - 305, 1941.
- Kottmeier, C.
- Die Vertikalstruktur nächtlicher Grenzschichtstrahlströme.  
Dissertation am Institut für Meteorologie und Klimatologie der Universität Hannover, 1982.
- Kraichnan, R.H.
- Model for Energy Transfer in Isotropic Turbulence.  
The Physics of Fluid, Vol 5, No. 5, p. 583, 1962.
- Krauspe, P.  
Swolinsky, M.  
Vörsmann, P.
- Wind Determination and Wind Shear Detection from Flight Test and Airline Flight Data.  
International Conference on Aviation Weather Systems, American Meteorological Society, Montreal, Que, May 1981.
- Krauspe, P.
- Beiträge zur Längsbewegung von Flugzeugen in Windscherungen.  
Dissertation, Fakultät für Maschinenbau und Elektrotechnik der TU Braunschweig, 1983.
- Küssner, H.G.
- Das zweidimensionale Problem der beliebig bewegten Tragflächen unter Berücksichtigung der Partialbewegung der Flüssigkeit.  
Luftfahrtforschung Band 17, Lfg 11/12 (1940).
- Lenschow, D.H.
- Probing the Atmospheric Boundary Layer.  
American Meteorological Society, Boston, Massachusetts, 1984.
- Lenschow, D.H.
- The Measurement of Air Velocity and Temperature Using the NCAR Buffalo Aircraft Measuring System.  
NCAR - TN/EDD - 74, 1972.
- Lumly, J.L.  
Panowsky, H.W.
- The Structure of Atmospheric Turbulence.  
John Wiley and Sons, New York, London, 1964.
- Meroney, R.N.
- WECS site screening by physical modeling.  
Proceedings Conference and Workshop on Wind Energy Characteristics and Wind Energy Siting DEO and AMS, Oregon, USA, 1979.

- Monin, A.S.  
Obuchow, A.M.      Fundamentale Gesetzmäßigkeit der turbulenten Vermischung in der bodennahen Schicht der Atmosphäre.  
in: Statistische Theorie der Turbulenz, Akademie-Verlag, Berlin 1958, S. 199-226.
- Prandtl, L.      Strömungslehre  
Vieweg-Verlag, Braunschweig, 1965.
- Pritchard, F.E.      Spectral and Exceedance Probability Models of Atmospheric Turbulence for Use in Aircraft Design and Operation.  
Air Force Flight Dynamic Laboratory, Wright-Patterson Air Force Base, Ohio, Rep. AFFDL-TR-65-122, (1965).
- Reichardt, K.      Gesetzmäßigkeiten der freien Turbulenz.  
VDI-Forschungsheft 414 (1942), 2. Auflage 1951.
- Schänzer, G.      Abschätzung von stochastischen Böenlasten unter Berücksichtigung instationärer Luftkräfte.  
Z. f. Flugwiss. u. Weltraumforsch. 9 (1985), Heft 3, S. 167-178.
- Schänzer, G.      The Effect of Gust and Wind Shear for Automatic STOL Approach and Landing.  
AGARD Conference Proceedings CP 140, "Flight in Turbulence", Bedfordshire 1973.
- Schänzer, G.      Influence of Wind Shear, Downdraft and Turbulence on Flight Safety.  
2nd International Symposium on Aviation Safety, Toulouse, Nov. 1986.
- Schänzer, G.      Flug in gestörter Atmosphäre.  
Vorlesung am Institut für Flugführung der TU Braunschweig.
- Schänzer, G.  
Heintsch, T.  
Hoyer, H.  
Tetzlaff, G.      Untersuchung der Scherwindverhältnisse an der Weidacher Höhe.  
Gutachten, 10.07.1987, Braunschweig.
- Schlichting, M.      Grenzschicht-Theorie.  
Verlag G. Braun, Karlsruhe 1982.
- Shangxiang, Zhu  
Etkin, B.      Fluid-dynamic Model of a Downburst.  
UTIAS-Report No. 271, April 1983.
- Shelkovnikov, M.S.      Strujnye techeniya na malykh vysotakh (Strahlstöße in geringer Höhe).  
Meteorologiya i gidrologiya, 1983, Nr. 11, Moskau, S. 44-46.
- Stieler, B  
Winter, H.      Gyroscopic Instruments and their Application to Flight Testing.  
AGARDograph No. 160, Vol. 15, September 1982.
- Swolinsky, M.      Beiträge zur Modellierung von Scherwind für Gefährdungsuntersuchungen.  
Thesis, Techn. Univ. Braunschweig, 1986.
- Swolinsky, M.  
Krauspe, P.      Windbestimmung aus Flugmeßdaten eines Linienflugzeugs.  
Meteorologische Rundschau 37, 72-81, Juni 1984.
- Taylor, G.I.      The Spectrum of Turbulence.  
Proceedings of the Royal Society, A 164, 476-490, 1938.
- Thorpe, A.S.  
Miller, H.H.  
Mono      Dynamic Models of Two-Dimensional Downdrafts.  
Quart. J. R. Met. Soc. (1980), 106, 463-484.
- Vörsmann, P.  
Swolinsky, M.      Wind Shear Detection from PCM-recorded MLS-Flight Data.  
12. ICAS Congress, Conference Proceedings, Munich, Oct. 1980.
- Vörsmann, P.      An On-Line Realization for Precise Wind Vector Measurements on Board the DO 28 Research Aircraft.  
14th Congress of the International Council of the Aeronautical Sciences, September 9-14, 1984, Toulouse, France.
- Vörsmann, P.      Ein Beitrag zur bordautonomen Windmessung.  
Dissertation am Institut für Flugführung der TU Braunschweig, 1984.
- Weiszäcker, C.F. v.      Das Spektrum der Turbulenz bei Großen Reynold'schen Zahlen.  
Zeitschr. f. Physik 124, 626, 1948.
- White, F.M.      Viscous Fluid Flow.  
Mc Craw-Hill Book Company, New York, 1974.
- Woodfield, A.A.  
Wood, J.F.      Worldwide Experience of Wind Shear During 1981-1982.  
AGARD CP No. 347, Athens, 10. - 13. May 1983.

9-16

Wuest, W.

Pressure and Flow Measurement.  
AGARDograph No. 160, Vol. 11., July 1980.

Zhu, S.  
Etkin, B.

Fluid-dynamic Model of a Downburst.  
UTIAS-Report No. 271, April 1983.

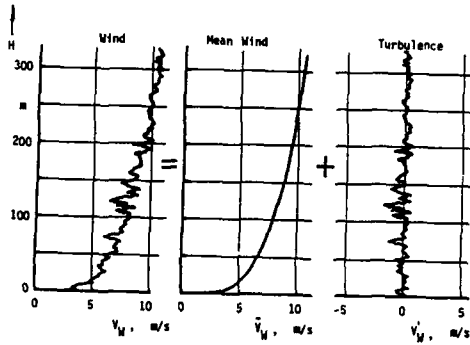


Fig. 1 Separation of turbulence

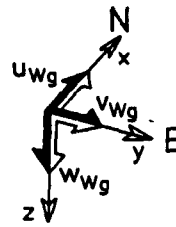


Fig. 2 Wind components in an earth fixed coordinate system

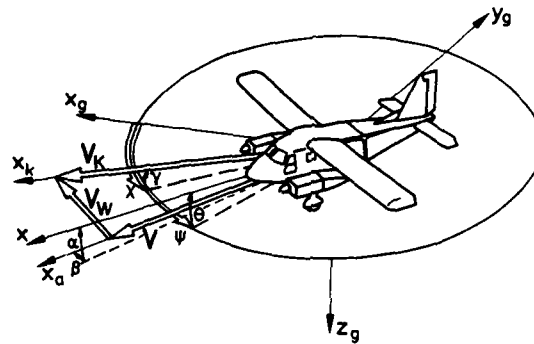


Fig. 3 Determination of the wind vector

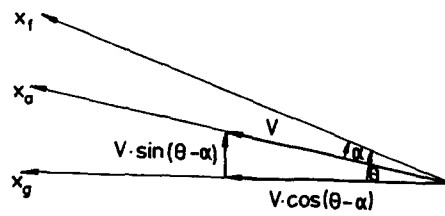


Fig. 4 Determination of the true airspeed components in the aircraft symmetrical plane

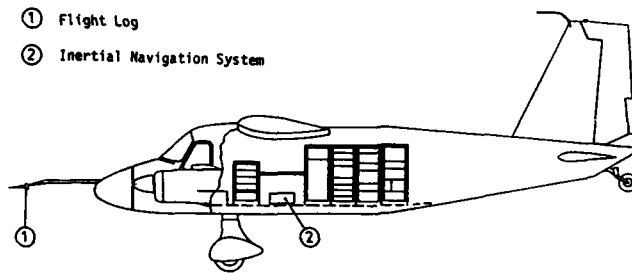


Fig. 5 Hardware location in a measurement aircraft

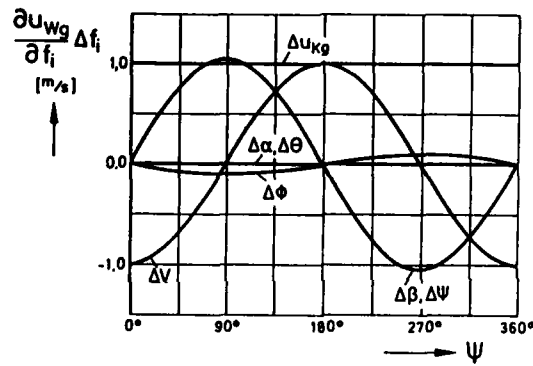


Fig. 6 Error of the  $u_{wg}$  component due to sensor errors

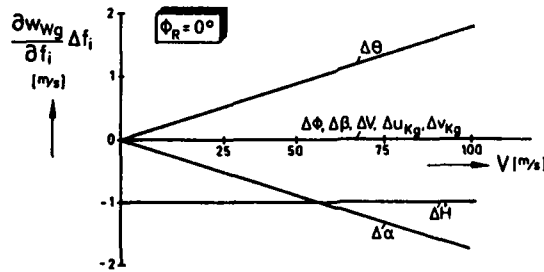


Fig. 7 Error of the  $w_{wg}$  component due to sensor errors

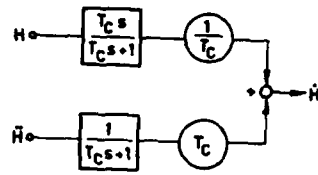


Fig. 8 Complementary filter for obtaining the vertical speed of the aircraft

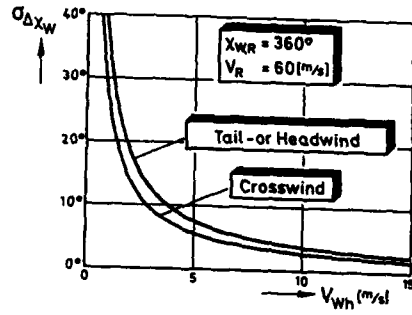


Fig. 9 Error in wind direction as a function of wind speed

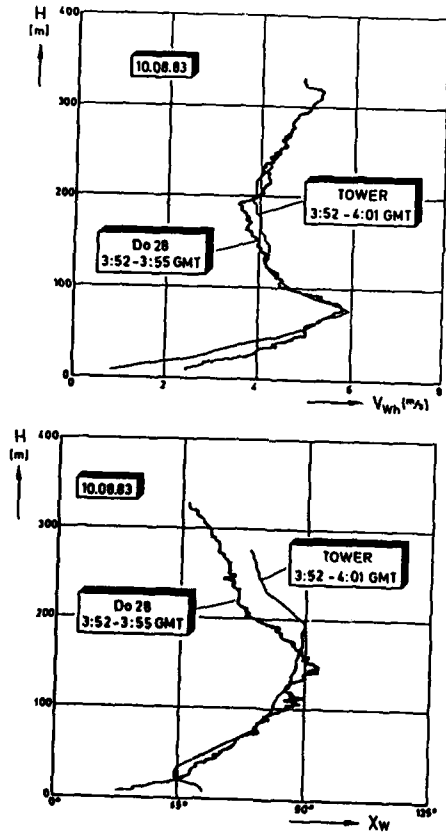


Fig. 10 Comparison of aircraft and tower wind

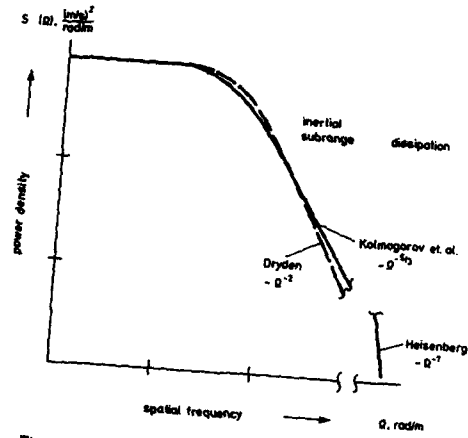


Fig. 11 Power density spectrum of turbulence

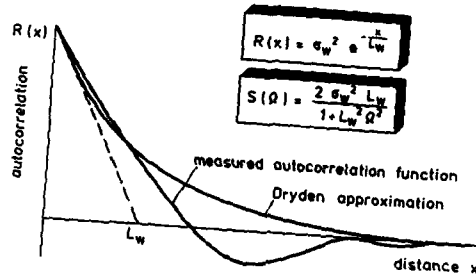


Fig. 12 Autocorrelation function of turbulence

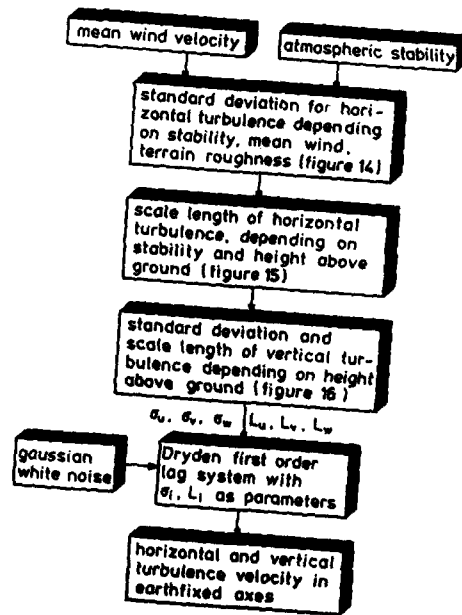


Fig. 13 Turbulence calculation model

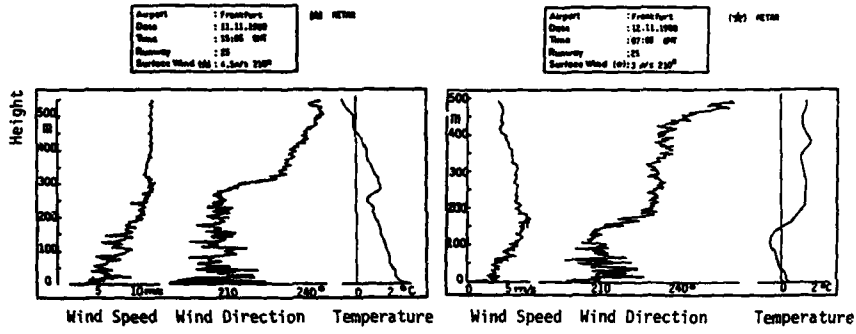


Fig. 14 Influence of temperature inversion on turbulence intensity

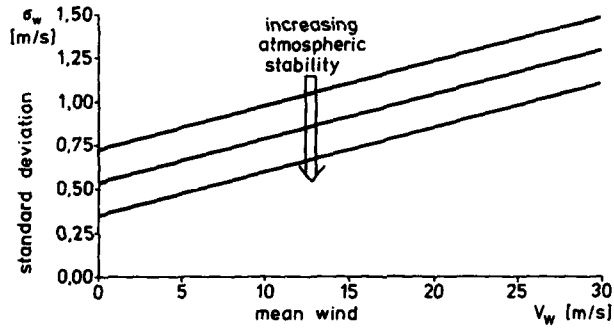


Fig. 15 Standard deviation versus mean wind velocity

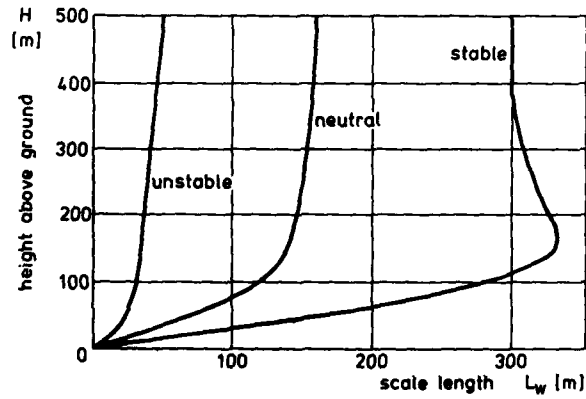


Fig. 16 Scale length versus height above ground

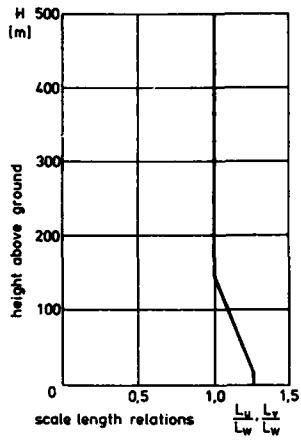


Fig. 17 Relation of scale length for horizontal and vertical turbulence components

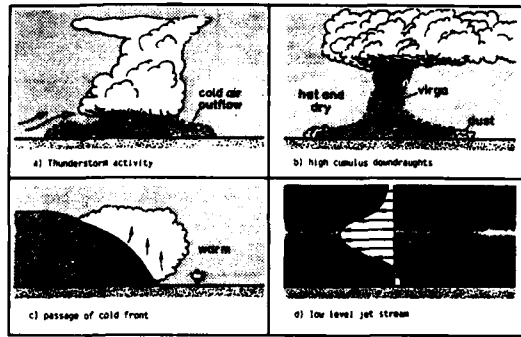


Fig. 18 Meteorological scenario significant for wind shear conditions

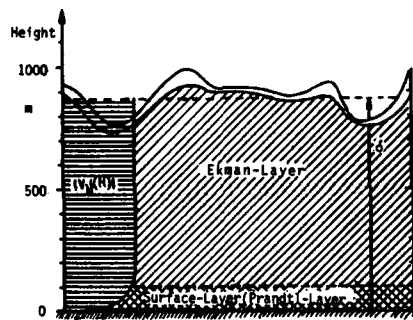


Fig. 19 Classification of planetary boundary layer

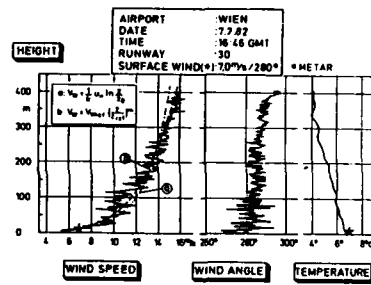


Fig. 20 A typical boundary layer wind profile compared with wind models

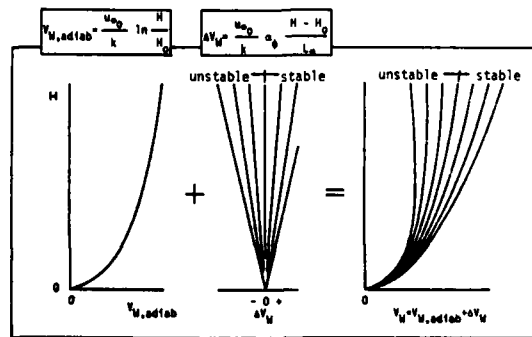


Fig. 21 Composition of the log-lin-profile

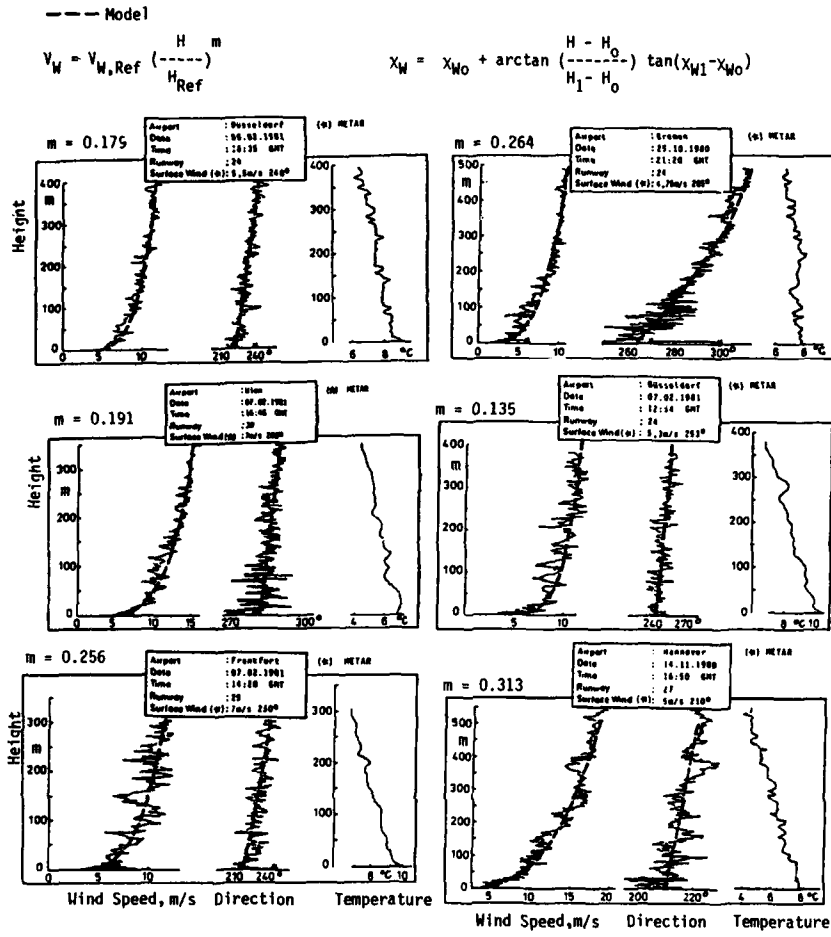


Fig. 22 Measured and modeled wind profiles

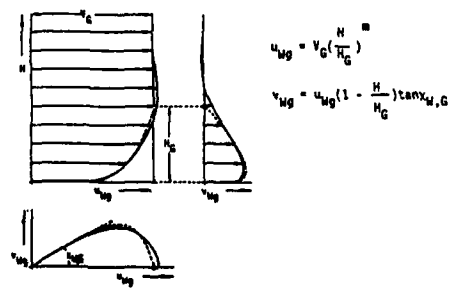


Fig. 23 Turbulent surface flow (PRANDTL)

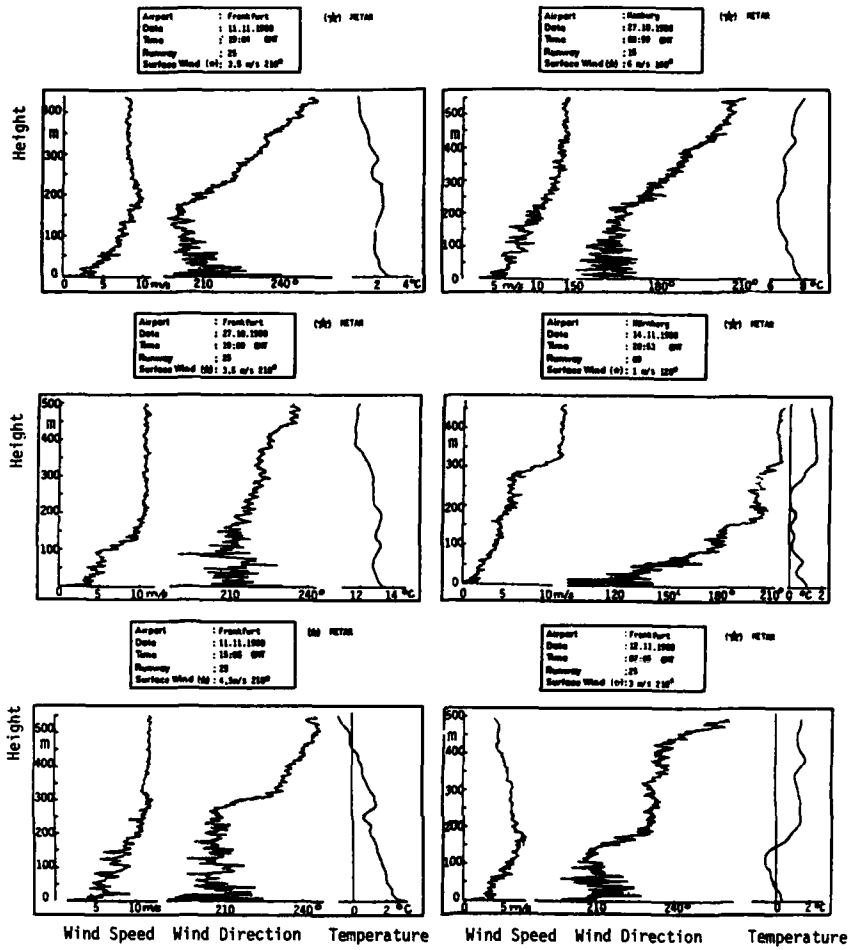


Fig. 24 Influence of temperature inversion to wind profile

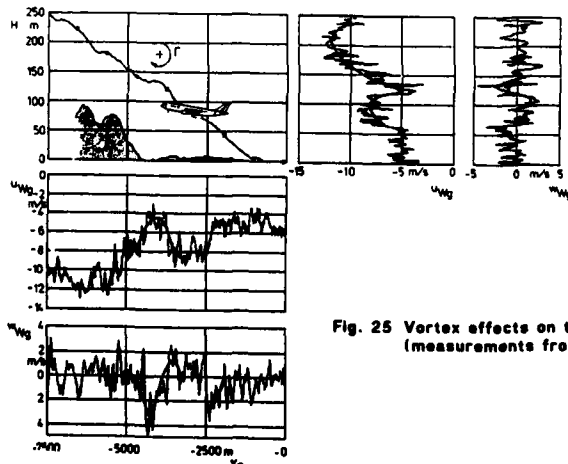


Fig. 25 Vortex effects on the wind components  $u_w$  and  $w_w$  (measurements from SCHÄNZER et al., 1987)

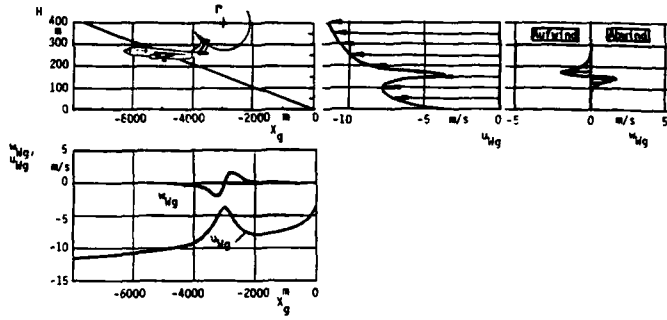


Fig. 26 Vortex effects on the wind components  $u_{wg}$  and  $w_{wg}$  (flight simulation)

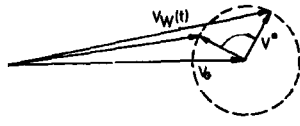


Fig. 27 Inertial oscillation supposed by BLACKADAR (1957)

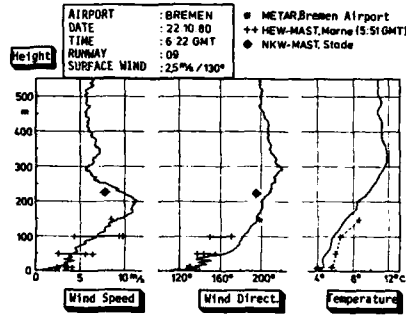


Fig. 28 Sample of flight measured low level jet

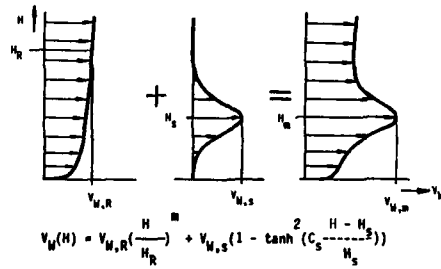


Fig. 29 Composition of the low level jet model

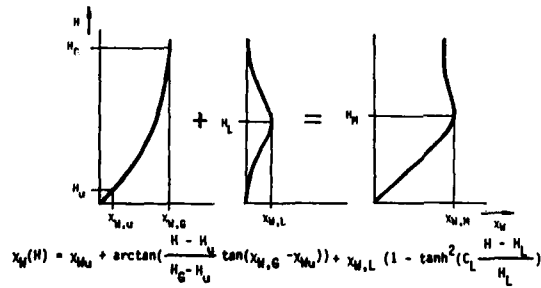


Fig. 30 Composition of the wind direction

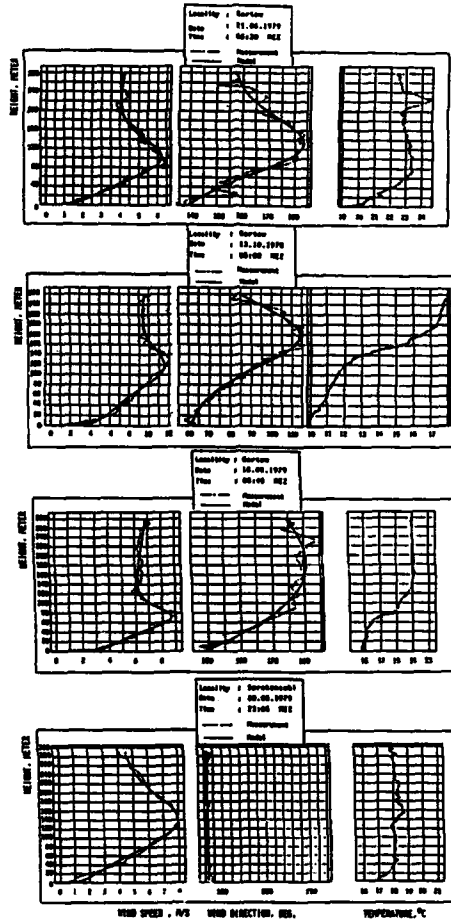


Fig. 31 Comparison of tower data with a low level jet model

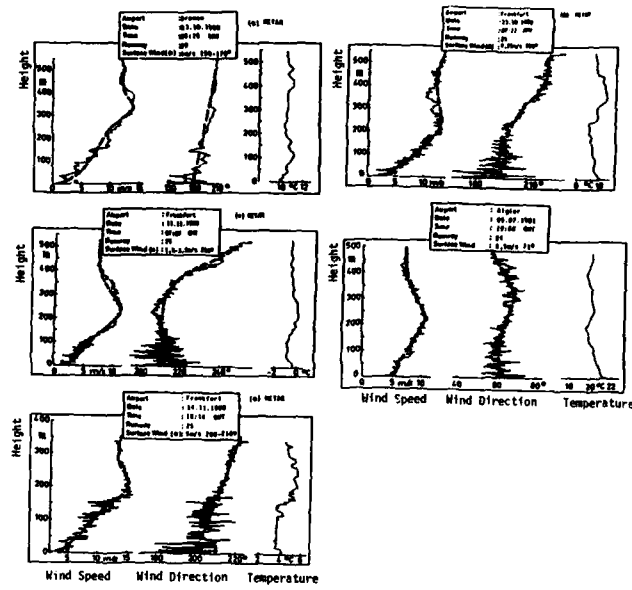


Fig. 32 Comparison of flight test data with a low level jet model

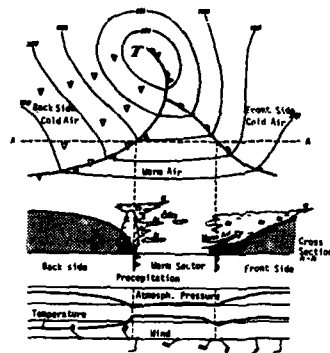


Fig. 33 The passage of a frontal system (England/Ulbricht, 1980)

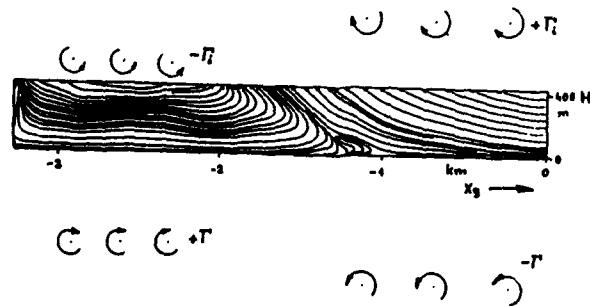


Fig. 34 Principle proceeding for the generation of a frontal flow field

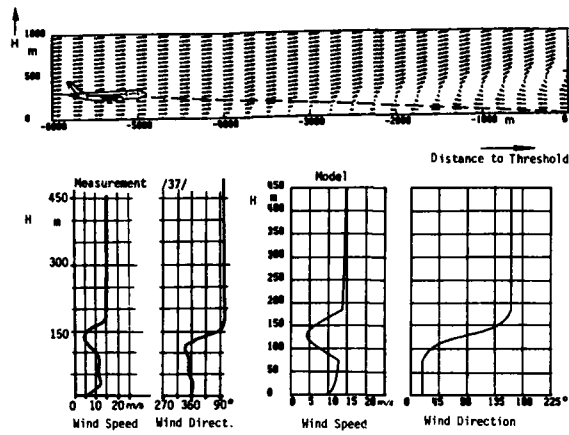


Fig. 35 Measured frontal wind speed and model data along a 3°-glide slope

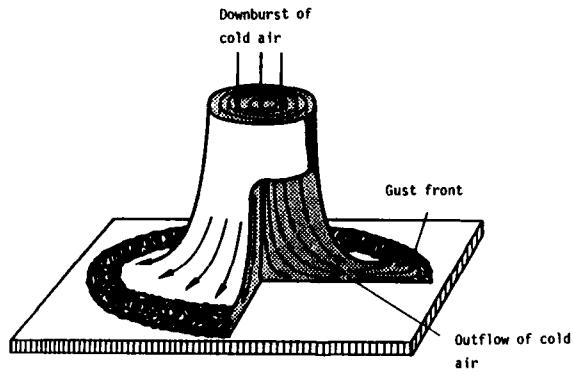


Fig. 36 Characteristic flow in a thunderstorm downburst (KRAUSPE, 1983)

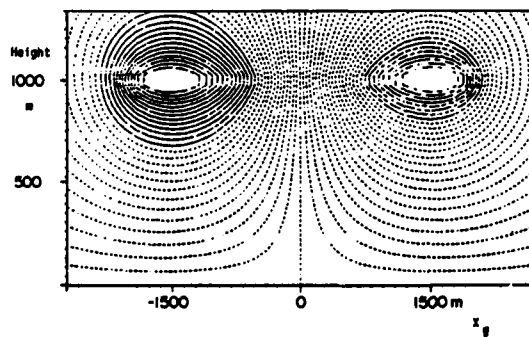


Fig. 37 Doublet sheet model (ZHU/ETKIN, 1983)

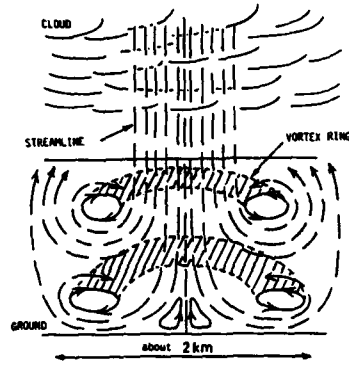


Fig. 38 Ring vortex model (WOODFIELD/WOOD, 1983)

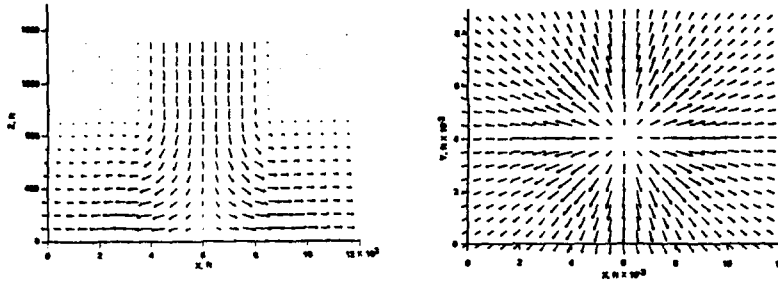


Fig. 39 Downburst model supposed by BRAY (1985)

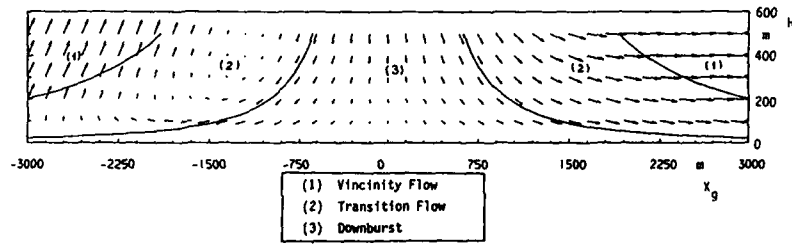


Fig. 40 Extended steady jet flow model

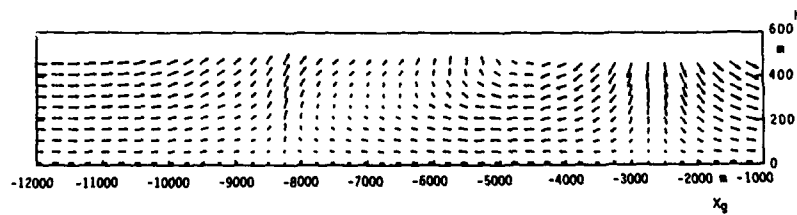
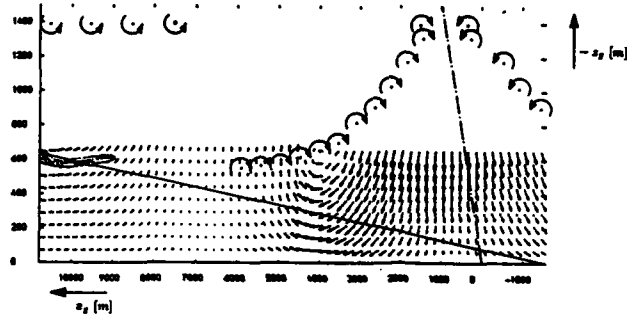
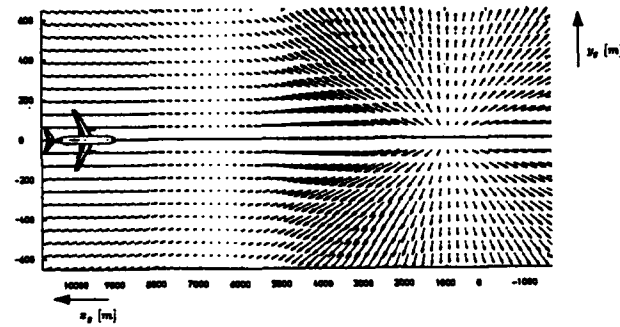


Fig. 41 Vortex superposition model



Flow field in the  $x_g/x_g$  plane



Flow field in the  $x_g/y_g$  plane

Fig. 42 Three-dimensional vortex superposition model

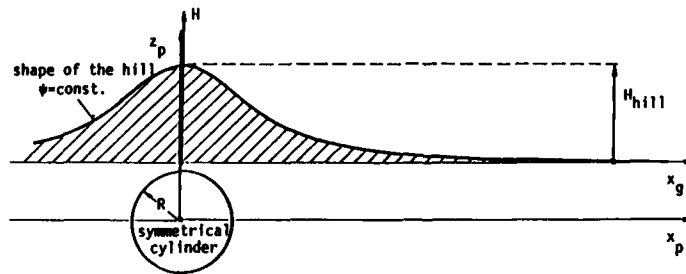


Fig. 43 Shape of the hill defined by a streamline of a cylinder (HAHN, 1986)

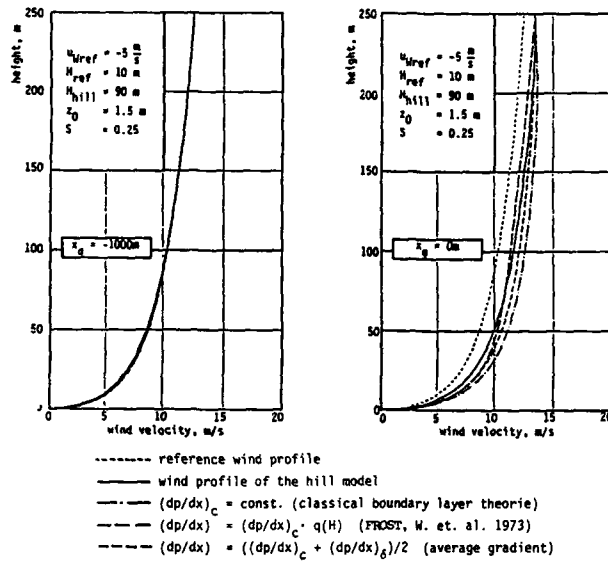


Fig. 44 Comparison of the hill model with results of a finite difference technique (HAHN, 1986)

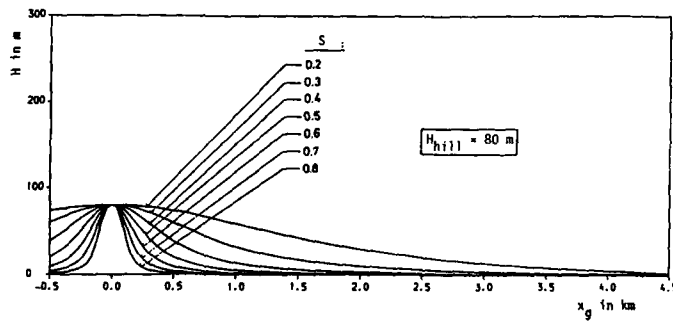


Fig. 45 Effect of the shear factor on the shape of a hill

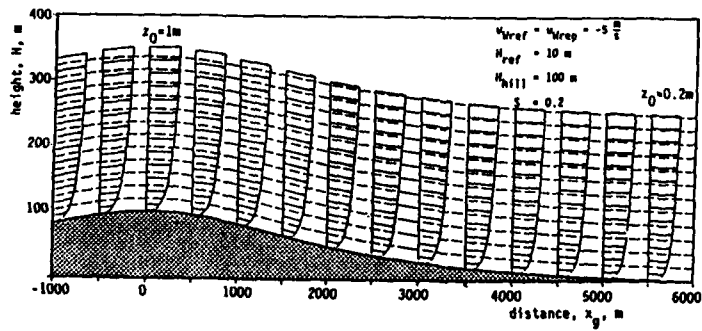


Fig. 46 Wind profiles and streamlines over the hill model (HAHN, 1986)

$f_i$	$\partial u_{Kg} / \partial f_i$	$\partial v_{Kg} / \partial f_i$	$\partial w_{Kg} / \partial f_i$
$\alpha$	$-V_R (\gamma_R \cos \gamma_R + \phi_R \sin \gamma_R)$	$-V_R (\gamma_R \sin \gamma_R - \phi_R \cos \gamma_R)$	$-V_R$
$\beta$	$V_R \sin \gamma_R$	$-V_R \cos \gamma_R$	$-V_R \phi_R$
$\theta$	$V_R \gamma_R \cos \gamma_R$	$V_R \gamma_R \sin \gamma_R$	$V_R$
$\phi$	$-V_R \alpha_R \sin \gamma_R$	$V_R \alpha_R \cos \gamma_R$	$V_R \alpha_R \phi_R$
$\gamma$	$V_R \sin \gamma_R$	$-V_R \cos \gamma_R$	0
$\nu$	$-\cos \phi_R$	$-\sin \gamma_R$	$\gamma_R$
$u_{Kg}$	1	0	0
$v_{Kg}$	0	1	0
$\dot{H}$	0	0	-1

Tab. 1 Approximations for the linear error model

**PART III**

**Impact of New On-Board Technologies  
on Aircraft Operation**

**AIRCRAFT TRAJECTORY – PREDICTION AND CONTROL  
IN THE  
AIR TRANSPORT FLIGHT MANAGEMENT COMPUTER SYSTEMS**

by

**Peter J. Howells**  
Senior Systems Design Engineer  
Smith Industries  
SLI Avionic Systems Corp  
4141 Eastern Ave. S.E.  
Grand Rapids, Michigan 49518-8727  
United States

## Summary

The declining cost of computing power and memory has enabled avionic manufacturers to develop sophisticated airborne computing systems. One of the most complex aircraft systems on modern air transport aircraft is the Flight Management Computer System (FMCS). The FMCS has reduced pilot workload by taking over the more mundane but complex functions – such as calculating the most economical speed – and, together with improvements in cockpit displays and monitoring systems, has allowed the transition from the three to two crew airline cockpit.

The FMCS can compute the most economical path from one airport to another and then fly the aircraft along that path. To achieve this the computer must be able to select the most economical speed schedules for each phase of flight, then predict the complex vertical and horizontal profile that the aircraft would fly and, when connected to the aircraft's autopilot, control the aircraft along that three dimensional flight path. The fourth dimension of time can also be selected as a control criteria, and the FMCS will compute the speed schedules and flight path based on a required time of arrival at a selected point along the flight plan. In addition to reducing pilot workload, air traffic control efficiency is increased because the airborne navigation data base can be used to select and accurately fly published arrival and departure procedures without supervision from the ground controllers.

This paper describes the algorithms used for the Smiths Industries 737 FMCS prediction and control functions. It identifies the requirements for successful implementation and some of the difficulties that may be encountered.

## 1 Introduction

In the deregulated USA airline environment there was a need to reduce operating costs by improving fuel efficiency and, where possible, by reducing the flight crew from three to two. This was the impetus for the aircraft manufacturers to increase the avionic capability of new aircraft and thus decrease pilot workload. A completely new aircraft system that was developed as a result of this cockpit revolution was the Flight Management Computer System (FMCS).

### 1.1 Operational Overview

The FMCS is composed of one or two Flight Management Computers (FMC) which contain the computing hardware and software. One unit may be installed if independent navigation is not required or if, as on the Boeing 737-300, an alternate "back up" navigation system within the control display unit is provided. A dual FMC system is installed on long haul aircraft where the loss of the primary navigation system would be unacceptable. Two Control Display Units (CDU) are also provided as an integral part of the FMCS and are used by the pilot and copilot to communicate.

This paper describes the FMCS installed on the 737-300/400/500 aircraft and represents one example of a unit meeting ARINC specification 702. The FMCS on other aircraft have basically the same capabilities but may differ in the way they are implemented. Also it is the nature of an FMCS development (and a tribute to flexibility of the FMCS design) that capabilities of the system tend to grow and evolve after the initial certification of a new aircraft model. This description, therefore, should be considered a snapshot of a particular design at a certain point in time.

### 1.2 System Capabilities

As its name suggests the FMC system is responsible for all aspects of flight management, these fall into one of the following functional areas:

**Navigation** This function uses aircraft sensors such as the aircraft inertial reference system, etc. and the internal FMCS navigation data base to generate an accurate estimate of aircraft position and velocity. This function also autotunes the aircraft's navigation radios.

**Flight Planning** Accepts and interprets pilot entries of flight plan data using an alpha numeric keyboard and display. The pilot may enter any of the following to generate the desired flight plan:

- **Waypoints** – Predetermined or pilot entered points on the ground, nav aids, airports, etc. can be selected by name and the position of these points are retrieved from the navigation data base. The pilot can also

define his own waypoints using latitude and longitude and bearing/distance or bearing/bearing definitions from other waypoints.

- Company Routes – Predefined lists of waypoints that correspond to normal airline routes.
- Departures and Arrivals – Single key selection of standard airport departure or arrival procedures, approaches, runways and transitions.
- Airways – Lists of waypoints on published airways.

All these entries are combined to form a complete airport to airport flight plan waypoint list. This list is used by other functions in the FMCS but can be easily modified by the pilot at any time during the flight.

**Display Support** Data transmission to the electronic flight instrument system (EFIS) of navigation data base information, flight plan and aircraft situation (position, track, wind, etc.).

**Performance** The FMCS contains a complete airframe and engine model. These models are used to generate the following aircraft and engine specific data:

- Throttle limits.
- Thrust and drag for defined throttle settings and environmental conditions.
- Optimum speeds and altitudes
- Maximum and minimum speeds and altitudes

**Predictions** An accurate emulation of the aircraft's four dimensional track in space. It provides an estimation of:

- Fuel remaining at each waypoint and at the destination.
- Speed and altitude at each waypoint.
- Estimated Time of Arrival (ETA) at each flight plan waypoint.

These dynamically updated predictions give a valuable indication of the effects of temporary or permanent modifications made by the pilot (such as raising cruise altitude) or changing environmental conditions (such as increasing headwind).

**Control** When connected to the aircraft's autopilot system the FMCS will automatically fly the predicted flight plan. The FMCS will use vertical and horizontal steering commands and speed target commands to direct the aircraft to the flight plan and to maintain predetermined profile from take-off to glideslope intercept at the destination.

### 1.3 Aircraft sensors

The FMCS relies on multiple aircraft sensors for the accuracy of its navigation and control. For this reason the optimum sensor configuration for maximum accuracy should be available on the aircraft. This should include a mix of long term and short term accurate position sensors for navigation and accurate attitude, altitude speed sensors for control. A typical sensor suite would be as follows:

**Position - Short term accuracy** Most modern aircraft are equipped with dual or triple Inertial Reference Units (IRUs). These units contain ring laser gyros which provide excellent attitude information and position information but will tend to drift as the flight progresses at a rate of up to 2 Nautical miles per hour.

**Position - Long term accuracy** An accurate position over the length of the flight is essential for correct operation. This can be provided from any of the following, singularly or in combination:

- Distance Measuring equipment (DME) – can be used in pairs to provide an accurate triangulated position. Only available on flights within direct line of sight of the ground equipment.
- VHF Omnidirectional Range (VOR) – can be used with a DME to provide a less accurate angle and distance based position
- Global Positioning System (GPS) – Uses satellites to provide a very accurate position. Available worldwide when all satellites are operational.
- Omega and LORAN – Less accurate but almost worldwide radio based systems.

The relatively long time between recalculations of these long term sensors means that they cannot normally be used as the sole source of navigation data but the combination of long and short term sensors provides a balanced configuration.

**Attitude** The IRUs provide very accurate attitude information and the addition of a Air Data Computer (ADC) provides the complementary long term altitude and speed data stability required for the FMCS control function.

### 1.4 FMCS displays

The primary display and entry unit of the FMCS is the control display unit (CDU). Two CDUs are normally provided in the cockpit and allow independent access to the FMCS. A typical CDU is shown in Figure 1 and is composed of the following:

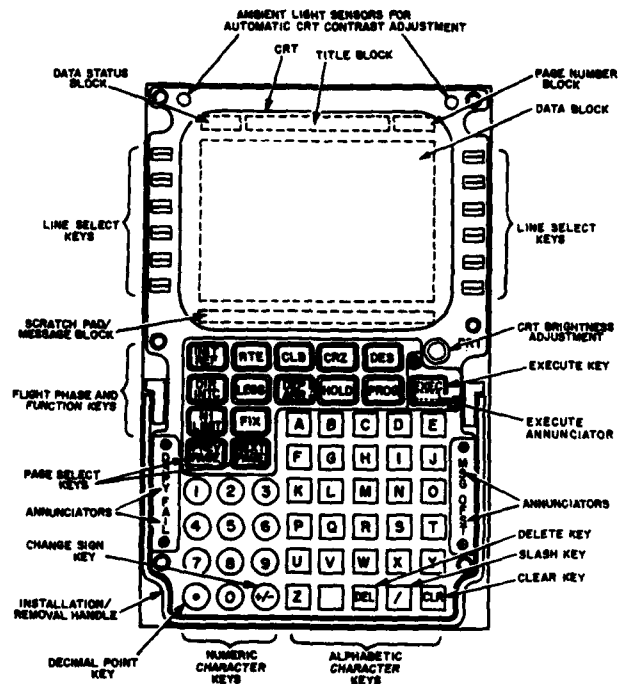


Figure 1: FMCS Control Display Unit

- A multi-line display unit with multi-function line select keys (LSKs) along each side. The display is used to present alphanumeric data which can be selected and entered using the LSKs.
- Mode keys that are used to select different pages of information.
- An alphanumeric keyboard that is used to enter data.

In addition to the CDU, the EFIS provides a graphical presentation of the flight plan and the progress along the flight plan and is, therefore, an important FMCS display interface to the pilot.

## 2 Predictions

An important function provided by the FMCS is the emulation of the entered flight plan profile and the prediction of aircraft parameters at points along that profile. When the required minimum amount of information has been entered about the proposed route, the predictions algorithm can "fly" the profile and predict the speed, altitude, fuel remaining, etc. at fixed waypoints along the plan and at the destination airport. The predictions algorithm also generates the courses to be flown between the waypoints using great circle path computations and identifies additional "vertical" waypoints such as top of climb, top of descent and deceleration points that are a function of aircraft performance and selected speeds.

A complete set of data for each vertical and lateral waypoints in the flight plan is stored and updated periodically for use by other functions in the FMCS such as display generation and aircraft control. In addition, predictions generates messages to the pilot if hazardous situations are detected. Examples of this are a selected cruise altitude that is above the maximum achievable altitude of the aircraft, or when the fuel on board is not enough to reach the destination.

The accuracy or fidelity of the predictions in an airborne system such as the FMCS is a compromise between speed of the hardware and response time requirements. It is in the predictions software, which is generally the most demanding on computer throughput, where innovative techniques and algorithms can be implemented.

To initialize the FMCS the pilot is required to enter a basic lateral flight plan which would include an origin airport, a destination airport and at least one in between waypoint. From this minimum entry a lateral profile can be generated and lateral control (LNAV) is available. In addition to the flight plan, the minimum performance parameters (described in section 2.1.3), as well as any known extra parameters that will improve the accuracy of the emulation, such as cruise wind and ISA deviation should be entered. From these entries and some default assumptions (such as standard day atmospheric conditions) a complete vertical profile can be generated and displayed to the pilot. Vertical control (VNAV) can then be engaged after take off and used to guide the aircraft through climb cruise and descent.

There are two timing requirements that affect the operation of the prediction algorithm and may influence the type of algorithms used. They are:

**Response time** The time between a major change to the flight plan by the pilot and the generation of whole new profile. Obviously, it is important that this time be as short as possible. The required system throughput for the whole FMCS can be estimated by calculating the processor throughput required to complete a full predictions run within the target response time.

**Update rate** The rate at which the predictions are rerun to account for changing environmental conditions. Predictions updates are usually a background task.

The accuracy of predictions is limited by the amount of extra data that is entered by the pilot. If the pilot has information on cruise winds or winds at a flight plan waypoint the predictions algorithm is able to refine the enroute flight times and fuel usage and generate a more realistic profile. However, predictions must also be able to adapt to unexpected actual conditions, such as an unforecasted cruise wind. Actual conditions are measured and then propagated along the flight plan in a realistic manner even if this conflicts with the pilot entered data.

## 2.1 Pilot Initialization

With the aircraft on the ground the pilot can enter data into the FMCS so that a lateral and vertical profile can be constructed. In general these are divided into flight plan related parameters either lateral (horizontal plane) or vertical; and performance related parameters such as aircraft weight, etc.. Although this data is entered on the ground all the parameters can be modified as required in the air to account for changing conditions or air traffic control requirements.

### 2.1.1 Lateral Profile Definition

The Lateral profile generally consists of an origin airport, a destination airport and a number of enroute waypoints. Normally the pilot is able to define this complete lateral flight plan (excluding the arrival procedure) on the ground before take off. The kind of entries made are:

**Company routes** The navigation data base (NDB) internal to the FMCS can be customized by an airline to include all its route structure. This means that a simple multi-character identifier can be used to automatically recall a stored airport pair flight plan. An example of this would be "SEASFO" which would give the normal flight plan from Seattle to San Francisco. This default flight plan can be easily modified through the CDU, if required.

**Departures and Arrivals** Once the flight plan between the airports has been defined the pilot can enter a departure procedure and possibly an arrival procedure. The departure and arrivals (DEP/ARR) page contains a list of the published runways, standard instrument departure (SID) and transitions for the origin airport and runways, standard terminal arrival route (STAR) procedures and transitions for the destination airport. These are selected by the pilot when allocated by air traffic control (ATC). These procedures contain all the necessary information needed to fly the procedure as described by the governing agency. The pilot can also enter an arrival procedure for the departure airport in case a return to origin is required.

**Special leg types** The departure and arrival procedures are composed of special legs and it is these that are the most challenging for the predictions and control algorithms. Examples of some of these special leg types are:

- **Heading to an altitude** - This leg type, usually found as the first leg of a flight plan, directs the FMCS to climb at constant heading until a defined altitude is reached. At that point the leg is terminated and a transition to the next leg is initiated.
- **Course to an intercept** - For this leg type the FMCS constructs a great circle path, at a specified track angle, from a waypoint to the point where the aircraft would intercept a specified radial into a defined navigation aid.

In general, all legs are defined as a lateral profile control type - such as heading or track - followed by a termination point - such as a waypoint, an altitude or an interception of a VOR radial or DME distance.

The full "toolbox" of leg types from which a procedure can be constructed is specified in the ARINC 424 specification.

To include all leg types in the lateral flight plan the predictions algorithm must be able to estimate where the termination point of each leg would be. To be able to do this the algorithm must be able to accurately estimate normal in flight acceleration or deceleration, rate of climb or descent and probable wind conditions. Some legs, however, deliberately have no termination points (called manually terminated legs or vectors) and when one of these legs are flown it is the responsibility of the pilot to "terminate" the leg and rejoin the remainder of the flight plan. The predictions algorithm, however, uses a default expected path to complete the profile.

In addition to the leg types described above, the predictions algorithm requires special processing for some standard flight plan leg combinations which can be entered as a single unit. These include:

**Holding patterns** These "race track" shaped paths can be specified in a number of ways and have strictly defined rules on entry path and exit method. Holds can be "attached" to an existing flight plan waypoint

or designated as present position (PPOS) holds that are inserted just ahead of the aircraft.

**Procedure turns** This standard combination of legs may be included as part of an approach procedure as a way of reversing course.

**Parallel Offset** This single selection allows the pilot to fly parallel to the predefined lateral flight plan at a defined distance to left or right. This feature allows ATC to allocate fast and slow aircraft on the same basic flight plan without one over-running the other.

### 2.1.2 Vertical profile definition

The vertical profile definition will include the minimum entry of selected initial cruise altitude and continue with optional manual entries such as speed or altitude constraints at waypoints. Speed and altitude constraints can also be introduced automatically through the selection of arrival or departure procedures or as a default such as airport restriction speeds (250 Kts below 10000 feet in the USA).

### 2.1.3 Performance initialization

Once the minimum lateral and vertical profile parameters have been entered, the performance predictions algorithm must be initialized with the minimum set of parameters that will enable the algorithm to construct a basic vertical profile. To these the pilot can add any refinements that may be available.

**Cost Index** The key to the vertical profile construction is a parameter called cost index (CI). This pilot-entered number is a function of current fuel price and crew costs. The CI speed schedule algorithm reduces overall flight cost by optimizing the requirements of lowering fuel usage by flying slower or reducing crew air time by flying faster. The CI value entered is a function of the current fuel cost and "cost" of time. In general, the lower the CI number the longer the flight will take, this would correspond to the high-fuel-cost, low-crew-cost operating environment. A high number entry indicates crew costs are high and a relatively high speed schedule will be chosen.

**Aircraft Weight** The aircraft gross weight can be calculated from the entry of zero fuel weight, provided the fuel weight is available from aircraft sensors. Or it can be entered directly.

**Refinements** If additional data is available then it can be entered into the system. These include:

- ISA Deviation or top of climb temp
- Anticipated average cruise wind
- Reported winds at waypoints in the flight plan
- Forecast descent winds - wind bearing and magnitude at designated altitudes
- Destination QNH
- Anti-ice on/off altitude

### 2.1.4 4D Navigation - Required Time of Arrival (RTA) Initialization

In FMC systems where the accuracy of predictions allows the precise calculation of estimated time of arrival (ETA) at any waypoint, a control loop can be implemented that modifies CI to meet a specified ETA at a waypoint in the flight plan. This form of four-dimensional navigation is called required time of arrival (RTA). To initialize the RTA algorithm the pilot needs to designate a waypoint in the flight plan and enter a required time of arrival.

## 2.2 Profile Prediction

With all initializations complete the predictions algorithm can begin. The algorithm is run differently if a completely new profile is required or if the profile is just being updated. A completely new profile would be required the first time all the data is entered and anytime a major modification is made. In this case all the phases of the flight plan would have to be identified and checks made on the reasonableness of the initialization entries. Predictions updates are run as a background task and includes such tasks as updating estimated wind values as actual winds are encountered.

### 2.2.1 Basic algorithm overview

A full predictions run on the Smiths Industries 737-300 FMCS contains the following steps:

**Flight plan division** The first task is to divide the lateral flight plan into approximate phases so that climb, cruise and descent can be properly allocated. The current phase of flight is determined from the present aircraft position. From that the remainder of the flight plan is broken up as follows:

- Determine the first restriction in descent (FRDS) and last restriction in climb (LRCL). This routine tries to anticipate the pilots' intention when altitude restrictions have been entered for flight plan waypoints. The algorithm first generates an approximate vertical profile that assumes the shallowest rate of climb and descent. The flight plan is then scanned for altitude constraints and these are labeled as climb or descent based on their position in the approximate profile. Particularly troublesome are high altitude restrictions -

i.e. aircraft to be at or below 25000ft when the waypoint is sequenced - in a short flight plan under these cases the routine has to determine whether the intention is to extend the climb phase or to descend early. This routine allocates FRDS and LRCL to lateral waypoints and predictions then knows that top of climb (T/C) and top of descent (T/D) are inside these points.

- Designated the end of descent (E/D) point as the last "hard" constraint in the flight plan. The point is typically the final approach fix, a point just before the destination airport runway, which has a specified speed and altitude allocated to it. This waypoint can then be used as a "pivot" point for descent; as the speed schedule (and hence rate of descent) varies, the top of descent moves along the flight plan but the E/D remains fixed.

Once these points have been allocated they will not change unless the flight plan is modified.

**Climb speeds** The economy climb speed target is calculated using a polynomial expression, and is a function of takeoff gross weight and cost index. The resulting Calibrated Airspeed (CAS) is checked against airframe limit values and used as a target speed for the climb segment.

**Initial Cruise speed** A constant value of climb fuel burn is used to calculate the approximate fuel used to climb to cruise altitude. The resultant T/C weight, cruise wind and cost index are then used in a polynomial expression to calculate the initial cruise mach. The initial cruise mach and the previously calculated climb CAS are then used to calculate the crossover altitude. The crossover altitude is the altitude at which the equivalent mach of the climb CAS (which decreases with altitude) matches the initial cruise mach. At this altitude in climb, the speed target to the autothrottle changes from a constant CAS target to a constant mach target. Tests are made on the cruise mach to ensure aircraft structural limits are not exceeded. The algorithm generates a message to the pilot if no target speed can be generated at the selected cruise altitude because of buffet limits etc.

**Climb modelling** Using the designated climb speed, the flight plan and a high fidelity aircraft performance model, the climb segment can then be emulated. A predefined climb throttle setting is used, which can either be the default maximum climb thrust or a pilot selected reduced climb thrust schedule to save engine wear or for noise abatement. To model the climb it is divided into small altitude steps. The fuel burn from the previous step is used to predict the gross weight at each altitude step. The available thrust is then calculated and hence the climb rate needed to maintain the target speed. From this integration technique the time taken, the horizontal distance traveled and the fuel used to climb to each altitude are calculated until the cruise altitude is reached. This point is inserted into the flight plan and designated as the top of climb (T/C).

**Cruise modelling** The cruise portion of the profile is emulated and estimates of fuel burn, distance traveled and ETA at each waypoint in the cruise phase are generated. The economy cruise mach speed target is calculated at steps along the cruise using a cost index based polynomial which is a function of the expected aircraft weight and predicted wind. The algorithm continues along the flight plan until the previously defined "shallow profile" top of descent point is reached.

**Descent speeds** The economy descent CAS target is a function of the entered cost index which, after limiting, is used to calculate the descent crossover altitude. As in climb, the final cruise mach target is used to calculate the crossover altitude. Again, above the crossover altitude the mach target is used and from crossover to E/D the constant descent CAS target is used. A constant descent fuel burn rate is then used to calculate the approximate aircraft weight at E/D.

**Descent modelling** The emulation of the descent profile starts at the destination airport and moves backwards along the flight plan. A fixed approach profile is used to calculate time, distance and weight increments from the runway to the end of descent waypoint. The descent profile emulation then continues back up the flight plan recalculating gross weight, thrust and lift at each waypoint. The emulation recognizes waypoint and airport speed constraints and modifies the descent rate accordingly. Idle thrust is used for the emulation. When the backward descent reaches the cruise altitude this point is designated as the top of descent and a vertical waypoint is inserted in the flight plan. The cruise emulation then continues from the approximate top of descent to the more accurate "backward descent" top of descent. A comparison is then made between the top of descent fuel derived from the backward descent (which used an approximate destination weight) and the actual top of descent fuel using the cruise emulation. If a large discrepancy is found, that may affect the descent profile, the backward descent emulation is run again using a revised estimate of destination weight.

**Destination parameters** When the difference in fuel is small (below 1000 pounds) the descent profile is assumed to be stable and any difference in top of descent fuel is added or subtracted to all the waypoints in the descent to give an accurate fuel at destination. Checks are made to ensure there is enough fuel to reach the destination and messages are generated if required.

**Airport restriction** A normal feature of the descent is the deceleration to the airport restriction speed at the airport restriction altitude. The ATC requirement is that the aircraft be below the restriction speed when the restriction altitude is reached. To accomplish this a "level off" is inserted in the flight plan where the aircraft will reduce the rate of descent to a minimum value (usually 1000 ft/min) so that the aircraft can slow down. The length of the

segment is calculated from aircraft performance parameters. The beginning and end of the deceleration points are inserted in the flight plan and displayed to the pilot.

### 2.2.2 Special predictions processing

The predictions algorithm described above assumes a normal flight plan with reasonable initialization entries. Special processing is required if these conditions are not met:

**Short flight plan** If the length of the flight plan is short and the entered cruise altitude can not be reached before it is time to descend (i.e. no cruise phase) a UNABLE CRUISE ALT message will be generated. The algorithm detects this situation when the backwards descent routine reaches the top of climb waypoint before cruise altitude.

**No end of descent** If no fixed altitude is provided at the destination airport then the descent segment of the profile can not be built. This is usually a temporary situation that will be rectified when an arrival procedure is provided as the aircraft nears its destination. Under these conditions the algorithm will construct a default descent profile and provide only the destination parameters (fuel, time, etc.). This default descent will not be displayed and the descent path can not be flown.

**Holding patterns** The FMCS allows the pilot to attach a holding pattern to any flight plan waypoint. However, the predictions algorithm assumes that if they are more than three minutes ahead that the holding patterns will not be flown and therefore does not include the distance around the holding pattern as part of the distance calculation. As a holding pattern is approached and the three minutes to go point is reached, it is assumed that the aircraft will travel at least once around the hold and this is then included in the predictions distance calculation.

**Floating waypoints and special legs** Where special leg types have been inserted in the flight plan, by an arrival or departure procedure, predictions calculates the position of the termination point using the best information available. The point is inserted in the flight plan but, knowing that the point will move as conditions change, it is identified as a "floating" waypoint.

**Discontinuities** If the flight plan has a gap in it due to the insertion of a "manual" leg, the pilot is expected to fly the aircraft manually and predictions assumes (in the absence of better information) that the pilot will fly a great circle path from the waypoint preceding the manual leg to the waypoint that follows the leg.

### 2.2.3 Parameters predicted

Predictions will generate the following waypoints that define the vertical profile:

- Top of climb
- Top of descent
- Bottom of descent
- Climb and descent crossover altitudes (if below cruise altitude)
- Transition altitude (above which altitudes are displayed in flight levels)
- Cabin repressurization altitude
- Anti-ice on and off altitudes
- Climb thrust revision altitude
- Speed change points – airport restriction deceleration point, etc..
- "Floating" and special leg type waypoints – estimate of the position of the leg terminators.

For each vertical and lateral waypoint in the flight plan the following data will be generated:

- Curve path transitions - the path that the aircraft will follow when it passes a waypoint. The type of transition is based on the angle of the turn and whether the aircraft is required to overfly the waypoint or not. The radius of any turn is based on the predicted ground speed and the shape of the transition can vary from a "cut the corner" turn up to a 360° loop. Curve path transitions apply to lateral waypoints only.
- Fuel Remaining – Used for fuel planning and gross weight estimation.
- Estimated Time of Arrival – Used by RTA for time control.
- Altitude
- Speed

### 2.3 RTA function predictions

The Required Time of Arrival (RTA) function is a 4D navigation (time control) performance mode. This function uses the data provided by the cost index based economy predictions algorithm to estimate the time of flight for each of the remaining phases of flight up to a specified waypoint. A delta time of flight algorithm is used to estimate the additional time taken to travel to a specific waypoint for a different cost index. This "quick predictions" algorithm calculates the new cost index average ground speed for each of the phases of flight and generates a new time of flight by assuming that the time of flight in each phase is inversely proportional to the ratio of the flight plan average ground speed and the new cost index average ground speed. The RTA function uses an iterative cost index search method and the quick predictions algorithm to find the cost index that produces an "estimated" ETA that matches the pilot entered required time of arrival. This matching cost index is then used by the predictions algorithm as if it had been entered by the pilot.

## 3 FMCS Control

The FMCS is designed to be a fully integrated multi-axis aircraft control function. However, because of the size and complexity of the software involved, the FMCS usually contains only outer-loop control. There is a deliberate policy of segregating the flight critical functions such as inner-loop control and autoland in the relatively small (with regard to software size) autopilot/flight controls system and the autothrottle system. This segregation simplifies initial certification because the certification "critical" functions that require expensive dissimilar and redundant hardware, parallel software development and detailed documentation are concentrated in smaller units. This partitioning also was chosen to separate the functions that will rarely change (inner-loop) from the more subjective convenience functions which will evolve and build. This separation, therefore, means that the FMCS can be relatively easily re-certified when new capabilities are added after initial certification.

### 3.1 Control Interface

The FMCS does not have direct access to the aircraft control functions but interfaces through a number of other systems. This simplifies the FMCS control function and allows the pilot to over-rule the FMCS if manual flying is required without modifying the original flight plan and calculated profile. The pilot can return to FMCS control following an unforeseen excursion and continue with the original flight plan. The interface with the flight controls systems is decided by the aircraft manufacturer and is a function of whether the FMCS is being fitted into an all new aircraft or whether the FMCS is being retrofitted into an existing airframe with existing autopilot and autothrottle units. The aim is to reduce duplication of functions wherever possible. For this paper the control interface of the 737-300 and later derivatives is described. On this aircraft a roll command is used for the horizontal axis, the existing autopilot pitch axis functions are used for vertical control and the autothrottle is controlled by speed targets. Other aircraft types could use a different control interface (such as pitch targets in the vertical axis). The 737-300 control interface is described below:

**Autopilot and Flight Director System (AFDS)** This system provides interface to the aerodynamic control surfaces of the aircraft. The pilot has direct input to the system for heading select, altitude hold, vertical speed, etc.. modes. The pilot can operate the system without connecting it to the control surfaces by selecting the flight director mode and following the displayed vertical and horizontal cue bars. The FMCS input can be selected as an alternate vertical or horizontal control mode by selecting the LNAV or VNAV mode keys. With the FMCS in control the autopilot monitors the FMC input for signals outside the FMCS control authority, and will automatically limit authority or disconnect if necessary. The pilot can arm other autopilot modes such as autoland and these will become active, and the FMCS will be disconnected, if the required engagement conditions are met (e.g. ILS glideslope valid).

**Autothrottle** This system provides automatic speed control and protection regardless of environmental conditions. The autothrottle is closely coupled to the autopilot system and takes its speed control targets from the system that is controlling the aircraft. If the FMCS VNAV mode is selected and engaged the autothrottle is being controlled by the FMC.

### 3.2 FMC Control Modes

The FMCS has two major control modes; lateral navigation (LNAV) and vertical Navigation (VNAV). With both these modes selected and engaged on the AFDS mode control panel, the FMCS controls the aircraft in two dimensions horizontally, in altitude vertically and controls the speed target to give the forth control dimension, time. Within these major modes are sub modes which are a function of flight plan phase and are controlled or monitored by the pilot through the FMCS CDU. The FMCS uses a mode annunciator panel to display to the pilot the current active mode and submode at all times.

### 3.3 Lateral Navigation (LNAV) Control

The LNAV interface with the autopilot is a roll command. The FMCS has up to 30 degrees of command authority with a nominal internal maximum of 25 degrees of bank.

For aircraft control a reference path buffer (RPB) is constructed which describes the leg from one flight plan waypoint to another. This leg is divided into segments that describe the actual path that will be flown over the ground. The buffer may contain up to fifteen individual path segments which can be one of four types, these are:

**Straight segment** This segment represents a great circle path with a constantly changing track angle. While flying this segment the entire buffer is updated every 60 seconds to recalculate the termination of the current segment and the attributes of any future segments (curve radius, etc.). For this type of segment, every 200 milliseconds the control algorithm calculates a new desired track. To steer along this segment a roll command is generated that is a function of the lateral abeam distance from the aircraft to the current segment of the reference path called the cross track error (XTK) and the Track angle error (TKE) which is the difference between the current aircraft track and the desired track.

**Curve segment** A curve segment is defined as a start point, end point and a constant radius curve between them. This type of segment is used for curved path transitions, etc.. Once the aircraft sequences onto a curve segment the curve radius is not updated. As in the straight segment, the desired track is constantly recalculated based on a constant radius curve. The radius of curve is calculated using current aircraft speed and a nominal bank angle. The resulting TKE and XTK are used for steering control.

**Heading segment** Is a straight path that maintains a constant heading along the segment. This segment type is updated every 60 seconds. The steering control for this type of segment is a simple function of the difference between the current aircraft heading and the desired heading from the flight plan (heading error). This means that the aircraft may drift laterally from the originally designated path and as this drift is propagated along the remaining segments, the position of the flight plan waypoint at the end of the leg (always a floating waypoint) will be moved.

**Track segment** Is a straight path that maintains a constant desired track on the ground. Like the heading segment the roll command is a function of TKE only. If there is no wind the heading segment and track segment are equivalent.

A reference path buffer is generated from the flight plan leg by translating the leg into a series of guidance segments. The number of segments can vary from two (a straight and a curve) for a simple leg between two waypoints, to fifteen for a holding pattern consisting of an entry path, the hold itself and the hold exit path.

A reference path buffer for the next leg in the flight plan is also generated so that a new buffer will be available when the waypoint is sequenced.

If the aircraft is off the flight plan when LNAV is first engaged the control algorithm will attempt to construct a capture path between present aircraft position and the flight plan. The capture leg will be constructed only if one of the following conditions are met:

1. The aircraft is within three nautical miles abeam of the current reference path segment, regardless of the present aircraft heading or track.
2. The aircraft is beyond the 3 nautical mile capture band but present aircraft heading will cause the aircraft to intercept the flight plan between present abeam point and the waypoint that terminates that leg. In other words, the aircraft is pointing back towards the flight plan. Under these conditions the aircraft is allowed to maintain its present track until it intercepts the path.

If the above capture criteria are not met, and LNAV engagement is attempted, a "NOT ON INTERCEPT HEADING" message will be displayed on the CDU.

There are a number of special flight plan situations that require extra translation processing when a reference path buffer is generated. Some examples are described below:

**Holding patterns** A holding pattern can be entered into the flight plan at any existing waypoint or at present position (PPOS). If the hold is rotated about the hold fix such that a special entry procedure is required, this is included in the buffer. An example of the breakdown of the segments in a holding pattern is shown in figure 2. It shows a hold with a "parallel" entry.

**Bypassed waypoints** If two waypoints are close and in such a relative position that the aircraft can not turn quickly enough to reach the second waypoint, then that waypoint is designated a "bypass" and the RPB for the two legs are combined into one and the aircraft is flown as close as possible to the second waypoint.

**ILS localizer capture** If the leg is designated as a localizer approach then the steering algorithm enters a special mode that allows it to sequence onto the glideslope early or late regardless of the path in the RPB. Once the aircraft sequences onto the glideslope intercept leg and is within 3 degrees of the runway centerline or 17 NM from the runway threshold (ILS coverage area) then the raw glideslope data is monitored. If the glideslope centerline is reached before the predicted glideslope intercept point, then steering will sequence the segment early. If, however, the aircraft reaches the predicted intercept point before glideslope capture is confirmed by the raw ILS beam data, a localizer capture path is generated which is a track segment with a track angle of the runway extended centerline plus or minus an appropriate intercept angle. This path is flown until the raw glideslope centerline is reached or the aircraft flies outside the predicted glideslope beam coverage boundaries.

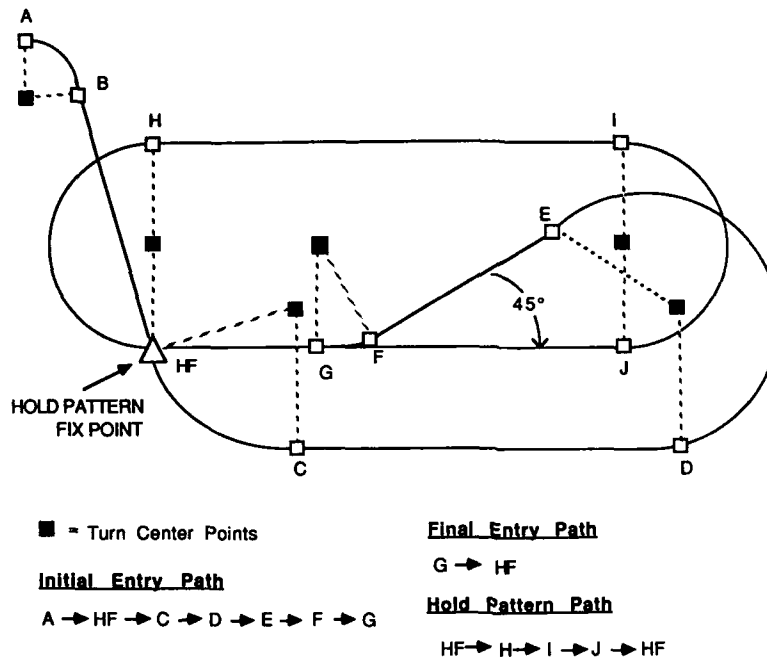


Figure 3: Reference path buffer segments of a holding pattern

### 3.4 Vertical Navigation (VNAV) Control

The VNAV mode of the FMCS uses existing modes of the autopilot *wherever possible so that inner loop control laws are not duplicated*. The FMCS uses mode selection and targets to duplicate the pilot entered values for the selected mode. Different modes are used in different phases and sub-phases and these are described in section 3.4.2

#### 3.4.1 VNAV interfaces

When in VNAV mode the 737-300 FMCS interfaces with the autopilot and autothrottle using the following output parameters:

- Autopilot mode requests - used to change the autopilot control mode including the following:
  - VNAV valid - Tells autopilot whether VNAV can be engaged or not
  - Vertical Speed mode request
  - Speed on elevator mode request
  - Altitude capture mode request
  - Altitude hold mode request
  - Level change mode request
- Vertical speed target - primary climb and descent control parameter
- Altitude target - used for altitude capture and altitude hold modes.
- Autothrottle mode requests - changes autothrottle modes
  - Speed mode request
  - Idle mode request
  - Level deceleration mode request
  - Thrust limit mode request - for each phase
  - T/O or Climb derate mode request
  - Derate thrust cut back required

- Engine-out mode request
- CAS or Mach identifier
- Speed target - either CAS or mach as appropriate
- Thrust limit values - for each flight phase

The FMCS receives back from the autopilot and autothrottle systems current active mode information and the current setting of the Mode Control Panel (MCP) altitude select window. This MCP window value is used by the pilot to control climb and descent by defining the altitude limit through which the aircraft must not pass. The pilot will set this window to the next clearance altitude above the aircraft in climb and below the aircraft in descent.

### 3.4.2 VNAV phases

When engaged in the VNAV mode the FMCS uses different modes for different phases of flight. A description of the interaction is described below:

**Take off and Climb phase** While on the ground the pilot can preselect, through the FMCS CDU, a derated take off thrust and special climb thrust profile. This is desirable at certain airports if environmental conditions permit, so full thrust is not used. If derate is selected, the FMCS will transmit reduced thrust limits to the autothrottle.

After takeoff the pilot selects desired climb performance option, which can be any of the following:

- Economy - The default performance option that uses the CI to calculate the most economical target speeds.
- Maximum angle - The FMCS calculates a target CAS that causes the aircraft to climb at the steepest angle.
- Maximum rate - The FMCS calculates a target CAS that causes the aircraft to climb at the highest rate of climb.
- Engine out - If an engine fails during climb the pilot can select an engine out climb with a speed target that maximizes climb gradient.
- Selected speed - The pilot can enter a specific speed that the aircraft will fly.
- Required time of arrival - The FMCS calculates the most fuel efficient speed target which meets a time constraint at a future waypoint

As soon as VNAV is engaged the FMCS selects the autopilot speed on elevator mode and sets the desired speed output dependent on the performance option selected. In this mode the autopilot controls the rate of climb so that the aircraft maintains the desired speed. The autothrottle is set to climb mode with a maximum thrust value equal to the limit supplied by the FMC. If a derated climb profile has been preselected the FMCS will modulate the limit in accordance with a predefined schedule. The FMCS will set the target altitude to the cruise altitude or the next waypoint altitude constraint if one exists. As the aircraft approaches that altitude the autopilot will automatically transition into altitude capture mode and then altitude hold at the requested altitude. The autothrottle will transition into speed mode at the FMCS target speed. If the level off is due to a waypoint constraint the aircraft will remain in altitude hold until the waypoint is sequenced and the FMCS will raise the FMCS target altitude to the next constraint and change the autopilot mode back to speed on elevator to continue the climb. If, however, the autopilot approaches the MCP window altitude the autopilot will capture that altitude regardless of the current FMCS target. The pilot is then required to select a higher altitude and reselect VNAV to continue the climb.

**Cruise phase** The cruise phase is flown in autopilot altitude hold mode and the autothrottle in speed tracking mode using the FMCS target mach output. During the cruise phase the pilot can climb to a higher altitude or descend to a lower altitude using the cruise climb or cruise descent modes. This is simply accomplished by selecting a new altitude in the MCP altitude window and then entering the new cruise altitude on the cruise page of the CDU. A cruise climb request will result in an autopilot speed on elevator mode at FMCS target mach and climb thrust on the autothrottle. A cruise descent request will cause the FMCS to request a vertical speed on elevator mode at -1000 ft/min and the autothrottle will maintain the FMCS target mach. The default FMCS target mach, economy, is based on the CI derived optimum speed. The pilot can select an alternate long range cruise mode or engine out mode if required and the FMCS will select the optimum mach target for those conditions. The pilot can also manually select a mach target.

**Descent phase** Descent is the most difficult phase for the FMCS to control. To maximize fuel efficiency the engines must be set to idle (minimum fuel flow). Slowing the aircraft down under these conditions requires the use of speed brakes which normally can only be operated by the pilot. The pilot can preselect one of two descent modes:

**Path descent mode** In this mode the FMCS controls the aircraft to a predefined profile constructed by predictions. When the aircraft approaches the top of descent point the pilot can, after gaining clearance from ATC, select a lower MCP window altitude. When the T/D point is reached the FMCS will set the altitude target to the first descent constraint and request a vertical speed on elevator mode for the autopilot. The

	ACT RTA PROGRESS	2 / 3	
	RTA WPT		RTA
1L	EPH	1012:00Z	1R
	RTA SPD	TIME ERROR	
2L	250/.633	EARLY 01:30	2R
	RECMD T/O	GMT	
3L	0909:21Z	0858:30Z	3R
	DIST-----TO EPH	-----ETA	
4L	125NM	1010:30Z	4R
	FIRST--T/O WINDOW--LAST		
5L	0900:30Z	0910:30Z	5R
	-----		
6L	<LIMITS		6R

RTA Progress Page (On-ground)

	ACT RTA PROGRESS	2 / 3	
	RTA WPT		RTA
1L	EPH	1012:00Z	1R
	RTA SPD	TIME ERROR	
2L	250/.633	EARLY 01:30	2R
	SPD REST	GMT	
3L	220/HOLD	0900:30Z	3R
	DIST-----TO EPH	-----ETA	
4L	120NM	1010:30Z	4R
	FIRST--RTA WINDOW--LAST		
5L	1008:23Z	1010:30Z	5R
	-----		
6L	<LIMITS		6R

RTA Progress Page (In-air)

Figure 3: On-ground and In-air RTA CDU display pages

autothrottle mode is set to idle (or high idle if anti-ice bleeds are being used). The FMCS then modulates the target vertical speed to match the descent profile. The profile descent gradient is based on the speed defined by the selected performance mode. The default mode is economy (from cost index), although the pilot could have entered a manual speed while in cruise and flown the resulting gradient.

The profile has built into it any level-off segments that are required to meet waypoint constraints or the airport restriction speed; therefore under normal conditions the FMCS can control the aircraft along this profile without deviating from the predefined vertical speed schedule. If, however, the aircraft drifts above or below the path (due to unpredicted winds) the FMCS must compensate using the limited control available. If the aircraft drifts above the path the FMCS will increase the vertical speed target and allow the airspeed to build. As the speed exceeds an acceptable deviation the pilot is requested (via a CDU message) to apply the speed brakes and slow the aircraft down. If the aircraft drifts below the path the FMCS will use the vertical speed target to return to the path which will cause the aircraft to slow down. As soon as the speed deviation exceeds an acceptable limit (15kts) the FMCS will request the autothrottle to temporarily transition into speed control mode and return the aircraft to the speed target.

If the aircraft drifts too far above the target speed (as would happen if the pilot did not apply the speed brakes) and approaches the aircraft structural limits the speed will be limited by the autopilot and the aircraft will deviate from the path.

**Speed descent mode** If a predefined descent path is not available the FMC will revert to a fixed speed or airmass descent mode. In this mode the FMC will control the descent using the autopilot "speed on elevator" mode. The autopilot modulates the descent rate to match the FMCS generated target speed without regard to the predictions profile. The pilot can also select this mode as an alternative to path descent. The target speed used in this mode defaults to the economy speed from CI although the pilot can override this by manually entering a speed.

In speed descent the FMCS puts the autothrottle into idle mode.

### 3.4.3 Required Time of Arrival (RTA - 4D)

The RTA function allows the pilot to designate a time of arrival (the required time) at a specified waypoint in the flight plan. The RTA function does not generate speeds directly but interfaces with the rest of the FMCS using the CI. When the pilot enters a RTA time the RTA function selects a new CI that will result in an ETA at the designated waypoint that meets the entered Required Time of Arrival.

In the air, the RTA function will recalculate the CI whenever the predicted ETA from the flight plan drifts outside a control limit. In addition to the RTA time the RTA function provides the pilot with maximum and minimum achievable times based on the maximum and minimum CI values. These times are displayed to the pilot so that he knows the FMCS time control authority limits.

On the ground the RTA function generates an advisory display page that identifies the earliest and latest take off times and also the most economical take off time based on the entered cost index. A time error display counts down the time until the first take off time.

Figure 3 shows a typical on-ground and in-air RTA progress page.

A typical operational scenario for the RTA function would be for the pilot to be assigned, by ATC, a waypoint that has been designated as the destination airport metering fix. This waypoint is used to control the flow of aircraft to the airport and the aim is to have the aircraft arrive at that waypoint in the same sequence as they will land. The ATC computer will assign a time at which each aircraft should arrive. An aircraft equipped with a RTA FMCS will be able to enter that assigned time and tell ATC the exact time the aircraft should take off to achieve that time. In addition, while flying in the RTA mode the pilot can tell ATC whether a revised RTA time is achievable or not.

## 4 Conclusion

The addition of powerful and flexible computing systems like the Flight Management Computer System to the cockpits of latest generation air transport aircraft has reduced pilot workload and increased safety. In addition, the optimization of flight profiles has increased fuel efficiency of the aircraft and increased the comfort level of the passengers. The recent addition of the Required Time of Arrival function has the potential for reducing flight delays despite the current air traffic build up. Studies also suggest that the addition of an RTA capability in only a limited number of aircraft would reduce air traffic control workload.

In the future, increased miniaturization coupled with increased computational throughput will allow FMCS manufacturers to pack more and more capabilities into smaller and smaller units. Concepts such as artificial intelligence may make the system easier to operate. Direct satellite communications will increase the accuracy of the FMCS by providing a way of trading information about environmental conditions such as wind and temperature, and flight plan changes such as airport closures and alternative airports.

Just as personal computers have revolutionized business and personal work habits so the FMCS and derivative systems will revolutionize the cockpit of the future.

IMPACT OF NEW TECHNOLOGY ON OPERATIONAL INTERFACE:  
FROM DESIGN AIMS TO FLIGHT EVALUATION AND MEASUREMENT

by

J.J. Speyer and C. Montell  
Operations Engineering, Flight Division  
Airbus Industrie, B.P. 33, 31707 Blagnac Cedex, France

and

R.D. Blomberg  
Dunlap & Associates Inc  
17, Washington Street, Norwalk, Connecticut 06854, USA

and

Dr J.P. Fouillot  
Laboratoire de Physiologie  
Faculté de Médecine, Cochin,  
24, Rue du Faubourg St-Jacques, F-75104 Paris, France

SUMMARY

Since the early 1980's Airbus Industrie has conducted a progressive research programme investigating the ergonomic, physiological and psychological factors affecting flight crew in their working environment, and progressively refining the data acquisition and analysis techniques.

This self-imposed commitment to a dedicated appreciation of man-machine aspects was met in two ways:

- . Informally, by stringent application of human engineering principles, although in short supply in as far as their explicit formulation is concerned,
- . Formally, by continuous development of statistical methods and engineering experiments, concentrating on pilot questionnaires, performance evaluations and workload models.

Although the title of this paper may not seem to be directly related to the topic addressed by this Agardograph a statistical workload calculation model will highlight the insidious link that enables to correlate pilot performance parameters (and hence aircraft trajectory) with estimates on the impact of new technology on the operational interface. The purpose of this paper is to review the span between initial design aims and subsequent flight evaluation and measurement.

Except for the general recommendations of Fitts, Wanner, Wiener and Curry, few fundamental design guidelines appear to be available in the scientific field of human factors. A practical review is presented of the operational objectives and technological modules that marked the outgrowth of the Airbus family of commercial aircraft. Progressively integrated, several waves of innovations engineered an evolutionary process that brought to bear growing functionality at the operational interface. The emerging role of the pilot is becoming more that of a systems monitor than that of a controls handler, devoting himself to overall intelligence functions which new technology features were precisely aimed to support. Several contemporary human factors views are mentioned in the paper suggesting that the pilot be brought back into a more active role to avoid automation- or design-induced errors. What has been achieved with the early 1980's A310/A300-600 cockpit however is, in our view, still in the vicinity of the Wiener and Curry philosophy on automation and cockpit design. In the step that was to be taken in the latter 1980's A320/A330/A340 designs aims have been intended to cover even more error-tolerance or -protection against incidents of the Wanner scheme.

Reviewing aircrew comments on design aims and achievements from flight evaluation became a practice in the early 1980's when soliciting crewmember opinions received considerable impetus. Conclusions are presented from questionnaire surveys on new technology aircraft conducted successively by Airbus Industrie, Wiener, Curry and Lufthansa. Commonly criticized on most new aircraft types are the autopilot/autothrottle interactions and the FMS whose training definitely needs more emphasis on basic know-how and practice. It appears that crews want automation even further developed to improve system integration and crew interface, with no significant fear for the possibilities of errors or potential loss of flying skill. But what also seems to be requested is intuitive design allowing the pilot to understand more straightforwardly

the automation systems at work and to monitor more easily their performance, limits and crew errors. Measuring the impact of new technology on the operational interface could precisely help setting up this human factors capability. Which in turn should eventually influence on design guidelines and specifications.

The success of the questionnaire technique prompted Airbus Industrie to use it again for its Fly-by-wire proof-of-concept experiment on the A300 testbed. The unanimous enthusiasm of airline & authority pilots for the sidestick/fly-by-wire combination was also confirmed by the fact that, as a group, they did not feel uncomfortable with the idea of being primarily responsible for the management of system interfaces rather than the direct operation of their aircraft. It would appear indirectly from these studies that older technology aircraft can more often be discredited on the basis of human factor principles than new ones. It is however with the coming of the latter that more emphasis was gradually put on human factors by all those concerned, manufacturers, airworthiness authorities, pilots and airlines. Even more systematic efforts on man-machine interface analyses were put in the wake of the crew complement question which triggered the development of several evaluation methods. One of these, the Performance Criteria Methodology, was developed to statistically investigate the impact of new technology features such as the EFIS, the FMS and Fly-by-Wire/ Sidestick. A brief review is given of engineering experiments' results for the first two to conclude on the contribution of this equipment towards improving smoothness of performance and alleviating workload. The advantages of a FbW system over conventional controls are operationally demonstrated with the third experiment. Performing analysis of variance on basic flight parameter measures allows again to demonstrate marked smoothness and stability improvements, flight efficiency, reduced task- and workload.

Our previous research suggested that workload ratings collected in minimum crew certification campaigns might be modelled using data extraneous to the pilot (aircraft flight performance parameters and flight status measures) and data intraneous to the pilot (heart rate variability measures). The aim was to achieve an objective analysis of an until-then subjective process (workload rating) which had received too little scientific attention. A computer model was evolved from the A310-200 certification process, which indeed conformed well with the subjective data. Certification of the A310-300, a generally similar but sufficiently different aircraft, provided a further check on the degree of objectivity attained, helped to simplify the model's formulation. As part of the development program for the A320, the A300 FbW flying testbed had numerous visiting pilots involved in extensive demonstrations as well as special manoeuvres such as simulated engine failure at take-off and a demonstration of the inherent stall protection of the control system. The model was again successfully applied to these flights in order to determine if it could cope with the new control system and the unusual profiles. Finally, the very first flight of the A320 also had both pilots equipped with heart rate monitoring equipment so as to test the model.

Cleared for experimental use, the Airbus Workload Model was then used in January 1988 for the A320 Minimum Crew Certification to generate second-by-second estimates of pilots' subjectively estimated workload. The purpose of this demonstration was to provide a range of low to high workload situations by means of 12 scenarios which provided varying flying problems. In all, 48 simulated line flights, which involved different levels of automation, were flown. Crew errors were also recorded and classified according to their severity and awareness. As a tool to investigate the impact of new technology, the Airbus Workload Model presents a novel opportunity to study workload and its relationship to both errors and automation. The findings are descriptive in nature because the certification data base was not constructed to support research on these issues. But they suggest that there is a relationship between the severity and type of error and workload, and that automation and workload are inversely related.

## 1. INTRODUCTION

Recent breakthroughs in display and control avionics constitute one of those remarkable technological milestones that from time to time will spur aircraft development and airline operations. Whether in technical areas or operational functions trade-offs between continuity and progress have steered the design and deployment of the Airbus family of aircraft. In particular, cockpit development has directly proceeded from a permanent process of monitoring new technology availability and problems, and of evaluating how best to improve the pilot's working environment within realistic airline constraints (economics, maintenance, training, ATC, human resources etc.). The drive of this adaptation and integration process through technology leaps and systems' interfacing ambitioned the eventual inclusion of the human operators in the safety loop, a goal long sought in the profession. While economic effectiveness and industrial feasibility were most important factors to be considered between possible solutions, the safety imperative has always been the prime parameter nonetheless.

In direct conjunction with this, Airbus Industrie has conducted an important research programme from the early 1980's onwards, gradually investigating the ergonomic, physiologic and operational factors affecting flight crew in their working environment, and progressively refining the data acquisition and analysis techniques (Speyer J.-J., Fort A., October 1982).

Underscoring the necessity to consider human factors issues in a broader systemic context was an early paper in 1977, titled "Controlled Flight into Terrain: System-Induced Errors" (Wiener E.L., 1977). The contradiction suggested in this title aims to indicate the difficulty for integrating two levels of system management: aircraft control (inner loop exercising psycho-motor skills) and aircraft monitoring (outer loop demanding cognitive abilities). The evolution of flight deck automation up to front line aircraft types of that time period (B-747, DC-10, L-1011, A300 B2/B4) was commented by Edwards (Edwards E., 1972 ; 1977) as owing much more to engineering and economic analyses than to ergonomics and systematic development of policy concerning the role of men in automated systems. Stressing the failure of the human factors profession to play a more significant role in the design process Wiener and Curry addressed the following operational interface aspects:

- vigilance problems and crew overload/underload,
- inadequate workplace design and extra-cockpit communication,
- faulty pilot-controller communication and crew coordination,
- unadapted, excessive or wrong automation,
- unheard or cancelled warning devices and visual illusions,
- confusing terminology and charts.

In the aviation transport area alone, some 75 % of accidents are amorphously catalogued as pilot error, the remainder being evenly split between purely technical and environmental causes. Their point here is that a majority of these accidents are design-induced referring to human engineering concepts (Wiener E.L., 1977), air traffic control (Wiener E.L., 1980) and automation (Wiener E.L., Curry R.E., 1980). Few fundamental design guidelines are available in the scientific field of human factors. They all appear to come "a posteriori" illustrating that this activity is an art in infancy. Except for the general human factors guidelines of Fitts, Wanner, Wiener, Curry and Nagel, we are short of standards sought by the industry since it is still evolving at a rapid pace (Fitts P.M., 1951 ; Wanner J.-C., 1969, 1984, 1989 ; Wiener E.L. and Nagel D.C., 1988). It is not really feasible to apply these at the technical design stage, but it was thought that the opposite approach, i.e. "a posteriori" evaluation and measurement of the human factors impact of new technology, would eventually benefit future design conceptions. Each new design should nonetheless command its specific human factors approach & analysis the results of which guidelines cannot dictate nor predict.

An "avant la lettre" human factors orientation gradually emerged from Airbus' partners and customers' collective memory of jet aircraft design and operating experience to date. Somehow, the systemic inclination that such an approach warrants mirrors the evolution towards functional/organizational matrix organizations at partners' design offices themselves. And by the same token it reflects Airbus' industrial marketing approach, which traditionally keeps its customers involved from the start of the design process through so-called task forces (Schmitt B., October 1984, Caesar H., November 1985). Fulfilling its role at the heart of this process, Airbus Industrie was all set for a judicious assessment of needs, requirements and capabilities and for a proper formulation of realistic design aims.

## 2. TECHNOLOGY EVOLUTION AND DESIGN AIMS

The forward facing crew cockpit of the A310 and A300-600 stems from A300 B2/B4 experience which itself proceeds from that of the Caravelle, Trident, BAC 1-11, VFW-614 and Concorde. In fairness to all, it is also a direct result of multiple discipline research programmes that included a human factors orientation such as the NASA Terminal Configuration Vehicle, the French Persepolis project and the BAE Advanced Cockpit Design.

Early consideration had been given to making the original A300 a 2-pilot crew aircraft. The technology then available did not permit such an approach with the necessary degree of confidence; the overall design goal being to ensure adherence to the "need to know" and "fail safe" principles which the 1970 to A300 cockpit did not fully satisfy:

- . side panel not fulfilling fail-safe criteria,
- . number of dials and displays giving unnecessary information during a large part of the flight,
- . necessity to scan in different places.

The innovations of this first wide-body proved a major credit to Airbus:

- automatic throttle (ATS) from brakes off to touchdown,
- automatic angle of attack protection and speed reference system (SRS), both being instrumental against windshear incidents,
- automatic two and one-engine go-around;
- thrust computer (TCC) linked to autothrottle, allowing derated engine operation/increased engine life.

The necessary evolution became possible in the early 1980's with the help of technology leaps providing concentration, standardization and flexibility (Baud P. and Ivanoff D., 1982). Design goals of the FFCC were then formulated as follows:

- . better crew integration and crossmonitoring,
- . better man-machine interface,
- . lower risk of flight/system management error,
- . automation of routine actions,
- . simplification of tactic actions in normal, abnormal and emergency procedures,
- . augmented availability for strategic flight actions,
- . clear presentation of predigested information for easier and quicker diagnosis and correction,
- . reduction of crew workload.

A definite consolidation trend developed as from the late 1980's with A320 design aims to be carried forward for A330/A340 projects (Ziegler B. and Durandeau M., 1984):

- . extension of pilot error-tolerance, -detection and -protection by safeguarding functioning points and operating envelopes,
- . continuing developments in digital technology and data transmission focusing on systems integration,
- . former FFCC breakthroughs refined and kept as mainstays for the future.

Progressively integrated, three successive waves of adaptive innovations have engineered a cascade evolutionary process that brought to bear growing functionality at the operational interface level (Speyer J.-J., September 1988).

The following modules were hereby successively introduced three by three:

- pushbuttons combining control, visual feedback and malfunction alert so as to reorganize cockpit real estate and enable systems management from an overhead-mounted panel, synoptically arranged (source to distribution) according to frequency of use (normal, abnormal, emergency),
- advanced system automation to avoid repetitive actions in normal operation or after a single failure (electrical, APU, fuel, pressurization, avionics cooling, air bleed, electronic engine control etc.),

- digital autoflight systems (AFS) with preselected functions, increased integration of guidance modes with autothrust (ATS) and flight director, clear and unambiguous operation, improved flight envelope protection and automatic landing potential to Cat III,
- cathode ray tubes for quantitative and qualitative monitoring of system's status in coordination with flight phases (ECAM):
  - . eliminating the need for frequent overhead panel scanning in normal conditions,
  - . applying a rigorous cockpit lights out philosophy, the absence of visual warnings corresponding to normal conditions,
  - . simplifying failure understanding (System Display) and orientation of corrective actions (Warning Display),
  - . reducing the number of discrete sounds to a bare minimum, basic attentions drawing the attention of the crew to warning display messages,
  - . adapting warnings to flight phases with inhibitions where safety mandates,
- electronic flight instruments (EFIS) replacing electromechanical ADI's for short term flight path control (PFD) and replacing HSI's for medium term navigation (ND) allowing direct access to predigested information by means of situation-adapted symbology,
- digital flight management systems (FMS) to command the autoflight system for full horizontal and vertical navigation and guidance with profile optimization for maximum economy,
- fly-by-wire in conjunction with sidesticks replacing mechanical flight controls to simplify conventional chains, extend flight envelope protection to include stall, windshear, manoeuver or attitude exceedances, transfer of command,
- full authority digital engine control to extend engine operational protection and to provide a wide array of power management functions,
- digital radio management panels to manage the frequency selections for all VHF, HF and SSR radio communications as well as ILS, VOR and DME radio navigation aids in case of FMGS-failure.

The first three modules characterize the mutation of the A300 towards the A300FF, the ensuing A310 being supplemented by the three following and the subsequent A320 being supplied with all nine.

### 3. DESIGN GUIDELINES AND PILOT ROLE

One of the more established principles particularly insists that man and machine should be used in complement to each other and according to respective areas of specialization.

Fitts Lists (Fitts P.M., 1951) indeed provide tips for the differentiation of tasks between man and machine recognizing human superiority with regard to overall intelligence, decision-making, error-correction, inductive reasoning and gradual overload.

Machines on the other hand would cope better with sudden overload, are much faster, consistent and powerful, good at deductive reasoning, better at complex computation and short-term memory. They also do a better job at monitoring, having no problems with concentration, motivation, vigilance, distraction and fatigue.

Developing his argumentation with regard to human factors and flight safety, J.C. Wanner (Wanner J.-C., 1969, November 1984, August 1987, March 1989) considers three classes of incidents that may be playing a pivotal role in aircraft mishaps:

- . pilotability incidents whereby the crew erroneously allowed the functioning point outside the authorized envelope with difficult or impossible reversion,
- . perturbation-sensitivity incidents whereby external (e.g. windshear) or internal perturbations (e.g. failures or fire) let the displaced functioning points go beyond limits, whether limits after perturbations are new or unchanged,
- . manoeuvrability incidents whereby the execution of a procedure (e.g. to modify trajectory or avoid obstacle) and the displacement of the functioning point as a result of incidents of the two preceding types brings the resulting functioning point closeby or past its limits.

Wanner identifies 5 basic human attributes that allow to derive a set of 8 proposed design rules covering pilotability incidents. Perturbation-sensitivity and manoeuvrability rules are in his view more of a regulatory nature, do not implicate the human operator as such but rather system redundancy and integrity and operational knowledge of mission and environment.

Wiener and Curry conclude their survey of cockpit automation and flight safety by proposing 15 recommendations for designing and using automated systems (Wiener E.L., Curry R.E., 1980). In need of a philosophy regarding automation they have persistently advocated the respect of at least three principles (Wiener E.L., October 1985):

- . to allow the crew more freedom to fly the plane and use automation in the manner it wishes, but surrounded by a multidimensional warning and alerting system that informs the crew if they are approaching some limit; as long as within the limits the crew would have freedom to conduct the flight according to its style; this concept of "an electronic cocoon" is called flight management by exception,
- . to use forecasting models and trend warnings to predict a penetration of the cocoon rather than waiting for it to happen and alarms to be activated when the system reaches a critical point; in order for the crew to have maximum control of the situation, values for the forecasting parameters could be selected by the crew; this concept is called exceptions by forecasting,
- . to allow the crew to inform the machine of its strategic goal or intent which would allow the computer to check crew inputs and system outputs to determine if they are logically consistent with the overall goal; if not an exception message would be issued; this concept is called goal sharing.

The evolution of the pilot's role is inevitably linked to that of the aircraft and its cockpit, triggered as it has been by economic and technological imperatives. Persistently, the pilot's role is now being compared to that of a manager. It may therefore be beneficial to reflect on what flight management entails from an organizational point of view (Speyer J.-J., October 1986).

Three levels can be considered as illustrated in Figure 1:

- . the strategic management level, which is the process of deciding on goals of the mission, on changes in these goals as a function of constraints, on the resources used to attain these objectives (for example evaluate and decide to perform a Cat II approach),
- . the tactical or functional management level, which is the process by which functions assure that resources are programmed, selected and used effectively and efficiently in the accomplishment of mission goals (for example planning and preparing a Cat II approach),
- . the operative or implementative control level is the process of assuming that specific tasks are carried out effectively and efficiently (for example execute and monitor a Cat II approach).

The task-related level is almost exclusively handled by computers and automation. No longer is the pilot just a simple controller or monitor. Rather, he dialogues with the aircraft, giving direction to the different systems and devoting himself to overall intelligence and general direction of his flight. Presented in this way the functional level is at crossroads between the crew and the aircraft, it is the interface level. The pilot's enlarged role as flight manager, systems supervisor and computer monitor centers around the four cognitive functions of planning, programming, maintaining and thrusting (Babcock G.L., Edwards W.W., Stone R.B., October 1982):

- . planning is a dynamic function that is never completed fully accurately and continuously involves mental representation and decision-making (models/pattern-matching, strategic evaluation, forecasting, risk-evaluation). The Navigation and Profile modes of the FMGS can be very effective in assisting in the planning of an arrival, the advisory mode of the ECAM is instrumental for forecasting,
- . programming is an anticipatory set-up function allowing systems to be instructed ahead of actual aircraft operation. Representative examples exist with pressurization and FMGS selections,
- . maintaining is a control function to manage system and subsystem failures and to monitor necessary back-up whether manually or automatically implemented. The overhead panel, its flight management by exception through the cockpit lights out philosophy and the overall ECAM system help to exercise this function,

thrusting is an active monitoring function requiring intelligence, understanding, patience and confidence to allow automation to operate without intervening. Goal sharing or the ability of the crew to communicate with the machine on its strategic mission goal or intent is of particular importance in thrusting. Monitoring navigation or approach progress through EFIS and FMGS are typical examples of this function.

Interacting with task- and mission-related flight elements, the contemporary pilot must be proficient in quickly and efficiently managing all available resources within a constrained working environment. New technology features were precisely aimed at supporting the above-mentioned interface functions of planning, programming, monitoring and thrusting.

Directing an automatic system rather than doing the job manually and coordinating with the other crewmember commands skills supplementary to those required in conventional cockpits. Supplementary since the skilled aviator still needs to remain proficient in manual handling in spite of much more frequent reliance on automatic modes. Airlines do insist however that pilots make full use of the automation offered in the modern cockpit. Manual flying for training purposes is being encouraged during routine operations. Mollet (Mollet C., February 1988) contends that "the laws governing the whole behaviour of (new technology) flight guidance systems are so complex that they are no longer (fully) transparent to the pilot". Not helping cockpit management, manual flying definitely has to be supplemented by good systems knowledge, by intuitive understanding of computers behaviour and limitations and by strict crew-coordination discipline when having to manage complex situations. Any feeling of "being along for a ride", ideas of underload, lack of vigilance, boredom and complacency, any sense of "being out of the loop" needs to be properly addressed by means of cockpit management techniques that help to foster the attitude that automation is just another resource to manage (Speyer J.-J., Fort A., October 1987).

While at NASA, John Lauber (Lauber J.K., March 1980 and August 1982) emphasized that the major impact of the inclusion of microprocessor and display technology in new generation transport aircraft would be the quality and quantity of real-time information available to the crew and the way this information would be manipulated and used to conduct a flight. As a result of previous accidents with conventional technology aircraft attributable to shortcomings in crew communication and coordination, the NTSB did recommend that the FAA urge operators to indoctrinate flightcrews in the principles of flightdeck resource management.

Pointing beyond the sterile cockpit, Wiener insists (Wiener E.L., 1985a) however that the evolution whereby pilots gradually began to serve as monitors of automatic devices must be reconsidered. In his view, shared by others, the pilot should be brought back into a more active role in the control loop to sustain alertness especially in view of very long range operations (Wiener E.L., August 1986). The vast literature on vigilance has indeed shown that the human, after all, is not a very effective monitor, less likely to detect system fault or wrong set-up, more likely to commit large blunders. For this reason, the famous doer versus monitor doctrine-placing the pilot rather as a monitor than as a doer- is being revisited. A recurrent theme, the implications with regard to design philosophy for control and monitoring systems being (Wiener E.L., Curry R.E., 1980):

- that the designer must specify to what extent the human should be included in the inner (aircraft control) and outer (aircraft monitoring) control loops and to what extent automation should assist him in multi-attribute decisions,
- that the designer must consider the single channel behaviour of the human and the integration of the numerous devices, alerting and warning systems and conditions to be monitored.

Potentially weak vigilance of the pilot and vulnerable aircraft systems suggest a growing need for the machine to monitor itself and the operator, diagnosing errors performed by the human. This well-identified need to develop automatic systems that monitor human operator performance rather than only the reverse has also been suggested in the aerospace medical world (Mollard R., Ignazi, October 1986).

Pelegrin, on the other hand (Pelegrin M., October 1986 ; September 1988), advocates increased automation, using new technology to include:

- automatic reconfigurations after failures,
- ongoing maintenance and systems status back- and updating,
- pilot assistance in abnormal situations not necessarily resulting from failures,
- crew error-tracking capabilities and crew interrogation systems.

He concludes from a detailed analysis of 7 accidents that their catastrophic outcome would have been avoided, should these (older technology) aircraft have been designed

with only slightly more automation just compatible with the level of technology then available. Pelegrin also advances that if automatized systems are going to enjoy further development the ensuing frontier between man and machine and the resulting tasksharing between both will imply the sharing of intelligence and knowledge of their interactions. Increased automation will therefore only be successful if non-deterministic human characteristics can be taken into account by means of Human Factors, (fuzzy-set) Behavioural Models and Artificial Intelligence.

In opposition to this, semi-automatic systems as they are known today: after a system failure the aircraft remains partially automatic and according to the incident the pilot may or may not have to take over, may or may not have to change operating modes. Conflicts sparkling from this duality and the need to maintain a permanent man-machine dialogue have led to the notion of operator assistance to better close the information loop and complement both operator and machine intelligence.

The error-protection capabilities of map-displays and fly-by-wire flight controls mentioned in the previous paragraph have somewhat paradoxically been accompanied by a renewed interest for error-tolerant systems as safety nets. Extensive analysis on human factors has revealed (Gerbert K. and Kemmler R., 1986) that -whether systematic or random- these can be interpreted as a four-dimensional structure: vigilance errors, perception errors, information-processing errors and sensorimotor errors. In particular, it was found that determinants and background variables of human factor incidents and accidents provide a model of basic man-machine system interaction which are useful and predictive of human error occurrence.

Seifert and Brauser have proposed two strategies for future flight deck design (Seifert R. and Brauser K., May 1983) equating the pilot's capabilities and needs:

- provision of sufficient feedback to allow the pilot to detect and correct unintentional performance errors before they affect system performance,
- introduction of fail safe and fail operational ergonomic design by means of human error detection and correction functions into the man-machine interface intelligence.

Models of human operator behaviour are also needed for incorporation of such error-tracking capability into automation themselves. This need for a better knowledge of the man-machine relationship prompted Airbus Industrie in cooperation with Dunlap and Associates and Cochin Faculty to develop and validate a predictive crew workload rating model (Speyer J.-J., Fort A., Blomberg R.D., Dr Fouillot J.-P., June 1987) based on heart rate variability, aircraft performance parameters and situational information (scenario, flight phase conditions, pilot role etc.). Section 6 presents the latest results of this work as applied to a fly-by-wire aircraft (A320) with an initial attempt to relate workload patterns with the level of automation, error awareness and error severity (Blomberg R.D., Schwartz A.L., Speyer J.-J., Fouillot J.-P., September 1988). Further work is however necessary to investigate how automation, workload, vigilance, performance and errors all relate to each other.

Trying to automate error completely away may merely displace the problem of pilot error, however. Being still the ultimate crosscheck and decision-maker, the piling up of "operator assistant systems" would make the crew even more dependant.

What has been achieved with the early 1980's A310/A300-600 cockpit is, in our view, still in the context of the Wiener and Curry philosophy on automation and cockpit design. In the step that was to be taken in the latter 1980's A320/A330/A340 designs have essentially been intended to cover more error-tolerance or protection against incidents of the Wanner scheme.

In the end these "a posteriori" rules and philosophies are not too far from the operational orientation that inspired the functional layout and organization of our new cockpits and associated systems. Design being an inextricable exercise of compromise, art and science, any "à la lettre" correspondence cannot be expected "a priori" however. Design engineers and test pilots do not work from the isolation of an ivory tower but have a very practical orientation to implement design concepts and objectives. Each new design is likely to command its own particular human factors evaluation as part of a broader systems analysis aimed at integrating it all.

#### 4 - QUESTIONNAIRES

The practice of systematically soliciting aircrew opinions received considerable impetus in the early 1980's when subjective evaluation of workload became a regular practice in crew complement certification. Practical methods and statistical analyses were developed, the only human factors issue that had to be formally examined at that stage being workload nonetheless. In parallel to these flight test activities and as early as 1983, Airbus Industrie performed more detailed pilot surveys to further investigate the quality of the man-machine interface itself, quite apart from its focus on workload.

A campaign debriefing questionnaire was prepared to undertake an anonymous opinion survey of those 17 pilots and observers that had participated to the flight and simulator campaigns for the A310's minimum crew determination. As a group, they covered an experience level corresponding to the operation of almost all commercial jet aircraft introduced to then with the exception of the B-767. The purpose of this

chapter is to review findings of surveys of this kind also performed by others, e.g. by Wiener, Curry and Neumann (Lufthansa) as they all relate to the impact of new technology on the operational interface.

#### 4.1 - Initial field work at AIRBUS

The initial A310-survey of Airbus was composed of more than 150 questions covering the whole spectrum of aircraft design issues that pertain to human engineering and ergonomics (Speyer J.-J., Fort A., 1983):

- . functional grouping of instruments/controls,
- . general presentation of flight systems information,
- . crew comfort,
- . overhead panel layout,
- . PFD information presentation, speed scale, mode annunciators etc...,
- . ND information presentation involving Arc Mode, Map Mode, Plan Mode, Weather Radar etc...,
- . ECAM information presentation involving Warning Display, System Display, etc...,
- . FMS Control & Display Unit, Manipulation, Pagination etc...,
- . AFS Flight Control Unit, Autothrottle operation, Thrust Rating Panel, Autopilot/Flight Director Procedures etc...,
- . Checklists and Procedures,
- . Outside appearance/mechanical ergonomics,
- . Tasksharing and worksharing,
- . Workload and error-inducing potential,
- . Intelligibility of hardware, procedures and mental ergonomics.

In answering that questionnaire pilots were asked to compare the A310 with the reference aircraft they considered most representative of their experience. Answering consisted in circling a number corresponding to their opinion on a 6-point agree-disagree type attitude measurement scale. The absence of a middlemark was meant to prevent participants from taking neutral and uncommitted positions.

More than 75 % of all questions received fairly high marks in the appreciation range of 4 to 5, pilots and observers refraining from making extreme position judgements. Where significant improvement was desirable for the future they felt free to rate in this direction. As confirmed in the other surveys the suggested areas for improvement concerned pilot seating, system software, use of real estate on the overhead panel, Flight Path Vector-information, attention-getting capability of some alarms on the PFD and on the ECAM, procedures with the FMS and interpretation of error messages, homogeneity of abnormal/emergency checklists with the ECAM Warning Display. As in every certification exercise we took advantage of this opportunity to do further homework having learnt throughout the years that more contact was going to be necessary to understand the pilot community. A step in the right direction was therefore prompted by the crew complement issue.

#### 4.2 - Curry and Wiener Surveys

In several subsequent studies Curry and Wiener (Curry R.E., May 1985 ; Wiener E.L., July 1985b) respectively investigate the human factors of new technology and automation as observed during the service introductions of the B-767 and MD-80. Both author's studies are based on questionnaires, interviews, discussion meetings and cockpit observations. Questionnaire forms used 5-point agree-disagree Likert-type intensity scales and matrix-type frequency-of-use tables.

On the positive side, these studies conclude that the new digital aircraft and their automatic features are overall considered as well-designed, reliable and useful. Much appreciation goes towards the automatic flight director systems and autothrottles, the electronic flight instruments and flight management systems and the electronic aircraft systems' monitors (EICAS). All these systems meet pilot's general agreement as for functions and implementation.

Pilots from airlines that did not use mechanical checklists felt they would be useful, many thinking these should be on EICAS. Some confusion was reported concerning the interaction of pitch autopilot and autothrottles, some other criticisms prevailing with regard to the respective designs of the mode control panel and control and display unit (CDU) of the flight guidance system on the MD-80 and of

the flight management system on the B-767. Many comments had also to do with the type of training desirable. Both authors believe that a gap seems to be gradually widening between system designers and airline pilots. The piecemeal introduction of new technology and automation appears to have alienated the end users to the point that an operational philosophy of aircraft utilization is not readily apparent at service introduction.

The large performance differences that appear to exist between pilots in their operation of the flight management and guidance systems may be related to computer literacy. Pilots who perform better may have more experience with computers outside their flying job, e.g. owning PC's and using them frequently. It would also appear that the coherence of the user's own cognitive organization is instrumental in achieving prime performance since functional knowledge is what best matches with the design and operation of these digital systems (Leplat J., 1985 ; Roske-Hofstrand R.J. and Paap K.R., 1986 ; Amalberti R., 1987).

Although automation was introduced as a means to reduce workload and eliminate human error it does not seem to raise unanimity however. After several years experience, it was found that automation would change only the locus and type of human error (Nagel D.C., 1988). Whereas small errors may be eliminated, Wiener and Curry point out that gross blunders can creep in such as systematic procedural or decision-making errors. From our observation of errors in the case of the A310 crew complement certification campaign, it was concluded that their mere existence - most having been minor slips, blunders, mishaps due to problems in resource management or insufficient familiarity with the aircraft - also made possible to establish learning loops (Speyer J.-J., Fort A., 1983). Some of the recommended improvements therefore concerned operational procedures and the training syllabus with particular emphasis on system knowledge and functional insight.

Mixed feelings towards automation's reduction in workload are reported in Wiener's study of B-757 pilots (Wiener E.L., 1988). While some would strongly agree (11 %) or agree (38 %) as to effective workload reduction, an equivalent proportion strongly disagrees (7 %) or disagrees (37 %), leaving the remaining 7 % uncertain about the actual effect of automation. Those who generally claim "workload reduction", would still add that new technology and automation overall commands a proportionally higher monitoring load due to the significant reallocation of workload from taskload into cognitive work. As Curry observes (Curry R.E., May 1985), performance with the new digital systems is less likely to be determined by traditional psychomotor skills but more by cognitive abilities: decision-making behaviour, systems knowledge, monitoring behaviour and crew coordination. Several features of new technology were nonetheless found to minimize mental operations or transformations: the speed trend, map display, altitude arc etc.

Fear of skill-erosion due to automation has pilots practice preventive hand-flying. But as Swissar's Mollet points out "if the basic training of the pilot has been sufficient (scanning technique, basic flying and navigation) a normally gifted pilot should have sufficient training to handle all normal and abnormal situations (Mollet C., February 1988)". The only relevant loss of performance seems to be attributable to monitoring problems particularly as a result of distractions. When operating with a lot of automation the effects of distraction do not manifest themselves as when practising instrument flying. Instruments flying will usually break down when the pilot concentrates on one important piece of information to the detriment of the other aspects. Feedback from improper monitoring of automatic equipment does not occur very often: only in the fairly rare and simultaneous conditions that automation fails to operate as intended and that the pilot is distracted. Another tendency is that some pilots would program a recovery and not turn off automation. This may be the result of simulator and line training where the emphasis would be put on proper operation of automatic equipment.

In an attempt to widen his human factors principles of automation (Curry R.E., May 1985), Curry estates the idea of displaying data, not commands. Removing the necessity for the pilot and command generator to have common objectives, it would allow pilot flexibility to modify his goals for existing conditions and would keep him in an active role without threatening vigilance because of underload. Examples that go along this idea are the flight path vector, the speed trend or the altitude arc prediction how all introduced in the genuine glass-type cockpits discussed here.

Although the B-767 was the only aircraft in his study, Curry reports very similar experiences in discussions with A310 operators. In this respect it is useful to review the A310-field study performed at Lufthansa (Neumann, Brandt N., May 1988).

#### **4.3 - LUFTHANSA Fleet Surveys**

This airline's policy is to establish a sound basis for future aircraft specifications from flight crews' experience. Feedback surveys were started to this effect as early as in 1976 covering the whole fleet operated at that time, B-707, B-727-200, B-737-100, B-747, DC-10, A300-B2 (Figure 2). Major technological innovations in store for new airplanes could already be expected and the question was whether and how to proceed with further automation than already available then. Another survey was launched shortly after the A310-200 and 737-200 Advanced introductions to enquire about pilot's acceptance of the new technologies.

Answers to questionnaires were provided by means of a 5-point evaluation scale exhibiting a neutral position as the Likert-scheme adopted by Wiener and Curry. The pilot questionnaire consisted of two main parts. The first dealt with overall cockpit lay-out, general handling qualities and airplane systems while the second was concerned with the electronic interfaces to the crew (ECAM, EFIS, AFS, FMS). Questions on the latter were divided into four man-machine interface areas:

- physical interface (reach and see): controls location, reach and handling, display location, readability, colour and lighting, etc...,
- operational interface (dialogue and understanding): operational rules, display rules, amount of necessary learning & training, etc...,
- tool interface (application): modes, usefulness, adequateness and importance,
- organizational interface (fit into the environment): reliability, logistics, ATC constraints, procedures update & improvement.

Pilots with more than 500 hours on the A310 generally judged the aircraft more positively than those with less.

- The ECAM's operating and display rules did not create any difficulties. Aural warnings were however considered as too loud attention catchers. The 1976-survey had on the other hand indicated a rejection of these since being found too numerous for proper discrimination. The principle of computer-aided-guidance during normal and abnormal operations was generally welcomed. But the procedures themselves as offered in the ECAM got rather limited pilot acceptance. They were criticised as sticking still too much to the flight engineer concept of the A300 B2/B4, containing too many unnecessary "monkey" switching actions. Because of missing capacity and redundancy of the ECAM, switching from screen to paper checklist and vice versa was also considered as potentially confusing. Overall it was claimed that thorough training and skill was necessary to handle complex failure situations. As the A310 is a fairly reliable aircraft, proficiency in dealing with these difficult cases does not build up in routine line operations. So only the simulator is left as an appropriate learning tool to develop the necessary abilities. Almost no pilots had ever seen any serious ECAM failure at all.
- The transfer from electromechanical to electronic flight instruments (EFIS) received overwhelming acceptance. It was clearly recognized that displaying on CRT's of flight parameters in an easy and self-explanatory way was leaving electro-mechanical techniques far behind. The primary flight display's (PFD) speed scale, radar height indication and aural transmission on short finals are much appreciated for instant situational awareness. The MAP-mode is considered to be the most important navigation display's (ND) feature followed by the PLAN, ROSE and ARC-modes. The drift angle presentation and flight path vector are not being likened with regard to importance, flyability and utilization. The location of the navigation display is found suboptimal since it is partly hidden behind the control column. Knowledge and practice with the display's symbology was found to be best acquired during simulator and line training.
- Most pilots found it important to have the readout of the automatic flight system's (AFS) flight control unit (FCU) repeated in the PFD or ND (e.g. altitude and V/S values). The existing information content of the A310 flight mode annunciator (FMA) is highly appreciated with regard to colour, quantity and arrangement. The amount of modes for lateral & vertical navigation and for thrust control is considered adequate. Most of the crews having more than 500 hours use virtually all possibilities of the AFS.
- As in the Curry & Wiener surveys on the B-767/MD-80 the coordination of AFS (lateral/vertical) and ATS (autothrust) is not considered fully satisfactory especially in altitude capture during descent or localizer capture in Land mode. At the time of the Lufthansa survey vertical navigation with the FMS was still in a fairly introductory stage with OP+ I7-status still far out. Most crews would take off in Navigation (NAV) & Profile (PROF) modes with a very minor portion relying solely on manual handling with flight director (FD). In descent the PROF mode was usually not being used at the time of the enquiry. Slightly more than half of the pilots would fly manual ILS approaches, a small proportion would fly manual non-precision approaches. Most visual approaches were flown manually with FD. Nearly all landings would be manual, without use of control wheel steering.
- The arrangement of the FMS's keys was fully accepted by the group having 500 hours, false inputs being considered possible nonetheless due to close location of parallel line-select keys. Fast slewing apparently would lead to stepping past pages, incorrect data format was often experienced. But the menu technique and scratchpad were highly appreciated, learning being best accomplished "on the job". Insertion of navids not in the database and of waypoints by means of the scratchpad was found to be an area for improvement. Some found that in rare instances it was hard to get quickly by specific data such as runway-, route-,

or way-point-changes or return to departure. As in the other surveys this one also confirmed FMS response times to require improvements. Overall, there was still satisfaction with the FMS, to the point of having aircraft control performed by this system rather than through the AFS's FCU (except for approach and landing because of the status of profile mode at the time of the questionnaire distribution).

- In conclusion, it emerged from the Lufthansa project that crews indeed wanted automation further developed in order to improve systems integration and crew interface. In particular, automation was found in need for improvement in as far as it would allow to become as good or better than manual operation. As Mollet reports (Mollet C., February 1988) pilots are not always in a position to realize how much better a safe and comfortable trajectory can be maintained using digital flight guidance systems. By the same token it also appears that copilots would tend to know more of their systems while captains would be less critical of them. While the ECAM/FMS would need further development and periodic update, training would require further adaptation and flexibility. In this respect the A320 should provide a promising check as to the improvements effectively reached.

Similar to the Curry study on the 767, the A310 study of Lufthansa confirms the preference of new technology aircraft (Figure 2), the absence of outright reluctance with regard to automation regardless of the possibilities of errors or loss of flying proficiency. This emerges particularly after having accumulated over 500 flying hours equivalent to about one year's airline rostering. Copilots are usually eager to see even more implementation functions than do captains who tend to accept systems as they are. Both would welcome initial training putting more emphasis on basics and practical hints to reinforce know how and general understanding.

What definitely appears to be required is intuitive design which should allow the pilot to understand more easily the automation systems at work to take over if necessary (Klopfstein M., May 1987). This type of transparency would help to monitor more straightforwardly automation performance and limits. Providing the pilot with such a flight management information system should relieve him of monitoring and decision-making since automation would serve as a watchdog, providing benchmarks & alternatives, assisting the pilot with automation resources, possibly tracking workload patterns and some day crew errors (Pelegriin M., October 1986 ; Speyer J.-J., October 1986 ; Wiener E.L., 1988 ; O'Donnell R.D., September 1988 ; Shingledecker C.A., September 1988).

#### 4.4 - AIRBUS Sidestick/Fly-by-wire Survey

The Lufthansa study makes several hints at improving specifications of next generation aircraft which incidentally were already implemented on the A320. Assertive of this airline-oriented approach to new technology development, Airbus performed a first phase "proof-of-concept" experiment in the second part of 1983 also supported by a questionnaire-interview approach.

A test installation of hybrid fly-by-wire was placed in the Airbus Industrie A300 flying testbed (MSN 003) the objective being to evaluate the concept associated with side-stick control. The conventional controls for the CMI or left-seated pilot were removed and replaced with a sidestick controller mounted on the pedestal to that pilot's left. Inputs from the sidestick went to a computer which simulated the functions and control laws of the EFCS (Electronic Flight Control System) and controlled the elevator, ailerons and pitch trim tabs through the autopilot. Some 75 flying hours were achieved with 48 pilots from 5 airworthiness authorities, 12 airlines and Airbus Industrie.

Here also qualitative assessment was made through a detailed questionnaire containing 42 questions filled in by each team of visiting aircrew; 25 such questionnaires were submitted the summary being available in Table 1 with as answering scale again the 6-point attitude scale that had been as exercised in the A310 survey. The overall result was extremely positive and showed no difficulties of adaptation to the side-stick, unanimous approval of the C\* pitch law, unanimous enthusiasm for the flight envelope protection especially at low speed and an unexpected necessity to further develop lateral control, a positive contribution towards design of this type of survey (Corps G.C., October 1986).

TABLE 1 - SIDESTICK/FLY-BY-WIRE EVALUATION A300 MSN 003

Summary of the Questionnaire Answers

	Unacceptable					Excellent
RATING SCALE	1	2	3	4	5	6
NUMBER OF ANSWERS	17	34	92	204	352	317
	1.6 %	3.2 %	8.8 %	19.4 %	33.6 %	30.2 %

- Unanswered questions 34 or 3.2 %
- Total number of answers 1050 from 25 questionnaires
- Note that 25 of the 51 answers in 1&2 were related to roll characteristics.

Questions submitted pertained the whole range of issues at stake:

- position architecture, range of movement of the controller and associated armrest,
- harmonization of pitch & roll control forces, operating forces and ease of making control inputs,
- absence of mechanical coupling between left & right controllers,
- little or no need for trim change in pitch,
- ease of precise control in pitch, effectiveness of flight control, protection at high speed or high incidence approaching the stall,
- ability of precise control in roll, effectiveness of flight control, protection at high bank angles,
- ability to accurately control the bank angle close to the ground at take-off & landing.

Pilots who participated were all well experienced in the operation of commercial jet aircraft. Some, still copilots, had no difficulties at all to change hands for switching from right to left hand seat. As a group they did not feel uncomfortable with the idea of being primarily responsible for the management of system interfaces rather than the direct operation of their aircraft.

#### 4.5 - Concluding comment

Most crews interviewed in field studies do indeed express high praise for the new "glass cockpits". These would essentially provide a more dynamic source of information and greater awareness of the aircraft with respect to the operating environment effectively making conventional electromechanical cockpits obsolete.

In fairness to all, Wiener also admits in a later paper (Wiener E.L., 1985a) that the negative side of automation should not be overstated. The number of automation- or design-induced incidents brought about by new technology has been very limited and their consequences very small. Most automation would seem to work with very high reliability and pilots themselves are very satisfied with new control and monitoring interfaces (Gannet J.R., October 1982 ; Nordwall B.D., November 1986) when compared to former equipment. The "good old days" fallacy is even repeatedly discredited with recent incidents and accidents having occurred on earlier technology aircraft (Machado F., 1984 ; Bruggink G., 1983 ; Int. Journal of Aviation Safety 1985 ; NTSB -Aircraft Accident Report- March 1986).

Caution with regard to the human factors impact of new technology will however remain to be exercised and all aircraft manufacturers are well aware of the support this new discipline will have to offer to aircraft design and systems integration if the industry intends to maintain its commitments to safety and efficiency.

### 5. PERFORMANCE EVALUATION OF NEW TECHNOLOGY

#### 5.1 - Principles of Engineering Experiments

Increased focus on man-machine interface analysis formally began in the aftermath of the US Presidential Task Force on crew complement which had recommended more emphasis in this area. Two experimental studies were performed in cooperation with DUNLAP & ASSOCIATES (Hartford, Connecticut, USA) to investigate the impact of new digital equipment that was to be installed in the A310.

Although described in detail in Agardograph N° 282 on the Practical Assessment of Pilot Workload it is useful to review the essentials in light of this paper's focus on the impact of new technology. The Performance Criteria Methodology developed in these engineering experiments (Lipson Ch., Narendra J.S., 1973) was also applied in a third study to investigate the impact of side-stick/fly-by-wire that would eventually equip the A320. This third application will be presented in more detail here.

The first two evaluation studies were undertaken to compare the overall performance of the pilot/aircraft system between flights using conventional, electromechanical primary flight instruments and those flown with the new, electronic flight instruments (EFIS) and the flight management system (FMS). Data collection for the EFIS experiment was undertaken in an A300 flight test & development aircraft (MSN 003) which for this purpose was specifically equipped with conventional instruments installed in front of the left seat position and EFIS installed in the right seat position. Data collection for the FMS experiment was undertaken in a production A310 which had both the EFIS and FMS at both pilot positions.

Both aircraft had on-board computerized recording of all relevant flight parameters at rates in excess of one per second. Both studies utilized a factorial experimental design in which relevant parameters were systematically varied as the experimental

subjects (senior Airbus test pilots who had never flown with EFIS nor FMS before) repeatedly flew specifically designed circuits.

### 5.2 - EFIS Performance Criteria Analysis

The pattern used in the EFIS experiment was a modified standard training circuit that posed a variety of flying problems for the pilots.

Altitudes, airspeeds, flaps and slats positions, a holding turn, climb and descent rates and bank angles were all precisely specified to ensure comparability of data from circuit to circuit. Three conditions were chosen to provide a range of situations under which the instruments would be compared and to vary workload for statistical comparison: FD (Flight Director and Autothrottle system on), ILS (Flight Director and Auto Throttle system off, raw data) and NDB (Flight Director, Autothrottle and ILS off, non-precision configuration). The circuit was designed so that the flying pilot, who wore a helmet-mounted hood, would have to utilize extensively the information on the primary flight displays or flight instruments. In all, 24 circuits were manually flown with each combination of two pilots, two displays / instruments and three conditions repeated once. The major analytical technique chosen for the instrument comparison was multi-dimensional analysis of variance: ANOVA (Lipson Ch., Narendra J.S., 1973)).

The results of this EFIS study implied some significant performance benefits from flying with CRT displays. Significantly higher control reversal rates with associated lower standard deviations of control positions when the test aircraft was flown from the right seat with the EFIS strongly suggest closer tracking of criterion values. This is likely because the EFIS provided better information for manoeuvring, particularly with respect to airspeed and pitch behaviour of the aircraft, than did the conventional instruments. The observed high control reversal rates when flying with the EFIS may be partially attributed to the total absence of lash in the displays and the thinner indicator lines and bars which likely enable the pilots to respond to changes they could not even detect reliably on the conventional, electro-mechanical instruments.

It can therefore be concluded that pilot/aircraft system performance was equivalent or better on all measures when the aircraft was flown using the EFIS than when conventional instruments were used. Measures of smoothness and precision of flight showed the greatest contrast between the EFIS and conventional instruments.

These findings must be interpreted with the understanding that neither pilot had extensive experience flying with the EFIS. Both were familiar with its principles and design, but neither pilot had amassed enough time with the instrument to be comfortable with it. Certainly, their experience with the EFIS was infinitesimal when compared to the large number of hours they had flown with conventional instruments. It is therefore reasonable to hypothesize that a greater level of pilot familiarity with the EFIS would have shown an even larger EFIS performance benefit when flying in the normal to moderately difficult flying situations experienced during this experiment.

### 5.3 - FMS Performance Criteria Analysis

The circuit for the FMS study consisted of a Standard Instrument Departure (SID) and a Standard Arrival Route (STAR) with a single procedure turn as a holding pattern. Altitude and airspeed changes were specified at prescribed points in the circuit to increase pilot workload and exercise the combined information on the PFD and ND. The total experiment consisted of flying the circuit 10 times in three different conditions, i.e. NAV (once by each pilot, FMS coupled to Autopilot), STANDARD (twice by each pilot, Autopilot without FMS), MANUAL (twice by each pilot, FMS for ND-map generation) without Autopilot.

Examination of the significant effects from the ANOVA's calculated from this engineering experiment showed clear patterns of findings directly linked with differences among the three studied conditions. The number of these differences and their logical consistency indicated that they were real and not chance findings. It was, therefore, particularly noteworthy that none of the significant findings indicated or even suggested a performance problem related to the FMS. Regardless of whether it was coupled with the autopilot or its information was used directly by the pilots, the FMS produced extremely consistent and high quality performance.

The performance benefits of the NAV condition were clearly documented by this study. The FMC appears capable of commanding the AP to navigate the aircraft in the horizontal plane with great precision and repeatability. This frees the pilots to attend to other tasks or simply reduces their workload and makes them more available to respond to unexpected occurrences. It is also important to realize that the performance benefits of the NAV condition were achieved without noticeably altering the "style" in which the aircraft flew the circuit. The tracks produced by the FMS appeared "normal," i.e., not unlike the intended track or the tracks produced when the pilots flew in the STANDARD condition. There was no apparent cause for concern that flight tracks flown with the FMS in command would differ materially from those flown by aircraft not equipped with an FMS. Hence, it could be concluded that the Airbus A310 and similarly equipped aircraft should blend smoothly and easily into the existing ATC environment regardless of the mode in which they are flown.

The results from the MANUAL condition led to several additional conclusions. First, the information displayed on the ND by the FMC was obviously accurate and consistent from trial-to-trial. Second, the pilots were clearly able to interpret the ND and use the information to fly precise and repeatable tracks. Finally, the response style of the pilots when flying manually suggests that they responded to smaller deviations from nominal flight parameter values than did the autopilot. This resulted in somewhat lower parameter standard deviations when the autopilot was engaged and somewhat higher control reversals and rates through zero when the pilots flew manually. Which leads to the logical conclusion that pilots can safely and accurately fly an FMS-equipped aircraft even if both autopilots were to fail as long as the FMS were available to drive the map mode of the ND. Moreover, the results lead to the strong implication that in critical flying situations in which track must be maintained with the greatest possible precision for short periods of time, it would likely be better to disengage the autopilot and allow the pilots to follow the ND display manually as they did in the MANUAL condition of this experiment.

Finally, the performance gains observed for both the EFIS and FMS were not associated with any increase in the workload perceived by the pilots in the experiments. In fact, they rated (on a 10-point numeric interruption scale) flying with the EFIS as a lower workload situation than flying with conventional instruments. Likewise, use of the FMS was associated with lower rated workload than trials flown without it. Although neither of these latter differences was statistically significant, the results provided the clear implication that pilot workload would be positively influenced by the introduction of these new, electronic flight instruments.

#### 5.4 - Sidestick/Fly-by-wire Performance Criteria Analysis

##### 5.4.1 - Experimental Design

With the experience gained in both preceding experiments it is quite obvious that a comparative test could also be conceived for the sidestick/fly-by-wire combination versus conventional controls. Since AIRBUS INDUSTRIE's flying testbed A300 (MSN 003) was involved in a first phase proof-of-concept exercise whereby the conventional controls for the CM1 (left) flying position were removed and replaced with a sidestick, arrangements were again made to perform an engineering experiment (Blomberg R.D., Speyer J.J., July 1988).

In order to assess the performance differences between flying with the sidestick/FBW system and conventional, manual controls, 12 experimental circuits were flown in December 1983. All circuits were flown from the left seat using the sidestick controller by two senior test pilots. These same pilots had previously flown 12 circuits from the same seat of the same aircraft with conventional controls. Since the testbed aircraft is equipped with extensive instrumentation to record most critical aircraft performance parameters, it was possible to undertake a detailed statistical comparison of the conventional controls and the FBW system. The circuit flown was the same as the one designed for the EFIS study with again the three different combinations of aircraft and approach configurations used to vary pilot workload (FD, ILS and NDB as detailed in 5.2). Go around was initiated at 100 feet ratio altitude for the FD and ILS conditions and at 300 feet for the NDB approaches.

The same four measures (mean, standard deviation, transitions through zero, reversal rates) were calculated as appropriate from the various flight parameters and used in an analysis of variance (ANOVA) to determine if differences existed which could confidently be attributed to the control system being used. Subjective ratings using the 10-point interruption scale referred to in sections 5.2 and 5.3 were again collected at various points to compare workload levels in either condition.

The results of this experiment, which are summarized in the following documented several major performance benefits of the sidestick/FBW system.

##### 5.4.2 - Smoothness and stability improvements

All measures of smoothness and stability favoured the sidestick/FBW system by a considerable margin. The standard deviations of roll and pitch angles were reduced significantly for the sidestick/FBW circuits as shown in Figure 3. This indicates that, on average, there were significantly smaller departures from the mean value of pitch and roll angle when the FBW system was used.

The standard deviations of roll, pitch and yaw rates (speeds) showed an even greater improvement in smoothness as depicted in Figure 4. At the same time, the number of transitions through zero for these three rates, dropped dramatically as illustrated in Figure 5. Together these results show that significantly more stable flight was achieved with the sidestick/FBW than with conventional controls. It is interesting to note that the benefits in roll and pitch, which are directly controlled by the FBW system, also extended to yaw rate likely because the smoother flight performance induced less yaw that had to be corrected by the yaw damper.

Accelerations on all three axes also showed a large benefit. In figure 6, which shows acceleration measured through the center of gravity of the aircraft, a large reduction in transitions through zero is readily apparent. This should relate

directly to both smoother system performance and increased passenger comfort. Further emphasizing the likely benefits in terms of passenger comfort was the sharp reduction in the average lateral acceleration for the 12 circuits flown with the sidestick/FBW system. Although lateral acceleration with either control system was small, the sidestick/FBW managed to reduce the absolute magnitude of this undesirable parameter by a factor of four from .004 g's to .001 g's.

#### 5.4.3 - Fuel efficiency

The improvements in smoothness and stability noted above suggest that the aircraft/pilot system performs more efficiently when flown with the sidestick/FBW controls. This in turn should yield lower fuel burn and reduced stress on the airframe. In fact, every parameter related to fuel burn showed significantly better values for the circuits flown with the sidestick/FBW system. For example, the standard deviation of rudder position was reduced significantly from 0.9 degrees for conventional controls to 0.6 degrees for the sidestick. This means that the excursions of the rudder from its mean value were much smaller with the sidestick thereby reducing drag.

The improved efficiency of the sidestick/FBW was also evident in the vertical speed parameter. The circuit flown by the pilots required them to establish and maintain precise rates of climb and descent while simultaneously holding target airspeed. They were able to accomplish their vertical speed tasks much more smoothly and with fewer changes when they flew with the sidestick. Vertical speed standard deviation was reduced from 362 feet per minute for the conventional controls to 326 feet per minute for the sidestick/FBW combination. At the same time, the rate of vertical speed transitions through zero fell dramatically from 8.7 per minute to 5.0 per minute. These effects were established at the  $P < 0.001$  level i.e. there is less than 1 chance in a 1000 they are due to coincidence. Together these results clearly show the improved efficiency possible with the new technology.

The increased efficiency resulting from the use of the FBW control system were directly evident in the N1 parameter. Figure 7 shows a graph of the standard deviation of this parameter separately for the two control systems and the three flight conditions. The results show several interesting effects. The values are clearly lower for the sidestick/FBW in all cases further confirming the efficiency benefits of this system. However, with the sidestick the standard deviation is much lower for the ILS and NDB conditions with the autothrottle system off than for the Flight Director (FD) condition in which the autothrottle system was on. This suggests that the pilots may have made many small corrections to ensure that the N1 did not deviate very far from its mean value. This assumption is confirmed by Figure 8 which shows the reversal rate for N1. The pilots made many more throttle inputs resulting in reversals of N1 when they flew with the sidestick and the autothrottle system off (ILS and NDB conditions). This leads to the assumption that the pilots had more time available to manage the throttle and input changes when they were flying with the sidestick. These effects were again established at the  $p < 0.001$  level.

#### 5.4.4 - Pilot taskload

The suggestion that the taskload of the pilots was reduced was confirmed by analyzing their inputs to the sidestick controller. The position of the sidestick was measured in terms of its pitch and roll angles. However, a pilot using the sidestick is free to move it in any direction to accomplish simultaneous control of pitch and roll. Therefore, the most meaningful measure of pilot inputs to the sidestick was a composite reversal rate. This rate was calculated by counting a single reversal for any second in which either or both pitch or roll angle reversed.

The comparison of the composite sidestick reversal rate for the sidestick-flown circuits with the summed reversals of the ailerons, elevators and pitch trim tabs for the circuits flown with the conventional controls provides a direct measure of any reduction in pilot taskload for controlling the pitch and roll of the aircraft. Any elevator, pitch trim or aileron surface movement in the conventional control trials was associated by definition with a control movement since all flying was under the manual control of the pilots. The results of comparing sidestick reversals with the sum of reversals for pitch trim, elevator and aileron is shown in Figure 9. Pilots achieved the smoother and more efficient performance described above with over a 50 percent reduction in control inputs. Considering a numeric filter to take away sidestick vibrations not introduced by the pilot (less than 0.02°/minute) it was possible to show even more alleviation.

The benefits of this greatly reduced task loading on the pilots are obvious. Their ability to cope with emergencies should clearly be enhanced. The accuracy associated with non-control tasks such as internal and external communications should be greatly improved while workload is simultaneously reduced.

#### 5.4.5 - Pilot workload

An examination of the table below shows a slightly lower mean workload for the sidestick/fly-by-wire flights but this effect was not statistically significant the

experiment not having concentrated specifically on this issue. Also apparent is that the expected ordering of conditions with respect to workload was again achieved.

These results show that the sidestick-FBW managed flights were not associated with any higher workload even with pilots who were very inexperienced in the use of these new flight controls at the time of the experiment.

	<u>Mean</u>	<u>Standard Deviation</u>
Conventional	6.7	2.3
Sidestick/FBW	6.4	2.2
Flight Director	5.7	1.8
ILS	6.9	2.2
NDB	7.2	2.5

## 6. WORKLOAD MODELLING APPLICATIONS

### 6.1 - Programme Evolution

Because of the cost and time pressures associated with minimum crew demonstration, Airbus Industrie decided to investigate the possibility of developing a mathematical model capable of predicting pilot workload ratings in a valid and reliable manner. If such a model could be validated, it would also have utility beyond the certification of new aircraft. Another use would be during the development of new aircraft to assess the potential implications of design decisions on workload. A valid model would also find use as a measure of training proficiency. Figure 10 illustrates the several steps that were already performed in view of this final goal and these are described in the following.

#### 6.1.1 - Identification of variables

- The first step in this process was to determine if there was any statistical relationship between the scale ratings given by pilots during flight and directly measurable aircraft system performance measures. As part of the EFIS performance criteria study performed with Dunlap & Associates Inc. in 1982 and referred to in 5.2, a number of multiple regression equations were developed providing a good fit between workload ratings and various aircraft performance measures as the independent variables. This work reported in Agardograph n° 282 (Speyer J.-J., Fort A., Blomberg R.D., Fouillot J.-P., June 1987) effectively suggested that a valid model could be built.
- Also included in this first step was the use of physiological variables to assess pilot workload. Since its inception in 1980 work in this field with the Cochin Laboratory of Physiology is founded on the assumption that these measures reflect the level of neurological arousal determined by the demands of flight performance. Largely based on the study of ECG's, work was not limited to that of heart rate average alone, modifications of which are well known since long for acute phases of flight such as take-off, landing, delicate manoeuvres or flight incidents (Dr Roscoe A.H., October 1986 ; November 1986 ; June 1987 ; September 1988 ; Tekaiia et al., 1981 ; Fouillot J.-P. et al., September 1988). In this context, the introduction of contemporary cockpit systems tends to reduce physical activity in pilot workload and increased the utility of heart rate variability as a potential indicator of mental workload and emotional stress. Following the A310 Minimum Crew Demonstration Dr. J.-P. Fouillot of the Cochin Laboratory of Physiology (Fouillot J.-P. et al., 1985 ; Tekaiia et al., 1985) demonstrated a significant correspondence between a set of heart rate variability indices and exponential heart rate averages (derived with Dunlap & Associates) and the subjective Airbus Workload Scale.
- Modelled after the Cooper-Harper scale, the Airbus Workload Scale was also adapted from workload theories developed at MIT by Simpson and Sheridan (January 1979) and in the ESAU by Wanner (Wanner J.-P., 1969). It consists of 7-points from 2 to 8 and offers one rating choice for the low workload category (2), two rating possibilities for the moderate (3, 4) and two for the high (5, 6) workload categories. The two remaining rating alternatives concern extreme (7) and supreme (8) workload cases that require cautious judgement during post-flight assessment. As demonstrated by means of Factorial Analysis of Correspondences (Bensecr J.-P. F., 1980) in Agardograph n° 282, higher pilot workload ratings tend to correspond with higher heart rate and lower heart rate variability while conversely lower ratings are associated with lower heart rate and higher variability measures.

#### 6.1.2 - Model development and calculation

- The second step was to choose a specific approach, collect enough data and actually calculate a model. With the research results mentioned in the above it was reasoned that workload ratings collected in minimum crew certification campaigns might be modelled using not only data extraneous to the crew (aircraft flight performance parameters and flight status measures) but also data intraneous to the pilots (heart rate measures). That work was accomplished using the data collected from the A310-200 crew complement demonstration held in early 1983. It provided an excellent basis for initial model development since the

60 flights of this campaign contained an abundance of data including subjective ratings, aircraft performance measures and heart rate recordings of the 14 participating pilots.

The flight scenarios used in this demonstration also covered a relatively wide range of normal, abnormal and emergency flight conditions representative of the range of situations that a useful model would be expected to predict. As reported in Agardograph n° 282 the coordinated effort between Airbus Industrie, Dunlap & Associates and Cochlin Laboratory of Physiology resulted in the calculation of over 50 different models of pilot workload. Stepwise Multiple Regression and General Linear Modelling (Neter J., Wasserman W., 1974) were used to by Blomberg derive these, the best of which was selected for application. Overall, the following data entered the development model:

- 22 aircraft performance measures (exponential averages, rates through zero, reversal rates, number of AFC modes on),
- 14 heart rate measures (level, difference-baseline and overall mean, trend-short & long term, variance-short & long term),
- 4 flight status variables (flight condition, flight phase, scenario group, pilot duty).

The model fit quite well ( $R = 0.665$ ) with actual pilot ratings and was statistically significant ( $F = 8.71$ ,  $p < 0.0001$ ). However it used 107 degrees of freedom and the coefficients of some of the terms in the model were not significantly different from zero. It also included some parameters, such as tailplane deflection and scenario group, which might not be widely applicable to other aircraft and flying situations.

#### 6.1.3 - Model validation and simplification

- The third step was therefore intended to reduce the complexity of the model by removing measures which are difficult to collect and those which might not have widespread applicability across aircraft types. Another objective was also to validate the revised model resulting from this simplification. To accomplish this an independent set of data was needed which contained all of the measures in the model and associated pilot ratings but which were not part of the data the model was built from. Route proving flights of the A310-300 in early 1986 provided the most reasonable way to attempt such a validation. It was reasoned that this generally similar but sufficiently different model would allow a fair initial test of the model while still providing an indication of its ability to predict reliably across aircraft types. The avionics software is for example a more advanced version than that used in the basic A310-200. The A310-300 also has a tail-mounted fuel tank which can be used to shift the aircraft's center of gravity for improved fuel economy.

Additional validation was also sought by including at least one pilot who had not participated in the A310-200 campaign. Two crews were consequently selected one of which had flown extensively in the previous program and was well represented in the data on which the model was built. The second crew was made of two airline pilots who regularly fly both A310 variants. One of them had participated in the previous campaign but contributed few ratings to the data the model was based on. The other pilot had not participated in any previous work at all. The four scenarios selected for the validation flights were chosen to represent the full range of observed ratings during the initial campaign and involved normal flight, flight without autothrottle, engine-out operation and flight without ECAM. Destinations, flight durations and routes were selected to be representative and similar to those used with the A310-200. Each scenario was flown twice, once by each crew, to accomplish a repeated-measures design for a total of eight flights.

The first development effort had utilized a split-half design to calculate a model and assess its validity. Under this approach, the data for the 1282 available ratings taken during the A310-200 certification flights were divided arbitrarily into two halves. A model had been calculated on one half and validated on the other. For the model simplification effort, an entirely new set of 775 ratings from 8 flights in a slightly different type of aircraft was available as validation data set. All of the 1282 data points in the development data could therefore be used for model building with the new data reserved solely for validation.

The task of revising and validating the model involved extensive data processing and management using similar measures and statistical techniques as in the initial development. Data management was again a major undertaking both because of the size of the data and because four different sets of information recorded in completely different ways had to be integrated, e.g. rating data, aircraft data, heart rate data and log data. The latter provided time-based references with respect to flight phase, flight condition, type(s) of failure(s) and

specifications of pilot flying/non flying. In short, the following type of data entered the revised model:

- 10 aircraft performance measures,
- 11 heart rate measures (rating pilot 4; non-rating pilot 7),
- 6 flight status variables, e.g.:
  - . flight condition,
  - . flight phase,
  - . pilot role,
  - . number of ECAM displays available,
  - . number of FMS's available,
  - . autothrottle available or not.

This represents a significant reduction in complexity from the original. The ability of the simplified model to predict accurately the ratings given by the pilots was not reduced meaningfully by the process of simplification. The multiple R for the revised model was 0.664 as compared to 0.665 for the original version. Also, the statistical properties of the revised model are superior to the original. It uses only 63 of the available degrees of freedom compared with 107 for the earlier version; its F-value is almost double that of the original ( $F = 15.21$ ,  $p < 0.0001$ ).

In addition to improved statistical properties, the revised model does not contain any aircraft measures which are not normally available on present and contemplated jet transport aircraft. It also does not contain any flight status measures which should present a data collection problem. The data for each of the measures used is typically recorded on standard flight recorders. The revised model was used to calculate predicted values for the 775 ratings collected during the eight A310-300 route proving flights. The calculated rating values were then correlated with the actual ratings. The Pearson product moment correlation coefficient between actual and calculated rating scores was 0.44 (significant with  $p < 0.0001$ ). Thus, it was possible to conclude that the model as developed in the A310-200 was valid and likely applicable across an even wider range of aircraft types and flying situations.

The successful validation of a workload calculation model meant that the model could be used confidently in certification and as an aid to aircraft development. There was still no practical evidence however of the applicability of the model to the next generation of Airbus aircraft which will all have sidestick controllers and fly-by-wire control systems. The model had been developed and validated in a conventional control environment. Since fly-by-wire control can change the response of an aircraft under certain flying conditions efforts had to be devoted to determine if the model could make the transition to fly-by-wire. Also, the output of the model can be considered as a pilot/aircraft system performance measure which could find application for pilot selection and training provided norms for pilot groups of interest can be established. But similarly, there were no insights on how the model might react in the various manoeuvres used in pilot training.

#### 6.1.4 - Model application to the fly-by-wire concept

- The fourth step in building a workload calculation system aimed therefore at examining the model's performance with sidestick/fly-by-wire and in specific manoeuvres more like training than any previous use of the model had allowed. Referred to earlier as part of the development program for the A320, demonstrations on flying testbed A300 n° 3 provided an ideal platform for further investigation. This aircraft was experimentally equipped with dual sidestick controllers and a hybrid fly-by-wire control system.

The flight plan for demonstrations to airline and Airworthiness Authority guest pilots involved extensive free flying as well as six special manoeuvres described as follows:

- . simulated engine failure at take-off rotation,
- . high g demonstration up to a 2 g load,
- . bank angle limiting demonstration with roll angle exceeding 35°,
- . low speed stall protection demonstration at high angle of attack,
- . transfer of command input demonstration after erratic take-over from the other pilot,
- . over-rotation at take-off to demonstrate transfer of command and flight envelope protection.

An additional objective was to assess the rationality of model calculations in the context of the type of flying conducted in these demonstrations. The nature and organization of this demonstration flight program did not permit the collection of actual ratings for which visiting pilots would have had to be trained. Previous collection of workload ratings in the A310-300 could provide a basis for determining if the model's operation was reasonable taking into account the flying problems presented and the fact that the pilots were having their first-ever fly-by-wire experience. Time pressure and other factors made it also impossible to have all guest pilots equipped with heart rate sensing equipment. So only a subset of the total number of flights was available for analysis.

The pattern of estimates by flight phase appears quite reasonable and consistent with both expectation and previous workload research. As depicted in figure 11 workload profiles are logically following what might be expected from flight phases. Also, the values for CM2/PNF- Airbus test pilots, three of which contributed to the data included -are below those of CM1/PF- experienced guest pilots, eight of which had been instrumented. This is not surprising since these eight flights were typically the first sidestick/fly-by-wire experiences for these visitors and for some their first flying an A300.

Another pattern of results concerns the relationship among the four flight conditions. Depending on the additive coefficients in the model, these conditions logically ranked themselves as failure with associated checklist being exercised, failure condition, normal situation with checklist being exercised or normal condition, these four being in order of decreasing values. As shown in Figure 11 the differences among flight conditions are greatest during the in-flight phases and least for the relatively low workload taxi phases. The consequences of diverting the attention of a crewmember to an emergency or checklist are certainly greater when the aircraft is in the air than when it is on ground.

Assessing individual flight graphs with normal flight conditions in Figure 11 also provides a feeling for the role that heart rate variability data play in the model since at any given time all other parameters are the same for CM1/PF and CM2/PNF estimates. Moreover, the extent to which the model's estimates for CM1/PF and CM2/PNF are equivalent in level and shape can be interpreted as a direct measure of how well the crew is coordinating and sharing workload.

An examination of Figure 12 reveals an excellent correspondence between the FbW demonstration data and the A310-300 validation study data, either actual or calculated. The actual and calculated values being highly correlated ( $r = 0.961$ ), the normal flying data for the demonstration flights also correlate well with these validation data ( $r = 0.759$ ). The major differences are for take-off, cruise and taxi before take-off and can easily be explained. The take-off data for the FbW demonstration flights are the guest pilots' first encounter with the fly-by-wire system which certainly could be expected to increase workload. The initial cruise phase in the FbW demonstration flights was relatively short lasting only 30 seconds on average. It was only at an altitude of 10,000 ft, with the guest pilot still unfamiliar with the aircraft and the autopilot not engaged. The cruise phases of the A310 validation flights were sustained periods of level flight at high flight levels usually involving the autopilot. The relatively low estimates for taxi before take-off are also attributable to the nature of the demonstration flights. There were no MEL items for pilots to deal with as in the A310 validation flights, CM2 was taxiing and the presence of a CM3-flight engineer further reduced any load on the pilots prior to take-off.

The flight program also included six special manoeuvres in order to demonstrate various aspects of the fly-by-wire control system to these guest pilots. Five of the six manoeuvres were essentially basic flying problems and were therefore assuming the normal flight condition. The simulated engine failure at take-off, however, was estimated as a failure flight condition. As graphically depicted, Figure 13 shows that each special manoeuvre was associated with an elevation in workload estimates for both crewmembers except for the bank angle limiting. An engine failure at take-off, a steep dive and pull up into a 2 g climb, approaches to stall/high alpha and seemingly irrational control inputs at critical points in the flight path (overrotation and transfer of command) would all be expected to cause workload to elevate. The absence of an increase in predicted workload for the bank angle limiting is not unexpected since it can be assumed that guest pilots often had banked aircraft beyond 35 degrees especially at safe altitude and airspeed. The purpose of this manoeuvre was to demonstrate the limiting properties of the control system and not to generate anything extreme. The extent of the increase of CM1 versus CM2 is also orderly. Workload for both pilots is highest for the engine failure at take-off. The overrotation and transfer of command manoeuvres elevate the workload for CM2 more than for CM1 because CM1 is flying the aircraft and making critical control inputs. Similarly, the high alpha approach causes a much greater increase for CM1 than for CM2. This is likely since contrary to the CM1 the CM2 is familiar with the fact that the fly-by-wire will prevent a stall while the alpha floor will trigger maximum thrust.

Whether for the normal flight phases or for the special manoeuvres one of the workload implications emerging from these demonstration flights is that absolute workload levels for guest pilots were not as high relative to the Airbus test pilots as might be expected for pilots just transitioning to sidestick/fly-by-wire. This supports the notion that transition to this new flight control should not present any major handling problems. Overall, the results clearly showed the ability of the model to produce realistic estimates for the various phases of flight and for the special manoeuvres even though these demonstrations departed dramatically from conditions inherent in the model's development and validation. Had there been any inherent problems in the model these would likely have been unveiled during this fourth step.

#### **6.1.5 - Model application to the first flight of A320**

Finally, the fifth development step was the application of the workload model to the very first flight of the A320 with both pilots equipped with heart rate monitoring sensors. This was not a formal experiment but, rather, an exploratory effort and a further chance to exercise the model under highly unusual circumstances. The internal consistency of the model's estimates for this first flight (Figure 14) again strongly suggested that it is a valid tool even with a sidestick/fly-by-wire aircraft. It was particularly noteworthy that the model was able to function acceptably even though the heart rates of both pilots were fairly high. These high rates were not unexpected in a situation with as much relative anxiety and excitement as a maiden flight of a new aircraft. However, the model's ability to cope with them, was a further indication of how robust it is to a wide range of flying situations.

It was therefore concluded that the model was ready for operational use as part of flight test and, in particular, as experimental tool for the A320 certification.

### **6.2 - Programme Application**

#### **6.2.1 - Objective of the Airbus Calculation System**

As the A320 approached certification it had, like all other commercial jet aircraft, again to demonstrate its ability to operate in the real-world environment of crowded airports and airways, flying a rigorous schedule covering the length and breath of Europe (Speyer J.-J., Monteil C., February 1988).

The main objective of this particular demonstration was indeed to satisfy certification requirements for the A320's minimum crew complement as laid out in FAR/JAR 25.

This was achieved by using different means to comply with the regulation:

- reviews of procedures and checklists resulting from flight debriefings and pilot comments,
- workload analyses of subjective workload rating evaluations as performed earlier for the A300 FF/A310 certifications, with pilot and observer assessments,
- workload calculations by means of aircraft parameters, physiologic and flight status measures as objective substantiation of pilot and observer assessments.

The first phase of these intensive trials were run for 8 days in January 1988 and involved a series of 50 real flights on a typical short/medium haul network flying up to 7 sectors a day. Four different crews took part: three were composed of an airline pilot (acting on behalf of the certification authorities) and of an Airbus Industrie test pilot, while two airworthiness authority pilots made up the fourth crew. A short campaign of 20 simulated flights took also place but is not being reviewed here since the workload model has neither been validated nor yet adapted to simulator use.

Subjective rating by pilots may bring an undesirable intrusion on the flying duties of the crew causing distractions particularly when workload is high and should be avoided by the observers. For example, across all 50 flights of the flight campaign, a total of only five ratings was requested during take-off and only twenty five were asked for during landing, compared to a total of more than 2.200 rating requests. Put to practical test, the Airbus Calculation System was therefore used to provide continuous estimates for each second of flight, an even wider and more valuable application than had been performed before.

#### **6.2.2 - Data collection procedures**

Data collection included acquisition of heart rate data for both pilots using portable recorders and aircraft data by using on-board recording equipment. Figure 15 schematizes the patent pending Airbus Workload Calculation system.

Cardiac periods were recorded from the electrocardiogram of each pilot by means of a portable microcomputer (VITALOG PMS8). A specific program enabled the identification of the heart rate record, its synchronization to the flight parameters, the test of each cardiac period and record. The resulting data was stored in solid-state memory for subsequent recovery and display by a personal computer acting as the Data Manager and installed in the A320. Saved in binary format after each flight, the physiologic data was subsequently converted in decimal format and transferred to a ground-based personal computer when returning to base to be checked and processed into heart rate variability indices. The aircraft data was also converted to a standard format, 9 track, 1.600 BPI magnetic tape for use by the calculation programs, all of which were designed to run on the PC-system.

Logging of flight events and crew activities by qualified observers and from closed-circuit video screens allowed to determine actual flight condition so as to have only one rating calculation rather than the 4 parametric possibilities according to normal/emergency or checklist/no checklist combinations. This observation was also synchronized with ECG-recordings by means of an identification signal at the start of observer logging.

Analysis included the determination of flight phases from the aircraft data followed by the calculation of workload estimates and the preparation of output tables and graphic presentations.

### 6.2.3 - Scenarios of the A320 Campaign

Having received somewhat limited training compared to genuine airline standards -not an exception at that stage of aircraft development- all crews had to demonstrate the necessary understanding and ability to handle problems and failures involved in sometimes very demanding scenarios. Their purpose in the context of minimum crew demonstration was to provide a range of low to high workload situations in order to determine the suitability of the A320 for operations with a crew complement of two pilots. Twelve different flight scenarios were drawn which each crew flew at least once.

With newly introduced FBW technology, an integrated FMGS (AFS + ATS + FMS) and a rearranged EIS architecture (EFIS + ECAM), the A320 exercise focused on simulated problems (flight and dispatch) pertaining to:

- Fly-by-wire computer failures (ELAC, SEC, FCDC) resulting in transitions to alternate and direct control or manual flight,
- Flight management and guidance failures resulting in manual flight, conventional navigation and loss of automatic radio and navaid selections,
- Automatic thrust control failures resulting in manual throttle handling,
- Electronic failures concentrating on ECAM (complete loss, loss of aural warnings, local warnings only, loss of red and amber cautions) or on EFIS,
- Electronic failures concentrating on EFIS (loss of display unit, electrical problems, flight controls unit failures causing the loss of the EFIS control panel and automatic selections on navigation displays).

As a result, these cases were covered by the first seven flight scenarios, the remainder concentrating on rather traditional themes also exercised in former demonstrations:

- pressurization loss followed by emergency descent or by manual control,
- electrical AC or DC problems,
- hydraulic failure resulting in gravity gear extension,
- incapacitation of captain or first officer.

In principle, an effort was made to limit the combined event probabilities to a realistic level of  $10^{-7}$ /flying hour but in several cases it was necessary to go beyond this objective in order to find the most judicious combinations of failures. The normal flight scenario was maintained on purpose to evaluate the impact on workload in these conditions. Weather was representative of winter operations, flights were routed through heavy traffic areas.

### 6.2.4 - Statistical tests

Two main products are derived from the Airbus Workload Calculation System: statistics and calculated timelines.

A series of analyses was undertaken to gradually determine the validity of using the model on the A320:

- correlation coefficient between actual and calculated ratings on a case-by-case basis,

- correlation coefficient between actual and calculated ratings per flight phase,
- correlation coefficient between actual and calculated mean ratings per scenario type,
- calculated mean ratings by flight phase and for each crewmember on a flight-by-flight basis.

It should be clearly kept in mind that the model produces an estimate on the same workload scale from two to eight as practised through dynamic workload rating by the pilots.

Overall, of the 2382 ratings for which data for both the model and the pilot's actual quotation were available, the correlation coefficient was 0.498. This is higher than for the A310-300 limited validation (0.44) and is also associated with much less than one chance in 10,000 that the finding is not real.

When the actual and calculated ratings for the in-flight-only phases (take-off, climb, cruise, descent, rapid descent, approach and landing) are correlated, the coefficient increases to 0.534. The correlation between actual and (predicted or processed) calculated mean ratings for the in-flight phases reaches 0.729. As shown in figure 16 the correlation by scenario mean is also excellent at 0.772. These high correlations leave virtually no doubt that the workload calculations stemming from the model are valid and further support the applications of this technique.

#### 6.2.5 - Timeline Plots

The validity of the workload model calculations having been shown, it became relevant to use the calculated rating values to analyse each flight in more detail than was possible with the number of actual ratings which yielded the calculated timelines.

Timelines were drawn for actual and calculated pilot ratings (every 15 seconds from the start of data acquisition) for all of the 50 flights of the campaign further providing graphical confirmation of good correspondences as exemplified by figure 17. Planned, simulated failures as part of the test scenario are indicated by triangles. When the failure was reset during flight, both a starting and ending triangle are shown. If the failure continued throughout the flight, only a single triangle is shown.

The relative shapes and position of the curves for CM1 and CM2 provide an indication of the workload imposed during the various phases of the flight by the scenario and the regular task of flying that route on that very day with its prevailing weather and ATC conditions. The curves also present a view of the degree to which the crew shared the workload throughout the flight. The staggered appearance of some curves (Figure 18) points to possibly pilot-induced lags in level, phase and tendency. It should be remembered that the pilot rating interrogation process is strictly under control of the observer and that the rating requests are sometimes delayed to avoid possible intrusion especially when workload is higher than usual. Being required to provide "an aggregate rating since last request" pilots may at times put more or less weight than appropriate to account for past workload trends especially when they asked for ratings soon enough after the onset of these workload increases or decreases. Too frequent requests in the absence of any really significant workload shifts can on the other hand induce serial dependencies. At some point here, the pilot may rate one category higher or lower because he either thinks the observer genuinely notices different workload from his side, either he decides to disrupt the monotoneous pattern of always providing the same rating.

#### 6.2.6 - Discussion

The calculated curves need to be assessed in the context of actual scenario progress. Figure 16 depicts an ECAM/FAC situation type with logical concordances between failure onset/cancellation and calculated model responses confirming workload trends stemming from subjective ratings. For crews with apparent lack of knowledge, training and experience some basic scenario combinations (as in Figure 19) appeared to add difficulties to the extent that some kind of adverse synergism contributed to create even higher workload than for each problem taken individually. Overall and in most planned scenarios workload was low to moderate with a smaller proportion of higher workload. Prolonged legs (Figure 20) with no technical failures nor operational difficulties brought some crewmembers to very low workload levels only to be incremented during descent and approach phases. This adds to the growing body of evidence that the long debated issue of pilot overload may have overshadowed an equally appropriate focus on just the opposite concern which is underload (Clauzel J.S. and G. Stone, November 1983).

Calculated ratings also provide additional information for those times and situations during which there were not too many actual ratings to reach a workload assessment. Special effects can be assessed such as FBW control law transitions from normal to alternate and reverse or from alternate to direct law prior to landing as respectively illustrated in Figures 17 and 18. In no cases did any of these transitions hamper pilots for landing. In a related way, an increased workload pattern for the PF in one of these certification flights was explained by a windshear encounter just prior to landing. Judgment and expertise need to be exercised to assess the calculated timelines with regard to workload acceptability and variability.

### 6.3 - Application to the study of errors and automation

One of the other advantages of calculating continuous measures of workload is that an attempt can be made to relate spontaneous crew errors to the workload level at the exact point in time that the error occurred. Crew workload is one of the most important human factors parameters in aviation because high workload can lead to errors. Sustained high workload levels will overtax the crew, limit spare capacity to attend to anything but the task at hand and hereby increase the probability of error and accident. Conversely, sustained low workload may also lead to errors since the pilot may lose situational awareness and have difficulty getting back into the loop.

Blomberg and Schwartz took the unique opportunity offered by the A320 minimum crew demonstration to investigate more fully the relationship between workload and errors. In these certification flights crew errors had to be detected by the pilot observers, recorded at the time they occurred and entered into the data collection system.

#### 6.3.1 - General approach

Errors were categorized by their severity as (Speyer, Monteil, February 1988):

- . Minor (M) - Slips or procedural problems which could be fixed promptly,
- . Important (I) - More serious deviations from proper procedures which were ultimately corrected or errors not related to safety which went uncorrected by the crew,
- . Safety-related (S) - Problems with the potential to degrade safety whether corrected or not.

Only one of the 75 identified errors was deemed of the "Safety-related" type by the observers. This error was one of the "knowledge-representation" type with momentary scenario interruption decided by the Flying Director subsequent to a complete loss of radiocommunications wrongly suspected by the crew. For the purpose of these analyses this error was combined with those in the "Important" category for a total of 17 in both categories. The remaining 58 errors were judged to be "Minor".

These same errors were also categorized as to the pilot's likely awareness of their occurrence (Blomberg, Schwartz et al, September 1988):

- . Unaware (U) - Errors not resulting in an alarm or any immediate or long term change in the aircraft performance or flying task,
- . Aware (A) - Errors resulting in an alarm or the almost sure need for remedial actions at some time relatively soon after the error had been committed.

Examples of the "Unaware errors" concern cases such as checklist omissions, slight deviations from target flight levels, and incorrect barometer settings. Examples of the "Aware-type" include failure to notice the autopilot was disconnected, lack of speed holding in climb, or forgetting that both autothrottle systems were lost.

The underlying assumption of this categorization is that error awareness produces different workload effects due to remedial activities or emotional reactions than errors that go unnoticed by the pilot.

Errors were located on the timeline plots of calculated workload ratings to assess:

- . the relative workload level at the time or the error with respect to the total workload profile, i.e. low, medium or high,
- . the workload trends prior to and immediately following the time of the error, i.e. increasing, decreasing or steady.

#### 6.3.2 - Results and Discussion

Whereas the M errors were approximately evenly distributed among low, medium and high relative workload segments, the "I+S" errors on the other hand were most likely to be observed during periods of medium and high prevailing workload and relatively unlikely to occur with low workload.

While "M" errors were to be associated with decreasing workload, "I+S" errors appeared to be rather linked with increasing workload. A significant statistical indication prevailed for almost half of the "pilot aware"-errors to happen in periods of increasing workload and half of the "pilot unaware"-ones to take place when workload was decreasing.

Error awareness was however not systematically related to any of the three prevailing workload levels themselves.

All of the "I+S" errors that occurred at a high workload level were associated with increasing workload just prior to the time of error and usually with decreasing workload thereafter. This suggests that when workload is high and increasing and an error occurs, that error will be severe.

Any workload decrease after the peak may be the result of the pilot "giving up" and shedding tasks, just as it may simply be an artifact of the exercise since expert assistance is always available from other specialists in the cockpit.

Conversely with workload decreasing before an "I+S" error, it was more likely to level off or increase further on which is consistent with the possible generation of workload by the higher severity errors.

Workload data could also be used for a more molar analysis to investigate the relationship between workload and automation.

In the A320 certification flights, scenarios were arranged to vary the flying problem presented to the pilots. In the process of creating scenarios, the automation level was not systematically varied. However, three of the 12 scenarios had different but relatively constant levels of automation for the majority of their in-flight periods. Aggregating both pilots' second-by-second model estimates by phase and for each of the three scenarios considered helped to derive a potentially strong inverse relationship between workload and automation level confirming practical experience. The lowest automation scenario that required conventional navigation on standby instruments shows the highest average workload. And the highest automation situation, which is normal flight, provides the lowest workload. Finally, the moderate automation case, which involved systems monitoring without the ECAM displays or cautions & warnings, lies in between.

#### 7 - CONCLUSION

As a tool to investigate the impact of new technology or the effect of human factors on the operational interface, the Airbus Workload Model opens new avenues in the study of workload and vigilance and their relationships to both errors and automation. One of the great strengths of the model is its ability to offer continuous data, a unique opportunity which no other documented workload technique offers throughout the entire duration of a real flight.

Much further work remains however to be done to evaluate the impact of aircraft technology. Which should be performed more thoroughly by also investigating the impact of the airline operational environment itself. The Airbus Workload Model will soon be put to test in actual airline operations teaming up with medical research as to the effect of monotony on vigilance and biomechanical behaviour (A. Coblenz, G. Ignazi, R. Mollard, M. Sauvignon, October 1986). In this context, the upcoming trend towards ultra long-haul operations will accentuate the issue due to low cruise workload and high automation, circadian rhythms, sleep disturbance/deprivation, duty time and ensuing fatigue (Wegmann H., Conrad B., Klein K., March 1983; Graeber C. et al, December 1986). Due consideration will be needed to assist the crew in maintaining sufficient vigilance by means of flight procedures or aircraft systems tailored around human performance and cognitive engineering. Ensuring a safe response from pilots even in periods of diffused arousal will need proper reactivation in order to bring them back into the informational loop and maximize their situational awareness if necessary (Nagano H, October 1985).

Inevitably, some of this work will some day have to focus on human performance capabilities, i.e. on the characteristics of good airmanship. A number of studies from Gopher (Gopher D., 1982; Gopher D. and Kahneman, 1982) have indeed indicated that good pilots significantly differentiated themselves from less well performing ones with regard to their mental attention and concentration capabilities.

More understanding of pilot knowledge representation and of learning and cognitive processes will also be required to better understand pilot behaviour with regard to new technology airplanes. The existence of a technically stimulating environment (as for test pilots), the pilot selection process, the training level of the airline, discipline in operations, personality traits and the high degree of functionality in new technology interfaces, all have brought to bear wide variations in perceptions and knowledge representation of aircraft systems. A number of studies from Boy (Boy, 1988) have also stressed on the organization of learned analytical knowledge and on its progressive transfer into compiled situational knowledge and controlled processes as a function of the topic's structure or problem to be solved.

Airbus Industrie is fully committed to human factors analysis in flight test development and operations engineering. But it has an even larger commitment to an informal human factors orientation in cockpit/aircraft procedures' design and operational review. The major emphasis being on safety and design-induced error tolerance it will maintain put an adapted emphasis on formal ergonomics studies. Research funds being limited Airbus Industrie will nonetheless continue to apply itself towards selected topics in the investigation of the impact of aircraft technology on the operational interface.

## REFERENCES

-----

GLOSSARY

AC : Alternative Current  
 ADI : Attitude Direction Indicator  
 AFC : Automatic Flight Control  
 AFCS : Automatic Flight Control System  
 AFS : Automatic Flight System  
 ANOVA : Analysis of Variance  
 APU : Auxiliary Power Unit  
 ATC : Air Traffic Control  
 ATS : Autothrottle system  
  
 BAe : British Aerospace  
  
 C\* : C-star fly-by-wire control law  
 CAT III/II : Category III/II  
 CDU : Control and Display Unit  
 CM1 : Crewmember 1: left seated pilot  
 CM2 : Crewmember 2: right seated pilot  
 CRT : Cathode Ray Tube  
  
 DC : Direct Current  
 DGAC : Direction Générale de l'Aviation Civile  
 DME : Distance Measurement Equipment  
  
 ECAM : Electronic Centralized Aircraft Monitor  
 ECG : Electrocardiogram  
 EFCS : Electronic Flight Control System  
 EFIS : Electronic Flight Instruments  
 EICAS : Engine Indicating Caution and Advisory System  
 EIS : Electronic Instrument System  
 ELAC : Elevator and Aileron Computer  
 ESAU :  
  
 FAA : Federal Aviation Agency  
 FAC : Flight Augmentation Computer  
 FADEC : Full Authority Digital Engine Control  
 FAR : Federal Airworthiness Regulations  
 FBW : Fly-by-wire flight control system  
 FCC : Flight Control Compute  
 FCDC : Flight Controls Data Concentrator  
 FCU : Flight Control Unit  
 FD : Flight Director  
 FFCC : Forward Facing Crew Cockpit  
 FMA : Flight Mode Annunciator  
 FMC : Flight Management Computer  
 FMGS : Flight Management and Guidance System  
 FMS : Flight Management System  
 FPV : Flight Path Vector  
 FWC : Flight Warning Computer  
  
 HF : High Frequency  
 HSI : Horizontal Situation Indicator  
  
 ILS : Instrument Landing System  
 INS : Inertial Navigation System  
 IRS : Inertial Reference System  
  
 JAR : Joint Airworthiness Regulations  
  
 MCDU : Multipurpose Control and Display Unit  
 MIT : Massachusetts Institute of Technology  
 MSN : Manufacturer's Serial Number  
  
 N1 : Engine fan speed thrust control parameter  
 NASA : National Aeronautics and Space Administration  
 NAV : Navigation: horizontal mode of the FMS  
 ND : Navigation Display  
 NDB : Non Directional Beacon  
 NSTB : National Transportation Safety Board  
  
 OP : Open Profile

PFD : Primary Flight Display  
 PROF : Profile: vertical mode of the FMS  
 RMP : Radio Management Panel  
 SD : System Display  
 SEC : Spoiler and Elevator Computer  
 SID : Standard Instrument Departure  
 SPD : Speed Mode of AFS-ATS  
 SRS : Speed Reference System  
 SSR : Secondary Surveillance Radar  
 STAR : Standard Arrival Route  
 TCC : Thrust Control Computer  
 VFW : Vereinigte Flugwerke  
 VHF : Very High Frequency  
 VOR : Very High Frequency Omni Directional Range  
 WD : Warning Display

#### BIBLIOGRAPHY

- AMALBERTI R., CERMA**  
 "Pilotes Superviseurs et Gestionnaires de Systèmes Automatiques.  
 Un nouveau rôle bien risqué pour la fiabilité du couple homme-machine",  
 in AGARD-CP-425, on the Man-machine Interface in Tactical Aircraft Design and Combat  
 Automation, September/October 1987
- BABCOCK G.L., EDMUNDS W.W., STONE R.B., ALPA**  
 "Information Transfer and the Changing Role of the Pilot", SAE paper 821413, October  
 1982
- BAUD P. & IVANOFF D., Airbus Industrie Flight Division,**  
 "Cockpit Display of A310",  
 Airbus Industrie presentation at International Symposium, Tokyo, August 1982
- BENZECRI J.-P. et BENZECRI F.**  
 Pratique de l'Analyse des Données,  
 Analyse des Correspondances DUNOD, Paris, 1980
- BLOMBERG R.D., Dunlap & Associates Inc, SPEYER J.-J., Airbus Industrie Flight Division**  
 "Fly-by-wire Performance Analysis", FAST  
 Airbus Technical Digest Number 9, July 1988
- BLOMBERG R.D., SCHWARTZ A.L., Dunlap & Associates Inc, SPEYER J.-J., Airbus Industrie  
 Flight Division, FOUILLOT J.-P., Cochin Faculty Laboratory of Adaptation Physiology,  
 Paris**  
 "Application of the Airbus Workload Model to the study of Errors and Automation", in  
 NATO Advanced Research Workshop Vigilance and Performance in Automatized Systems.  
 Org.: Prof A. Coblentz  
 Laboratoire d'Anthropologie et d'Ecologie Humaine - Université René Descartes, PARIS,  
 September 1988
- BOY G., CERT-Onera**  
 "Assistance à l'Opérateur: Une Approche de l'Intelligence Artificielle",  
 Editions TECHNEA, Toulouse, France, September 1988
- BRUGGINK G.**  
 "Reflections on the Potomac",  
 International Journal of Aviation Safety (1), 5-12, 1983  
 "Report on accident of MH 684 at Kuala Lumpur",  
 "Report on accident of SAS 901 at JFK, New York",  
 International Journal of Aviation Safety (3,3), 218-222, 1985
- CAESAR H., Lufthansa**  
 "Design Philosophies of New-Technology Aircraft and Consequences for its Users",  
 Flight Safety Foundation presentation at the 38th Annual International Air Safety  
 Seminar, Boston, November 1985
- COBLENTZ A., IGNAZI G., MOLLARD R., SAUVIGNON M.**  
 Laboratoire d'Anthropologie Appliquée, Université René Descartes - Paris V  
 "Effect of Monotony on Vigilance and Biomechanical Behaviour"  
 In: Commission of European Communities-Proceeding of the Workshop  
 "Vigilance: Methods, Models and Regulation"  
 Leonard J. Ed., Dusseldorf, October 1986

- CORPS G.C., Airbus Industrie Flight Division**  
Airbus A320 Side Stick and Fly-By-Wire, An update",  
SAE paper 861801, October 1986
- CURRY R.E., NASA Ames Research Center, Moffett Field, CA**  
"The Introduction of New Cockpit Technology: A Human Factors Study", NASA Technical Memorandum 86659, May 1985
- CLAUZEL J.S. and STONE G., Douglas Aircraft Company**  
"Flight Crews and Advanced Technology Cockpits - The Safety Challenge",  
Flight Safety Foundation presentation at the 36th Annual International Air Safety Seminar, Rio de Janeiro, November 1983
- EDWARDS E., University of Aston in Birmingham**  
"Man and Machine: Systems for Safety",  
Proceedings of the BALFA Technical Symposium, London, 1972
- EDWARDS E., University of Aston in Birmingham**  
"Automation in Civil Transport Aircraft"  
Applied Ergonomics, 8.4, 194-198, 1977
- FITTS P.M.**  
"Engineering Psychology and Equipment Design", in "Handbook of Experimental Psychology" Stevens SS (Ed), John Wiley & Sons, New York, 1951
- FOUILLOT J.-P., REGNARD J., SPEYER J.-J., TEKAJA F., DROZDOWSKI T., LEBLANC A., RIEU M.**  
"Ambulatory Monitoring of Air Crew Heart Rate Variability", presented at the 1985 ISAM Symposium. Proceedings of the Fifth International Symposium on Ambulatory Monitoring, 1985
- FOUILLOT J.-P., TEKAJA F., BLOMBERG R.D., BENAODIA M., SPEYER J.-J.**  
"Etude de la Variabilité Cardiaque de Pilotes d'Airbus",  
NATO Advanced Research Workshop Vigilance and Performance in Automatized Systems.  
Org.: Prof A. Coblentz  
Laboratoire d'Anthropologie et d'Ecologie Humaine - Université René Descartes, PARIS,  
September 1988
- GANNETT J.R.**  
"The Pilot and the Flight Management System", Symposium on Behavioral Objectives in Aviation Automated Systems, SAE, October 1982
- GERBERT K., KEMMLER R., German Air Force Institut of Aerospace Medicine**  
"The Causes of Causes: determinants and background variables of human factor incidents and accidents"  
ERGONOMICS, 25(11), p. 1439-1453, 1986
- GOPHER D.**  
"A selective attention tests as a predictor of success in flight training"  
Human Factors, 24, p. 173-183, 1982
- GOPHER D. and KAHNEMAN D.**  
"Individual differences in attention and the prediction of flight criteria"  
Perceptual and Motor Skills, 33, p. 1335-1342, 1982
- GRABER C. (Ed.), NASA-Ames Research Center, Moffset Field, CA, USA**  
"Sleep and Wakefulness in International Aircrews"  
A Cooperative Study by DFVLR, Jikei University School of Medecine, NASA-Ames Research Center, RAF Institute of Aviation Medecine, Stanford University School of Medecine
- KLOPFSTEIN M., CENA**  
"Image mentale et représentation des informations de pilotage des avions"  
Séminaire Erreurs Humaines et Automatisation, Ecole Nationale d'Aviation Civile,  
Toulouse, 19 et 20 Mai 1987
- LEPLAT J.**  
"Les Représentations Fonctionnelles dans le Travail" in Psychologie Française, 30  
(314), p. 269-275, 1985
- LIPSON Ch., NARENDRA J.S.**  
"Statistical Design and Analysis of Engineering Experiments", McGraw Hill Inc, 1973
- LAUBER J.K., NASA**  
"Aviation Technology and the Flight Crew"  
International Aeronautical Symposium, Tokyo, August 1982
- LAUBER J.K., NASA**  
"Resource Management on the Flight Deck" in Proceedings of a NASA/Industry workshop,  
San Francisco, CA  
Report NASA CP-220, March 1980

- MACHADO F.**  
 "The destruction of KAL 007: How did it happen?"  
 International Journal of Air Safety (2), 5-14, 1984
- MOLLARD R., IGNAZI G., Université René Descartes**  
 "Automatisation et Performance : Dessins et Perspectives"  
 Proceedings of EEC-workshop on Effects of Automation on Operator  
 Performance, Laboratoire d'Anthropologie Appliquée,  
 Université René Descartes, Paris, October 1986
- MOLLET C., Swissair**  
 "Training to and from the Automated Cockpit" in Proceedings of the 7th General Flight  
 Crew Training Meeting, IATA, February 1980
- NAGANO H., Japan Airlines**  
 "Mental Fitness for Duty and Control of Arorisal State", SAE paper 851778,  
 October 1985
- NAGEL D.C.**  
 "Human Error in Aviation Operations" Ch. 9 in "Human Factors in Modern Aviation", p.  
 263-303, Wiener E.L. and Nagel D.C. (Eds), New York, Academic Press, 1988
- NETER J. and WASSERMAN W.,**  
 "Applied Linear Statistical Models", Housewood, Illinois, Irwin, 1974
- NEUMANN and BRANDT N., Lufthansa**  
 "Cockpit/Systems Survey - A310"  
 Paper presented at the 5th Airbus Industrie Performance and Operations Engineering  
 Conference Proceedings, Ch. 39 p. 1-26, Honolulu, Hawaii, May 1988
- NORDWALL B.D.**  
 "Electronic Cockpits are making Conventional Cockpits Obsolete", Aviation Week and  
 Space Technology, Issue of November 3rd 1986
- NTSB Aircraft Accident Report**  
 China Airlines Boeing 747-SP, N4522V, 300 Nm Northwest of San Francisco, CA,  
 19 February 1985 (NSTB-AAR-86/03), Washington D.C., March 1986
- O'DONNELL R.D. MTI Inc,**  
 "Performance Assessment Requirements for Future Cockpit Systems"  
 NATO Advanced Research Workshop Vigilance and Performance in Automatized Systems.  
 Org.: Prof A. Coblenz  
 Laboratoire d'Anthropologie et d'Ecologie Humaine - Université René Descartes, PARIS,  
 September 1988
- PELEGRIN M., CERT-Onera**  
 "Difficulties and Risks of the Semi-Automatic Control" (namely piloting modern  
 aircraft)  
 Proceedings of the EEC - workshop on Effects of Automation on Operator Performance,  
 Laboratoire d'Anthropologie Appliquée,  
 Université René Descartes, Paris, October 1986
- PELEGRIN M., CERT-Onera**  
 "Man and Systems"  
 Proceedings of the International Conference on Human-Machine Interaction and  
 Artificial Intelligence in Aeronautics & Space, Org. G. BOY, CERT-Onera,  
 September 1988
- ROSCOE A.H. and GRIEVE B.S.**  
 "The Impact of New Technology on Pilot Workload"  
 SAE paper 861773, October 1986
- ROSCOE A.H., Britannia Airways**  
 "Introduction to Practical Assessment of Pilot Workload"  
 p. 1-13, Ch. 1 of the Proceedings from Symposium on the Practical Assessment of Pilot  
 Workload, Ed. H.C. Muir and A. Roscoe, MD  
 Flight Systems Bedford Department Royal Aircraft Establishment, November 1986
- ROSCOE A.H., Britannia Airways**  
 "In-Flight Assessment of Workload Using Pilot Ratings and Heart Rate" p. 78-82, Ch.  
 12 of AGARD AG-282,  
 The Practical Assessment of Pilot Workload, Ed. by Dr A. Roscoe, June 1987
- ROSCOE A.H., Britannia Airways**  
 "Flight Deck Automation and Pilot Workload"  
 NATO Advanced Research Workshop Vigilance and Performance in Automatized Systems.  
 Org.: Prof A. Coblenz  
 Laboratoire d'Anthropologie et d'Ecologie Humaine - Université René Descartes, PARIS,  
 September 1988

- ROSKIE-HOFSTRAND R.J. & PAAP K.R., Aerospace Human Factors Division, NASA-Ames and Department of Psychology, New Mexico State University, USA**  
 "Cognitive networks as a guide to menu organization: An application in the automated cockpit"  
 Ergonomics, Vol 29, No 11, 1301-1311, 1986
- SCHMITT B., Swissair**  
 "Using Operational Experience in Designing Effective Flight Decks", Flight Safety Foundation presentation at the 37th Annual International Air Safety Seminar, Zurich, October 1984
- SEIFERT R. and BRAUSER K., MBB**  
 "New Flight deck Design in the light of Operational Capabilities", AGARD, Conference Proceedings n° 347, May 1983
- SHERIDAN T.B. and SIMPSON R.W., MIT, Cambridge, Massachusetts, USA**  
 "Towards the Definition and Measurement of the Mental Workload of Transport Pilots"  
 Final Report, Massachusetts Institute of Technology, Contract DOT-OS-70055, January 1979
- SHINGLEDECKER C.A., NTI Inc**  
 "Performance Assessment Techniques in Advanced Cockpit Systems"  
 NATO Advanced Research Workshop Vigilance and Performance in Automatized Systems. Org.: Prof A. Coblenz  
 Laboratoire d'Anthropologie et d'Ecologie Humaine - Université René Descartes, PARIS, September 1988
- SPEYER J.-J. and FORT A., Airbus Industrie Flight Division**  
 "Human Factors Approach in Certification Flight Test", SAE paper 821340, October 1982
- SPEYER J.-J. and FORT A., Airbus Industrie Flight Division**  
 "A310 Two-Man Crew Workload Analysis and Questionnaires", Report AI/V-F 383/83, 1983
- SPEYER J.-J., Airbus Industrie Flight Division**  
 "Premiers Développements vers une Intelligence Embarquée sur Airbus"  
 Proceedings of the Conference on Human-Machine Interaction and Artificial Intelligence in Aeronautics & Space, CERT-Onera, Matra, Airbus Industrie, p. 34-63, October 1986
- SPEYER J.-J. and FORT A., Airbus Industrie Flight Division, BLOMBERG R.D., Dunlap & Associates Inc, FOUILLOT J.-P., Cochin Faculty**  
 "Assessing Workload for Minimum Crew Certification" p. 90-115, Ch. 14 of AGARD AG-282, "The Practical Assessment of Pilot Workload", Ed. by Dr. A Roscoe, June 1987
- SPEYER J.-J. and FORT A., Airbus Industrie Flight Division**  
 "Communications: The Inside Track in Resource Management", SAE paper 871889, p. 245-259, October 1987
- SPEYER J.-J. and MONTKIL C., Airbus Industrie Flight Division**  
 A320-100/200 Certification Flight Test Report AI/E-V0 n° 474 411/87, February 23rd 1988
- SPEYER J.-J., Airbus Industrie Flight Division**  
 "Towards Design-Induced Error Tolerance"  
 Proceedings of the International Conference on Human-Machine Interaction and Artificial Intelligence in Aeronautics & Space, CERT-Onera, Matra, Dassault-Breguet, Aerospatiale, Airbus Industrie, p. 69-94, September 1988
- TEKAJA F., FOUILLOT J.-P., DROZDOWSKI T., REGNARD J., SPEYER J.-J., RIEU M.**  
 "Incidence des Contraintes Psychiques et Intellectuelles sur la Fréquence Cardiaque", Les Cahiers de l'Analyse des Données, Vol. 6 n° 2, p. 175-185, 1981
- TEKAJA F., FOUILLOT J.-P., DROZDOWSKI T., REGNARD J., LEBLANC A., SPEYER J.-J., RIEU M.**  
 "The Nearest Neighbors: Application to Workload and Heart Rate Variability", presented at the 1985 ISAM Symposium. Proceedings of the Fifth International Symposium Ambulatory Monitoring, 1985
- WANNER J.-C.**  
 Etude de la Sécurité des Aéronefs en Utilisation (ESAU)  
 Publication Service Technique Aéronautique, Ministère de la Défense, France, 1969
- WANNER J.-C.**  
 "Facteur Humain et Sécurité",  
 Académie Nationale de l'Air et de l'Espace,  
 Colloque International sur la Sécurité Aérienne, Novembre 1984 - Actualisé Août 1987
- WANNER J.-C.**  
 Partie Modélisation de l'Opérateur Humain dans "Catastrophe Non Merci", Carino A., Nicollet J.-L. and Wanner J.-P., Masson (Ed) March 1989

- WEGMANN H-M, CONRAD B. and KLEIN K., DVFLR-Institute for Aerospace Medicine, Cologne, W. Germany**  
 "Flight, Flight Duty, and Rest Times: A Comparison Between the Regulations of Different Countries"  
 Aviation, Space, and Environmental Medicine 54(3): p. 212-217, March 1983
- WIENER E.L., University of Miami, Coral Gables, Florida, USA**  
 "Controlled Flight into Terrain Accidents: System-Induced Errors",  
 Human Factors, 19(2), p. 171-181, 1977
- WIENER E.L., University of Miami, Coral Gables, Florida, USA**  
 "Midair Collisions: The Accidents, the Systems and the Realpolitik",  
 Human Factors, 22(5), p. 521-533, 1980
- WIENER E.L. & CURRY R.E.**  
 "Flight-deck Automation: Promises and Problems",  
 Human Factors, 23(10), p. 995-1011, 1980
- WIENER E.L., NASA Ames Research Center, Moffett Field, CA**  
 "Human Factors of Cockpit Automation: A Field Study of Flight Crew Transition", NASA Contractor Report 177333, July 1985b
- WIENER E.L., University of Miami, Coral Gables, Florida, USA**  
 "Cockpit Automation: in Need of a Philosophy", SAE paper 851956, October 1985
- WIENER E.L., University of Miami, Coral Gables, Florida, USA**  
 "Beyond the Sterile Cockpit", Human Factors, 27(1), p. 75-90, 1985a
- WIENER E.L., University of Miami, Coral Gables, Florida, USA**  
 "Fallible Humans and Vulnerable Systems: Lessons learned from Aviation"  
 NATO Workshop on Failure Analysis of Information Systems, Bad Windsheim, Germany, August 1986  
 NATO ASI Series. Vol F32, Information Systems: Failure Analysis, Ed. J.A. Wise and A. Debons Springer-Verlag Berlin Heidelberg 1987
- WIENER E.L., University of Miami, Coral Gables, Florida, USA**  
 "Cockpit Automation" Ch. 13 in "Human Factors in Modern Aviation" p. 433-461,  
 Wiener E.L. and Nagel D.C. (Eds), New York, Academic Press, 1988
- WIENER E.L. & NAGEL D.C.**  
 "Human Factors in Aviation",  
 Academic Press Series in Cognition and Perception, 1988
- ZIEGLER B., DURANDEAU M., Airbus Industrie**  
 "Flight Control System on Modern Aircraft", 14th ICAS Congress, Toulouse, September 1984

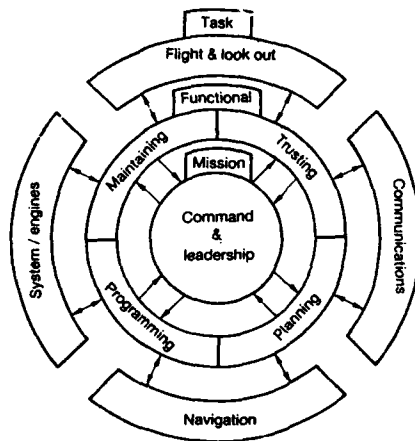


FIGURE 1 - Mission, Functional and task levels

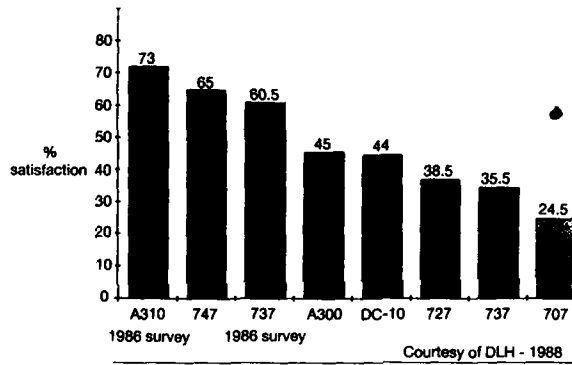


FIGURE 2 - Lufthansa Cockpit / Systems Survey

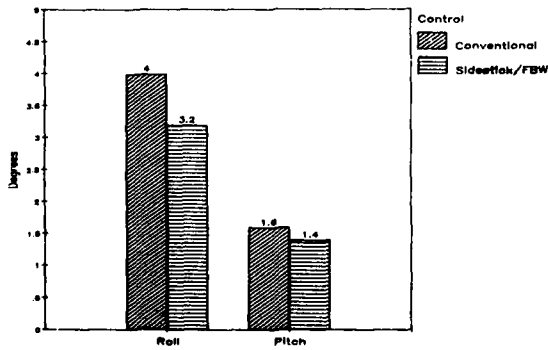


FIGURE 3 - Roll and Pitch Angles Standard Deviation

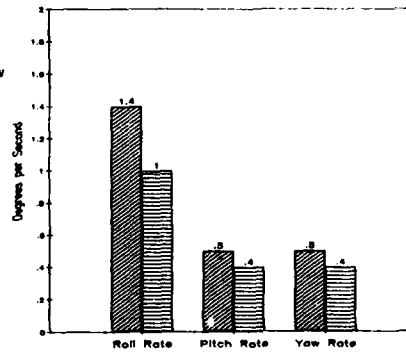


FIGURE 4 - Roll, Pitch and Yaw Rates Standard Deviation

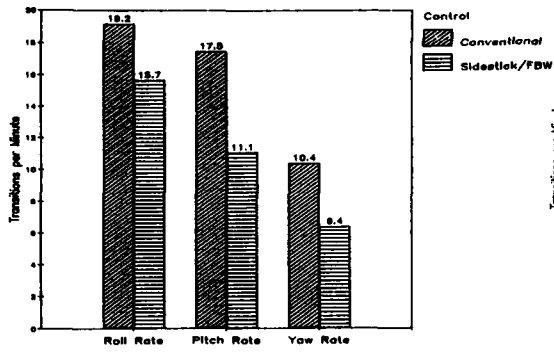


FIGURE 5 - Roll, Pitch and Yaw Rates Transitions through Zero

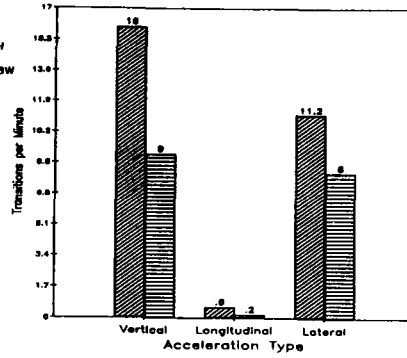


FIGURE 6 - Accelerations Transitions through Zero

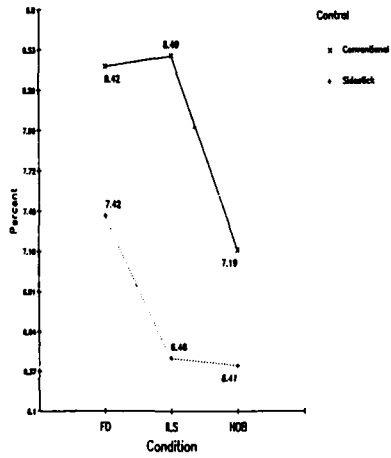


FIGURE 7 - N1 Engine Nr 1 Standard Deviation

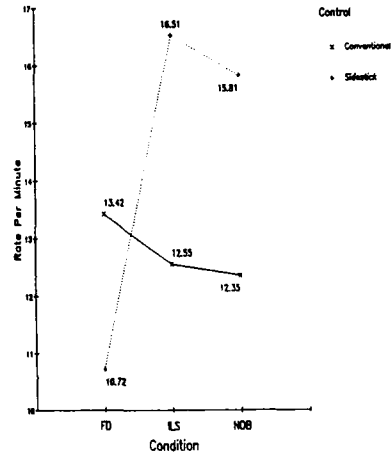


FIGURE 8 - N1 Engine Nr 1 Reversal Rate

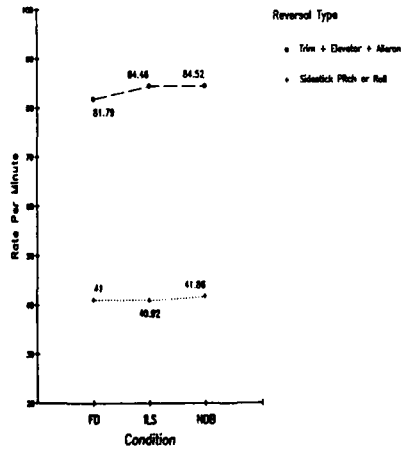


FIGURE 9 - Pitch Trim + Elevator + Aileron Reversals versus Any Sidestick Reversal

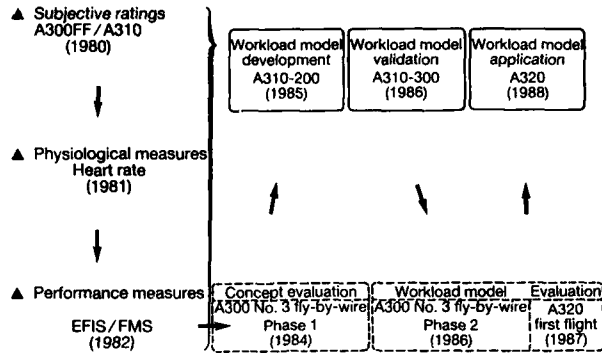


FIGURE 10 - Progress in Research & Development  
From Subjective Rating to Objective Workload Estimation

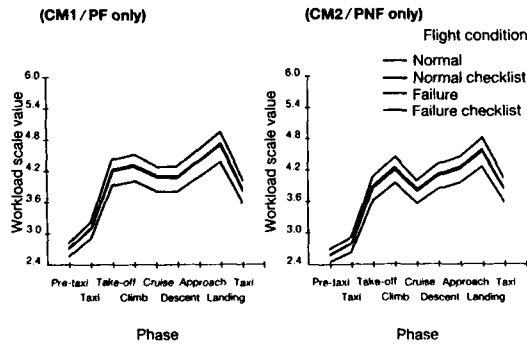


FIGURE 11 - A300 Sidestick/Fly-by-wire demonstration phase 2 (1986)  
Model Estimates by phase and flight condition

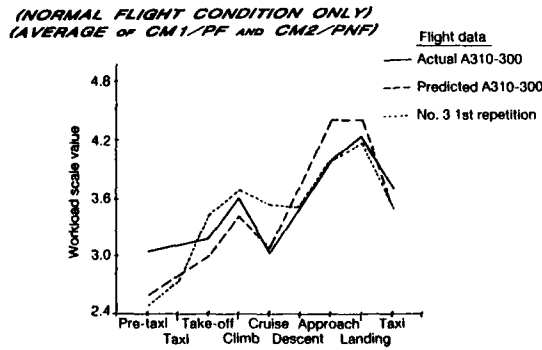
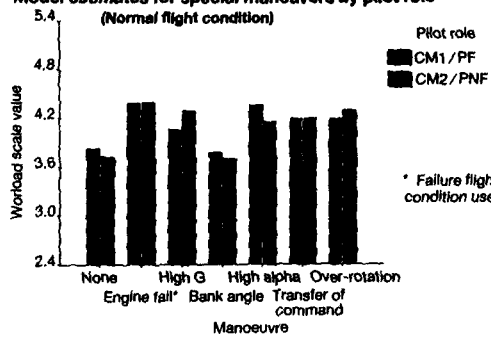


FIGURE 12 - A300 Sidestick/Fly-by-wire demonstration phase 2 (1986)  
Comparison of Estimates by flight phase with A310-300 validation

**Model estimates for special maneuvers by pilot role**  
(Normal flight condition)



**FIGURE 13 - A300 Sidestick/Fly-by-wire demonstration phase 2 (1986)**  
Model estimates for special manoeuvres by pilot role

**Model estimates by phase and flight condition**  
(CM1/PF) (CM2/PNF)

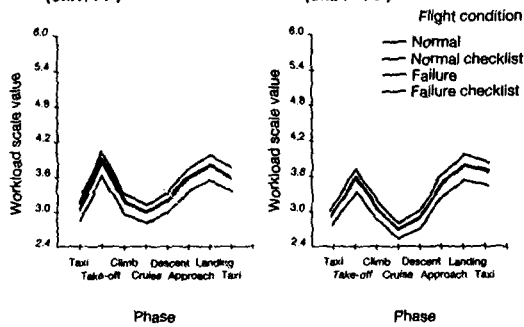


**FIGURE 14 - A320 1st Flight**  
Model estimates by phase and flight condition

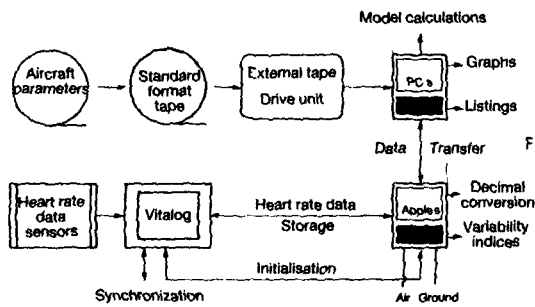


**FIGURE 15 - Airbus Workload Calculation System**  
Schematic of Data Acquisition Process

**Model estimates and actual ratings by scenario**

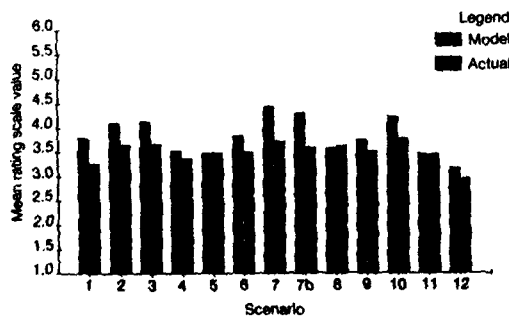


**FIGURE 16 - A320 Crew Complement Campaign**  
Comparison of pilot workload estimates  
Model estimates and actual ratings  
by scenario

Flight AIB 2534 - FRA/AMS (Jan. 25, 1988) scenario 6

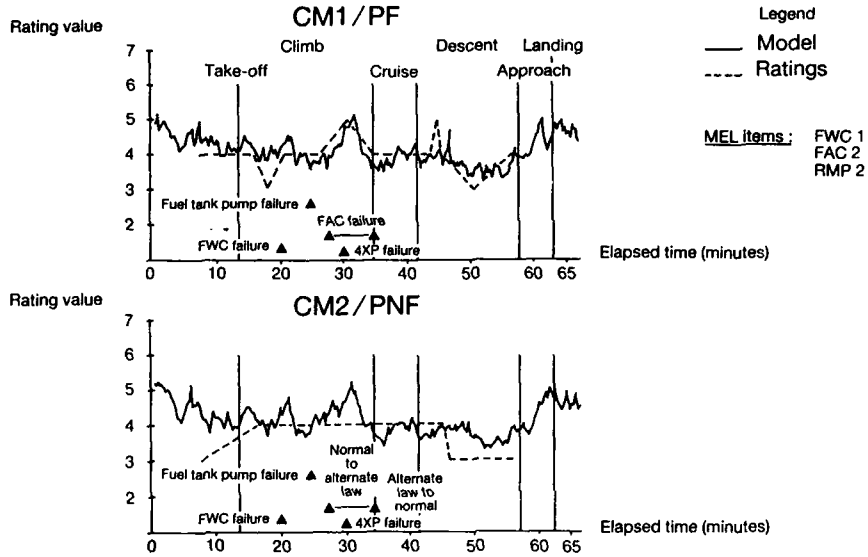


FIGURE 17 - A320 Crew Complement Campaign  
Flight's Timeline with Model Estimates and Actual Ratings:  
Example of good correspondances

Flight AIB 2915 - LHR/BST (Jan. 29, 1988) scenario 1

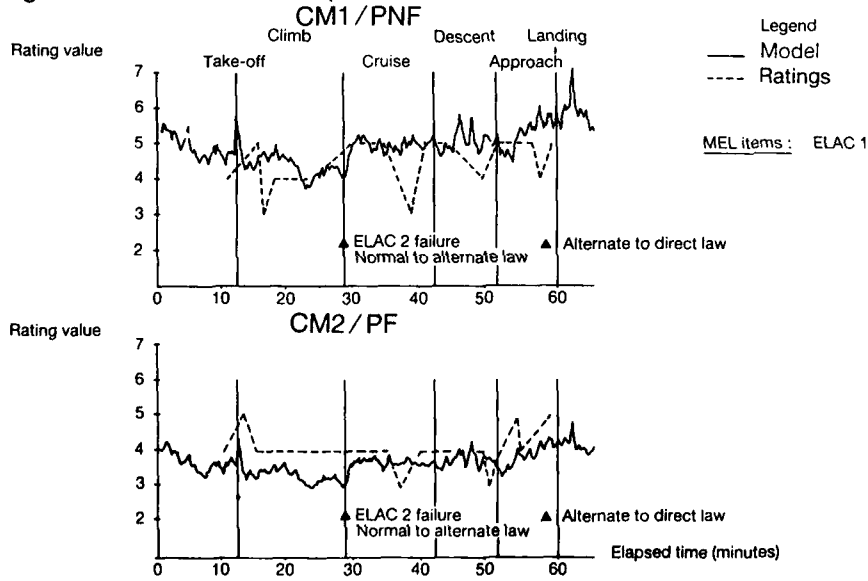


FIGURE 18 - A320 Crew Complement Campaign  
Flight's Timeline with Model Estimates and Actual Ratings:  
Example of staggered appearance

**Flight AIB 2846 - AMS/ORY (Jan. 28, 1988) Scenario 10**

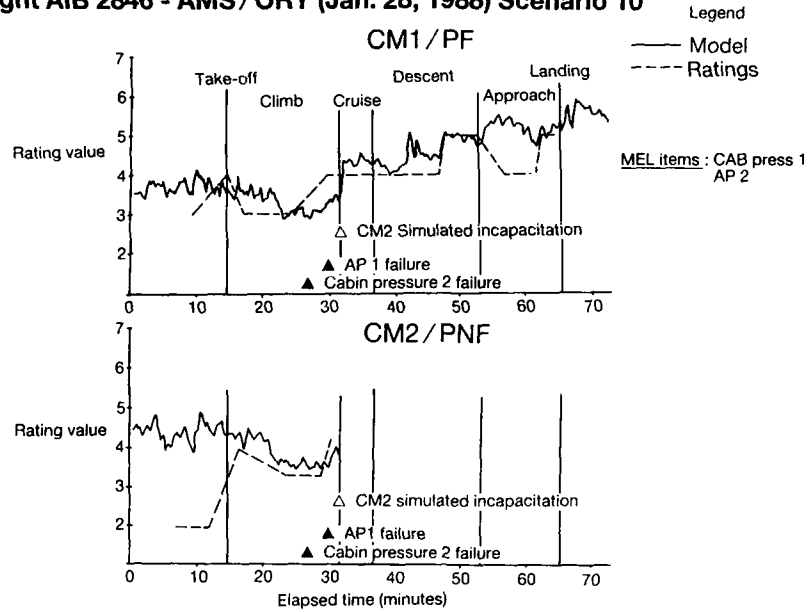


FIGURE 19 - A320 Crew Complement Campaign  
Flight's Timeline with Model Estimates and Actual Ratings:  
Example of workload synergism

**Flight AIB 3021 TLS/ATH (Jan. 30, 1988) Scenario 12 (normal flight)**

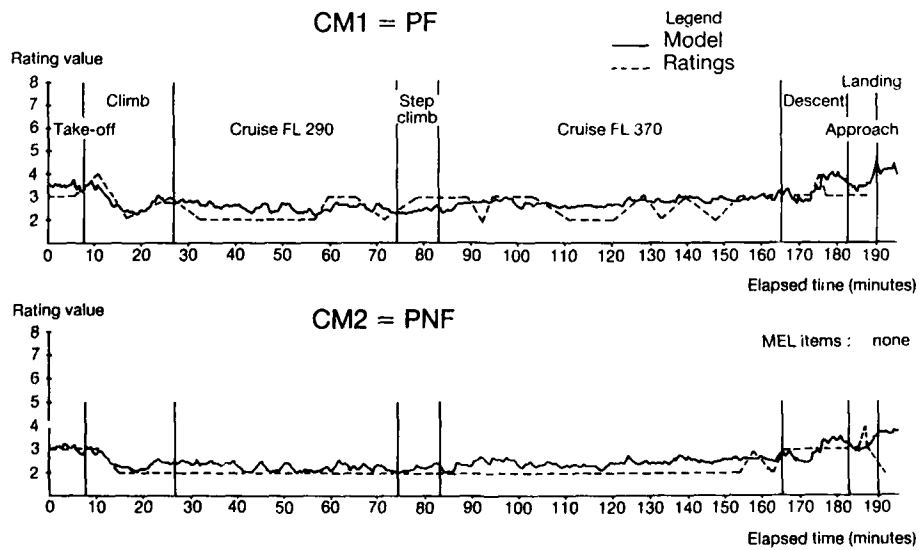


FIGURE 20 - A320 Crew Complement Campaign  
Flight's Timeline with Model Estimates and Actual Ratings:  
Example of very low workload levels

REPORT DOCUMENTATION PAGE															
1. Recipient's Reference	2. Originator's Reference AGARD-AG-30 Volume 1	3. Further Reference ISBN 92-835-0547-6	4. Security Classification of Document UNCLASSIFIED												
5. Originator	Advisory Group for Aerospace Research and Development North Atlantic Treaty Organization 7 rue Ancelle, 92200 Neuilly sur Seine, France														
6. Title	AIRCRAFT TRAJECTORIES -- Computation -- Prediction -- Control VOLUME 1														
7. Presented at															
8. Author(s)/Editor(s) Various	Edited by André Benoit		9. Date March 1990												
10. Author's/Editor's Address Various			11. Pages 268												
12. Distribution Statement	This document is distributed in accordance with AGARD policies and regulations, which are outlined on the Outside Back Covers of all AGARD publications.														
13. Keywords/Descriptors	<table border="0"> <tr> <td>Aircraft trajectories (computation--prediction--control)</td> <td>→ Flight simulation</td> </tr> <tr> <td>Aircraft models</td> <td>Genesis of wind</td> </tr> <tr> <td>Crew/automation</td> <td>Guidance laws</td> </tr> <tr> <td>Effect of wind variation</td> <td>Optimal trajectories</td> </tr> <tr> <td>Flight management computer system</td> <td>Wind models</td> </tr> <tr> <td>Flight in critical atmosphere</td> <td>Windshear</td> </tr> </table>			Aircraft trajectories (computation--prediction--control)	→ Flight simulation	Aircraft models	Genesis of wind	Crew/automation	Guidance laws	Effect of wind variation	Optimal trajectories	Flight management computer system	Wind models	Flight in critical atmosphere	Windshear
Aircraft trajectories (computation--prediction--control)	→ Flight simulation														
Aircraft models	Genesis of wind														
Crew/automation	Guidance laws														
Effect of wind variation	Optimal trajectories														
Flight management computer system	Wind models														
Flight in critical atmosphere	Windshear														
14. Abstract	<p>This volume is part of a set of three -- is composed of a preface and 11 papers covering respectively,</p> <ul style="list-style-type: none"> <li>— FUNDAMENTALS: General outline; Optimal trajectories; Non-linear models of aircraft.</li> <li>— FLIGHT IN CRITICAL ATMOSPHERIC CONDITIONS: Genesis of wind and influence on airplane trajectories; Flight control in windshear; Flight simulation.</li> <li>→ IMPACT OF NEW ON-BOARD TECHNOLOGIES ON AIRCRAFT OPERATION: Flight management in air transport; Crew/automation interface.</li> </ul> <p>This AGARDograph has been sponsored by the Guidance and Control Panel of AGARD.</p>														

<p>AGARDograph No.301 Volume 1 Advisory Group for Aerospace Research and Development, NATO <b>AIRCRAFT TRAJECTORIES: COMPUTATION — PREDICTION — CONTROL. VOLUME 1</b> Edited by André Benoit Published March 1990 268 pages</p> <p>This volume — part of a set of three — is composed of a preface and 11 papers covering respectively,</p> <p>— <b>FUNDAMENTALS:</b> General outline; Optimal trajectories; Non-linear models of aircraft.</p> <p>P.T.O.</p>	<p>AGARD-AG-301 Vol.1</p> <p>Aircraft trajectories (computation—prediction—control) Aircraft models Crew/automation Effect of wind variation Flight management computer system Flight in critical atmosphere Flight simulation Genesis of wind Guidance laws Optimal trajectories Wind models Windshear</p>	<p>AGARDograph No.301 Volume 1 Advisory Group for Aerospace Research and Development, NATO <b>AIRCRAFT TRAJECTORIES: COMPUTATION — PREDICTION — CONTROL. VOLUME 1</b> Edited by André Benoit Published March 1990 268 pages</p> <p>This volume — part of a set of three — is composed of a preface and 11 papers covering respectively,</p> <p>— <b>FUNDAMENTALS:</b> General outline; Optimal trajectories; Non-linear models of aircraft.</p> <p>P.T.O.</p>	<p>AGARD-AG-301 Vol.1</p> <p>Aircraft trajectories (computation—prediction—control) Aircraft models Crew/automation Effect of wind variation Flight management computer system Flight in critical atmosphere Flight simulation Genesis of wind Guidance laws Optimal trajectories Wind models Windshear</p>
<p>AGARDograph No.301 Volume 1 Advisory Group for Aerospace Research and Development, NATO <b>AIRCRAFT TRAJECTORIES: COMPUTATION — PREDICTION — CONTROL. VOLUME 1</b> Edited by André Benoit Published March 1990 268 pages</p> <p>This volume — part of a set of three — is composed of a preface and 11 papers covering respectively,</p> <p>— <b>FUNDAMENTALS:</b> General outline; Optimal trajectories; Non-linear models of aircraft.</p> <p>P.T.O.</p>	<p>AGARD-AG-301 Vol.1</p> <p>Aircraft trajectories (computation—prediction—control) Aircraft models Crew/automation Effect of wind variation Flight management computer system Flight in critical atmosphere Flight simulation Genesis of wind Guidance laws Optimal trajectories Wind models Windshear</p>	<p>AGARDograph No.301 Volume 1 Advisory Group for Aerospace Research and Development, NATO <b>AIRCRAFT TRAJECTORIES: COMPUTATION — PREDICTION — CONTROL. VOLUME 1</b> Edited by André Benoit Published March 1990 268 pages</p> <p>This volume — part of a set of three — is composed of a preface and 11 papers covering respectively,</p> <p>— <b>FUNDAMENTALS:</b> General outline; Optimal trajectories; Non-linear models of aircraft.</p> <p>P.T.O.</p>	<p>AGARD-AG-301 Vol.1</p> <p>Aircraft trajectories (computation—prediction—control) Aircraft models Crew/automation Effect of wind variation Flight management computer system Flight in critical atmosphere Flight simulation Genesis of wind Guidance laws Optimal trajectories Wind models Windshear</p>

<ul style="list-style-type: none"> <li>- FLIGHT IN CRITICAL ATMOSPHERIC CONDITIONS: Genesis of wind and influence on airplane trajectories; Flight control in windshear; Flight simulation.</li> <li>- IMPACT OF NEW ON-BOARD TECHNOLOGIES ON AIRCRAFT OPERATION: Flight management in air transport; Crew/automation interface.</li> </ul> <p>This AGARDograph has been sponsored by the Guidance and Control Panel of AGARD.</p> <p style="text-align: right;">ISBN 92-835-0547-6</p>	<ul style="list-style-type: none"> <li>- FLIGHT IN CRITICAL ATMOSPHERIC CONDITIONS: Genesis of wind and influence on airplane trajectories; Flight control in windshear; Flight simulation.</li> <li>- IMPACT OF NEW ON-BOARD TECHNOLOGIES ON AIRCRAFT OPERATION: Flight management in air transport; Crew/automation interface.</li> </ul> <p>This AGARDograph has been sponsored by the Guidance and Control Panel of AGARD.</p> <p style="text-align: right;">ISBN 92-835-0547-6</p>
<ul style="list-style-type: none"> <li>- FLIGHT IN CRITICAL ATMOSPHERIC CONDITIONS: Genesis of wind and influence on airplane trajectories; Flight control in windshear; Flight simulation.</li> <li>- IMPACT OF NEW ON-BOARD TECHNOLOGIES ON AIRCRAFT OPERATION: Flight management in air transport; Crew/automation interface.</li> </ul> <p>This AGARDograph has been sponsored by the Guidance and Control Panel of AGARD.</p> <p style="text-align: right;">ISBN 92-835-0547-6</p>	<ul style="list-style-type: none"> <li>- FLIGHT IN CRITICAL ATMOSPHERIC CONDITIONS: Genesis of wind and influence on airplane trajectories; Flight control in windshear; Flight simulation.</li> <li>- IMPACT OF NEW ON-BOARD TECHNOLOGIES ON AIRCRAFT OPERATION: Flight management in air transport; Crew/automation interface.</li> </ul> <p>This AGARDograph has been sponsored by the Guidance and Control Panel of AGARD.</p> <p style="text-align: right;">ISBN 92-835-0547-6</p>

AGARD

NATO  OTAN

7 rue Ancelle · 92200 NEUILLY-SUR-SEINE  
FRANCE

Telephone (1)47.38.57.00 · Telex 610 176

DISTRIBUTION OF UNCLASSIFIED  
AGARD PUBLICATIONS

AGARD does NOT hold stocks of AGARD publications at the above address for general distribution. Initial distribution of AGARD publications is made to AGARD Member Nations through the following National Distribution Centres. Further copies are sometimes available from these Centres, but if not may be purchased in Microfiche or Photocopy form from the Sales Agencies listed below.

NATIONAL DISTRIBUTION CENTRES

**BELGIUM**

Coordonnateur AGARD -- VSL  
Etat-Major de la Force Aérienne  
Quartier Reine Elisabeth  
Rue d'Evere, 1140 Bruxelles

**LUXEMBOURG**  
See Belgium

**NETHERLANDS**

Netherlands Delegation to AGARD  
National Aerospace Laboratory, NLR  
Kluyverweg 1  
2629 HS Delft

**CANADA**

Director Scientific Information Services  
Dept of National Defence  
Ottawa, Ontario K1A 0K2

**DENMARK**

Danish Def  
Veø Idræts  
2100 Cope.



National Aeronautics and  
Space Administration

Washington, D.C.  
20546

**SPECIAL FOURTH CLASS MAIL  
BOOK**

Postage and Fees Paid  
National Aeronautics and  
Space Administration  
NASA-451



Official Business  
Penalty for Private Use \$300

**FRANCE**

O.N.E.R.A.  
29 Avenue  
92320 Chât

**GERMANY**

Fachinform:  
Karlsruhe  
D-7514 Egg

**GREECE**

Hellenic Air  
Air War Col  
Scientific and  
Dekelia Air  
Dekelia, Ath

**ICELAND**

Director of Aviation  
c/o Flugrad  
Reykjavik

Defence Research Information Centre  
Kentigern House  
65 Brown Street  
Glasgow G2 8EX

**ITALY**

Aeronautica Militare  
Ufficio del Delegato Nazionale all'AGARD  
3 Piazzale Adenauer  
00144 Roma/EUR

**UNITED STATES**

National Aeronautics and Space Administration (NASA)  
Langley Research Center  
M/S 180  
Hampton, Virginia 23665

THE UNITED STATES NATIONAL DISTRIBUTION CENTRE (NASA) DOES NOT HOLD STOCKS OF AGARD PUBLICATIONS, AND APPLICATIONS FOR COPIES SHOULD BE MADE DIRECT TO THE NATIONAL TECHNICAL INFORMATION SERVICE (NTIS) AT THE ADDRESS BELOW.

SALES AGENCIES

National Technical  
Information Service (NTIS)  
5285 Port Royal Road  
Springfield  
Virginia 22161, USA

ESA/Information Retrieval Service  
European Space Agency  
10, rue Mario Nikis  
75015 Paris, France

The British Library  
Document Supply Centre  
Boston Spa, Wetherby  
West Yorkshire LS23 7BQ  
England

Requests for microfiche or photocopies of AGARD documents should include the AGARD serial number, title, author or editor, and publication date. Requests to NTIS should include the NASA accession report number. Full bibliographical references and abstracts of AGARD publications are given in the following journals:

Scientific and Technical Aerospace Reports (STAR)  
published by NASA Scientific and Technical  
Information Branch  
NASA Headquarters (NIT-40)  
Washington D.C. 20546, USA

Government Reports Announcements (GRA)  
published by the National Technical  
Information Services, Springfield  
Virginia 22161, USA



Printed by Specialised Printing Services Limited  
40 Chigwell Lane, Loughton, Essex IG10 3TZ

ISBN 92-835-0547-6